Auger electron radionuclide therapy utilising F3 peptide to target the nucleolus

Christopher Hillyar MSc (Oxon)

CRUK/MRC Oxford Institute for Radiation Oncology
Jesus College, University of Oxford
Submitted for the degree of Doctor of Philosophy in Radiobiology
Trinity Term, 2015

Word count: 37,648

OXFORD INSTITUTE FOR RADIATION ONCOLOGY

Abstract

Auger electron radionuclide therapy utilising F3 peptide to target the nucleolus

Christopher Hillyar
CRUK/MRC Oxford Institute for Radiation Oncology
Jesus College, University of Oxford
Submitted for the degree of Doctor of Philosophy in Radiobiology
Trinity Term, 2015

F3 is a 31 amino acid peptide that possesses tumour homing capability and binds to nucleolin (NCL) expressed on the cell surface of malignant cells. Exposure of osteosarcoma (U2OS) cells to F3 peptide was found to shift the distribution of NCL and nucleophosmin (NPM) from the nucleolus to the nucleoplasm, and increase the level of Ki-67 in the nucleoplasm. ^{111}In-labelled F3 (^{111}In-DTPA-F3) was successfully radiosynthesised and was found to be significantly radiotoxic to MCF7, HCT116, MDA-MB-231/H2N, H322 and MDA-MB-435 cells, but not U2OS cells. ^{111}In-DTPA-F3 was shown to be taken up, and to deposit radiation dose, in the nucleolus. The level of cell kill produced by ^{111}In-DTPA-F3 was highly variable (19 fold range in surviving fraction) depending on the malignant cell line, and was correlated with the localisation of cell-bound ^{111}In-DTPA-F3 in the nucleus. The induction of γH2AX foci by ^{111}In-DTPA-F3 was found to be determined by the volume of the nucleolus. In conclusion, ^{111}In-DTPA-F3 is a promising Auger electron-emitting radiotherapeutic agent that targets the nucleolus, the radiosensitivity of which may vary depending on the malignant cell line.

Acknowledgements

I would like to thank Professor Katherine Vallis for the opportunity to complete a DPhil under her expert supervision; and Dr Bart Cornelissen and Professor Boris Vojnovic for their expert advice as cosupervisor and thesis committee member. I am extremely grateful to Dr Nadia Falzone who calculated the S-values in the Appendix of this thesis. I would also like to thank Dr Veerle Kersemans for advice on radiation protection; Professor Peter O'Neill and Dr Vincenzo D'Angiolella for assessing my Transfer of Status and Confirmation of Status; Professor Yvonne Jones and Professor Erika Mancini for great encouragement as Jesus College Advisors; and Dr Rebekka Hueting and Dr Cristiana Kartsonaki for technical assistance. Last but no means least, I would like to thank my family – Deborah, Simon, Ben, Jamie and Chloe – and my fiancée – Anjan – for their endless love and support during the highs and lows of my DPhil.

Abbreviations

AF488	AlexaFluor-488
AF488-WGA	AlexaFlour-488-conjugated wheat germ agglutinin
AF555	AlexaFluor-555
Ag-NOR	Silver staining nucleolar organiser region
AR	Androgen receptor
ARF	Human $p14^{ARF}$, mouse $p19^{ARF}$
ATM	Ataxia telangiectasia mutated kinase
BCA	Bicinchonic acid
BnDTPA	Benzyl-DTPA
BSA	Bovine serum albumin
CDK1	Cyclin-dependent kinase 1
Cy	Cytoplasm
D_0	Slope of the linear portion of the survival curve
DFC	Dense fibrillar centre
DMSO	Dimethyl sulfoxide
DNA	Deoxyribonucleic acid
DOTA	Tetraazacyclododecase tetraacetic acid
DSB	Double-strand break
DTPA	Diethylenetriamine pentaacetic acid
EC	Electron capture
EC_{50}	50% effective dose
EGF	Epidermal growth factor
EGFR	Epidermal growth factor receptor
ERK	Extracellular signal-regulated kinase
F3	F3 peptide
FC	Follicular centre
FISH	Fluorescence in situ hybridisation
FITC	Fluorescein isothiocyanate
GC	Granular centre
HCV	Hepatitis C virus
HDM2	Human double minute 2
HIV	Human immunodeficiency virus
HMGN2	High mobility group nucleosome binding domain 2
HPV	Human papilloma virus
HRP	Horse radish peroxidase
HSV-1	Herpes simplex virus 1
IC	Internal conversion
IC_{50}	50% inhibitory concentration

IGFR	Insulin-like growth factor receptor
IR	Ionising radiation
LD_{37}	Dose of γ-radiation (Gy) required to reduce surviving fraction to 0.37
LET	Linear energy transfer
MAPK	Mitogen-activated protein kinase
MDM2	Mouse double minute 2
Me	Membrane
MIRD	Medical internal radiation dose
mRNA	Messenger RNA
MS	Mass spectrometry
mTOR	Mammalian target of rapamycin
NAT	Noradrenaline transporter
NCL	Nucleolin
NDF	Nucleolar derived foci
NLS	Nuclear localisation sequence
NPM	Nucleophosmin
No	Nucleolus
NOPdb	Nucleolar protein database
NOR	Nucleolar organiser region
Np	Nucleoplasm
Nu	Nucleus
PARP-1	Poly(adenosine diphosphate-ribose) polymerase
PBS	Phosphate buffered saline
PENELOPE	Open-source Monte Carlo software
PET	Positron emission tomography
PHAX	Phosphorylated adapted RNA export protein
PIC	Pre-initiation complex
PI3K	Phosphatidylinositde 3-kinase
PKR	Protein kinase R
PNB	Pre-nucleolar body
Pol	Polymerase
PR	Perichromosomal region
Pre-rRNA	Pre-ribosomal RNA
PRRT	Peptide-receptor radiotherapy
RAS	Rapidly accelerated fibrosarcoma kinase
RBE	Relative biological effectiveness
rDNA	Ribosomal DNA
RGD	3-mer peptide (Arg-Gly-Asp)
RIT	Radioimmunotherapy
RNA	Ribonucleic acid
RNAi	RNA interference

RNP	Ribonucleoprotein
ROS	Reactive oxygen species
RP/r-protein	Ribosomal protein
rRNA	Ribosomal RNA
SD	Standard deviation
SDS	Sodium dodecyl sulfate
SEM	Standard error of the mean
SILAC	Stable-isotope labelling by amino acids in cell culture
siRNA	Small interfering RNA
SL-1	Selectivity factor
SMN	Survival of motor neurone protein
snoRNA	Small nucleolar RNA
snoRNP	Small nucleolar RNP
SPECT	Single photon emission computed tomography
TAF1C	TBP-associated factor 1C
TAT	HIV-1 TAT protein
TATA box	*Cis*-regulatory element
TBP	TATA box-binding protein
TBST	Tris-buffered saline with Tween-20
TIF-1A	Transcription intermediary factor 1-alpha
TF	Transcription factor
TGS1	Trimethylguanine synthase 1
tRNA	Transfer RNA
TRT	Targeted radiotherapy
TTF1	Thyroid transcription factor 1
Ub	Ubiquitin
UBF	Upstream binding factor
UdR	Deoxyuridine
UV	Ultraviolet radiation
VEGF	Vascular endothelial growth factor
VHL	Von Hippel-Lindau tumour suppressor
γH2AX	Phosphorylated (Ser-139) form of the H2A histone variant H2AX

Contents

Figures

Tables

Chapter 1. Introduction

1.1. Overview of radionuclide therapy

Haematological cancers can be treated with a combination of systemic chemotherapy, myeloablative therapy and transplantation, while solid tumours can be treated with a combination of surgery, systemic chemotherapy and locally delivered radiotherapy. External radiotherapy is used in 40% of cancer patients as a stand-alone modality or in combination with chemotherapy. Although external radiotherapy is effective in the treatment of locally confined disease, it is less effective against small metastatic lesions, diffuse or metastatic, disseminated disease. Radionuclide therapy encompasses the use of radioisotopes that are selectively taken up by malignant lesions through interactions with transporters or by interactions with tumour antigens targeted via a vector to which the radionuclide is attached.

Accumulation of therapeutic radionuclides in malignant tissue results in the deposition of radiation dose in tumour cells. The radionuclide ^{131}I (sodium-[^{131}I]iodide; t½, 8 days) is selectively taken up by thyroid tissue and thyroid carcinomas that overexpress the sodium-iodide symporter (Dohan*, et al.*, 2003). Accumulated ^{131}I deposits radiation dose in iodine-avid thyroid carcinoma through the emission of high energy beta particles during radioactive decay to ^{131}Xe ($^{131}_{53}\mathrm{I} \rightarrow {}^{131}_{54}\mathrm{Xe} + {}^{0}_{-1}\mathrm{e}$) (Schlumberger, 1998; Sherman, 2003). In contrast, the beta-emitter ^{89}Sr ([^{89}Sr]strontium-chloride; t½, 50 days) and the alpha-emitter ^{223}Ra ([^{223}Ra]radium-chloride (Alpharadin®); t½, 11.4 days) are calcium analogues used

for palliation of bone metastasis and are selectively taken up via the sodium-calcium antiporter expressed by overactive osteoblasts in bone lesions (D'Angelo*, et al.*, 2012; McGann and Horton, 2015; Pandit-Taskar*, et al.*, 2014).

More frequently, however, radiopharmaceuticals are radiosynthesised by coupling a radionuclide to a vector, which acts as a delivery vehicle that targets the radionuclide to a target moiety overexpressed by malignant cells. Vectors for preclinical or clinical studies include small molecules ($^{125/131}$I-labelled metaiodobenzylguanidine (MIBG)) (Weber*, et al.*, 1996); peptides (^{111}In/^{177}Lu-labelled octreotide/octreotate) (Kam*, et al.*, 2012; Pasieka*, et al.*, 2004); proteins (^{111}In-labelled epidermal growth factor (EGF)) (Reilly*, et al.*, 2000); or an affibody, antibody or antibody fragment (^{90}Y/^{131}I-labelled anti-CD20 antibody) (Goldsmith, 2010).

^{90}Y-labelled ibritumomab tiuxetan (Zevalin®) and ^{131}I-labelled tositumomab (Bexxar®) are radiolabelled anti-CD20 antibodies (Goldsmith, 2010). Both ^{90}Y-labelled ibritumomab tiuxetan and ^{131}I-labelled tositumomab are effective treatments for non-Hodgkin lymphomas (Kaminski*, et al.*, 2001; Witzig*, et al.*, 2002). ^{111}In- and ^{125}I-labelled antibodies against CD20, CD74 and HLA-DR have also shown promise in preclinical studies of metastatic B-cell lymphoma (Michel*, et al.*, 2005). The expression level of tumour target antigens (e.g. CD22) has been found to be predictive of the efficacy of RIT agents (e.g. ^{90}Y-labelled epratuzumab) (Linden*, et al.*, 2005).

In contrast to haematological malignancies, RIT of solid tumours is less effective, due to reduced radiosensitivity, poor vascularisation and elevated interstitial pressure that results in heterogeneity of uptake of the radiopharmaceutical and

absorption of radiation dose (usually giving a mean tumour dose of <15 Gy) (Hillyar*, et al.*, 2014). In contrast to RIT agents, the small size of PRRT agents (<5,000 Da) compared to antibodies (~155,000 Da) may enable PRRT agents to diffuse deeper into solid tumours. Radiolabelled somatostatin analogues for treatment of neuroendocrine tumours are the most extensively studied PRRT agents. These PRRT agents interact with the somatostatin receptor type 2 (sst2) at the cell membrane of malignant neuroendocrine cells (de Jong*, et al.*, 1999a; De Jong*, et al.*, 1999b; Hofland*, et al.*, 1999; Wang*, et al.*, 2003). Radiolabelled somatostatin analogues include ^{111}In-labelled octreotide (Valkema*, et al.*, 2002), ^{90}Y-labelled Tyr-octreotide (Otte*, et al.*, 1999; Valkema*, et al.*, 2006; Waldherr*, et al.*, 2002), ^{111}In-labelled pentetreotide (Anthony*, et al.*, 2002) and ^{177}Lu-labelled Tyr-octreotate (Kwekkeboom*, et al.*, 2003).

1.2. Biophysical properties of therapeutic radionuclides

Theoretically, the mechanism of radiation action of any radionuclide depends on the probability of the induction of damage due to ionisations in a set of critical target molecules, e.g. deoxyribonucleic acid (DNA), that must be inactivated to induce cell death. The probability of ionisations in a critical target molecule depends on the traversal of the emitted radiation directly through the target molecule (direct ionisations), or in its near vicinity where ionisations in water molecules generate reactive oxygen species (ROS; e.g. $\cdot O_2^-$, H_2O_2, $\cdot OH$, and OH^-) that diffuse over ~4 nm distances to ionise a target molecule (indirect ionisations) (Adelstein, 1993). The ratio of direct-to-indirect ionisations depends on the ‘quality’ of the emitted particle,

i.e. the linear energy transfer (LET; energy deposition per unit track length (eV/μm)). Thus, the deposition of ionisations in a target moiety is determined by the spatial position of the decaying atom with respect to the target moiety as well as the physical characteristics of the emitted particulate radiation.

Charged particles emitted by therapeutic radionuclides can be compared based on their biophysical properties (Figure 1.1). Beta particles (β^-) are high energy (0.498 to 2.280 MeV), long range (0.05 to 11.8 mm in water), negatively charged electrons emitted from the nucleus of a radionuclide (e.g. ^{90}Y, ^{131}I, or ^{177}Lu) at a rate of one per decay. Beta particles are sparsely ionising with low LET (0.2 keV/μm), except over a few nanometres at the end of the track length. As beta particles traverse matter their track paths become increasingly contorted due to scattering. Scattering results from elastic collisions with atomic nuclei and electrons (causing changes in direction with no energy loss) and inelastic collisions with atomic nuclei (producing Bremsstrahlung or braking radiation) and electrons (producing ionisations and excitations).

Alpha particles have equal mass (4 Da) and positive charge (+2) to that of helium nuclei. The emission of an alpha particle from the nucleus of a radionuclide (e.g. ^{211}At, ^{212}Pb, ^{213}Bi, ^{223}Ra, ^{225}Ac, or ^{227}Th) produces a daughter nucleus that has 2 fewer protons and 2 fewer neutrons. Alpha particle energies range from 5 to 9 MeV, resulting in a linear track length on the order of the diameter of a few mammalian cells (20 to 80 μm in water). Alpha particles have very high LET (80 to 100 keV/μm), increasing to ~300 keV/μm at the Bragg peak at the end of the track. The ratio of DNA single-strand breaks-to-double-strand breaks induced by α particle emitters is

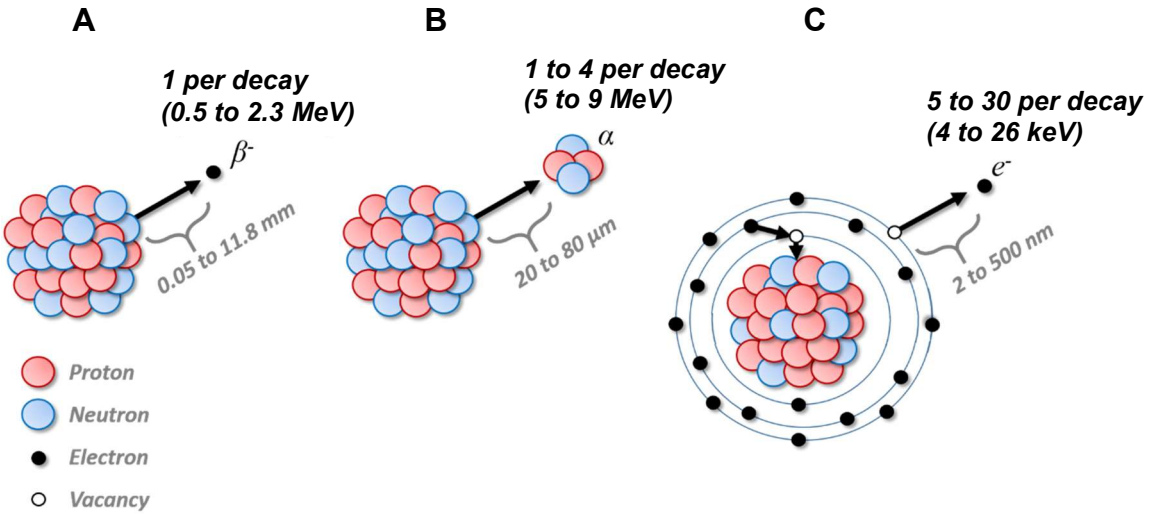

Figure 1.1. Biophysical properties of beta-, alpha-, and Auger electron-emitting radionuclides

(A) Beta particles (β^-) are high energy, long range, negatively charged electrons emitted from the nucleus of a radionuclide at a rate of one per decay. (B) Alpha particles (α) consist of two protons and two neutrons, are positively charged (2+) and are emitted from the nucleus of a radionuclide. (C) Auger electrons are low energy, short range, negatively charged electrons emitted as a result of electron capture (EC) or internal conversion (IC) decay. During EC (shown), a proton rich nucleus captures an inner shell electron and a vacancy is formed (usually in the K shell). During IC, an excited nucleus interacts with an inner shell electron, causing the electron to be ejected, forming a vacancy. In both EC and IC, a cascade of electron transitions rapidly moves the vacancy to the outermost shell. This is accompanied by the emission of 5 to 30 Auger electrons from the electron mantle of the radionuclide.

20, compared to 60 for low LET ionising radiation (IR) such as X-rays (Brons*, et al.*, 2001).

Auger electrons are predominantly (>90%) low energy (4 to 26 keV), short range (2 nm to 500 nm in water), negatively charged electrons that have high-LET-like properties. During electron capture or internal conversion, a vacancy is formed (usually in the K shell) and a cascade of electron transitions rapidly moves the vacancy to the outermost shell. This is accompanied by the emission of characteristic X-ray photons and 5 to 30 Auger, Coster-Kronig or super Coster-Kronig electrons (collectively termed Auger electrons) from the electron mantle of the radionuclide (e.g. ^{111}In, ^{123}I, or ^{125}I) (Kassis, 2004; Kassis, 2011). As Auger electrons traverse matter, their track paths become contorted due to scattering and multiple ionisations occur in the local vicinity of the decay site (4 to 26 keV/μm) (Cole, 1969), depositing highly localised energy over very small volumes of several cubic nanometres (10^2 to 10^5 Gy) (Kassis, 2004; Kassis, 2011; Pomplun*, et al.*, 1987). ^{111}In ($t_{½}$, 2.8 days), for example, emits an average of 14.7 Auger electrons (0.04 to 25.60 keV) and 2 γ-ray photons (171.3 and 245.4 keV) per decay. Thus, ^{111}In is suitable for Auger electron radionuclide therapy as well as single photon emission computed tomography (SPECT) imaging (Hillyar, 2015).

1.3. Auger electron radionuclide therapy

Auger electrons were discovered in 1922 by Lise Meitner (Meitner, 1922) and Pierre Auger (Auger, 1923). The biophysical properties of Auger electron-emitting radionuclides is shown in Table 1.1. Direct comparison of Auger electron emitters

	^{99m}Tc	^{111}In	^{123}I	^{125}I	^{201}Tl
Half-life (days)	0.25	2.80	0.55	59.4	3.04
Number of Auger electrons emitted per decay	4	14.7	14.9	24.9	36.9
Average Auger electron energy per decay (keV)	0.9	6.8	7.4	12.2	15.3
Auger electron energy range (keV)	0.2–17.8	0.04–25.6	0.02–30.35	0.02–30.3	0.07–66.9
Track range of Auger electrons in water (nm)	13–6,500	0.25–13,600	0.5–13,500	1.5–14,000	3–40,000
Conversion electrons emitted per decay	1.1	0.2	0.2	0.9	1.1
Average conversion electron energy per decay (keV)	15.4	25.9	20.2	7.2	30.2
Conversion electron energy range (keV)	100–140	145–245	127–159	3.7–35	1.6–153
Track range of conversion electrons in water (μm)	70–112	145–245	100–130	0.7–16	0.2–126
Energy of gamma emissions (keV)	140.5	171.3, 245.4	159	3,535	138.5
Total released energy per decay (keV)	142.6	419.2	200.4	61.4	138.5
Total energy deposited in water per decay (x10^{-14} Gy kg/Bq/s)	2.3	7	3.2	1	2.2

Table 1.1. Biophysical properties of Auger electron-emitting radionuclides

Adapted with permission from (Cornelissen and Vallis, 2010)

is highly complex, due to differences in the number of electrons emitter per decay and the range of energies of the emission spectra. A unifying attribute is the relationship between each Auger electron's kinetic energy in eV (which confers a range in nm) and LET (keV/μm). Greater than 90% of all Auger electrons have an energy of 2 to 4,000 eV (ranges of ~2 to 500 nm), and high LET of 4 to 25 keV/μm (Kassis, 2011).

The radiotoxic effects of Auger electron-emitting radionuclides are caused by decay-induced ionisations, excitations, nuclear recoil, chemical transmutations and local charge effects (Kassis, 2011). A body of evidence suggests Auger electron emitters are not highly radiotoxic when localised in the extracellular space (Bradley*, et al.*, 1975; Kassis*, et al.*, 1983; Kassis*, et al.*, 1987a; Kassis*, et al.*, 1987b; Miyazaki and Shinohara, 1993), cell membrane (Warters and Hofer, 1977) or cytoplasm (Hofer*, et al.*, 1975; Kassis*, et al.*, 1980; Kassis*, et al.*, 1985; Kassis*, et al.*, 1987b). These reports support the widely-held view that DNA damage (in particular DNA double-strand breaks) is the principle cause of radiation-induced cell death (Radford*, et al.*, 1988).

However, contradictory evidence suggests that ^{125}I is more radiotoxic to breast (4T1) and ovarian (SK-OV-3) carcinoma cells when localised on the cell membrane by non-internalising antibodies, than when ^{125}I is localised in the cytoplasm by internalising antibodies, and is equally as radiotoxic to SK-OV-3 cells as nuclear localisation (Pouget*, et al.*, 2008). Specifically, ^{125}I-labelled non-internalising anti-CEA (35A7) antibodies have been found to be equally as radiotoxic to SK-OV-3 cells when localised on the cell membrane, than when ^{125}I is localised in the nucleus by the internalising anti-HER2 antibody trastuzumab (Herceptin®) (Pouget*, et al.*,

2008). ^{125}I-labelled non-internalising antibodies also caused significant tumour growth delay *in vivo* (Santoro*, et al.*, 2009). Recently, a mean nuclear dose of 1.2 Gy deposited by non-internalising ^{125}I-labelled anti-CEA monoclonal antibodies was shown to be as effective at reducing the clonogenic survival of colon carcinoma (HCT116) cells as 43 Gy deposited in the nucleus by internalising ^{125}I-labelled anti-HER1 monoclonal antibodies (Piron*, et al.*, 2014). Further, ^{125}I-labelled acridines have been postulated to cause toxic effects in melanoma cells by causing the leaking of toxic compounds through the deposition of localised dose in cytoplasmic acidic vesicles into which they are internalised (Gardette*, et al.*, 2014).

Despite these contradictory reports, the prevailing view is that Auger electron-induced cell killing is, at least in part, a consequence of energy deposition in DNA, the 'quintessential genetic target' for all forms of radiation therapy including Auger electron radionuclide therapy (Kassis, 2004).

Microdosimetric modelling has shown that the amount of energy deposited in DNA is ~30 fold greater when the Auger electron emitter is placed in the nucleus compared to when placed on the cell membrane (Faraggi*, et al.*, 1994; Goddu*, et al.*, 1994). The radiotoxic effects of Auger electron emitters is mainly (~80% to 90%) mediated by indirect mechanisms, i.e. the ionisation of nearby water molecules that generates ROS that diffuse over short distances (~4 nm) to damage DNA (Bishayee*, et al.*, 2000a; Bishayee*, et al.*, 2000b; Walicka*, et al.*, 1998a; Walicka*, et al.*, 2001; Walicka*, et al.*, 2000; Walicka*, et al.*, 1999). Thus, the yield of DNA double-strand breaks induced when ^{99m}Tc, ^{123}I or ^{125}I is located close to chromatin DNA decreases in the presence of the ·OH radical scavenger dimethyl sulfoxide (DMSO)

(Chung*, et al.*, 2014; Kassis*, et al.*, 2000; Lobachevsky and Martin, 2004; Walicka*, et al.*, 1998b).

Early studies with ^{125}I showed that the incorporation of the thymidine analogue 5-[^{125}I]-iodo-2'-deoxyuridine (^{125}I-UdR) was highly radiotoxic to mammalian cells (D_0 <100 disintegrations per cell), producing a cell survival curve with an exponential reduction in clonogenic survival, i.e. a high-LET-like survival curve without a shoulder (Bradley*, et al.*, 1975; Chan*, et al.*, 1978; Hofer*, et al.*, 1975; Koch and Burki, 1975; Porteous, 1971). The Auger emitters ^{77}Br, ^{123}I, ^{125}I and $^{193m/195m}$Pt covalently bound to DNA via thymidine analogues (^{77}Br-UdR and ^{123}I-UdR), DNA-intercalating agents (^{125}I-labelled acridines), DNA-adduct-forming agents ($^{193m/195m}$Pt-labelled *cis*-/*trans*-platinum), and DNA-minor-groove-binding agents (^{125}I-Hoechst-33358), have also been shown to produce survival curves without a shoulder, typical of that of high-LET radiation (Howell*, et al.*, 1994; Karagiannis*, et al.*, 2000; Kassis*, et al.*, 1982; Kassis*, et al.*, 1989; Kassis*, et al.*, 1987b; Martin*, et al.*, 1979). Similarly, experiments with ^{123}I and ^{125}I showed that nuclear translocation of ^{123}I- and ^{125}I-labelled oestrogens produced high-LET-like exponential decreases in survival (^{125}I-estradiol has a D_0 of 28 decays/cell, similar to that of ^{125}I-UdR, i.e. D_0 of 30 decays/cell) (Bloomer*, et al.*, 1983; DeSombre*, et al.*, 2000; Epperly*, et al.*, 1991; Kearney*, et al.*, 1999; McLaughlin*, et al.*, 1989; Yasui*, et al.*, 1996; Yasui*, et al.*, 2001b).

Delivery of the Auger emitter to the nucleus, aims to deposit extremely high radiation dose in DNA within the local vicinity of the decay site ($3x10^6$ Gy/^{77}Br decay, 10^7 Gy/^{125}I decay) (Kassis, 2004; Kassis*, et al.*, 1982). DNA-incorporated ^{125}I (^{125}I-UdR) produces ~1 to 5 DNA double-strand breaks per decay, over ranges of 1.5 to 2 nm

from the decay site, i.e. on the order of the diameter of the DNA helix (Kassis*, et al.*, 2000; Krisch*, et al.*, 1976; Krisch*, et al.*, 1978; Krisch and Ley, 1974; Krisch and Sauri, 1975; Schmidt and Hotz, 1973). The ratio of DNA double-strand break induction for DNA-incorporated ^{123}I versus DNA-incorporated ^{125}I is 0.63 (^{123}I:^{125}I) (Lobachevsky and Martin, 2004). However, DNA-incorporated ^{99m}Tc produces a relatively low number of DNA double-strand breaks (0.011 DSB per decay) in a manner dependent on indirect mechanisms (0.0005 DSB per decay in the presence of DMSO) (Chung*, et al.*, 2014).

The nuclear translocation of Auger emitters increases the dose deposited in DNA. Nuclear accumulation has been achieved by 1) covalent incorporation into DNA ($^{123/125}$I-labelled iododexyuridine or iodothiodeoxyuridine), 2) binding of radiolabelled oligonucleotides or peptide nucleic acids to DNA, 3) receptor-mediated nuclear translocation via the somatostatin receptor (^{111}In-labelled octreotide), epidermal growth factor receptor (EGFR; ^{111}In-labelled EGF) or oestrogen receptor (ER; ^{125}I-labelled tamoxifen or estradiol), and 4) the conjugation of a nuclear localisation sequence (NLS) into a radiolabelled oligonucleotide, peptide, protein or antibody (Cornelissen and Vallis, 2010).

To gain entry to the nucleus, small molecules are small enough to diffuse freely through the nuclear pore complex. However, larger NLS-containing conjugates over ~50 kDa in size must first bind to importins α and β to gain entry to the nucleus through Ran-GTPase-dependent translocation via the nuclear pore complex. Dissociation of the NLS-containing conjugate from the α and β importins then occurs inside the nucleus (Kersemans*, et al.*, 2008b). Also, endosomal escape sequences have been suggested to be useful to potentiate endosomal escape, thereby

reducing hydrolysis of the radiopharmaceutic agent in the endo-lysosome (Cornelissen and Vallis, 2010). Notwithstanding advances in the nuclear translocation of Auger emitting radiotherapeutics, DNA double-strand break induction is nevertheless dependent on the structure of chromatin. Indeed, the histone deacetylase inhibitor suberanilohydroxamic acid (SAHA; vorinostat) has been shown to increase the number of γH2AX foci (markers of DNA double-strand breaks) induced by ^{111}In-labelled growth factors that translocate to the nucleus of growth factor receptor-positive breast carcinoma (MDA-MB-468) cells (Terry and Vallis, 2012).

1.4. Auger electron-emitting radiopharmaceutic agents

Radiopharmaceuticals that incorporate a vector are collectively referred to as targeted radionuclide therapy (TRT) agents. TRT agents that contain antibodies or peptides are divided into radioimmunotherapy (RIT) agents and peptide-receptor radionuclide therapy (PRRT) agents, respectively. In this section Auger electron-emitting TRT agents are discussed, including small molecules, oligonucleotides, PRRT agents, proteins, and RIT agents.

1.4.1. Small molecules

Radioiodinated nucleotides, such as ^{125}I-UdR, are efficiently incorporated into the DNA of S-phase cells (Bloomer and Adelstein, 1977). After intracellular internalisation, ^{123}I-UdR and ^{125}I-UdR are phosphorylated by thymidine kinase, thereby trapping the radioiodinated deoxynucleotide inside the cell. Nuclear

localisation of ^{125}I-UdR in tumour tissue has been demonstrated *ex vivo* using microautoradiography (Bodei*, et al.*, 2003; Mariani*, et al.*, 1993).

DNA-incorporated ^{125}I-UdR is retained in the nucleus during the life of the cell and is transmitted to post-mitotic daughter cells, while unincorporated ^{125}I-UdR is dehalogenated by thymidylate synthase or rapidly catabolised to iodouracil (Commerford and Joel, 1979; Garrett*, et al.*, 1979; Kassis*, et al.*, 1987a; Kinsella*, et al.*, 1986; Le Mevel*, et al.*, 1973). However, the disadvantage of ^{125}I-UdR is that DNA incorporation only occurs in tumour cells in S phase, i.e. the proliferating fraction of tumour cells. The radiotoxicity of ^{125}I-UdR is nonetheless potentiated by bystander effects that may affect non-radiolabelled/non-proliferating cells *in vivo* (Boyd*, et al.*, 2006; Xue*, et al.*, 2002).

Tumour washout of ^{125}I-UdR is rapid and tumour uptake is relatively low (Bodei*, et al.*, 2003). In the liver, ^{125}I-UdR is efficiently dehalogenated, increasing the injected dose required to achieve therapeutic ratios in cancer cells. The injected dose is limited however by uptake of ^{125}I-UdR in proliferating stem cell niches which produces toxic side effects, such as aloepecia and neutropenia (Bagshawe*, et al.*, 1991; Calabresi*, et al.*, 1961; Hampton and Eidinoff, 1961; Kriss*, et al.*, 1962; Prusoff, 1963).

As well as radioiodinated nucleotides, radioiodinated catecholamine analogues, such as ^{123}I-MIBG which penetrates into neuroendocrine spheroids, have also been studied (Mairs*, et al.*, 1991b; Walker*, et al.*, 1990). In the case of neuroblastoma and phaeochromocytoma, ^{123}I-MIBG interacts with the catecholamine type I active uptake (uptake-1) noradrenaline transporter (NAT). Once internalised via the uptake-1 NAT, ^{123}I-MIBG is packaged and stored in adrenergic vesicles (McEwan,

et al., 1985). Gene therapy with NAT expression vectors holds promise as a means to increase ^{123}I/^{131}I-MIBG uptake and cell kill (Boyd*, et al.*, 1999; McCluskey*, et al.*, 2013).

Early experiments showed that when MIBG was labelled with the short range Auger electron-emitter ^{123}I it was more effective at reducing the growth of smaller spheroid volumes than larger ones, and it was therefore suggested that MIBG would be more effective against small tumour volumes when labelled with a short range particle emitter (Gaze*, et al.*, 1992; Mairs*, et al.*, 1991a). However, subsequent experiments showed that ^{123}I-MIBG and the long range beta-emitter ^{131}I-MIBG were equally as effective at reducing the growth of spheroids 100 μm in diameter, while ^{131}I-MIBG was more effective than ^{123}I-MIBG at reducing the growth of spheroids 200 μm in diameter (Weber*, et al.*, 1996). In the clinical setting, ^{131}I-MIBG is routinely used to treat metastatic neuroblastoma, while ^{123}I-MIBG is mainly used for SPECT imaging. Radioiodinated oestrogens bind to the oestrogen receptor (ER) at the cell membrane. After binding ERs, which include a family of nuclear receptors activated by 17β-oestradiol, radioiodinated oestrogens translocate to the nucleus. Preclinical studies of oestrogens and androgens that internalise and translocate to the nucleus have utilised the Auger electron emitters ^{80m}Br, ^{123}I and ^{125}I (Bloomer*, et al.*, 1983; DeSombre*, et al.*, 1988; DeSombre*, et al.*, 1992). ^{123}I-labelled oestrogen reduces the growth of monolayer and spheroid cultures of oestrogen receptor-transfected Chinese hamster ovary (CHO) cells and oestrogen receptor-positive breast carcinoma (MCF7) cells *in vitro* (DeSombre*, et al.*, 2000; DeSombre*, et al.*, 1996; DeSombre*, et al.*, 1992; Kearney*, et al.*, 1999; Schwartz*, et al.*, 1996; Yasui*, et al.*, 2001a). Further, radiation dose-dependent ^{123}I-labelled oestrogen-induced DNA

double-strand breaks, single-strand breaks and chromosome aberrations, have all been inversely correlated with survival (Schwartz*, et al.*, 1996).

The ER agonist diethylstilbestrol has also been radiodinated with ^{123}I and ^{125}I, producing reductions in survival (Fischer*, et al.*, 2008). Similarly, ^{123}I-, ^{124}I-, and ^{125}I-labelled androgen receptor (AR)-targeting agents have been shown in pre-clinical studies to 1) internalise into prostate (LNCaP, DU145 and PC-3) carcinoma cells in an AR-dependent manner, translocate to the nucleus and associate with DNA *in vitro* (Han*, et al.*, 2014); and 2) deliver therapeutic radiation doses to a murine tumour model *in vivo* (Kortylewicz*, et al.*, 2015). No radiolabelled steroids have been studied clinically.

Radiolabelled chemotherapeutic agents, such as bleomycin (^{111}In-bleomycin), have been shown to deliver radioactivity to head and neck squamous cell carcinomas and gliomas (Kairemo*, et al.*, 1997; Kairemo*, et al.*, 1996; Korppi-Tommola*, et al.*, 1999). Autoradiography experiments have shown that ^{111}In-bleomycin is 1.6 to 5.3 fold more efficacious compared to non-radiolabelled bleomycin. A high proportion of ^{111}In-bleomycin (78%) translocates to the nucleus, reducing survival of squamous cell carcinoma, glioma and human small cell lung cancer cells and inducing more chromosomal aberrations compared to non-radiolabelled bleomycin (Hou*, et al.*, 1989a; Hou*, et al.*, 1985a; Hou*, et al.*, 1985b; Hou and Maruyama, 1990; Hou and Maruyama, 1992; Hou*, et al.*, 1992; Hou*, et al.*, 1989b; Jaaskela-Saari*, et al.*, 2005). The Auger electron emitters ^{191}Pt, ^{193m}Pt and ^{195m}Pt can replace the platinum core of the chemotherapy agent cisplatin. ^{191}Pt-cisplatin (167 MBq/mg) has been shown to be 4 fold more effective than non-radiolabelled cisplatin (IC_{50} of 0.76±0.13 μg/mL versus 3.24±0.08 μg/mL, respectively) at reducing the survival of cervical carcinoma

(ME-180) cells *in vitro* (Areberg*, et al.*, 2000). ^{191}Pt-cisplatin also retards the growth of human squamous cell carcinoma (AB) xenografts in mice *in vivo* (Areberg*, et al.*, 2001).

1.4.2. Oligonucleotides

Synthetic oligonucleotides can deliver Auger electron emitters to within nanometre distances of DNA and messenger RNA (mRNA) sequences by base-pairing with complementary sequences. Auger electrons emitted by radiolabelled oligonucleotides can damage DNA and mRNA, thereby perturbing cellular function and reducing detectable mRNA levels. ^{125}I-labelled antisense oligonucleotides have been shown to cause breaks in the mRNA for the human multidrug-resistance gene (*mdrl*) *in vitro* (Gaidamakova*, et al.*, 2004). Nanoparticles have been used to deliver short ^{111}In-labelled oligonucleotides with complementarity to the human *N-myc* gene overexpressed by human neuroblastoma (SK-N-DZ) cells (Watanabe*, et al.*, 2006). ^{111}In-labelled N-myc oligonucleotides reduced N-myc mRNA levels and inhibited the growth of neuroblastoma (SK-N-DZ) cells *in vitro* and SK-N-DZ xenografts *in vivo* (Watanabe*, et al.*, 2006).

1.4.3. PRRT agents

^{111}In-labelled 8-mer somatostatin analogues, such as ^{111}In-labelled octreotide (Valkema*, et al.*, 2002) and ^{111}In-labelled pentetreotide (Anthony*, et al.*, 2002), are the best studied Auger electron-emitting PRRT agents. Upon binding to sst2 at the cell membrane, the ^{111}In-labelled somatostatin analogues translocate to the nucleus

(de Jong*, et al.*, 1999a; De Jong*, et al.*, 1999b; Hofland*, et al.*, 1999; Wang*, et al.*, 2003). Preclinical studies have found that the Auger electron-emitter ^{57}Co-DOTA-octreotate (0.6 to 7.1 keV) was significantly more effective than ^{111}In-DOTA-octreotate (3.4 to 26.0 keV) at killing pancreatic carcinoma (AR42J) cells *in vitro* (Thisgaard*, et al.*, 2014). Nevertheless, a clinical study showed that 55% of patients experienced clinical improvement after treatment with ^{111}In-DTPA-octreotate (Valkema*, et al.*, 2002).

To improve the internalisation and retention of ^{111}In-labelled octreotide, the SV40 large-T antigen nuclear localisation sequence (NLS) has been conjugated to ^{111}In-DOTA-Tyr(3)-octreotide, forming ^{111}In-DOTA-Tyr(3)-octreotide-NLS (Ginj*, et al.*, 2005). ^{111}In-DOTA-Tyr(3)-octreotide-NLS has 6 fold higher intracellular retention in sst2-positive rat pancreatic carcinoma (AR4-2J) cells compared to ^{111}In-DOTA-Tyr(3)-octreotide lacking the NLS. Increased intracellular retention was attributed to the ability of the SV40 large-T antigen NLS to potentiate nuclear translocation (45 fold) (Ginj*, et al.*, 2005).

The radiotoxicity of PRRT agents (e.g. ^{111}In-labelled exendin-4, which binds GDL-1R expressed on neuroendocrine tumour cells) to organs such as the kidneys can be reduced through the administration of anti-angiogenic agents (vatalanib) that produce therapeutic synergy. 1.1 MBq of ^{111}In-labelled exendin-4 with 100 mg/kg of vatalanib was as effective as 28 MBq of ^{111}In-labelled exendin-4 alone in the treatment of a transgenic mouse model of pancreatic neuroendocrine tumours, without causing radiation damage to the kidneys (Wicki*, et al.*, 2014).

Improving the tumour localisation (tumour-to-normal tissue ratio) of Auger electron-emitting PRRT agents has been achieved by formulating bispecific agents that

increase the probability of binding to tumour antigens. An example is ^{111}In-DTPA-octreotate-RGD, which, in addition to sst2, recognises $\alpha_v\beta_3$ integrin via the 3-mer peptide RGD (Arg-Gly-Asp) (Capello*, et al.*, 2004). ^{111}In-DTPA-octreotate-RGD induced higher levels of apoptosis compared to ^{111}In-DTPA-octreotate *in vivo.* ^{99m}Tc-labelled RDG has also been conjugated to the HIV-1 TAT protein, a cell penetrating peptide, to drive ^{99m}Tc internalisation into $\alpha_v\beta_3$ integrin-expressing glioma (C6) xenografts in mice (Ocampo-Garcia*, et al.*, 2013). Due to significant intracellular internalisation, ^{99m}Tc-labelled RDG-TAT is potentially useful for imaging and therapy of tumours expressing $\alpha_v\beta_3$ integrin.

1.4.4. Proteins

Growth factors, such as EGF and vascular endothelial growth factor (VEGF), can be utilised to deliver Auger electron emitters to cancer cells. ^{111}In-labelled EGF is significantly more radiotoxic to breast carcinoma cells (MDA-MB-468) expressing high levels of the EGF receptor (EGFR) compared to breast carcinoma cells (MCF7) expressing low levels of EGFR (Bailey*, et al.*, 2007; Reilly*, et al.*, 2000). Experiments using fluorescence resonance energy transfer have shown that fluorophore-labelled EGF interacts with EGFR in the cytoplasm and the nucleus of MDA-MB-468 cells *in vitro* (Cornelissen*, et al.*, 2011a). When EGF binds to EGFR, ~10% of the total EGF:EGFR complex formed on the cell membrane translocates to the nucleus, because EGFR contains a putative nuclear localisation sequence (underlined) at residues 645–657, RRRHIVRKRTLRR (Cornelissen*, et al.*, 2011a; Lin*, et al.*, 2001; Lo*, et al.*, 2006; Reilly*, et al.*, 2000). The nuclear translocation of ^{111}In-labelled EGF can be enhanced using the EGFR tyrosine kinase inhibitor gefitinib, the anti-HER2

monoclonal antibody trastuzumab (Herceptin®) or the prenyltransferase inhibitor L-788,123 (Bailey*, et al.*, 2007; Cornelissen*, et al.*, 2011a). Thus, the effect of ^{111}In-labelled EGF on survival can be potentiated by enhancing nuclear translocation (Bailey*, et al.*, 2007).

Preclinical pharmacokinetic, biodistribution, toxicology and dosimetry studies for ^{111}In-labelled EGF have been completed in mice and rabbits (Reilly*, et al.*, 2006). The safety, pharmacokinetics, biodistribution and radiation dosimetry of ^{111}In-labelled EGF has also been studied in a Phase I human trial of patients with EGFR-positive metastatic breast cancer (Vallis*, et al.*, 2014).

In contrast to ^{111}In-labelled EGF, ^{111}In-labelled VEGFA$_{165}$ targets the tumour neovasculature to cause anti-tumour effects. Tumour neovasculature is readily accessible and, unlike tumour cells, the radiopharmaceutic agent is not required to diffuse from the capillary lumen to bind to tumour endothelial cells. The SV40 large-T antigen NLS has been conjugated to ^{111}In-labelled VEGFA$_{165}$ to increase translocation to the nucleus (1.5 fold), enhance DNA double-strand break formation (27.5 fold) and reduce clonogenic survival (4 fold) (Chan*, et al.*, 2010).

1.4.5. RIT agents

Since the 1980s, antibodies, such as ibritumomab tiuxetan and tositumomab, have had their antibody-dependent immune cell-mediated cytotoxicity enhanced by radiolabelling with high energy beta emitters (Kaminski*, et al.*, 2001; Witzig*, et al.*, 2002). Ibritumomab tiuxetan and tositumomab are non-internalising antibodies that remain associated with the cell membrane after binding to CD20 rather than translocating to the nucleus. Despite evidence that the cell membrane may be

sensitive to Auger electrons (Pouget*, et al.*, 2008), radiolabelled non-internalising antibodies have not been utilised extensively by the field of Auger electron RIT. Instead, internalising antibodies, such as 17-1a which recognises epithelial cell adhesion molecule (Ep-CAM), have been studied for Auger electron RIT. ^{125}I-labelled 17-1a is significantly radiotoxic and induces higher levels of chromosomal damage and micronuclei compared to ^{125}I-labelled R11D10, a non-internalising anti-Ep-CAM antibody (Woo*, et al.*, 1989).

Clinically utilised Auger electron-emitting RIT agents include ^{125}I-labelled monoclonal antibody 425 (mAb-425), an anti-EGFR antibody developed to treat glioblastoma multiforme (Bender*, et al.*, 1992; Derui*, et al.*, 1992; Quang and Brady, 2004). ^{125}I-labelled mAb-425 inhibited the growth of EGFR-overexpressing glioma (U-87MG, A1207 and F39) cells *in vitro* and glioma (87MG) xenografts *in vivo* (Bender*, et al.*, 1992). In Phase I/II studies, treatment of 192 patients with glioblastoma multiforme with ^{125}I-labelled mAb-425 alone or ^{125}I-labelled mAb-425 in combination with temozolamide produced a median survival of 14.5 months and 20.2 months, respectively, compared to a median survival of 10.2 months for a historical control group of 39 patients not treated with ^{125}I-labelled mAb-425 (Li*, et al.*, 2010).

To enhance nuclear translocation, RIT agents have been conjugated to the SV40 large-T antigen NLS. ^{111}In-labelled anti-CD33 antibody HuM195 conjugated to 8 NLS peptides (^{111}In-labelled anti-CD33-NLS) increased the localisation of the Auger electron emitter (up to 6 fold) and reduced the clonogenic survival of CD33-positive promyelocytic leukaemia (HL-60) cells *in vitro* (Chen*, et al.*, 2006). ^{111}In-labelled anti-CD33-NLS has also been shown to be effective at reducing the survival of the

HL-60-MX-1 cell line, a methotrexate- and mitoxantrone-resistant derivate of the HL-60 cell line (Kersemans*, et al.*, 2008a).

Similarly, the internalisation of ^{111}In-labelled anti-HER2 antibody (trastuzumab) was increased (2 to 5 fold) when conjugated to 6 NLS peptides, enhancing its effect on the survival of HER2-positive breast carcinoma (SK-BR-3, MDA-MB-361 and MDA-MB-231) cell lines *in vitro* (2 to 5 fold) and reduced the growth of MDA-MB-361 tumour xenografts *in vivo* (Costantini*, et al.*, 2007; Costantini*, et al.*, 2010). Also, the internalisation of an ^{111}In-labelled anti-EGFR monoclonal antibody (nimotuzumab) into EGFR-positive breast carcinoma (MDA-MB-468) cells was enhanced (7 fold) when conjugated to an NLS conferring higher uptake in tumour xenografts (Fasih*, et al.*, 2012).

^{111}In-labelled anti-γH2AX antibodies have also been conjugated to the HIV-1 TAT protein NLS (^{111}In-DTPA-anti-γH2AX-TAT) to detect, and be retained at sites of DNA double-strand break damage induced by external IR or bleomycin (Cornelissen*, et al.*, 2012a; Cornelissen*, et al.*, 2011b). ^{111}In-DTPA-anti-γH2AX-TAT has also been used to detect pre-neoplastic mammary lesions in athymic mice with elevated γH2AX levels (Cornelissen*, et al.*, 2014). During oncogenic stress or following exposure to IR, ataxia telangiectasia mutated (ATM) kinase and other PI3K-like kinases phosphorylate Ser-139 on multiple copies of the histone variant H2AX extending from sites of DNA double-strand break damage (Jackson and Bartek, 2009). γH2AX foci induced by IR can be detected and amplified by ^{111}In-DTPA-anti-γH2AX-TAT, reducing clonogenic survival of breast carcinoma (MDA-MB-231/H2N and MDA-MB-468) cells *in vitro*. The growth of breast carcinoma (MDA-MB-231/H2N) xenografts in athymic mice was also significantly inhibited by

IR in combination with ^{111}In-DTPA-anti-γH2AX-TAT compared to IR or ^{111}In-DTPA-anti-γH2AX-TAT alone (Cornelissen*, et al.*, 2012a). A cleavable version of ^{111}In-DTPA-anti-γH2AX-TAT that was also modified with EGF has been radiosynthesised to enhance uptake in EGFR-positive breast carcinoma (MDA-MB-468) cells. The tumour uptake of bivalent ^{111}In-labelled anti-γH2AX radioimmunoconjugates modified with EGF (^{111}In-DTPA-anti-γH2AX-SS-EGF) was increased in an EGFR-dependent manner after inducing γH2AX with externally delivered IR (Cornelissen*, et al.*, 2013). Irradiation with external IR resulted in increased nuclear translocation and nuclear retention of ^{111}In-DTPA-anti-γH2AX-SS-EGF and reduced survival of MDA-MB-468 cells (Cornelissen*, et al.*, 2013).

1.5. Potential non-DNA nuclear targets for Auger electrons

In the early 1990s, Hofer *et al*. (1993) conducted experiments in which asynchronous CHO cells were exposed to ^{125}I-UdR for 12 h. Cells were then synchronised by mitotic selection, replated and harvested 1 h (early G_1), 3 h (late G_1), 5 h (early S), 7 h (mid S) and 9 h (late S/G_2) after plating. After harvesting, cells were cells were frozen in liquid nitrogen for 5 days, before being thawed and plated for clonogenic survival assays. Results from clonogenic survival assays produced D_0 values (equal to the reciprocal of the straight portion of the slope of the survival curve) of 39 (early G_1), 41 (late G_1), 53 (early S), 72 (mid S), and 84 (late S/G_2) ^{125}I-decays/cell, respectively. These D_0 values suggested that target multiplicity increased while cycling through the cell cycle (Figure 1.2.A). Subsequent experiments were performed in which asynchronous CHO cells were exposed to

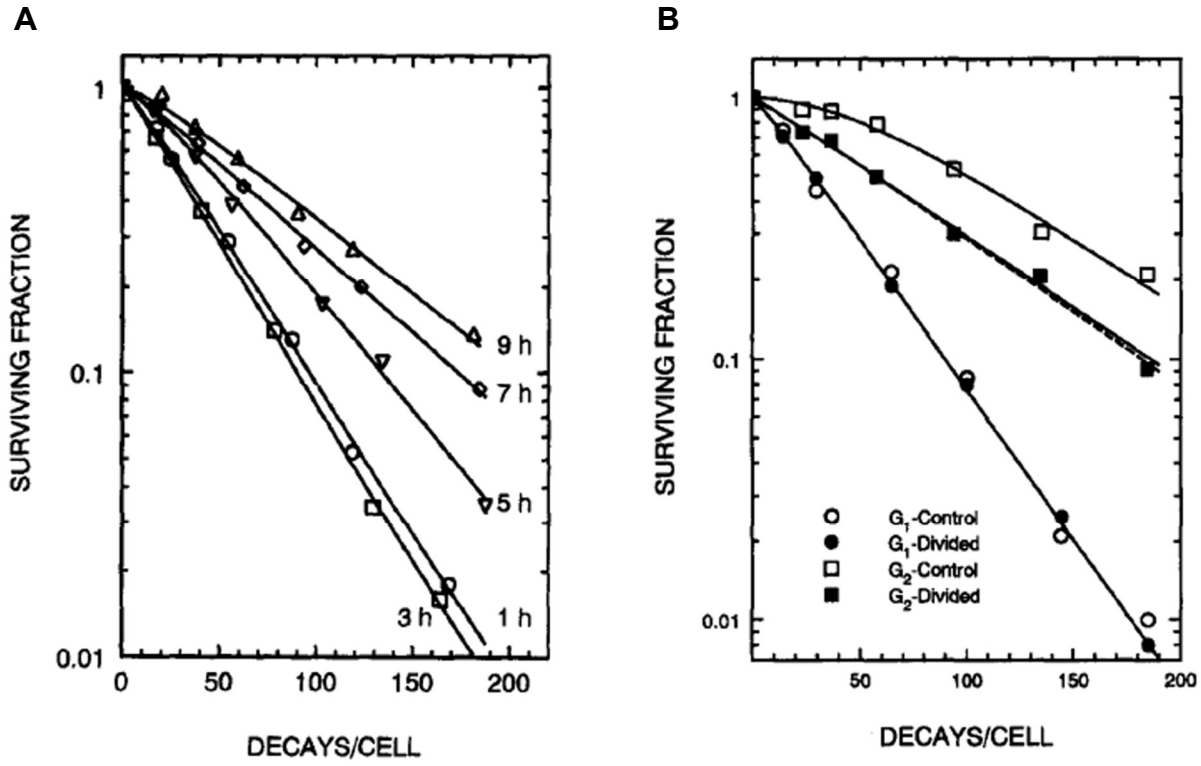

Figure 1.2. Survival of CHO cells exposed to ^{125}I-UdR

(A) Survival of CHO cells as a function of cell cycle position at the time of ^{125}I decay accumulation. Asynchronous CHO cells were labelled with ^{125}I-UdR for 12 h, synchronised by mitotic selection, replated, and harvested 1, 3, 5, 7 or 9 h after plating. (B) Survival of G_1- or G_2-phase CHO cells plated for colony formation in the same cell cycle after exposure to ^{125}I-UdR (G_1-control, G_2-control) or the next cell cycle (G_1-divided, G_2-divided). Reprinted from (Hofer*, et al.*, 1993) with permission from Taylor and Francis Group (www.tandfonline.com).

^{125}I-UdR for 12 h, then synchronised by mitotic selection, replated and harvested 1 h (early G_1) or 9 h (late S/G_2) after plating. After harvesting, cells were frozen in liquid nitrogen for 5 days, before being thawed and plated for clonogenic survival assays in the same cell cycle (G_1-control, G_2-control). Replicates were also plated but allowed to pass through one cell division before being replated in the next cell cycle (G_1-divided, G_2-divided). Each G_1-control and G_2-control cell was expected to give rise to a single colony if both (live-live pairs) of post-mitotic daughter cells or just one (live-dead pairs, dead-live pairs) of the post-mitotic daughter cells survived. G_1-divided and G_2-divided cells however were separated by trypsinisation and therefore the presence of live-dead pairs of post-mitotic daughter cells and dead-live pairs of post-mitotic daughter cells was revealed. Survival curves for G_1-control and G_1-divided cells were superimposed and lacked a shoulder, while survival curves G_2-control and G_2-divided cells were significantly different, with a shoulder and not comprising a shoulder, respectively (Figure 1.2.B). These data suggested that the targets that replicated during S-phase were independent entities that were damaged by ^{125}I located in DNA, leading to death of one daughter cell but not the other. Hofer *et al.* (1993) concluded that the primary target of this model (replicated independent target model) may be 1) the DNA that replicated during S-phase, with both daughter helices acting as independent targets, and/or 2) a non-DNA target closely associated with DNA such as a higher-order nuclear structure (Hofer*, et al.*, 1993).

Nucleoli are non-DNA higher-order structures closely associated with DNA that are replicated during S-phase (Celis*, et al.*, 1987), the components of which are distributed to daughter cells during mitosis. Chromosomes bearing ribosomal DNA

(rDNA; chromosomes 13, 14, 15, 21 and 22) cluster together to form one of a number of given nucleoli during interphase. In prophase of mitosis, increases in nucleolar cyclin B1-cyclin-dependent kinase-1 (CDK1) levels causes hyperphosphorylation of components of the ribosomal DNA (rDNA) transcription machinery (which impairs an interaction between SL-1 and UBF), resulting in transient loss of RNA polymerase I (Pol I) subunits (RPA16, RPA20, RPA39 and RPA194) in parallel with the dissolution of the nuclear envelope (Heix*, et al.*, 1998; Leung*, et al.*, 2004). rRNA processing factors are redistributed from the nucleolus to the cytoplasm or become associated at the surface of condensed chromosomes in a region called the perichromosomal region (PR) (Gautier*, et al.*, 1992). During anaphase, the PR distributes nucleolar proteins, along with the condensed chromosomes, between daughter cells. Nucleolar-derived foci (NDF), which form in the cytoplasm and contain early and late rRNA-processing proteins, are also distributed between daughter cells.

At the end of mitosis, nucleoli reassemble as rDNA transcription resumes (Dimario, 2004; Hernandez-Verdun, 2006; Leung*, et al.*, 2004; Olson and Dundr, 2005), concentrating factors involved in ribosome biogenesis (Kressler*, et al.*, 2010). Decreases in the level of cyclin B1-cyclin-dependent kinase-1 (CDK1) in late anaphase/early telophase reactivates rRNA transcription and triggers the reformation of the nuclear envelope (Sirri*, et al.*, 2000). The NDF disappear in early G_1, the contents of which, along with the contents of the PR, are transferred to fibro-granular bodies called pre-nucleolar bodies (PNBs) that are formed on the surface of the daughter chromosomes (Dundr*, et al.*, 2000). Subsequently, the nucleolus reforms through the recruitment of the contents of PNBs to the rDNA genes via

'bridges' formed by thin threads of granular material that can be visualised by electron microscopy and links the PNBs to the reforming nucleolus (Dundr*, et al.*, 2000; Savino*, et al.*, 2001). Finally, rDNA-bearing chromosomes coalesce, resulting in the fusion of some nucleoli. The nucleolus, then, fits the replicated independent target model proposed by Hofer *et al.* (1993) to explain why ^{125}I-UdR incorporated into DNA caused either the death of both post-mitotic daughter cells (dead-dead pair), only one daughter cell (dead-live pair, live-dead pair) or neither of the daughter cells (live-live pair) (Hofer*, et al.*, 1993).

Another line of evidence also suggested that damage to DNA may not be the only determinant of cell kill. In 2001, Yaqui *et al*. (2001) demonstrated that the number of DNA double-strand breaks does not determine the relative biological effectiveness of Auger electron-emitting radiopharmaceutic agents. In experiments that quantified DNA double-strand breaks and clonogenic survival, the yield of DNA double-strand breaks was 8 fold higher for ^{125}I-oestrogen compared to ^{125}I-UdR, but the efficiency of cell killing was similar for ^{125}I-oestrogen (D_0 = 28 decays/cell) and ^{125}I-UdR (D_0 = 30 decays/cell) (Yasui*, et al.*, 2001a). The relative biological effectiveness (RBE) of ^{125}I-oestrogen compared to X-rays was found to be 18.8 for double-strand breaks and 4.8 for cell kill, while for ^{125}I-UdR the RBE for double-strand breaks was 2.3, but the RBE for cell kill was 4.5. Similar levels of cell killing by ^{125}I-oestrogen and ^{125}I-UdR, but disparity between the number of DNA double-strand breaks suggests either 1) that the nature of the DNA double-strand breaks is different, with those induced by ^{125}I-oestrogen being less deleterious than those induced by ^{125}I-UdR and/or 2) that ^{125}I-UdR causes higher levels of irradiation of a non-DNA target closely associated with DNA.

1.6. The nucleolus as a target for Auger electrons

The first independent observations of the nucleolus were made by the German physiologists Rudolph Wagner (Wagner, 1835) and Gabriel Valentin (Valentin, 1836; Valentin, 1839) in 1835–9, but it was not until almost a century later that it was discovered that nucleoli arise at sites of repeated rDNA genes (Heitz, 1931; McClintock, 1934). In metabolically active eukaryotic cells, the nucleolus contains tens to hundreds of rRNA genes which account for approximately half of total cellular RNA synthesis (Grummt and Pikaard, 2003). In human diploid cells, >600 rDNA genes are located on the short arms of five pairs of acrocentric chromosomes (chromosomes 13, 14, 15, 21 and 22), with a transcribed sequence and an intergenic spacer arrayed head-to-tail in tandem repeats that are collectively termed nucleolar organiser regions (NORs). NORs readily stain with silver and so are also called Ag-NORs.

1.6.1. Potential for interfering with ribosome biogenesis

Ribosome biogenesis, i.e. the synthesis of the 40S and 60S ribosome subunits (r-subunits), is an energy-expensive process driven by Pol I-mediated transcription of rDNA genes (Fatica and Tollervey, 2002; Olson*, et al.*, 2002; Rudra and Warner, 2004). In yeast, the synthesis of rRNA represents ~60% of total transcriptional activity (Warner, 1999). A proliferating HeLa cell produces approximately 7,500 ribosomes per min, a process which requires the transcription of 150 to 200 rDNA genes and 300,000 ribosomal proteins (r-proteins) (Mayer and Grummt, 2006). The efficiency of Pol I transcription of the active rDNA genes, which constitute less than

half of the >600 rDNA genes, is modulated by the transcription factors TIF-1A, SL-1 and UBF (McStay and Grummt, 2008; Moss*, et al.*, 2007). The activity TIF-1A, SL-1 and UBF is positively regulated by the mTOR, phosphatidylinositol-3-kinase (PI3K), RAS-ERK, and mitogen activated protein kinase (MAPK) pathways. Together, the mTOR, PI3K, RAS-ERK, and MAPK pathways ensure the growth and survival of the cell, by coupling metabolic status, nutrient levels and growth factor signalling to the synthesis of ribosomes in the nucleolus (Grummt, 2003; Hardie, 2005; Mayer and Grummt, 2006; Sengupta*, et al.*, 2010; Xiao and Grove, 2009).

The synthesis of the ~7,000 nucleotide long 47S pre-rRNA leads to its co-transcriptional and post-transcriptional processing and modification by small nucleolar ribonucleoproteins (snoRNPs) and small nucleolar RNAs (snoRNAs), forming the 28S, 5.8S and 18S rRNAs in the nucleolus. SnoRNAs and snoRNPs mediate 2′-O-ribose methylation and pseudouridine formation during the processing of the 47S pre-rRNA (Matera*, et al.*, 2007). SnoRNAs act as guide RNAs during rRNA-specific modification (Dieci*, et al.*, 2009). The 5S rRNA and r-proteins are transcribed in the nucleoplasm by polymerase III (Pol III) and polymerase II (Pol II), respectively. The synthesis of mRNA encoding r-proteins accounts for ~50% of pol II transcription in yeast (Warner, 1999). In eukaryotic cells, the 5S rRNA and r-proteins are transported to the nucleolus and assembled with the 28S, 5.8S and 18S rRNAs to form the pre-ribosome 40S and 60S r-subunits. Pre-ribosome r-subunit assembly is facilitated by transient interactions with snoRNPs and non-ribosomal proteins (Fatica and Tollervey, 2002; Tschochner and Hurt, 2003). The near-mature pre-ribosome r-subunits are then exported from the nucleus to the cytoplasm in a Ran-GTP-dependent manner (Moy and Silver, 1999), where they

undergo the final processing steps to become the mature 40S and 60S r-subunits (Figure 1.3).

Nucleolar organisation is highly conserved from yeast to human (Kressler*, et al.*, 2010). The nucleolus has a tripartite structure that reflects the concentration of transcription and processing factors within sub-regions termed the fibrillar centre (FC), dense fibrillar component (DFC) and granular component (GC) (Raska, 2003). Pre-rRNA is transcribed in the FC, which is enriched with components of the Pol I transcription machinery. The snoRNPs and snoRNAs that process the pre-rRNA transcripts are concentrated in the DFC, whereas most proteins concentrated in the GC participate in pre-ribosome subunit assembly and late rRNA processing (Boisvert*, et al.*, 2007; Sirri*, et al.*, 2008).

In 1964, Donald Brown and John Gurdon reported that anucleolated *Xenopus* embryos that lack a functional nucleolus arrest in development because they are unable to synthesise ribosomes (Brown and Gurdon, 1964). Thus, the premise for Auger electron radionuclide therapy targeting the nucleolus is to inactivate the nucleolus and arrest the growth of malignant cells by interfering with ribosome biogenesis.

1.6.2. Potential for inducing the nucleolar stress response

Targeting the nucleolus aims to induce the nucleolar stress response, which couples disparate stress pathways in the regulation of p53 stabilisation, cell cycle arrest and apoptosis. Proteomic analysis has revealed that only ~30% of the >4,500 proteins associated with the nucleolus are involved in ribosome biogenesis (Ahmad*, et al.*, 2009; Andersen*, et al.*, 2005). Indeed, emerging evidence suggests that the

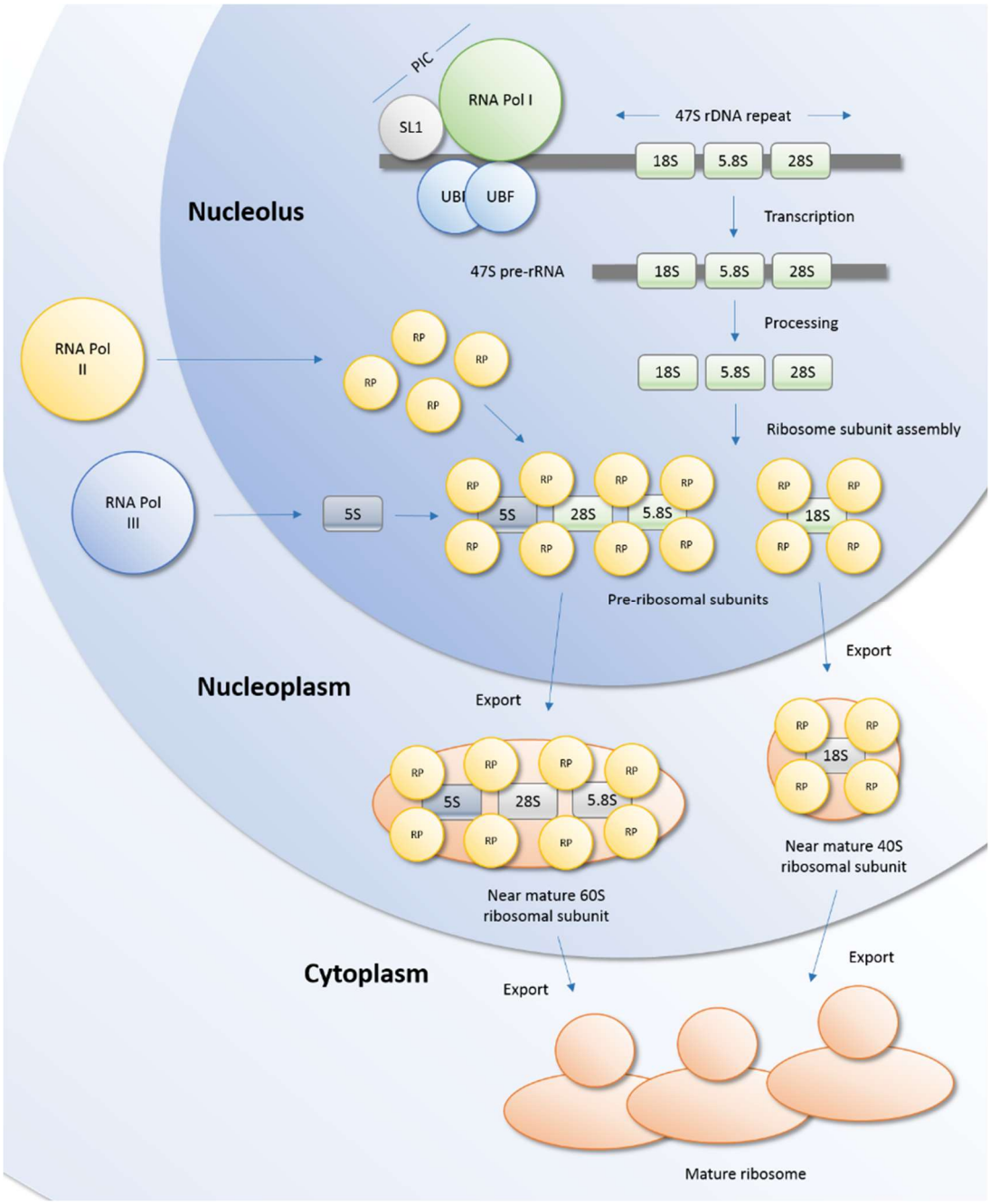

Figure 1.3. Ribosome biogenesis

During ribosome biogenesis, Pol I-mediated transcription of rDNA genes is modulated by the transcription factors SL-1 and UBF. Pol I transcription of the rDNA gives rise to the 47S pre-rRNA, which is post-transcriptionally processed in the nucleolus by snoRNPs and snoRNAs to form the 18S, 5.8S and 28S rRNAs. The 5S rRNA and r-proteins (RP) are transcribed in the nucleoplasm by Pol III and Pol II, respectively. The 5S rRNA and r-proteins are transported to the nucleolus where they are assembled with the 28S, 5.8S and 18S rRNAs to form the pre-ribosomal subunits. After pre-ribosomal subunits undergo maturation, the near-mature ribosome subunits are then exported from the nucleus to the cytoplasm, where they undergo the final processing steps to become the mature 40S and 60S ribosome subunits. Adapted with permission from (Hein, *et al.*, 2013).

nucleolus is a plurifunctional stress sensor, with many non-canonical functions besides its role as a factory for ribosome biogenesis. In addition to ribosome biogenesis, the nucleolus is also involved in the assembly of the signal recognition particle, the processing and export of mRNAs and tRNAs, virus infection control, maturation of non-nucleolar RNAs and ribonucleoproteins (RNPs), regulation of telomerase and senescence, regulation of the cell cycle, tumour suppressor and oncogene activities and the regulation of the MDM2-p53 pathway (Gerbi*, et al.*, 2003; Grosshans*, et al.*, 2001; Handwerger and Gall, 2006; Jacobson and Pederson, 1998; Mekhail*, et al.*, 2005; Olson and Dundr, 2005; Olson*, et al.*, 2002; Pederson, 1998).

Different types of cellular stress are accompanied by complex reorganisations of nucleolar components. Nucleolar responses to different types of cellular stress are shown in Table 1.2. DNA damage caused by ultraviolet (UV) radiation, Pol I transcription inhibition or topoisomerase II inhibition is accompanied by nucleolar segregation (Al-Baker*, et al.*, 2005; Govoni*, et al.*, 1994; Shav-Tal*, et al.*, 2005). Nucleolar segregation is characterised by the condensation and separation of the FC and GC, along with the formation of ‘nucleolar caps’ around a nucleolar remnant (Shav-Tal*, et al.*, 2005). In contrast, DNA damage caused by IR is accompanied by nucleolar disruption, which leads to the unravelling of the FC into necklace-like structures. Nucleolar fragmentation is distinct from nucleolar segregation in that it only occurs in response to inhibition of Pol II or protein kinase, but not Pol I inhibition (David-Pfeuty, 1999; Haaf and Ward, 1996; Shav-Tal*, et al.*, 2005). Nucleolar disruption is used hereafter in place of either nucleolar segregation or fragmentation (Vlatkovic*, et al.*, 2014).

Stress Type	Trigger	p53 Stabilisation	Effects on Nucleolus	Effects on Cajal bodies	References
DNA damage/genotoxic stress	UVC	Yes	Nucleolar segregation, delocalisation of Ki-67	Cajal body disruption and coilin in nucleoplasmic microfoci	(Al-Baker, *et al.*, 2005; Cioce and Lamond, 2005; Rubbi and Milner, 2003)
	IR (DSB)	Yes	Nucleolar disruption, ATM-dependent inhibition of RNA Pol I activity	No major effect on coilin distribution	(Cioce and Lamond, 2005; Rubbi and Milner, 2003)
	Camptothecin Bleomycin	Yes	Nucleolar disruption	N/A	(Rubbi and Milner, 2003)
Temperature change	Heat shock	Yes	Nucleolar disruption	Cajal Bodies smaller; micro-Cajal Bodies in Xenopus	(Carmo-Fonseca, *et al.*, 1993; Handwerger, *et al.*, 2002; Rubbi and Milner, 2003)
	Cold shock			Cajal Bodies bigger	(Carmo-Fonseca, *et al.*, 1993)
Hypoxia	–	Yes	Nucleolar disruption, VHL-dependent reduction of rRNA transcription	N/A	(Mekhail, *et al.*, 2006; Rubbi and Milner, 2003)
Viral infection	Adenovirus, Coronavirus, HCV, HIV, HPV, HSV-1, Poliovirus, West Nile virus	N/A	Changes in nucleolar morphology and proteome	Coilin in nucleoplasmic microfoci and rosettes (adenovirus); accumulation of coilin at damaged centromeres (HSV-1)	(Greco, 2009; James, *et al.*, 2010; Morency, *et al.*, 2007; Schillaci and Simonetti, 2004)
Nutrient stress	Serum starvation	N/A	Reduction in ribosomal biogenesis	Cajal body number decreases	(Andrade, *et al.*, 1993; Mayer and Grummt, 2006; Murayama, *et al.*, 2008; van Riggelen, *et al.*, 2010; Zhou, *et al.*, 2009)

Table 1.2. Different types of cellular stress with effects on the nucleolus

Reprinted under creative common licence from (Boulon, *et al.*, 2010).

Stress Type	Trigger	p53 Stabilisation	Effects on Nucleolus	Effects on Cajal bodies	References
Inhibition of RNA polymerase I and/or II	Actinomycin D	Yes	Nucleolar disruption, release of r-proteins into the nucleoplasm	Coilin in nucleolar caps	(Carmo-Fonseca*, et al.*, 1993; Lindstrom, 2009; Shav-Tal*, et al.*, 2005; Warner and McIntosh, 2009; Zhang and Lu, 2009)
	Doxorubicin	Yes	Nucleolar disruption	Nucleolar association of coilin	(Rubbi and Milner, 2003)
	α-Amanitin	Yes	Nucleolar disruption	Coilin in cap-like structures associated with the nucleolus	(Carmo-Fonseca*, et al.*, 1993; Rubbi and Milner, 2003)
Inhibition of nuclear export	Leptomycin B	Yes	No disruption of nucleolar integrity	Nucleolar association of coilin	(Rubbi and Milner, 2003; Sleeman*, et al.*, 2001)
Inhibition of phosphatases	Okadaic acid	N/A	N/A	Accumulation of coilin in the nucleolus	(Lyon*, et al.*, 1997)
Inhibition of DNA and RNA synthesis	5-Fluorouracil	Yes	Nucleolar disruption, release of r-proteins into the nucleoplasm and p53 stabilisation. rRNA processing disrupted	N/A	(Burger*, et al.*, 2010; Lindstrom, 2009; Warner and McIntosh, 2009; Zhang and Lu, 2009)
Alteration of proteasome activity	MG132	Yes	No disruption of nucleolar integrity, inhibition of late rRNA processing	No disruption of Cajal bodies	(Burger*, et al.*, 2010; Rubbi and Milner, 2003)
	Overexpression of PA28γ	N/A	N/A	Disruption of Cajal bodies	(Cioce*, et al.*, 2006)
Alteration of snRNP biogenesis	Depletion of SMN, PHAX, TGS1	N/A	N/A	Disruption of Cajal bodies and nucleolar localization of coilin	(Lemm*, et al.*, 2006)

Table 1.2. Different types of cellular stress with effects on the nucleolus

Reprinted under creative common licence from (Boulon*, et al.*, 2010).

Stress Type	Trigger	p53 Stabilisation	Effects on Nucleolus	Effects on Cajal bodies	References
Oncogenic stress	C-myc or Ras activation	Yes	Up regulation of nucleolar proteins p14ARF and NPM	N/A	(Chen*, et al.*, 2010; Kruse and Gu, 2008; Lee and Gu, 2010)
Alteration of ribosome subunit biogenesis	Malfunction of nucleolar proteins (e.g. Bop1, NPM, nucleostemin)	Yes	Release of r-proteins into the nucleoplasm following, in most cases, nucleolar disruption	N/A	(Fumagalli*, et al.*, 2012; Lindstrom, 2009; Warner and McIntosh, 2009; Zhang and Lu, 2009)

Table 1.2. Different types of cellular stress with effects on the nucleolus

Reprinted under creative common licence from (Boulon*, et al.*, 2010).

The nucleolar localisation of many nucleolar components and non-nucleolar components is altered by stress induced by the cell cycle, differentiation, transformation, modulation of cell growth, transcription inhibition or DNA damage (Boisvert*, et al.*, 2007; Grummt and Pikaard, 2003; Olson*, et al.*, 2002). Proteomic and dynamic imaging analysis of isolated nucleoli from cells exposed to actinomycin D, viral infection, UV or IR, has revealed that the protein content of the nucleolus is highly dynamic and responds differently to different types of stress (Boisvert*, et al.*, 2010; Boisvert and Lamond, 2010; Emmott*, et al.*, 2010; Lam*, et al.*, 2010; Moore*, et al.*, 2011).

The localisation in the nucleolus of tumour suppressor proteins and oncoproteins, such alternative reading frame (ARF; mouse $p19^{ARF}$, human $p14^{ARF}$), nucleophosmin (NPM), and mouse double minute 2 (mouse MDM2; human HDM2), regulates the p53 pathway (Colombo*, et al.*, 2002; Gjerset and Bandyopadhyay, 2006). To control p53 stabilisation, the oncoprotein MDM2 binds to p53, interfering with p53's ability to transactivate Pol II by binding the acidic activation domain of p53 (Momand*, et al.*, 1992; Oliner*, et al.*, 1993), and marks p53 with ubiquitin on its C-terminal lysines (K370, K372, K373, K381, K382, and K386), promoting nuclear export and proteosome-dependent degradation of p53 in the cytoplasm (Haupt*, et al.*, 1997; Kubbutat*, et al.*, 1997; Lee and Gu, 2010; Rodriguez*, et al.*, 2000). Under normal conditions, nuclear export of ubiquitin (Ub)-modified p53 involves the co-transport of the Ub-p53:MDM2 complex with the r-proteins RPL5 and RPL11 or the rRNAs 5.8S or 5S during ribosome biogenesis (Fontoura*, et al.*, 1992; Riley and Maher, 2007; Zhang and Lu, 2009). Nuclear export of p53 involves two distinct pathways in which p53 is poly- or mono-ubiquitylated and subsequently exported from the nucleus via the nucleolus or the nucleoplasm, respectively (Boyd*, et al.*, 2011). Nucleolar disruption is

required for DNA damage to result in the stabilisation of p53 (Rubbi and Milner, 2003), suggesting that the nucleolus is a central stress sensor that functions to suppress p53 stabilisation.

Under stress conditions, r-proteins (RPS5, RPS6, RPL11, RPL23, and RPL26), rRNAs (5.8S and 5S), and nucleolar proteins (nucleolin (NCL) and NPM) are released from the nucleolus into the nucleoplasm (Boisvert*, et al.*, 2010; Boisvert and Lamond, 2010; Boisvert*, et al.*, 2007; Colombo*, et al.*, 2002; Daniely*, et al.*, 2002; Gjerset and Bandyopadhyay, 2006; Zhang and Lu, 2009). In the nucleoplasm, RPL5, RPL11, RPL23 and RPS7 associate with MDM2 and inhibit MDM2's E3 ligase activity, thereby releasing p53 from MDM2 regulation (Zhang and Lu, 2009). Under normal physiological conditions, RPL11 is sequestered in the nucleolus by PICT1 due to NEDD8-dependent NEDDylation of RLP11. However, under stress conditions RPL11 is de-NEDDylated and released into the nucleoplasm, where it interacts with MDM2, promoting p53 stabilisation (Sasaki*, et al.*, 2011; Sundqvist*, et al.*, 2009). RPL11 and RPL23 can bind to MDM2 simultaneously, forming an inactive ternary complex (Lindstrom*, et al.*, 2007), while RPL5 and RPL11 co-operate to cause synergistic MDM2 inhibition (Horn and Vousden, 2008). Also, reduction in the levels of RPS6 abrogates 40S but not 60S r-subunit biogenesis and causes RPL5- and RPL11-dependent p53 stabilisation, while reduction in RPS23 and RPS7 inhibits ribosome biogenesis and causes RPL11-dependent p53 stabilisation (Fumagalli*, et al.*, 2009).

Release of RPL11 from the nucleolus to the nucleoplasm is triggered by changes in the bioavailability of 18S and 28S rRNAs. Interactions between RPL11 and MDM2 are favoured during stress conditions that disrupt ribosome biogenesis (Fumagalli*, et al.*, 2012; Holzel*, et al.*, 2010), while disruption of the 40S r-subunit leads to the upregulation of RPL11 mRNA (Fumagalli*, et al.*, 2009). In response to DNA damage,

RPL26 and NCL bind to the 5'-untranslated region of p53 mRNA, enhancing its translation (Takagi*, et al.*, 2005). However, MDM2 inhibits this interaction and drives the proteasome-dependent degradation of RPL26 by mediating its polyubiquitylation (Ofir-Rosenfeld*, et al.*, 2008).

It is hypothesised that damage caused by Auger electrons to rDNA and rRNAs (47S, 28S, 18S, 5.8S and 5S) may interfere with interactions with r-proteins in the nucleolus, releasing r-proteins (RPL5, RPL11, RPL23, RPS6 and RPS7) into the nucleoplasm, inducing p53 and promoting p53-dependent cell cycle arrest and apoptosis. Stabilised p53 represses Pol I and Pol III transcription (upregulated in malignancy due to oncogene activation), leading to the further release of r-proteins that mediate the stabilisation of p53. p53 stabilisation inhibits Pol I-mediated transcription by interfering with the formation of the pre-initiation complex (PIC). Formation of the PIC relies on UBF-dependent recruitment of the SL-1 complex to the Pol I transcription machinery. p53 binds to the SL-1 complex subcomponents TATA box-binding protein (TBP) and TBP-associated factor 1C, preventing the recruitment of SL-1 to the Pol I transcription machinery (Zhai and Comai, 2000). p53 also inhibits Pol III-mediated transcription of 5S rRNA by disrupting the interactions between promoter occupancy by TFIIIB and disrupting the interaction between Pol III and TBP, thereby decreasing ribosome subunit biogenesis (Crighton*, et al.*, 2003; Zhai and Comai, 2000). In contrast, the activation of p53 upregulates Pol II-transcribed genes such as p21, Bax, Puma and Noxa, initiating cell cycle arrest and driving the mitochondrial apoptotic pathway in the cytoplasm (Lee and Gu, 2010).

Conceptually, the nucleolus is a 'barrier' that needs to be surmounted for p53 stabilisation to take place (Rubbi and Milner, 2003). If the integrity of the nucleolus and ribosome biogenesis is compromised, the cellular processes that monitor Pol I

transcription and assembly of the r-subunits induce cellular checkpoints and apoptosis through the stabilisation and activation of p53 (Boisvert*, et al.*, 2007; Boulon*, et al.*, 2010). The nucleolar stress response pathway therefore consists of non-mutually exclusive mechanisms that couple the bioavailability of components of ribosome biogenesis with the MDM2-p53 pathway following the sensing of cellular stress by the nucleolus (Figure 1.4).

Targeting the nucleolus with Auger electrons may not only interfere with ribosome biogenesis by causing damage to rDNA and rRNA, but may also induce p53-dependent cell cycle arrest and apoptosis as a consequence of damage to proteins involved in rRNA transcription, r-subunit assembly and export of p53 to the cytoplasm.

1.6.3. Effects of targeting the nucleolus in cancer

The aim of this section is to argue that the nucleolus is a potential target for Auger electron radionuclide therapy of malignant disease. Cell growth and metabolism is driven by the size and number of nucleoli, which is linked to nucleolar activity. The rate of ribosome biogenesis is higher in proliferating cells than in resting cells (Derenzini and Ploton, 1991). Indeed, the size of the nucleolus is inversely related to the tumour doubling time, directly related to growth fraction of proliferating tumour cells, tumour aggressiveness and worse disease prognosis (Derenzini*, et al.*, 2009; Derenzini*, et al.*, 2000; Derenzini*, et al.*, 1998; Pich*, et al.*, 2000).

During oncogenesis, hyperactivation of rDNA transcription is caused by the up-regulation of signalling components and oncogenes that interact with the rDNA promoter or Pol I transcription machinery. Activated RAS-RAF-ERK and PI3K-AKT-mTOR pathways transmit signals to Pol I (and Pol III), thereby upregulating rRNA

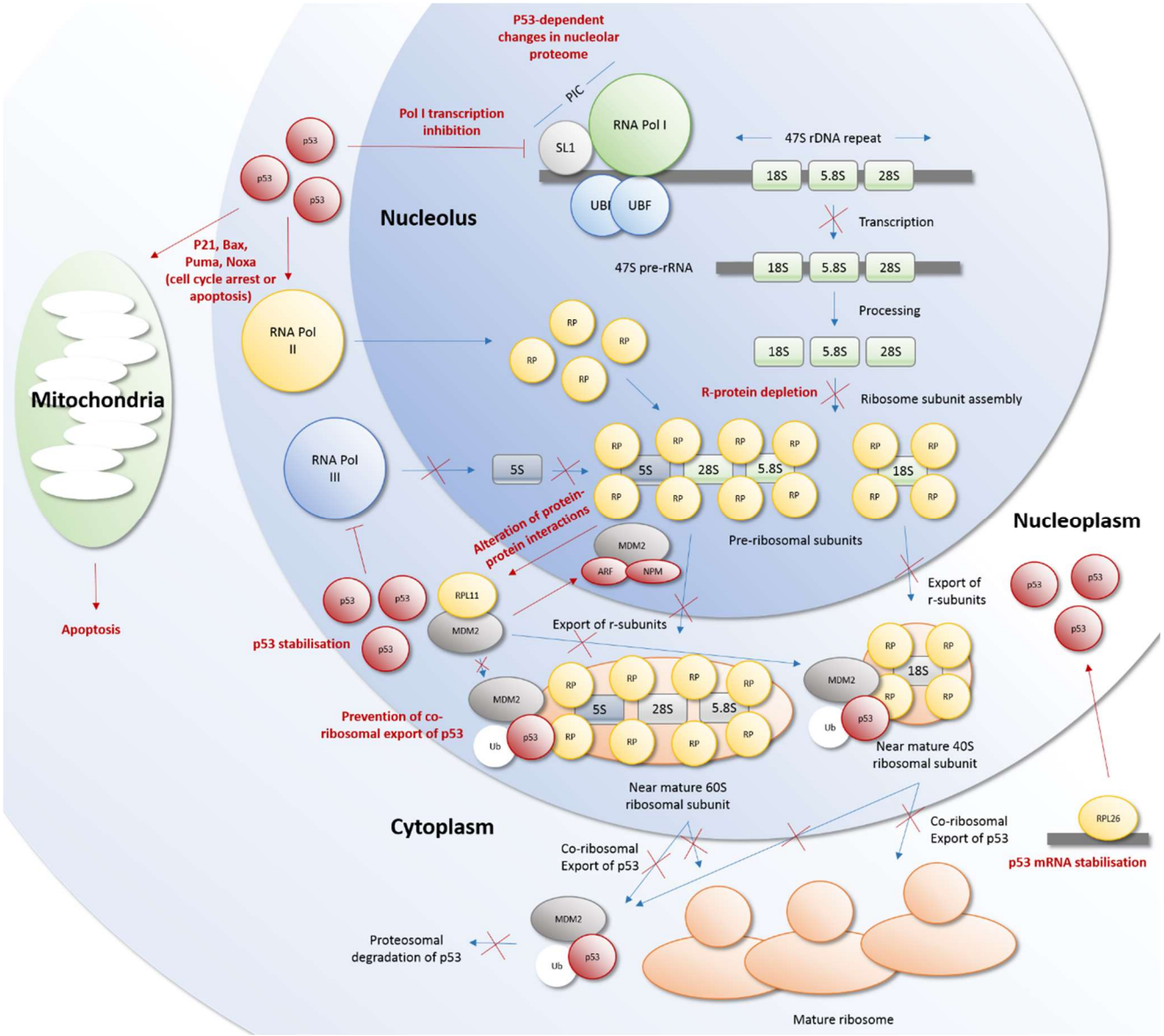

Figure 1.4. The nucleolar stress response

The nucleolar stress response pathway consists of non-mutually exclusive mechanisms that couple alterations in protein-protein interactions, mRNA stability, and ribosomal export with the MDM2-p53 pathway. The outcomes of the nucleolar stress response are shown in red and include inhibition of Pol I-mediated rRNA transcription, r-protein depletion in the nucleolus, increased p53 levels, upregulation of p53 target genes (p21, Bax, Puma and Noxa), cell cycle arrest and apoptosis. Adapted with permission from (Hein, *et al.*, 2013) and adapted under creative common licence from (Boulon, *et al.*, 2010).

synthesis (Chan*, et al.*, 2011; Drygin*, et al.*, 2010; Hannan*, et al.*, 2013; Stefanovsky*, et al.*, 2001; Zhao*, et al.*, 2003). Overexpression of RPS3a suppresses apoptosis while overexpression of the 5S rRNA has been linked to tumour formation in mouse tissues (Marshall*, et al.*, 2008; Naora*, et al.*, 1998).

On the other hand, haploinsufficiency of *DKC1* (the gene encoding the rRNA processing factor dyskerin) is linked to dyskeratosis congenita, a disease of premature ageing and increased cancer susceptibility (Ruggero*, et al.*, 2003), while mutation of the *RMRP* gene, which encodes an RNase essential for pre-rRNA processing, is linked to cartilage hair hypoplasia, a disease typified by short stature, immunodeficiency and a predisposition for cancer (Ridanpaa*, et al.*, 2001). Further, the cancer prone diseases Diamond-Blackfan anaemia and $5q^-$ syndrome have been linked to mutations affecting *RPL5*, *RPL11*, *RPS7*, *RPS14, RPS17, RPS19, RPS24* and *RPS35A*, the first three of which encode MDM2-binding proteins (Draptchinskaia*, et al.*, 1999; Ebert*, et al.*, 2008; Gazda*, et al.*, 2008).

The oncogene Myc drives malignant transformation by upregulating Pol I transcription by binding the rDNA promoter (Arabi*, et al.*, 2005; Grandori*, et al.*, 2005). Myc also interacts with SL-1 to stabilise the PIC at rDNA repeats (Grandori*, et al.*, 2005) and enhances Pol II-mediated transcription of Pol I subunits and transcription factors, such as RRN3 and UBF (Poortinga*, et al.*, 2004; Poortinga*, et al.*, 2011), and rRNA processing proteins such as NCL, fibrillarin and NPM (Schlosser*, et al.*, 2003; van Riggelen*, et al.*, 2010; Zeller*, et al.*, 2001). In collaboration with TFIIIB, Myc also regulates Pol III-mediated transcription of the 5S rRNA (Gomez-Roman*, et al.*, 2003; Kenneth*, et al.*, 2007). Other oncogenes that drive Pol I transcription include the truncated form of Netrin-1 (Δ-Netrin-1), nucleostemin, the leukaemogenic AML1-ETO fusion protein, RSK2, CK2, CDK2–4, AMPK and PTEN (Bakshi*, et al.*, 2008; Delloye-

Bourgeois*, et al.*, 2012; Hannan*, et al.*, 2013; Romanova*, et al.*, 2009). However, inhibition of Pol I with small molecules has been shown to block malignant transformation driven by oncogenes such as myc (Bywater*, et al.*, 2012).

On the other hand, oncogenic transformation is also driven by perturbations to the normal function of tumour suppressors such as p53. Mutation of the *TP53* gene occurs in all types of cancer at a rate of 5 to 50% (Olivier*, et al.*, 2010). The inhibitory function of p53 on Pol I (and Pol III) transcription is also frequently lost in malignancy (Budde and Grummt, 1999; Deisenroth and Zhang, 2010; Stein*, et al.*, 2002; Wade*, et al.*, 2013; Zhai and Comai, 2000). In normal cells, pRB prevents UBF from binding SL-1 at the rDNA Pol I promoter (Hannan*, et al.*, 2000a; Hannan*, et al.*, 2000b) and prevents TFIIIB from biding TFIIIC2 at the Pol III promoter (Chu*, et al.*, 1997; Hannan*, et al.*, 2000b; White*, et al.*, 1996). However, the function of the G_1/S checkpoint regulator retinoblastoma-associated protein (pRB) is also frequently lost in cancer (Bartek*, et al.*, 1996; Chinnam and Goodrich, 2011). Thus, the dysregulation of Pol I transcription causes malignant transformation through the hyperactivation of ribosome biogenesis, although paradoxical evidence in zebrafish suggests that insufficiency of several r-proteins involved in ribosome biogenesis can also lead to the development of malignant tumours of the peripheral nerve sheath (Amsterdam*, et al.*, 2004).

Many anti-cancer therapeutics have been found to inhibit Pol I transcription and rRNA processing (Table 1.3). However, no drugs are highly selective for Pol I, with the exception of a new class of Pol I inhibitors that include CX-3453 and CX-5461. CX-3453 binds G-quadruplex DNA structures within the rDNA repeat genes and specifically prevents NCL-G-quadruplex complex formation (Drygin*, et al.*, 2009). Accumulation of CX-3453 in nucleoli has been shown to be accompanied by rapid relocalisation of NCL from the nucleolus to the nucleoplasm and depletion of pre-rRNA

Drug	Mechanism of action	Impact on ribosome biogenesis	Impact on nucleolus	Cancer type(s)	References
Mitomycin C	Interstrand DNA crosslinking via alkylating 5-CpG-3 guanosine	Inhibition of Pol I transcription	Nucleolar disintegration	Adenocarcinoma, stomach, pancreas, anal, bladder, breast, cervical, colorectal, head, neck, and non-small cell lung cancer	(Burger*, et al.*, 2010; Rey*, et al.*, 1993)
Cisplatin	DNA crosslinking via alkylating DNA bases	Inhibition of Pol I transcription	Nucleolar disintegration	Testicular, bladder, lung, oesophagus, stomach, and ovarian sarcoma; and lymphoma	(Burger*, et al.*, 2010; Jordan and Carmo-Fonseca, 1998)
Oxaliplatin	DNA crosslinking via alkylating DNA bases	Inhibition of Pol I transcription	Nucleolar disintegration	Oesophagus and stomach cancer; and colorectal carcinoma	(Burger*, et al.*, 2010; Kidani*, et al.*, 1980)
Mitoxantrone	Topoisomerase II inhibitor and intercalates into DNA	Inhibition of Pol I transcription	Nucleolar disintegration	Breast, prostate, and liver cancer; myeloid leukaemia and non-Hodgkin's lymphoma	(Alberts*, et al.*, 1980; Burger*, et al.*, 2010)
Doxorubicin	Intercalates into DNA and inhibits Topoisomerase II	Inhibition of Pol I transcription	Nucleolar disintegration	Bladder, breast, stomach, lung, ovarian, and thyroid cancer; leukaemia, Hodgkin's lymphoma, and myeloma	(Burger*, et al.*, 2010)
Camptothecin (Topotecan and Irinotecan)	Inhibits Topoisomerase I	Modulates early rRNA processing	Nucleolar disintegration	Ovarian, lung, colon, and cervical cancer	(Burger*, et al.*, 2010; Gallo*, et al.*, 1971)
Temsirolimus Everolimus	mTOR inhibitors	Inhibition of Pol I transcription	No effect	Renal cell carcinoma, progressive neuroendocrine tumours of pancreatic origin, subependymal giant cell astrocytoma associated with tuberous sclerosis, and hormone receptor-positive, HER2-negative breast cancer	(Mahajan, 1994)

Table 1.3. Anti-cancer drugs with effects on the nucleolus

Reprinted with permission from (Hein*, et al.*, 2013).

Drug	Mechanism of action	Impact on ribosome biogenesis	Impact on nucleolus	Cancer type(s)	References
5-Fluorouracil	Thymidylate synthase, incorporates into 47S pre-rRNA	Impairs late rRNA processing	No effect	Colon, oesophageal, gastric, rectum, breast, biliary tract, stomach, head and neck, cervical, pancreas, renal cell, and carcinoid cancer	(Burger, *et al.*, 2010; Ghoshal and Jacob, 1997)
Homoharringtonine	Translation inhibitor, prevents elongation	Impairs late rRNA processing	No effect	Chronic myelogenous leukaemia	(Burger, *et al.*, 2010; Hsu, 1980; Sun, *et al.*, 2007)
Actinomycin D	Intercalates into GC-rich duplex DNA	Inhibits Pol I transcription at low nanomolar concentrations	Nucleolar disintegration	Wilms tumour and Ewing sarcoma	(Burger, *et al.*, 2010; Fetherston, *et al.*, 1984)
CX-3543	Disrupts NCL:rDNA G-quadruplex complexes	Selective inhibition of Pol I transcription (elongation)	Redistribution of NCL, no effect on fibrillarin	Phase I clinical trial Carcinoid and neuroendocrine tumours	(Drygin, *et al.*, 2009)
CX-5461	Inhibits SL-1 preinitiation complex formation at the rDNA promoter	Selective inhibition of Pol I transcription (initiation)	Nucleolar disintegration	Phase I clinical trial acute myeloid leukaemia, multiple myeloma and lymphoma	(Bywater, *et al.*, 2012; Drygin, *et al.*, 2011)
Ellipticine	Impairs SL-1 rDNA promoter binding and preinitiation complex assembly	Pol I transcription (initiation)	Not determined	Phase I and II clinical trial	(Andrews, *et al.*, 2013; Mathe, *et al.*, 1970)

Table 1.3. Anti-cancer drugs with effects on the nucleolus

Reprinted with permission from (Hein, *et al.*, 2013).

in malignant alveolar basal epithelial (A549) cells (Drygin*, et al.*, 2009). Inhibiting Pol I transcription due to the intercalation of CX-3453 into GC-rich rDNA caused apoptosis *in vitro* and delayed growth of breast carcinoma (MDA-MB-231) and pancreatic carcinoma (MIA Paca-2) xenografts *in vivo* (Drygin*, et al.*, 2009). A Phase I trial has demonstrated that CX-3453 was well tolerated and displayed clinical benefit to human patients with neuroendocrine tumours (Drygin*, et al.*, 2010).

In contrast, CX-5461 inhibits Pol I-mediated pre-rRNA synthesis by competing with the transcription factor SL-1 for binding to the rDNA promoter (Drygin*, et al.*, 2011). CX-5461 has 300 to 400 fold higher selectivity for Pol I than Pol II or Pol III and exhibited an anti-proliferative effect on a wide range of cancer cell lines that varied from an IC_{50} of ~3 nM to ~4,000 nM, suggesting that cancer cells are differentially sensitive to inhibition of ribosome biogenesis (Drygin*, et al.*, 2011). CX-5461 induces autophagy but not apoptosis in melanoma (A375) and pancreatic carcinoma (MIA Paca-2) cells *in vitro* and delays growth of A375 and MIA Paca-2 xenografts *in vivo* (Drygin*, et al.*, 2011). In contrast, Pol I inhibition with CX-5461 did induce apoptosis in a p53-dependent manner in Myc overexpressing murine lymphoma cells *in vitro* (Bywater*, et al.*, 2012). In Myc overexpressing murine lymphoma cells, exposure to CX-5461 caused the stabilisation of p53, transactivation of p53 target genes (p21 and Puma), inhibition of 47S pre-rRNA synthesis, and cleavage of caspase-3. Nucleoli were also found to have perturbed staining for fibrillarin, NCL and NPM, while the r-proteins RPL5 and RPL11 were found to associate with MDM2 after exposure to CX-5461 (Bywater*, et al.*, 2012). *In vivo*, CX-5461 was shown to prolong survival of a murine model of B cell lymphoma (Bywater*, et al.*, 2012). Thus, inhibition of ribosome biogenesis has been shown to have highly variable effects on the survival of malignant

cells *in vitro*, promoting both p53-independent cell death via an autophagic pathway and p53-dependent cell death via apoptosis.

1.7. Targeting the nucleolus with radiolabelled F3 peptide

1.7.1. Radiotoxicity of radiolabelled F3 peptides

In 2002, phage-display experiments that screened for peptides that homed to human leukaemia (HL-60) and breast carcinoma (MDA-MB-435) xenografts in mice, yielded a cDNA fragment that encoded a 31 amino acid fragment of human high mobility group nucleosome binding domain 2 (HMGN2) that binds to NCL (Porkka*, et al.*, 2002). Although it is the most abundant nucleolar phosphoprotein, NCL has also been shown to shuttle to the cell membrane of a wide range of cell lines (Table 1.4).

F3 peptide has been modified to deliver a wide range of cargos to non-malignant cells and malignant cells *in vitro* and *in vivo* (Table 1.5). In 2009, Drecoll *et al*. (2009) radiolabelled a dimeric form of F3, DTPA-$[F3]_2$, with the alpha particle-emitter ^{213}Bi (half-life of 45.6 min). In soft agar clonogenic experiments, exposure of EMT-6, MDA-MB-435, MIAPACA, OVCAR-3 and CMT-93 cells for 12 h to a range of concentrations of ^{213}Bi-DTPA-$[F3]_2$ (11.2 MBq/μg) was found to be effective at reducing colony forming potential and significantly increased the number of trypan blue-positive dead cells compared to control conditions (Drecoll*, et al.*, 2009). Conversely, non-radiolabelled DTPA-$[F3]_2$ was not found to reduce colony forming potential or cause cell death.

In tumour prevention studies, 1.85 MBq of ^{213}Bi-DTPA-$[F3]_2$ was i.p. injected on days 4, 6, 8, 10, 12 and 14 into SCID mice that were previously inoculated i.p. on day 0

Cell membrane NCL-positive cell lines	Cell type/tissue of origin	References
BHK	Hamster kidney cells	(Inder, *et al.*, 2009)
CVEC, HMEC, HUVEC	Proliferating endothelial cells	(Aldi, *et al.*, 2009; Ding, *et al.*, 2012; Hovanessian, *et al.*, 2010; Huang, *et al.*, 2006)
THP-1	Monocytes and macrophages	(Hirano, *et al.*, 2005)
MV4-11	Myeloid leukaemia cells	(Soundararajan, *et al.*, 2009)
MDA-MB-231, MDA-MB-231/H2N	Breast carcinoma cells	(Christian, *et al.*, 2003; Cornelissen, *et al.*, 2012b; Hovanessian, *et al.*, 2010; Tajrishi, *et al.*, 2011)
HeLa	Cervical carcinoma cells	(Chen, *et al.*, 2008; Hovanessian, *et al.*, 2010)
Caco-2	Colon carcinoma cells	(Dean and Kenny, 2011)
MKN-1	Gastric carcinoma cells	(Fujiki, *et al.*, 2014)
A431	Squamous cell carcinoma cells	(Aldi, *et al.*, 2009)
MDA-MB-435	Melanoma	(Christian, *et al.*, 2003; Hovanessian, *et al.*, 2010)
16HBEo	Human bronchial epithelial cells	(Chen, *et al.*, 2008)

Table 1.4. Cell membrane NCL-positive cell lines identified in pre-clinical studies

Construct	Malignant cell line(s) targeted	*In vitro* studies	*In vivo* studies	Reference
Fluorophore- or phage-labelled F3	HL-60, MDA-MB-435	Cell internalisation	Tumour homing	(Porkka*, et al.*, 2002)
F3-decorated siRNA-functionalised quantum dots	HeLa	RNA silencing, internalisation		(Derfus*, et al.*, 2007)
Oligonucleotide-labelled F3	HUVEC, EOMA, MDA-MB-435	Nuclear localisation	Tumour vasculature targeting, tumour vasculature growth inhibition	(Henke*, et al.*, 2008)
F3-decorated nanoparticles encapsulating photoferin	MDA-MB-435, 9L	Cell binding, photodynamic-dependent cytotoxicity	T2-weighted MRI imaging, photodynamic therapy	(Reddy*, et al.*, 2006)
F3-decorated nanoparticles encapsulating paclitaxel	C6	Cell internalisation, spheroid penetration	Near-infrared imaging, biodistribution, survival studies	(Hu*, et al.*, 2013)
F3-decorated nanoparticles encapsulating cisplatin	MTEC, HTEC, SKOV3, A2780, ID8	Cell binding, cytotoxicity	Tumour growth inhibition, survival studies	(Winer*, et al.*, 2010)
^{125}I-labelled F3	MDA-MB-435	Cell internalisation	SPECT imaging, biodistribution	(Bhojani*, et al.*, 2011)
^{225}Ac- and ^{213}Bi-labelled F3 monomer or dimer	MDA-MB-435, OVCAR-3, CMT-93, MIA-Paca	Cell internalisation, cytotoxicity	Biodistribution, survival studies, tumour prevention/reduction	(Drecoll*, et al.*, 2009; Essler*, et al.*, 2012; Vallon*, et al.*, 2012)
^{111}In-labelled F3	MDA-MB-231/H2N	Cell internalisation, cytotoxicity, γH2AX immunofluorescence	SPECT imaging, biodistribution, survival studies	(Cornelissen*, et al.*, 2012b)

Table 1.5. Modification of F3 for pre-clinical anti-cancer studies

with 10^7 MDA-MB-435-luc cells expressing firefly luciferase (a bioluminescent reporter system). Control mice were injected with 1.85 MBq of ^{213}Bi-DTPA or 100 µL of PBS. Optical imaging revealed that tumour growth was inhibited in SCID mice treated with ^{213}Bi-DTPA-$[F3]_2$. The mean survival time of SCID mice treated with ^{213}Bi-DTPA or PBS was 51 and 53 days, respectively, while mice treated with ^{213}Bi-DTPA-$[F3]_2$ survived for an average of 93.5 days ($P < 0.001$) (Drecoll*, et al.*, 2009). In tumour reduction studies, 1.85 MBq of ^{213}Bi-DTPA-$[F3]_2$, ^{213}Bi-DTPA or PBS were i.p. injected on days 16, 18, 20, 22, 24 and 26 into SCID mice bearing large intraperitoneal tumours. The mean survival time of SCID mice treated with ^{213}Bi-DTPA or PBS was 57 and 48, respectively, while SCID mice treated with ^{213}Bi-DTPA-$[F3]_2$ survived for an average of 78 days ($P = 0.04$) (Drecoll*, et al.*, 2009). Thus, ^{213}Bi-DTPA-$[F3]_2$ was shown to reduce colony forming potential *in vitro* and extend the survival of MDA-MB-435-luc xenograft-bearing SCID mice *in vivo*.

In comparison, Vallon *et al.* (2012) demonstrated that the efficacy of a monomeric form of up to 740 kBq/mL of ^{213}Bi-labelled F3 (^{213}Bi-DTPA-F3; 25 MBq/nmol) on the survival of OVCAR-3 cells was enhanced when administered in combination with paclitaxel (60 ng/mL), producing a greater therapeutic effect *in vitro* than ^{213}Bi-DTPA-F3 alone (Vallon*, et al.*, 2012). The effect of ^{213}Bi-DTPA-F3 on the survival of OVCAR-3 cells was dose-dependent and was enhanced by paclitaxel, except at the highest concentration of 740 kBq/mL of ^{213}Bi-DTPA-F3. Flow cytometry revealed that the caspase-3 inhibitor Z-VAD-FMK inhibited the induction of apoptosis in OVCAR-3 cells exposed to ^{213}Bi-DTPA-F3, paclitaxel or ^{213}Bi-DTPA-F3 + paclitaxel, suggesting that ^{213}Bi-DTPA-F3 induces apoptosis. The induction of apoptosis over 48 h by ^{213}Bi-DTPA-F3, paclitaxel or ^{213}Bi-DTPA-F3 + paclitaxel was also confirmed by probing OVCAR-3 cell lysate for the presence of cleaved caspase-3 using Western blotting.

Further, flow cytometry revealed that OVCAR-3 cells arrested in G_2/M phase after 24 h exposure to ^{213}Bi-DTPA-F3 (Vallon*, et al.*, 2012).

The *in vitro* toxicity of ^{213}Bi-DTPA-F3 and paclitaxel translated into inhibition of tumour growth *in vivo.* Inhibition of tumour growth by ^{213}Bi-DTPA-F3 + paclitaxel significantly increased the survival (121 days) of the SCID mice bearing OVCAR-3-luc xenografts compared to the other treatment groups (PBS, P = 0.00051; ^{213}Bi-DTPA-F3, P = 0.002; paclitaxel, P = 0.00055). In comparison, paclitaxel did not significantly increase the survival of SCID mice (40 days) compared to PBS (P = 0.34), although ^{213}Bi-DTPA-F3 did significantly increase survival (84 days) compared to PBS (P = 0.000074) and paclitaxel (P = 0.000083) (Vallon*, et al.*, 2012).

To compare the short half-life (45.6 min) of ^{213}Bi-DTPA-F3 with an alpha emitter with a longer half-life, Essler *et al*. (2012) also radiolabelled F3 with ^{225}Ac, which has a half-life of 10 days. In clonogenic assays, the ability of ^{225}Ac-labelled F3 (^{225}Ac-DOTA-F3; 0.07 MBq/nmol) to reduce colony forming potential of murine breast carcinoma (EMT6) cells was compared with ^{213}Bi-DTPA-F3 (28.04 MBq/nmol). The IC_{50} values for ^{225}Ac-DOTA-F3 and ^{213}Bi-DTPA-F3 as tested on EMT6 cells were 67 Bq/mL and 53 kBq/mL, respectively (Essler*, et al.*, 2012). Essler *et al*. (2012) suggested that ^{225}Ac-DOTA-F3 was approximately 1000 fold more radiotoxic than ^{213}Bi-DTPA-F3 (Essler*, et al.*, 2012). ^{213}Bi-DTPA-F3 has also been compared to ^{225}Ac-DOTA-F3 *in vivo* using SCID mice bearing i.p. MDA-MB-435-luc xenografts. Interestingly, the median survival of the ^{225}Ac-DOTA-F3 and ^{213}Bi-DTPA-F3 treatment groups was 95 and 97 days, respectively; there was no significant difference in survival of SCID mice between these two groups, despite the 1000 fold difference in the dose of radioactivity (6 x i.p. injections of 1.85 kBq or 1.85 MBq, respectively) (Essler*, et al.*, 2012). However, differences in the rate of tumour growth were detected using bioluminescence

imaging. In mice treated with ^{225}Ac-DOTA-F3, the tumour mass increased until 8 to 22 days after the last treatment, and then gradually decreased. Yet in mice treated with ^{213}Bi-DTPA-F3 the tumour mass increased until 1–8 days after the last treatment, and then decreased until a minimum size was reached at 29 days after the last treatment, but then increased again until finally causing the death of the animal. Despite these discrepancies, no differences were observed during the histological analysis of tumour composition, necrotic fraction or size after treatment with ^{225}Ac-DOTA-F3 or ^{213}Bi-DTPA-F3. Thus, F3 radiolabelled with the alpha particle- emitter ^{225}Ac was found to be more radiotoxic than when radiolabelled with ^{213}Bi.

1.7.2. Internalisation and biodistribution of radiolabelled F3 peptides

The cellular internalisation of ^{213}Bi-DTPA-F3 by OVCAR-3 cells was studied in Vallon *et al*. (2012). Approximately 10% of 37 kBq/ml of ^{213}Bi-DTPA-F3 (25 MBq/nmol) was found to become bound/internalised by OVCAR-3 cells after a 1 h exposure *in vitro*, while less than 1% of ^{213}Bi-DTPA became bound/internalised over the same time interval. Exposure of OVCAR-3 cells to the endocytosis inhibitor phenylarsine oxide significantly reduced the percentage of bound/internalised ^{213}Bi-DTPA-F3 from 10% to 4%, but did not significantly reduce the percentage of bound/internalised ^{213}Bi-DTPA (<1%). This suggested that approximately 6% of ^{213}Bi-DTPA-F3 had been internalised by OVCAR-3 cells *in vitro* (Vallon*, et al.*, 2012). Thus, Vallon *et al*. (2012) showed that ^{213}Bi-DTPA-F3 internalises into OVCAR-3 cells at favourable levels in comparison to ^{213}Bi-DTPA which lacked F3.

The internalisation of ^{213}Bi-DTPA-$[F3]_2$ has also been investigated in Drecoll *et al*. (2009). ^{213}Bi-DTPA-$[F3]_2$ was found to accumulate in MDA-MB-435 cells *in vitro*, with

the peak concentration of radioactivity being observed in the nuclei of MDA-MB-435 cells as early as 5 min (Drecoll*, et al.*, 2009). In repeat experiments, MDA-MB-435 cells were exposed for 30 min to 40 ng/mL of ^{213}Bi-DTPA-[F3]$_2$ in the presence or absence of 400 ng/mL of DTPA-[F3]$_2$ (10 fold excess) not radiolabelled with ^{213}Bi. Excess unlabelled DTPA-[F3]$_2$ reduced the amount of radioactivity associated with MDA-MB-435 cells that were simultaneously exposed to ^{213}Bi-DTPA-[F3]$_2$. This demonstrated consistency in the binding specificity between ^{213}Bi-DTPA-[F3]$_2$ and DTPA-[F3]$_2$ (Drecoll*, et al.*, 2009). However, if the intention was to demonstrate the specificity of binding of ^{213}Bi-DTPA-[F3]$_2$ to NCL, then a NCL-specific blocking agent that is dissimilar to DTPA-[F3]$_2$ (i.e. an anti-NCL antibody) should have been used.

In SCID mice, i.p injected ^{213}Bi-DTPA-[F3]$_2$ was found to accumulate at high levels in i.p MDA-MB-435 xenografts *in vivo* (32% injected dose per gram (ID/g)); the tumour-to-blood and tumour-to-intestine ratios were also relatively high at 17.6:1 and 10.4:1, respectively. The highest amount of radioactivity was observed in the kidney, although a high serum creatinine level (indicative of renal damage) was not observed (Drecoll*, et al.*, 2009). Thus, ^{213}Bi-labelled F3 was shown to accumulate at high levels in MDA-MB-435 cells *in vitro* and MDA-MB-435 xenografts *in vivo.* Interestingly, Drecoll *et al*. (2009) were also able to visualise i.p. MDA-MB-435 xenografts by positron emission tomography (PET) imaging by i.p. injecting 7.4 MBq of dimeric ^{68}Ga-labelled F3 (^{68}Ga-DOTA-[F3]$_2$).

Bhojani *et al*. (2011) developed AlexaFluor-532- and AlexaFluor-647-labelled F3 (AF532-F3Cys and AF647-F3Cys) for optical imaging of MDA-MB-435 cells *in vitro* and MDA-MB-435 xenografts *in vivo*. Exposure of MDA-MB-435 cells to 2 μg/mL of AF532-F3Cys showed localisation of AF532-F3Cys on the cell surface, cytoplasm and the nucleus of cells grown in serum-containing medium, while AF532-F3Cys was

predominantly nuclear in serum starved cells. In MDA-MB-435 xenograft- and lung carcinoma (A549) xenograft-bearing athymic mice, tumour uptake of AF647-F3Cys was observed at 2 h post i.v. injection (Bhojani*, et al.*, 2011).

In addition, ^{125}I-labelled F3 (^{125}I-IBMF3) was radiosynthesised for cellular uptake and SPECT imaging studies. The cellular uptake of ^{125}I-IBMF3 was measured by calculating the fold-difference in the radioactivity associated with MDA-MB-435 cells exposed to ^{125}I-IBMF3 for 4 h compared to cells exposed to ^{125}I-IBMF3 in media that was immediately removed after the addition of the radiopeptide (Bhojani*, et al.*, 2011). A 7 fold increase over baseline radioactivity was observed after 4 h, indicating ^{125}I-IBMF3 uptake over time. However, this result cannot readily be compared with the uptake of ^{213}Bi-DTPA-F3 or ^{213}Bi-DTPA-$[F3]_2$ *in vitro,* because uptake of ^{125}I-IBMF3 was not given as an amount of radioactivity or percentage of total radioactivity. SPECT imaging showed tumour accumulation of ^{125}I-IBMF3 (21.09–22.6 MBq in 100 µL of PBS:EtOH (95:5)) as early as 15 min post i.v. injection in MDA-MB-435 xenograft-bearing athymic mice. Biodistribution studies showed relatively low tumour accumulation at 30 min (1.05% ID/g) and the tumour-to-muscle ratio was 4.3 and tumour-to-blood ratio was 2.1 at 60 min. The highest amount of uptake was observed in the kidney, consistent with the renal uptake that was observed for AF647-F3Cys (Bhojani*, et al.*, 2011) and for ^{213}Bi-DTPA-$[F3]_2$ (Drecoll*, et al.*, 2009). Thus, fluorophore-labelled F3 was found to accumulate in MDA-MB-435 cells *in vitro* and MDA-MB-435 xenografts *in vivo*, while radioiodinated F3 was found to accumulate over time in MDA-MB-435 cells *in vitro* and at low levels in MDA-MB-435 xenografts *in vivo* (1.05% ID/g).

1.7.3. ^{111}In-labelled F3 as a tool for targeting the nucleolus

Recently, Cornelissen *et al.* (2012) fluorophore-labelled F3 and radiolabelled F3 with the Auger electron-emitter ^{111}In, forming FITC-F3 and ^{111}In-BnDTPA-F3, respectively. 34% of internalised FITC-F3 translocated to the nucleus of breast carcinoma (MDA-MB-231/H2N) cells *in vitro* (Cornelissen*, et al.*, 2012b). Within the nucleus, a proportion of FITC-F3 was shown to colocalise with NCL, the most abundant protein present in the nucleolus (Cornelissen*, et al.*, 2012b). Internalisation experiments in which MDA-MB-231/H2N cells were exposed to ^{111}In-BnDTPA-F3 for 2 h showed that internalisation was low *in vitro* (0.51±0.03% of 1 μM of ^{111}In-BnDTPA-F3 (6 MBq/μg) over 2 h) (Cornelissen*, et al.*, 2012b). When 100 fold molar excess of cold, non-radiolabelled F3 or anti-NCL antibody (ZN004) was used to saturate binding to NCL the internalisation of ^{111}In-BnDTPA-F3 was significantly reduced ($P < 0.001$). Of the internalised fraction of ^{111}In-BnDTPA-F3, 37% was found to translocate to the nucleus after 30 min (0.15±0.05%) (Cornelissen*, et al.*, 2012b).

Unlike ^{68}Ga-DOTA-[F3]$_2$, however, ^{111}In-DTPA-F3 was deemed unsuitable as an imaging agent for the detection of tumours *in vivo*. SPECT imaging of MDA-MB-231/H2N tumour xenografts 3 h after i.v. injection of athymic mice with ^{111}In-DTPA-F3 (3 μg; 6 MBq/μg) showed that tumour uptake (0.80±0.28% ID/g) and the tumour-to-muscle ratio (1.1) was low (Cornelissen*, et al.*, 2012b). This result was similar to the low uptake of i.v. injected ^{125}I-IBMF3 in MDA-MB-435 xenografts *in vivo* (1.05% ID/g) reported in Bhojani *et al*. (2011), but contradictory to the high uptake (32% ID/g), tumour-to-blood ratio (17.6:1) and tumour-to-intestine ratio (10.4:1) that was reported for i.p. injected ^{213}Bi-DTPA-[F3]$_2$ in Drecoll *et al*. (2009). These differences may have been due to the i.p. versus i.v. injection. Although it also should be noted that

differences in monomeric or dimeric form, the type of radionuclide, chelator, and cell line may affect the level of uptake of radiolabelled F3. Interestingly, Vallon *et al.* (2012) found that 6% of monomeric ^{213}Bi-DTPA-F3 had internalised into OVCAR-3 cells after 1 h *in vitro*, which is in contrast to the <1% of ^{111}In-BnDTPA-F3 that was found to internalise into MDA-MB-231/H2N cells *in vitro* (Cornelissen*, et al.*, 2012b; Vallon*, et al.*, 2012).

The internalisation assays that were carried out in Vallon *et al*. (2012) and Cornelissen *et al*. (2012) were different in that $1x10^7$ cells suspended in 1 mL of media in tubes were exposed to ^{213}Bi-DTPA-F3, but $2x10^5$ cells attached to the surface of 24-well plates were exposed to ^{111}In-BnDTPA-F3 in 200 µL of media. Thus, performing the internalisation assay with cells in suspension might have resulted in higher levels of uptake compared to cells attached to a substrate, since suspension cells could be expected to have a greater surface area of cell membrane, and therefore a higher number of receptors with which a construct can bind.

Despite low internalisation and tumour accumulation of ^{111}In-BnDTPA-F3 in MDA-MB-231/H2N cells *in vitro* and MDA-MB-231/H2N xenografts *in vivo*, incubation of MDA-MB-231/H2N cells with up to 5 µM of ^{111}In-BnDTPA-F3 (20.6 MBq/nmol) for 2 or 24 h has been shown to induce γH2AX foci in a dose-dependent manner and also in a manner that is linearly dependent on specific activity *in vitro* (Spearman R = 0.99; P = 0.0028) (Cornelissen*, et al.*, 2012b). The number of γH2AX foci after exposure of MDA-MB-231/H2N cells for 2 h to concentrations of ^{111}In-BnDTPA-F3 (20.6 MBq/nmol) of over 0.2 to 5 µM was not significantly different from exposure to external γ-rays (4 Gy) (P > 0.05).

Exposure of MDA-MB-231/H2N cells for 24 h to increasing concentrations (up to 3 µM) of ^{111}In-BnDTPA-F3 with a specific activity of 6 MBq/µg reduced clonogenic survival

down to 10% *in vitro* ($P < 0.001$), while exposure to non-radiolabelled F3 peptide did not significantly reduce survival (Cornelissen*, et al.*, 2012b). Similarly, exposure of MDA-MB-231/H2N cells for 24 h to increasing specific activities (0 to 9 MBq/μg) of a 2 μM concentration of ^{111}In-BnDTPA-F3 resulted in a 4.6 fold decrease in survival (from 75% to 16%), whereas equivalent amounts of ^{111}In chloride only resulted in a 2 fold decrease.

In athymic mice bearing MDA-MB-231/H2N xenografts, i.v. injection of ^{111}In-BnDTPA-F3 (3 μg; 6 MBq/μg) significantly inhibited tumour growth compared to mice treated with non-radiolabelled F3 or PBS (growth rate of 4.3×10^{-3}, 8.0×10^{-2} and 8.2×10^{-2} mm^3/day, respectively; $P = 0.0031$). Inhibition of tumour growth produced a significant increase in survival only in animals treated with ^{111}In-BnDTPA-F3 ($P = 0.0073$).

In summary, these data suggested that ^{111}In-BnDTPA-F3 was internalised into MDA-MB-231/H2N cells at modest levels via cell membrane NCL, translocated to the nucleus where it colocalised with NCL in the nucleolus, produced dose-dependent and specific activity-dependent induction of DNA double-strand breaks, and significant reduction in clonogenic survival *in vitro*. Further, ^{111}In-BnDTPA-F3 i.v. injected into mice was taken up by MDA-MB-231/H2N tumour xenografts at modest levels, but produced significant growth delay of tumour xenografts and significantly increased survival of MDA-MB-231/H2N xenograft-bearing mice. Given that FITC-F3 was found to colocalise with NCL in the nucleolus, these results led to the hypothesis that the nucleolus is relatively radiosensitive to short range (nm-μm) Auger electrons and that the irradiation of the nucleolus by ^{111}In-BnDTPA-F3 may have been, at least in part, responsible for the reduction in clonogenic survival of MDA-MB-231/H2N cells *in vitro* and the growth delay of MDA-MB-231/H2N xenografts *in vivo*.

An average of 14.7 Auger electrons are emitted by each atom of ^{111}In and deposit a very high dose of up to 5,000 Gy over 10 nm (Kassis, 2004; Kassis, 2011). Therefore, translocation of modest levels of ^{111}In-labelled F3 to the nucleolus may deposit high levels of energy in rDNA, rRNA and other nucleolar components. F3 peptide has been shown to bind to NCL, which represents 10% of the nucleolar proteome and possesses DNA/RNA helicase and DNA-dependent ATPase activities that are essential for Pol I transcription (Christian*, et al.*, 2003; Cornelissen*, et al.*, 2012b; Rickards*, et al.*, 2007; Tuteja*, et al.*, 1995; Tuteja*, et al.*, 1991). ^{111}In-labelled F3 peptide may also damage the NCL phosphoprotein, thereby inhibiting its multiple functions. Functions of NCL include 1) binding to the histone H1 to modulate chromatin condensation by unwinding DNA in the 5' to 3' direction, potentiating rDNA transcription in a growth factor-dependent manner in highly proliferating cells (Bouvet*, et al.*, 1998; Egyhazi*, et al.*, 1988; Erard*, et al.*, 1988; Escande-Geraud*, et al.*, 1985); 2) pre-rRNA processing through the recruitment of the U3 snoRNP (Ginisty*, et al.*, 1998); 3) phosphorylation- and calcium-dependent nuclear-cytoplasmic-membrane shuttling and ligand internalisation (Borer*, et al.*, 1989; Hovanessian*, et al.*, 2010; Schmidt-Zachmann and Nigg, 1993); 4) p53-dependent relocalisation from the nucleolus to the nucleoplasm in response to cellular stress caused by IR- and camptothecin-induced DNA damage (Daniely*, et al.*, 2002); and 5) repression of p53 translation and regulation of p53 stabilisation (Bhatt*, et al.*, 2012; Chen*, et al.*, 2012).

1.8. Aims

The main aim of this thesis was to investigate whether the nucleolus is a radiosensitive target for Auger electron radionuclide therapy. It was hypothesised that F3 peptide

was capable of delivering ^{111}In to the nucleolus, due to its interaction with NCL, and that once placed in the nucleolus the low-energy, short-range Auger electrons emitted by ^{111}In might cause damage to nucleolar components. Damage caused to nucleolar components might interfere with ribosome biogenesis and/or trigger the nucleolar stress response, thereby triggering cell death. To investigate whether F3 has effects on nucleolar structure, fluorescence imaging of nucleolar components was performed using cells exposed to F3. To investigate a link between cell death and the placement of ^{111}In in the nucleolus, clonogenic survival assays and internalisation experiments were carried out in conjunction to demonstrate that the uptake of radioactivity in the nucleolus was associated with the induction of cell death when exposing cells to ^{111}In-labelled F3 (^{111}In-DTPA-F3). To analyse whether ^{111}In-DTPA-F3 has the property of concentrating absorbed radiation dose in the nucleolus, the mean absorbed radiation dose deposited in subcellular compartments was modelled using a range of different cell lines and this parameter was also correlated with the level of cell death. The volume of the nucleolus and the number of γH2AX foci was also quantified so that correlations between nucleolar volume and the number of DNA double-strand breaks induced by ^{111}In-DTPA-F3 could be analysed.

Chapter 2. Materials and Methods

2.1. Materials

2.1.1. Cell culture

HCT116 (colon carcinoma), H322 (non-small cell lung cancer), MDA-MB-231/H2N (parental MDA-MB-231 breast carcinoma cells stably transfected to overexpress HER2), MDA-MB-435 (melanoma), U2OS (osteosarcoma), and MCF7 (breast carcinoma) cell lines were cultured in Dulbecco's modified Eagle's medium (DMEM; Sigma) supplemented with 1000 mg/L of glucose, L-glutamine and $NaHCO_3$; pyridoxine.HCl; 10% fetal bovine serum; and 100 units of penicillin and 0.1 mg of streptomycin per mL (Sigma). MDA-MB-231 breast carcinoma cells stably transfected with the HER2 gene (MDA-MB-231/H2N) were a gift from Dr R Kerbel (Sunnybrook Health Sciences Centre, Toronto, ON). MDA-MB-435 and MCF7 cells were a gift from Dr Bart Cornelissen, U2OS cells were a gift from Dr Mark Jackson, and HCT116 cells were a gift from Dr Abul Azad. H322 cells were acquired from ATCC. Cells were authenticated by the supplier and used for a maximum of 20 weeks after recovery from liquid nitrogen storage. Mycoplasma testing was carried out every three months.

2.1.2. Antibodies

2.1.2.1. Immunocytochemistry

Primary antibodies: Anti-NCL (1:1000; mouse; ab13541; Abcam), anti-Ki-67 (1:1000; rabbit; AB9260; Millipore), anti-NPM (1:1000; mouse; ab10530; Abcam) and anti-γH2AX antibody (1:1000; mouse; JBW301; Millipore). Secondary antibodies: AlexaFluor488-conjugated anti-mouse (1:250; goat; A11029; Life Technologies) and AlexaFluor555-conjugated anti-rabbit (1:250; goat; A11001; Life Technologies).

2.1.2.2. Western blotting

Primary antibodies: Anti-beta-actin (1:1000; rabbit IgG1; ab8227; Abcam), anti-fibrillarin (1:1000; rabbit IgG; ab5821; Abcam), anti-H2AX (1:1000; rabbit IgG; ab11175; Abcam). Secondary antibodies: Horse radish peroxidise (HRP)-conjugated anti-mouse (1:5000; goat IgG; 616520; Invitrogen) and HRP-conjugated anti-rabbit (1:5000; goat IgG; 656120; Invitrogen).

2.2. Methods

2.2.3. Fluorescence imaging of nucleolar components

$2.5x10^4$ HCT116, H322, MDA-MB-231/H2N, MDA-MB-435, U2OS or MCF7 cells were seeded in culture medium (400 µL) in 8-well glass chamber slides (Lab-Tek, Yeovil, Somerset, UK) and incubated at 37^0C/5% CO_2 overnight. Cells were left unexposed or were exposed to F3, IR, or F3 + IR. To achieve this, culture medium was aspirated

and fresh medium (200 µL) either containing or not containing F3 was added. After incubation at 37^0C/5% CO_2 for 3 h, cells were irradiated with a 10 Gy dose of γ-radiation using a ^{137}Cs irradiator or were removed from the incubator but left unirradiated. Cells were replaced in the incubator at 37^0C/5% CO_2 for a further 15 min, and were then washed (PBS), fixed (4% paraformaldehyde in PBS for 10 min at room temperature), permeabilised (1% triton-X in PBS for 15 min at room temperature) and blocked (2% bovine serum albumin (BSA) in 0.1% triton-X in PBS for 1 h at 37^0C). Cells were stained for NCL, NPM or Ki-67 using antibodies at 1:1000 dilution in 2% BSA in 0.1% triton-X in PBS for 1 h at 37^0C. Cells were washed (PBS) and exposed to fluorophore-conjugated secondary antibody (1:250) in 2% BSA in 0.1% triton-X in PBS for 30 min at room temperature. Cells were washed (PBS) again and DNA was stained with Hoechst-33342 (1 µg/mL in PBS) for 10 min at room temperature. Samples were mounted using Mowiol-488 (Sigma). Fluorescence images were acquired using a LSM-710 confocal microscope (Zeiss, Cambridge, UK).

ImageJ software was used to quantify the relative nucleolus intensity of protein components (NCL, NPM or Ki-67) for populations of cells that were either unexposed or exposed to F3, IR, or F3 + IR. A region of interest (ROI) was drawn around a given nucleolus visualised from a single unexposed cell, and the total intensity of the protein component and the area of that particular nucleolus was measured. This was repeated for every nucleolus that was visualised from single cell to give the sum total nucleolus intensity and sum nucleolus area of a single cell. Sum total nucleolus intensity was divided by sum nucleolus area to give the mean nucleolus intensity of a single cell, and this process was repeated for up to 50 cells to give the mean nucleolus intensity of a population of unexposed cells, i.e. the mean baseline nucleolus intensity. To calculate the relative nucleolus intensity of a single cell, the mean nucleolus intensity

of a single cell was divided by the mean baseline nucleolus intensity. The relative nucleolus intensity of the population of unexposed cells was calculated by taking the mean of the values of the relative nucleolus intensity for up to 50 cells. For the population of unexposed cells this gave a relative nucleolus intensity of 1 (± SEM). This entire procedure was repeated, using the baselines nucleus intensity, to give the relative nucleolus intensity of populations of cells that were exposed to F3, IR or F3 + IR.

The relative nucleus intensity was quantified in a similar manner. A ROI was drawn around the nucleus visualised from a single unexposed cell, and total nuclear intensity and nucleus area was measured. Total nucleus intensity was divided by nucleus area to give the mean nucleus intensity of a single cell, and this process was repeated for up to 50 cells to give the mean nucleus intensity of a population of unexposed cells, i.e. the mean baseline nucleus intensity. To calculate the relative nucleus intensity of a single cell, the mean nucleus intensity of a single cell was divided by the mean baseline nucleus intensity. The relative nucleus intensity of the population of unexposed cells was calculated by taking the mean of the values of the relative nucleus intensity for up to 50 cells. For the population of unexposed cells this gave a relative nucleus intensity of 1 (± SEM). This entire procedure was repeated, using the baselines nucleus intensity, to give the relative nucleus intensity of populations of cells that were exposed to F3, IR or F3 + IR.

The relative nucleoplasm intensity of was also quantified. Using single unexposed cells, the sum total nucleolus intensity was subtracted from the total nuclear intensity, and the sum nucleolar area was subtracted from the nuclear area, giving the total nucleoplasm intensity and nucleoplasm area, respectively. The total nucleoplasm intensity was then divided by the nucleoplasm area to give the mean nucleoplasm

intensity of a single cell, and this process was repeated for up to 50 cells to give the mean nucleoplasm intensity of a population of unexposed cells, i.e. the mean baseline nucleoplasm intensity. To calculate the relative nucleoplasm intensity of a single cell, the mean nucleoplasm intensity of a single cell was divided by the mean baseline nucleoplasm intensity. The relative nucleoplasm intensity of the population of unexposed cells was calculated by taking the mean of the values of the relative nucleus intensity for up to 50 cells. For the population of unexposed cells this gave a relative nucleoplasm intensity of 1 (± SEM). This entire procedure was repeated, using the baselines nucleoplasm intensity, to give the relative nucleoplasm intensity of populations of cells that were exposed to F3, IR or F3 + IR.

The nucleolus-to-nucleoplasm ratio of the protein components of a single cell was quantified by dividing the mean nucleolus intensity by the mean nucleoplasm intensity. This process was repeated for up to 50 cells to give the mean nucleolus-to-nucleoplasm ratio for a population of cells that were either unexposed or exposed to F3, IR or F3 + IR. For each condition, up to 50 cells were counted from duplicate experiments.

2.2.1. Synthesis of ^{111}In-DTPA-F3

F3 peptide (KDEPQRRSARLSAKPAPPKPEPKPKKAPAKK, MW = 3432 g/mol) was obtained from Cambridge Peptides. 50 µg (14.57 nmol) of F3 peptide (in 50 µL of 0.1 M sodium bicarbonate, pH 8.5) was reacted with a 1.5 fold molar excess (7.80 µg; 21.85 nmol) of diethylenetriaminepentacetic anhydride (DTPA; MW = 357.32 g/mol; Sigma) dissolved in dry dimethyl sulfoxide (DMSO; Sigma) at room temperature for 1 h, forming DTPA-F3 (step 1). Unconjugated DTPA was removed by gel filtration (Bio-

Gel P2; Bio-Rad). DTPA-F3 was eluted in 100 µL fractions using 0.1 M sodium citrate, pH 5.0 (step 2). The DTPA conjugation rate was determined by mixing the unpurified reaction mixture from 'step 1' with 1 MBq ^{111}In chloride (in 0.02 M of H.Cl) for 1 h at room temperature. Then, gel filtration as per 'step 2' was performed to separate ^{111}In-DTPA from ^{111}In-DTPA-F3 and the amount of radioactivity in each 100 µL fraction was measured using an automated gamma counter (Perkin Elmer). To determine the rate of conjugation of DTPA to F3, the amount of radioactivity in fractions 900–1200 µL (which represented ^{111}In-DTPA-F3) was divided by the total activity in all fractions plus the column (representing ^{111}In-DTPA and unbound ^{111}In). Since F3 does not absorb UV (280 nm) it was impossible to determine the concentration of DTPA-F3 using spectrophotometric analysis. Instead, DTPA-F3 in fractions 1000–1100 µL was pooled and its concentration was determined by multiplying the total number of moles of DTPA-F3 (14.57 nmol) in the original reaction by the percentage of ^{111}In-DTPA-F3 in fractions 1000–1100 µL (calculated by dividing the amount of radioactivity in fractions 1000–1100 by the total activity in fractions 900–1200 µL). To radiolabel DTPA-F3 for use in experiments, 22.17 MBq of ^{111}In chloride (in 0.02 M of H.Cl) was added per nmol of DTPA-F3, forming ^{111}In-DTPA-F3. After incubation at room temperature for 1 h, radiolabelling efficiency was determined using instant thin layer chromatography (ITLC; Amersham Health) in 0.1 M sodium citrate, pH 5.0. ITLC strips were measured using autoradiography and were routinely >95% (Cyclone Plus, Perkin Elmer).

2.2.2. Clonogenic survival assays

5x10^3 HCT116, H322, MDA-MB-231/H2N, MDA-MB-435, U2OS, and MCF7 cells were seeded in culture medium (100 µL) in 96-well plates and incubated at 37^{0}C/5% CO_2

overnight. For clonogenic assays using ^{111}In-DTPA-F3, culture media was aspirated and fresh media (50 µL) was added which contained ^{111}In-DTPA-F3 (0.1 µM; 22.17 MBq/nmol) or an equimolar control (DTPA, F3, DTPA-F3, ^{111}In chloride, ^{111}In-DTPA or ^{111}In chloride + F3). After incubation at 37^{0}C/5% CO_2 for 3 h, cells were detached using trypsin (50 µL). MDA-MB-231/H2N, MDA-MB-435, and U2OS cells were then reseeded in T25 culture flasks (in 4 mL of fresh medium), while HCT116, H322, and MCF7 cells were reseeded in 6-well plates (in 2 mL of fresh medium). For clonogenic assays using γ-radiation, cells in 96-well plates were exposed to 0, 2, 4, 8 or 10 Gy of γ-radiation using a ^{137}Cs irradiator (~1 Gy/min). Cells were then detached using trypsin (50 µL) and reseeded in T25 culture flasks (in 4 mL of fresh media). After incubation at 37^{0}C/5% CO_2 for 12 days, colonies were stained with methylene blue (2% methylene blue in water/methanol 1:1) and counted. 2–3 replicates were performed per condition. Surviving fraction (SF) was calculated using the following equations:

$$SF = \frac{[Clonies\ counted]}{[Cells\ seeded] \times ([Plating\ efficiency]/100)}$$

$$Plating\ efficiency = \frac{[Clonies\ counted]}{[Cells\ seeded]}$$

2.2.3. γH2AX assay

2.5x10^4 HCT116, H322, MDA-MB-231/H2N, MDA-MB-435, U2OS or MCF7 cells were seeded in culture medium (400 µL) in 8-well glass chamber slides (Lab-Tek, Yeovil, Somerset, UK) and incubated at 37^{0}C/5% CO_2 overnight. Culture medium was aspirated and fresh medium (200 µL) containing ^{111}In-DTPA-F3 (1 µM; 22.17

MBq/nmol) or an equimolar control lacking F3 (^{111}In-DTPA) was added. After incubation at 37^{0}C/5% CO_2 for 3 h, cells were washed (PBS), fixed (4% paraformaldehyde in PBS for 10 min at room temperature), permeabilised (1% triton-X in PBS for 15 min at room temperature) and blocked (2% bovine serum albumin (BSA) in 0.1% triton-X in PBS for 1 h at 37^{0}C). Cells were stained for γH2AX using anti-γH2AX antibody (1:1000) in 2% BSA in 0.1% triton-X in PBS for 1 h at 37^{0}C. Cells were washed (PBS) and exposed to fluorophore-conjugated secondary antibody (1:250) in 2% BSA in 0.1% triton-X in PBS for 30 min at room temperature. Cells were washed (PBS) again and DNA was stained with Hoechst-33342 (1 μg/mL in PBS) for 10 min at room temperature. Samples were mounted using Mowiol-488 (Sigma). Fluorescence images were acquired using a LSM-710 confocal microscope (Zeiss, Cambridge, UK). The number of γH2AX foci per cell was measured by creating a mask from an 80% threshold of the γH2AX staining using ImageJ software. Then γH2AX foci below the optical resolution of the 63x objective were excluded from the analysis by selecting to analyse particles with an area greater than 0.03 μm^2. Then, the number of γH2AX foci was counted automatically by selecting find maxima. γH2AX foci were counted from up to 50 cells from duplicate experiments per condition.

2.2.4. Internalisation assay

Internalisation of ^{111}In-DTPA-F3 into membrane, cytoplasm, nucleoplasm and nucleolus was determined by adapting a previously reported nucleolar fractionation technique (Lam, 2006). Briefly, 2x T75 flasks of confluent cells were suspended in 1 mL of culture medium in a 15 mL Falcon canonical centrifuge tube (Fischer Scientific). For HCT116, H322, MDA-MB-231/H2N, MDA-MB-435, U2OS, and MCF7 cells, 2x

T75 flasks of confluent cells provided $5.60x10^7$, $6.69x10^7$, $5.98x10^7$, $2.73x10^7$, $2.41x10^7$ and $6.27x10^7$ cells per mL, respectively. ^{111}In-DTPA-F3 (1 μM; 22.17 MBq/nmol), or an equimolar control lacking F3 (^{111}In-DTPA), was then added. Cells were incubated at 37^0C/5% CO_2 with gentle mixing. After 3 h, cells were centrifuged for 5 min at 4^0C (1000 rpm; Sorvall RT-7 Plus refrigerated centrifuge) and supernatant was retained (cell free fraction). Cells were then washed (1 mL of PBS) and centrifuged for 5 min at 4^0C (1000 rpm), before the supernatant was added to the cell free fraction. Cells were then resuspended in acid wash (0.1 M glycine, pH 2.5) for 6 min on ice to remove ^{111}In-DTPA-F3 or ^{111}In-DTPA attached to the membrane. Cells were centrifuged for 5 min at 4^0C (1000 rpm) and the supernatant was retained (membrane fraction). Cells were then washed (1 mL of PBS) and centrifuged for 5 min at 4^0C (1000 rpm), before the supernatant was added to the membrane fraction. Cells were resuspended in 1 mL of buffer A (10 mM Hepes, 10 mM H.Cl, 1.5 mM $MgCl_2$, 0.5 mM dithiotreitol, pH7.9) for 6 min on ice. The swollen morphology of the cells was checked under phase contrast (LED illumination microscope, Leica). The membrane of the cells was then ruptured using a Dounce homogeniser (12 strokes with the pestle) on ice. The integrity of the intact nuclei was checked under phase contrast. Cells were then centrifuged for 5 min at 4^0C (1000 rpm) and the supernatant was retained (cytoplasmic fraction). The pellet was resuspended in 1 mL of S1 solution (0.25 M sucrose, 10 mM $MgCl_2$), and this was then layered over 1 mL of S2 solution (0.35 M sucrose, 0.5 mM $MgCl_2$). The nuclei were centrifuged for 5 min at 4^0C (2500 rpm), before the supernatant was added to the cytoplasmic fraction. The nuclei were resuspended in 1 mL of S2 solution, before being sonicated (Vibra Cell) for 4x three second bursts (with three second intervals) at 50% amplitude. The disruption of the nuclei and the presence of dense, refractory bodies (nucleoli) was checked under phase contrast.

The sonicated sample was layered over 1 mL of S3 solution (0.88 M sucrose, 0.5 mM $MgCl_2$) and centrifuged for 10 min at 4^0C (3000 rpm), before the supernatant was retained (nucleoplasm fraction). Finally, the pellet was resuspended in 1 mL of S2 solution and retained (nucleolus fraction). The radioactivity in the membrane, cytoplasm, nucleoplasm and nucleolus fractions was measured using an automated γ-counter (Wizard, Perkin Elmer). 2–3 replicates were performed per condition. The fractionation process provided well-separated membrane, cytoplasm, nucleoplasm and nucleolus fractions as validated by Western blotting. β-actin, H2AX, and fibrillarin were used as cytoplasm, nucleus, and nucleolus markers in Western blots, respectively.

2.2.5. Western blotting

Western blotting was performed using samples containing 12.5 μg of protein. The protein concentration of each sample was determined by Pierce BCA assay as per the standard protocol (Thermo Scientific). Protein samples (in NuPage LDS sample buffer containing reducing agent; Life Technologies) were denatured by incubation at 70^0C for 10 min. Denatured samples were run on 4–12% NuPage Bis-Tris gels (Life Technologies) in NuPage MSPS SDS running buffer (Life Technologies) at 200 V (3.00 A) at room temperature for 50 min. Proteins from gels were transferred onto 0.45 μm nitrocellulose membrane (Bio-Rad) in transfer buffer:methanol (20:1) at 100 V (3.00 A) at room temperature for 1 h. Nitrocellulose membranes were blocked using 5% BSA in Tris-buffered saline with Tween-20 (TBST; 50 mM Tris, 150 mM Na.Cl and 0.05% Tween-20 at pH 7.6) at 4^0C overnight. Primary antibodies were applied in 5% BSA in TBST at 4^0C overnight. After PBS washes (3x), secondary HRP-conjugated

antibodies were applied in 5% BSA in TBST at room temperature for 1 h. After further PBS washes (3x), ECL Western blotting substrate (Pierce) was applied for 60 sec to nitrocellulose at a volume of 0.125 mL per cm^2. The nitrocellulose and 18 x 24 cm X-ray film (Fujifilm) were then placed in a 24 x 30 cm X-ray film screen (Genetic Research Instruments) for 30 sec. The X-ray film was developed in the dark, using a Compact X4 Imaging System (Xograph).

2.2.6. Single cell models and radiation dose calculations

Cell and nucleus dimensions were determined from fluorescence microscopy analysis. Briefly, $2.5x10^4$ HCT116, H322, MDA-MB-231/H2N, MDA-MB-435, U2OS or MCF7 cells were seeded in culture medium (400 µL) in 8-well glass chamber slides (Lab-Tek) and incubated at 37^0C/5% CO_2 overnight. To stain the membrane, cells were washed (PBS) and exposed to 2 µg/mL of AlexaFlour-488-conjugated wheat germ agglutinin (AF488-WGA, which binds to N-acetyl-D-glucosamine and sialic acid) for 15 min at room temperature. Then, cells were washed (PBS), fixed (4% paraformaldehyde in PBS for 10 min at room temperature), permeabilised (1% triton-X in PBS for 15 min at room temperature) and blocked (2% BSA in 0.1% triton-X in PBS for 1 h at 37^0C). Cells were washed (PBS) again and DNA was stained with Hoechst-33342 (1 µg/mL in PBS) for 10 min at room temperature. Samples were mounted using Mowiol-488 (Sigma). To stain nucleoli, cells were washed (PBS), fixed (4% paraformaldehyde in PBS for 10 min at room temperature), permeabilised (1% triton-X in PBS for 15 min at room temperature) and blocked (2% BSA in 0.1% triton-X in PBS for 1 h at 37^0C). Cells were stained for NCL using anti-NCL antibody (1:1000) in 2% BSA in 0.1% triton-X in PBS for 1 h at 37^0C. Cells were washed (PBS) and

exposed to fluorophore-conjugated secondary antibody (1:250) in 2% BSA in 0.1% triton-X in PBS for 30 min at room temperature. Cells were washed (PBS) again and DNA was stained with Hoechst-33342 (1 μg/mL in PBS) for 10 min at room temperature. Samples were mounted using Mowiol-488 (Sigma). Z-stacks with 1 μm intervals were acquired using a LSM-710 confocal microscope (Zeiss). The radius of the cell was calculated from a volume obtained by adding the areas inside the AF488-WGA-stained membrane over 1 μm intervals. The radius for the nucleus and the nucleolus was calculated in a similar manner using the volume of the Hoechst-33342-stained nuclei and NCL-stained nucleoli, respectively. Volumes were measured using ImageJ software. An average volume was calculated from 10 cells.

For simulation purposes a concentric geometry was adopted (homogeneous spheres of density 1 g/cm^3). Single cell doses were calculated, assuming uniformly distributed radioactivity in the following cellular compartments: Membrane (Me; taken as hollow sphere from the radius of the cell with thickness of 8 nm), cytoplasm (Cy; taken as hollow sphere 8 nm from the radius of the cell to the radius of the nucleus), nucleoplasm (Np; taken as hollow sphere from the radius of the nucleus to the radius of the nucleolus) and nucleolus (No; taken as a sphere from the radius of the nucleolus). Cellular S-values were calculated by Dr Nadia Falzone using event-by-event simulation with the general purpose Monte Carlo code PENELOPE (Salvat, 2011). A total of 2x10^9 primary particles were simulated in each run, with a statistical uncertainty ≤1.3%. Following the MIRD formalism (Goddu, 1997), the Author then calculated the cumulated radioactivity in the subcellular compartments, $\tilde{A}_h$, by extrapolating back from 0 to 3 h the radioactivity in source region r_h, and correcting for decay due to the half-life of ^{111}In (2.8 days). The mean absorbed radiation dose $\overline{D}_k$ to

a target region r_k from a source region r_h was calculated by the Author using the following formula:

$$\overline{D}_k = \tilde{A}_h S(r_k \leftarrow r_h)$$

Where $\tilde{A}_h$ is the cumulated radioactivity in source region r_h, and $S(r_k \leftarrow r_h)$ is the S-value for the radiation dose to the target region r_k per cumulated radioactivity in the source region r_h.

2.2.7. Statistics

GraphPad Prism 6 software was used to perform statistical analysis. Where statistical analysis was performed, information regarding the particular statistical test is provided in the figure legend.

Chapter 3. F3 peptide and ionising radiation alter the localisation of nucleolar proteins

3.1. Introduction

Before 2002, 121 human proteins had been reported to localise in the nucleolus, with 90% of these being known to be involved in ribosome biogenesis (Leung*, et al.*, 2003). Then in two landmark studies, Andersen *et al*. (2002) and Scherl *et al*. (2002) identified ~350 different nucleolar proteins that have since been recorded in the nucleolar proteome database (NOPdb). Since 2002, the NOPdb has grown to include 50,000 peptides that correspond to >4,500 nucleolar proteins (http://www.lamondlab.com/NOPdb3.0/) (Ahmad*, et al.*, 2009; Leung*, et al.*, 2006).

In 2005, a subset of nucleolar proteins were found to accumulate in the nucleolus after exposure of cells to actinomycin D, while the steady state levels of most nucleolar proteins (e.g. Pol I and exosome components) were found to become reduced in the nucleolus after exposure to actinomycin D (Andersen*, et al.*, 2005). In 2010, dynamic changes in the nucleolar proteome of adenovirus-infected HeLa cells showed that the majority of nucleolar proteins were unaffected by adenovirus infection, with very few proteins exhibiting significant changes in levels (Lam*, et al.*, 2010). Thus, the nucleolus responds distinctly to different types of perturbation (a list of the known nucleolar responses to different types of stress is given in Chapter 1, Table 1.1).

Boisvert *et al*. (2010) demonstrated that in colon carcinoma (HCT116) cells exposed to the topoisomerase II inhibitor etoposide (50 μM) for 1 h, most nucleolar proteins

became enriched in the nucleolus, except for r-proteins which were found to redistribute from the nucleolus to the cytoplasm upon etoposide-induced DNA damage (Boisvert*, et al.*, 2010). In a separate study, Biosvert and Lamond (2010) found that 1 h exposure to etoposide (50 μM) caused changes in the distribution of proteins between the nucleolus and the nucleoplasm that were dependent on p53 (Boisvert and Lamond, 2010). In particular, DNA damage produced by etoposide caused r-proteins to be redistributed from the nucleolus to the cytoplasm in p53 wild-type but not p53-null HCT116 cells.

DNA damage can be produced by UV and IR. UV causes DNA helix distorting bulges, cyclobutane pyrimidine dimers and 6-4 photoproducts, while IR causes DNA double-strand breaks. UV-induced DNA damage is repaired by the nucleotide excision repair pathway (Friedberg, 2001; Ravanat*, et al.*, 2001), but IR-induced DNA damage is repaired by the non-homologous end-joining or homologous recombination repair pathways (Wyman and Kanaar, 2006). UV causes the inhibition of Pol I transcription of rDNA in the nucleolus and Pol II transcription of non-ribosomal genes in the nucleoplasm. However, IR is not generally considered to inhibit transcription, though recent evidence suggests that IR-induced chromosome breaks do transiently inhibit Pol I transcription (Kruhlak*, et al.*, 2007).

Moor *et al*. (2011) found that NPM intensity in the nucleolus was reduced by 6 h after exposure to UVC, whereas fibrillarin and UBF relocalised into nucleolar caps. These changes were not evident 6 h after exposure to IR, except that the intensity of NPM reduced slightly in the nucleolus (~20%) (Moore*, et al.*, 2011). Changes in the nucleolar proteome were also evident after exposure of WS-1 cells to UVC or IR. A marked progressive change in the nucleolar proteome over 16 h was observed in response to UVC, while IR induced a change in the nucleolar proteome that was

described as ‘rapid’ and most pronounced at 15 min post-exposure (Moore*, et al.*, 2011). Fluorescence imaging experiments revealed that the intensities of AATF, GNL3, DDX56 and Ku70 was also found to be significantly reduced in the nucleolus 16 h after exposure to UVC, with AATF, GNL3 and DDX56, but not Ku70, being redistributed to the nucleoplasm, as shown by a reduction in the ratio of the nucleolar-to-nucleoplasmic intensities (Moore*, et al.*, 2011). Thus, the nucleolar proteome displays distinctly different stress responses to UVC and IR.

F3 peptide is a 31 amino acid (KDEPQRRSARLSAKPAPPKPEPKPKKAPAKK) fragment of human high mobility group nucleosome binding domain 2 (HMGN2). F3 was discovered during phage display experiments that screened for homing to human leukaemia (HL-60) and melanoma (MDA-MB-435) xenografts in athymic mice (Porkka*, et al.*, 2002). The receptor for F3 is NCL, which is the most abundant protein of the nucleolus, but has been shown to shuttle between the nucleus and the cytoplasm (Borer*, et al.*, 1989). NCL has been found to be present on the cell membrane of a wide range of malignant cell lines (Chapter 1, Table 1.3).

The main aims of the work presented in this chapter were to investigate if F3 has an effect on proteins that localise in the nucleolus and to compare the effect with the effect of IR. F3 has been shown to colocalise with NCL in the nucleolus (Cornelissen*, et al.*, 2012b) and, because the level of nucleolar proteins in the nucleolus changes dynamically in response to exposure of cells to a wide range of different cellular stresses, it was hypothesised that exposure of cells to F3 might cause changes in the levels of NCL and other proteins in the nucleolus. The localisation of proteins between the nucleolus and the nucleoplasm has also been shown to be altered in response to exposure of cells to cellular stress. Therefore, it was also hypothesised that F3 might also cause the localisation of nucleolar proteins to be altered. Thus, the levels and

localisation of NCL, NPM and Ki-67 in the nucleolus and the nucleoplasm were investigated following exposure of osteosarcoma (U2OS) cells to F3, IR or F3 + IR. These proteins were chosen because F3 has been found to bind to NCL, which has been shown to translocate from the nucleolus to the nucleoplasm in response to exposure of cells to IR (Daniely*, et al.*, 2002). NCL is known to form a 140 kDa complex with nucleophosmin (NPM) during interphase and cytokinesis (Liu and Yung, 1999). The NCL:NPM complex can form in the nucleolus and nucleoplasm following relocalisation of NCL and NPM from the nucleolus to the nucleoplasm (Liu and Yung, 1999). NPM levels reduce in the nucleolus after exposure of cells to IR and UV (Moore*, et al.*, 2011) and NPM translocation from the nucleolus to the nucleoplasm correlates with the cytotoxicity of a number of agents (Chan*, et al.*, 1996). Therefore, it was hypothesised that if F3 had an effect on the levels and localisation of NCL in the nucleolus, F3 might also produce a similar effect on NPM. Ki-67 is a nucleolar protein that is associated with, and may be necessary for cell proliferation (Scholzen and Gerdes, 2000). Unlike NPM, Ki-67 is not known to interact with NCL, but Ki-67 levels do become reduced in the nucleolus following transcription inhibition (Andersen*, et al.*, 2005). Ki-67 also redistributes from the nucleolus to the nucleoplasm after exposure of cells to UV (Al-Baker*, et al.*, 2005). The effect of F3 on Ki-67 was investigated to explore if F3 was able to produce effects on the levels and localisation of a nucleolar protein that is not known to interact with NCL or NPM. To quantify the levels and distribution of NCL, NPM and Ki-67 in the nucleolus and nucleoplasm, immunofluorescence imaging was used to measure the intensity of NCL, NPM and Ki-67 in the nucleolus and the nucleoplasm, because it is a relatively simple technique that can be readily applied to the quantification of a range of different proteins of interest for which commercial antibodies are available. U2OS cells were fixed 3 h after

exposure to F3, because this time-point coincided with the maximum uptake of F3 (Cornelissen*, et al.*, 2012b), while a time-point of 15 min time-point was chosen for fixation of cells exposed to IR, because this time-point coincided with the maximum response of the nucleolar proteome after exposure to IR (Moore*, et al.*, 2011). To image cells exposed to F3 + IR, cells were exposed to F3 for 3 h and then exposed to IR before being fixed 15 min later.

3.2. Results

3.2.1. F3 and IR cause nucleolin to be redistributed from the nucleolus to the nucleoplasm

To analyse and quantify the effect of exposure to F3, IR or F3 followed by IR (F3 + IR) on the levels of NCL in the nucleus, nucleoplasm and nucleolus, fluorescence imaging was performed using confocal microscopy to determine the intensity of NCL in the nucleus, nucleoplasm and nucleolus of U2OS cells. U2OS cells were exposed to F3 (1 μM) for 3 h (F3) or exposed to IR (10 Gy) and incubated for 15 min (IR) or exposed to F3 (1 μM) for 3 h and subsequently exposed to IR (10 Gy) and incubated for 15 min (F3 + IR). See Figure 3.1 for a schematic of the fluorescence imaging protocol.

Fluorescence imaging revealed that the size (cross-sectional area) of the nucleoli in U2OS cells that were exposed to F3 was significantly larger (1.26 fold) compared to untreated conditions ($P = 0.0264$). However, the size of the nucleoli in U2OS cells that were exposed to IR, or IR + F3 was not significantly different compared to the other groups (Figures 3.2). The number of nucleoli in U2OS cells that were exposed to F3, IR, or F3 + IR was not significantly different compared to untreated conditions. Thus,

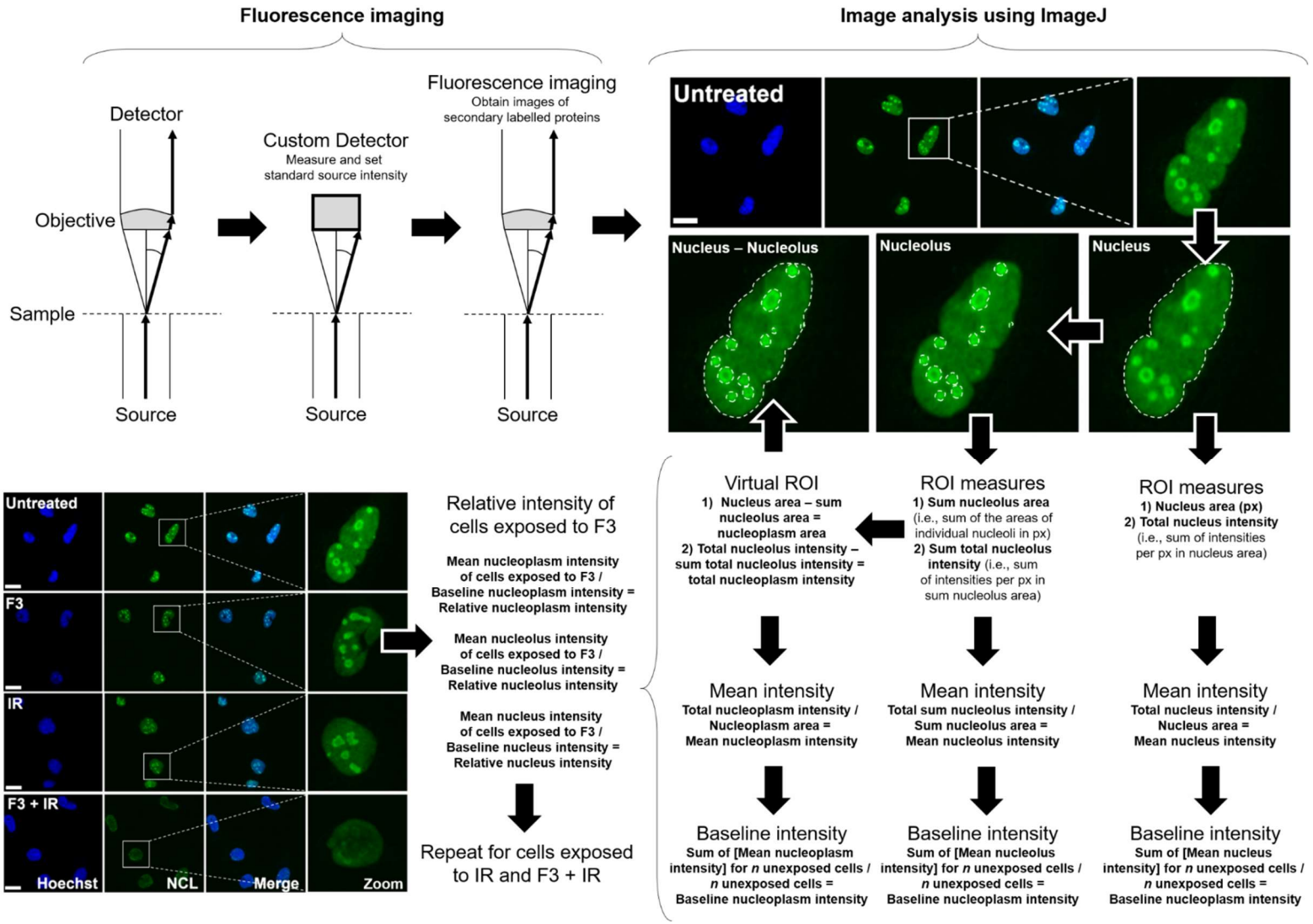

Figure 3.1 Schematic of fluorescence imaging protocol

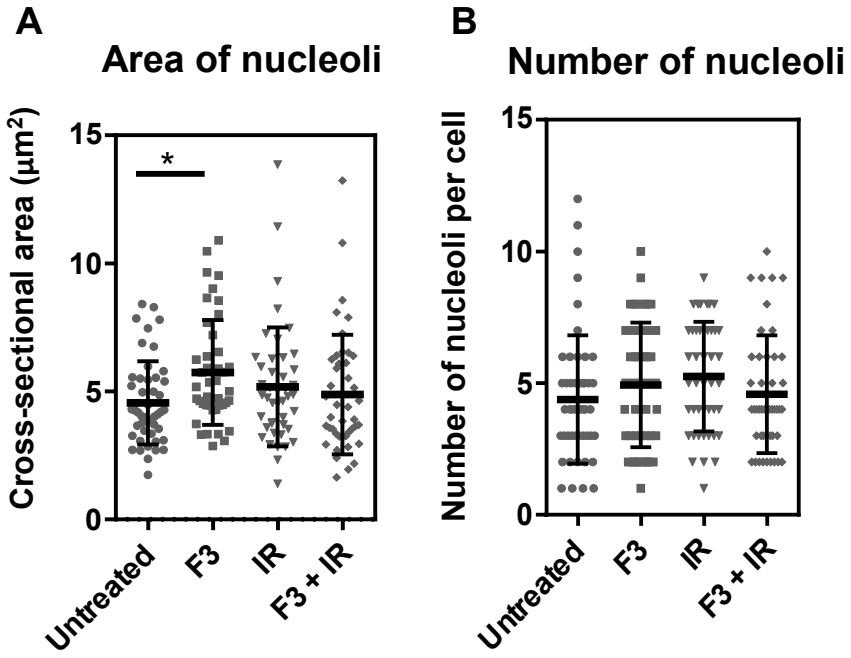

Figure 3.2. The size and number of nucleoli in U2OS cells exposed to F3, IR or F3 + IR

Quantification of (A) the size (cross-sectional area, μm^2) of nucleoli and (B) the number of nucleoli per cell for U2OS cells exposed to F3, IR (10 Gy), or F3 + IR, compared to untreated conditions. Values show mean ± SD, n = 43–50. GraphPad Prism 6 software was used to test if the data followed a Gaussian distribution using a D'Agostino-Pearson omnibus test, and then means were compared using an non-parametric Kruskal-Wallis one-way Anova (confidence level of 0.05) with multiplicity adjusted P values (Dunn's post-hoc test). *, $P < 0.05$.

exposure of U2OS cells to F3 caused enlargement of the nucleolus, although it should be noted that this result may have been influenced by the location on the z-axis of the image field which was placed at the largest section through the nucleolus.

By defining regions of interest, the relative levels of NPM were quantified by measuring the intensity of NPM in the nucleus, nucleoplasm and nucleolus using fluorescence imaging (Figure 3.3.A), in order to show that the levels in, and distribution between the nucleolus and the nucleoplasm of a protein known to interact with F3 becomes altered after exposing cells to F3 or IR. The mean NCL levels were used to calculate the fold-change (relative to untreated conditions) in the relative level of NCL in the nucleus, nucleoplasm and nucleolus due to exposure of U2OS cells to F3, IR, or F3 + IR. The relative level of NCL in the nucleus was significantly reduced 0.78±0.05 fold ($P = 0.0015$), 0.66±0.03 fold ($P < 0.0001$), and 0.62±0.03 fold ($P < 0.0001$) in response to exposure of U2OS cells to F3, IR, or F3 + IR, respectively. The relative level of NCL in the nucleus was significantly lower after exposure to F3 + IR compared to exposure to F3 ($P = 0.0475$) (Figure 3.3.B). Thus, exposure of U2OS cells to F3, IR, or F3 + IR reduced the relative level of NCL in the nucleus, while exposure to F3 + IR further reduced the relative level of NCL in the nucleus in comparison to exposure to F3.

In the nucleoplasm, the relative level of NCL was also significantly reduced 0.80±0.05 fold ($P = 0.0028$), 0.70±0.04 fold ($P < 0.0001$), and 0.65±0.03 fold ($P < 0.0001$) in response to exposure of U2OS cells to F3, IR, or F3 + IR, respectively (Figure 3.3.C). Thus, exposure of U2OS cells to F3 or IR reduced the relative levels of NCL in the nucleoplasm.

In the nucleolus, the relative level of NCL was significantly reduced 0.69±0.04 fold ($P < 0.0001$), 0.58±0.03 fold ($P < 0.0001$), and 0.54±0.03 fold ($P < 0.0001$) in response to exposure of U2OS cells to F3, IR, or F3 + IR, respectively (Figure 3.3.D). The

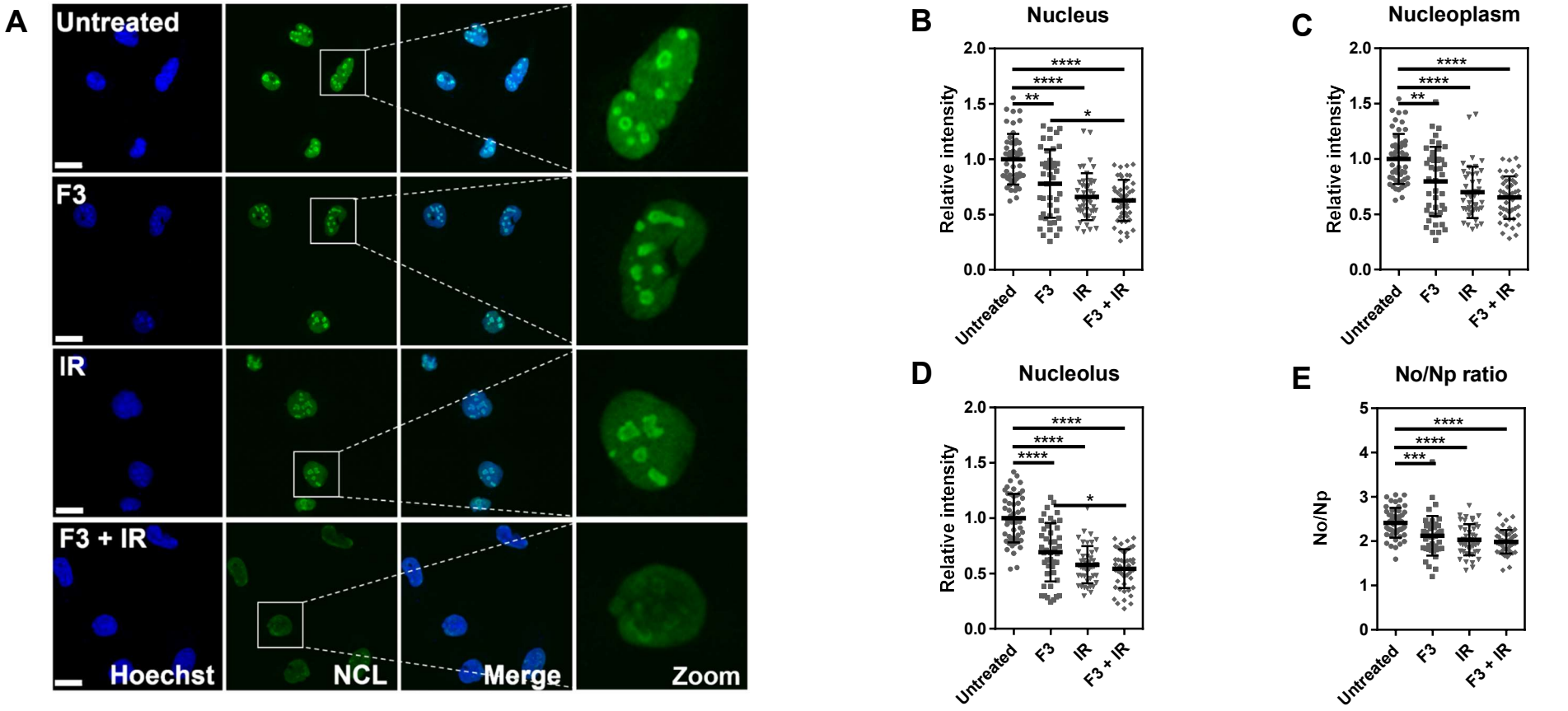

Figure 3.3. Intensity and distribution of NCL in U2OS cells exposed to F3, IR, or F3 + IR

(A) Fluorescence images of NCL levels in the nucleolus and the nucleoplasm of U2OS cells exposed to F3, IR, or F3 + IR, compared to untreated conditions. Blue, DNA. Green, NCL. Scale, 20 μm. (B–E) Fold-change in mean intensity of NCL in the (B) nucleus, (C) nucleoplasm and (D) nucleolus, and (E) the nucleolus/nucleoplasm ratio for U2OS cells exposed to F3, IR, or F3 + IR, compared to untreated conditions. Values show mean ± SD, n = 43–50. NCL, nucleolin; No/Np ratio, nucleolus/nucleoplasm ratio. GraphPad Prism 6 software was used to test if the data followed a Gaussian distribution using a D'Agostino-Pearson omnibus test, and then means were compared using a non-parametric Kruskal-Wallis one-way Anova (confidence level of 0.05) with multiplicity adjusted P values (Dunn's post-hoc test). *, $P < 0.05$; **, $P < 0.01$; ***, $P < 0.001$; ****, $P < 0.0001$.

relative level of NCL in the nucleolus was significantly lower after exposure to F3 + IR compared to exposure to F3 (P = 0.0363). Thus, exposure of U2OS cells to F3 or IR reduced the relative level of NCL in the nucleolus, while exposure to F3 + IR further reduced the relative level of NCL in the nucleolus in comparison to exposure to F3.

Interestingly, exposure of U2OS cells to F3, IR, or F3 + IR did not reduce the relative level of NCL in the nucleoplasm to the same extent as the nucleolus, suggesting that the distribution of NCL between the nucleolus and the nucleoplasm was altered by exposure of U2OS cells to F3, IR, and F3 + IR. The distribution of NCL between the nucleolus and the nucleoplasm was analysed and quantified by using the mean NCL intensity to calculate the nucleolus-to-nucleoplasm ratio (No/Nu ratio) of the level of NCL. The No/Nu ratio of the level of NCL in untreated U2OS cells was 2.41±0.05, indicating that NCL was present at a higher level in the nucleolus compared to the nucleoplasm. As expected, the distribution of NCL significantly shifted from the nucleolus to the nucleoplasm in U2OS cells exposed to F3, IR, and F3 + IR, in comparison to untreated conditions (2.12±0.07 No/Nu ratio, P = 0.0005; 2.03±0.05 No/Nu ratio, P < 0.0001; 1.98±0.04 No/Nu ratio, P < 0.0001; respectively) (Figure 3.3.E). Thus, exposure of U2OS cells to F3, IR, or F3 + IR shifted the distribution of NCL from the nucleolus to the nucleoplasm.

Together, these observations suggest that F3 reduced the relative level of NCL in the nucleoplasm and the nucleolus to a similar extent as IR, while the combination of F3 + IR further reduced the relative levels of NCL in the nucleolus (and therefore the nucleus) in comparison to the reduction meditated by F3. F3 shifted the distribution of NCL from the nucleolus to the nucleoplasm to a similar extent as IR and F3 + IR.

3.2.2. F3 and IR cause nucleophosmin to be redistributed from the nucleolus to the nucleoplasm

Similar to NCL, relative levels of NPM were quantified by measuring the intensity of NPM in the nucleus, nucleoplasm and nucleolus using fluorescence imaging (Figure 3.4.A), in order to show that the levels in, and distribution between the nucleolus and the nucleoplasm of a protein known to interact with NCL becomes altered after exposing cells to F3 or IR. The relative level of NPM in the nucleus was significantly reduced 0.84±0.05 fold ($P = 0.0093$), 0.66±0.02 fold ($P < 0.0001$), and 0.69±0.03 fold ($P < 0.0001$) in response to exposure of U2OS cells to F3, IR, or F3 + IR, respectively (Figure 3.4.B). The relative level of NPM in the nucleus was significantly lower after exposure to IR compared to exposure to F3 ($P = 0.0345$). Thus, exposure of U2OS cells to F3, IR, or F3 + IR reduced the levels of NPM in the nucleus, while exposure to IR further reduced the levels of NPM in the nucleus in comparison to exposure to F3.

In the nucleoplasm, the relative level of NPM was not significantly changed in response to exposure of U2OS cells to F3 (0.94±0.05 fold) (Figure 3.4.C). However, the relative level of NPM in the nucleoplasm was significantly reduced 0.78±0.03 fold ($P = 0.0021$) and 0.80±0.04 fold ($P = 0.0138$) in response to exposure of U2OS cells to IR or F3 + IR, respectively. Thus, exposure of U2OS cells to IR or F3 + IR reduced the level of NPM in the nucleoplasm, while exposure to F3 did not significantly change the level of NPM in the nucleoplasm.

The mean intensity of NPM in the nucleolus revealed that the relative level of NPM was significantly reduced 0.68±0.04 fold ($P < 0.0001$), 0.55±0.02 fold ($P < 0.0001$), and 0.54±0.02 fold ($P < 0.0001$) in response to exposure of U2OS cells to F3, IR, or F3 + IR, respectively (Figure 3.4.D). Thus, exposure of U2OS cells to F3, IR or F3 +

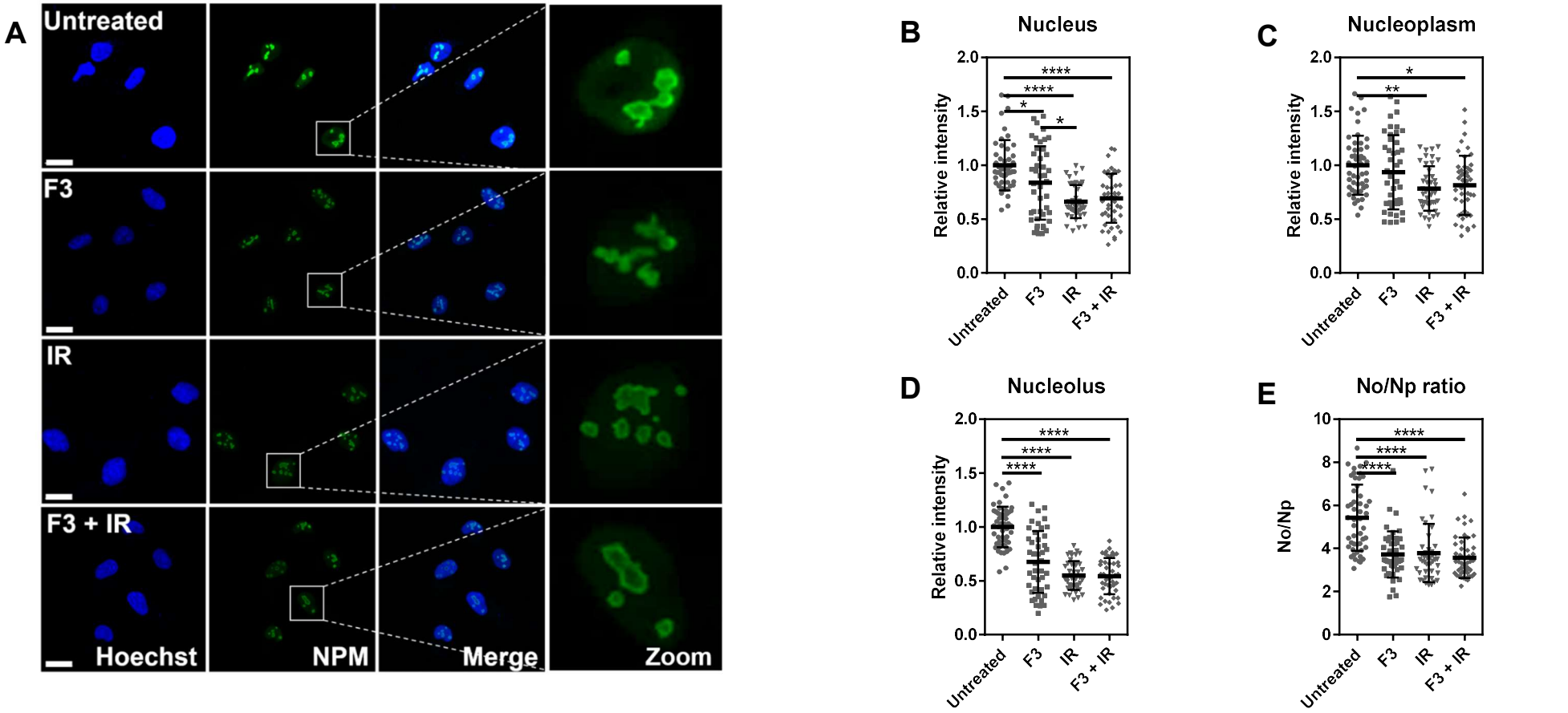

Figure 3.4. Intensity and distribution of NPM in U2OS cells exposed to F3, IR, or F3 + IR

(A) Fluorescence images of NPM levels in the nucleolus and the nucleoplasm of U2OS cells exposed to F3, IR, or F3 + IR, compared to untreated conditions. Blue, DNA. Green, NPM. Scale, 20 μm. (B–E) Fold-change in mean intensity of NPM in the (B) nucleus, (C) nucleoplasm and (D) nucleolus, and (E) the nucleolus/nucleoplasm ratio for U2OS cells exposed to F3, IR, or F3 + IR, compared to untreated conditions. Values show mean ± SD, n = 43–48. NPM, nucleophosmin; No/Np ratio, nucleolus/nucleoplasm ratio. GraphPad Prism 6 software was used to test if the data followed a Gaussian distribution using a D'Agostino-Pearson omnibus test, and then means were compared using a non-parametric Kruskal-Wallis one-way Anova (confidence level of 0.05) with multiplicity adjusted P values (Dunn's post-hoc test). *, $P < 0.05$; **, $P < 0.01$; ****, $P < 0.0001$.

IR reduced the level of NPM in the nucleolus.

Similar to observations for NCL, exposure of U2OS cells to F3, IR, and F3 + IR did not reduce the level of NPM in the nucleoplasm to the same extent as the nucleolus, suggesting that the distribution of NPM between the nucleolus and the nucleoplasm was altered by exposure of U2OS cells to F3, IR, and F3 + IR. The No/Nu ratio of NPM levels in untreated U2OS cells was 5.42±0.21, indicating that NPM was present at a higher level in the nucleolus versus the nucleoplasm. Similar to NCL, the distribution of NPM significantly shifted from the nucleolus to the nucleoplasm in U2OS cells exposed to F3, IR, and F3 + IR, compared to untreated conditions (3.72±0.16 No/Nu ratio, $P < 0.0001$; 3.79±0.20 No/Nu ratio, $P < 0.0001$; 3.56±0.13 No/Nu ratio, $P < 0.0001$; respectively) (Figure 3.4.E). Thus, exposure of U2OS cells to F3, IR, and F3 + IR shifted the distribution of NPM from the nucleolus to the nucleoplasm.

Together, these observations suggested that F3 and IR cause different effects on the relative level of NPM in the nucleoplasm and the nucleolus, with F3 causing reductions in the relative level of NPM in the nucleolus but not the nucleoplasm, and IR causing reductions in NPM in the nucleolus and the nucleoplasm.

3.2.3. F3 causes Ki-67 to accumulate in the nucleoplasm

Similar to NCL and NPM, the relative level of Ki-67 was quantified by measuring the intensity of Ki-67 in the nucleus, nucleoplasm and nucleolus using fluorescence imaging (Figure 3.5.A), in order to show that the levels in, and distribution between the nucleolus and the nucleoplasm of a protein not known to interact with NCL becomes altered after exposing cells to F3 or IR. The relative level of Ki-67 in the nucleus was significantly increased 1.41±0.10 fold ($P = 0.0054$) in response to exposure of U2OS

cells to F3 (Figure 3.5.B). In contrast, the relative level of Ki-67 in the nucleus was not significantly changed in response to exposure of U2OS cells to IR or F3 + IR (1.10±0.11 fold and 1.13±0.09 fold, respectively). Thus, exposure of U2OS cells to F3, but not IR or F3 + IR, increased the levels of Ki-67 in the nucleus.

In the nucleoplasm, the relative level of Ki-67 was significantly increased 1.43±0.10 fold in response to exposure of U2OS cells to F3 ($P = 0.0011$) (Figure 3.5.C). In contrast, the relative level of Ki-67 in the nucleoplasm was not significantly changed in response to exposure of U2OS cells to IR or F3 + IR (1.13±0.10 fold and 1.13±0.09 fold, respectively). Thus, exposure of U2OS cells to F3, but not IR or F3 + IR, significantly increased the relative level of Ki-67 in the nucleoplasm.

Although Ki-67 levels in the nucleoplasm increased after exposure to F3, the levels of Ki-67 in the nucleoplasm after exposure of U2OS cells to F3 + IR were similar to untreated conditions. Therefore, IR antagonised the increase in Ki-67 levels in the nucleoplasm due to exposure of U2OS cells to F3.

In the nucleolus, the relative level of Ki-67 was not significantly changed in response to exposure of U2OS cells to F3, IR, or F3 + IR (1.23±0.10 fold, 1.01±0.11 fold, and 1.12±0.10 fold, respectively) (Figure 3.5.D). Thus, exposure of U2OS cells to F3 or IR did not mediate effects on the relative level of Ki-67 in the nucleolus.

The increase in Ki-67 levels in the nucleoplasm, but not in the nucleolus following exposure of U2OS cells to F3, but not IR or F3 + IR, did not cause a significant change in the No/Nu ratio for Ki-67 levels. In untreated U2OS cells, the No/Nu ratio of Ki-67 levels was 1.69±0.06, indicating that Ki-67 was present at a higher level in the nucleolus versus the nucleoplasm during untreated conditions. However, the increase in the levels of Ki-67 in the nucleoplasm of U2OS cells exposed to F3 compared to untreated conditions did not significantly reduce the No/Nu ratio of 1.47±0.04 (Figure

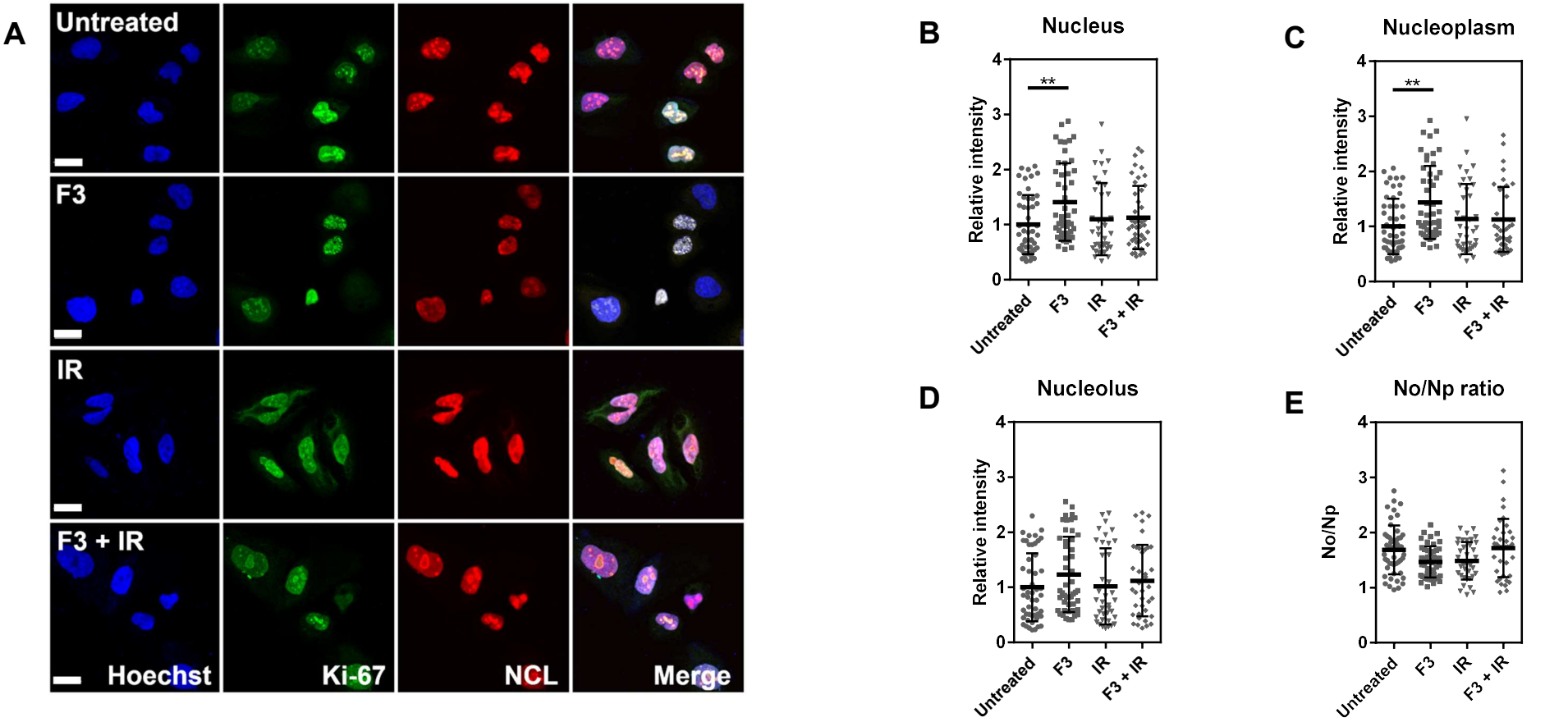

Figure 3.5. Intensity and distribution of Ki-67 in U2OS cells exposed to F3, IR, or F3 + IR

(A) Fluorescence images of Ki-67 levels in the nucleolus and the nucleoplasm of U2OS cells exposed to F3, IR, or F3 + IR, compared to untreated conditions. Co-staining for NCL was used to delineate the nucleolus. Blue, DNA. Green, Ki-67. Red, NCL. Scale, 20 μm. (B–E) Fold-change in mean intensity of Ki-67 in the (B) nucleus, (C) nucleolus, (D) nucleoplasm, and (E) the nucleolus/nucleoplasm ratio for U2OS exposed to F3, IR, or F3 + IR, compared to untreated conditions. Values show mean ± SEM, n = 38–50. No/Np, nucleolus/nucleoplasm ratio. GraphPad Prism 6 software was used to test if the data followed a Gaussian distribution using a D'Agostino-Pearson omnibus test, and then means were compared using a non-parametric Kruskal-Wallis one-way Anova (confidence level of 0.05) with multiplicity adjusted P values (Dunn's post-hoc test). **, $P < 0.01$.

3.5.E). Similarly, no significant difference was observed for the No/Nu ratio for Ki-67 levels compared to untreated conditions following exposure of U2OS cells to IR or F3 + IR (1.49±0.06 No/Nu ratio and 1.72±0.08 No/Nu ratio, respectively). Thus, exposure of U2OS cells to F3, IR, or F3 + IR, did not cause a significant change in the distribution of Ki-67 between the nucleoplasm and the nucleolus. Together, these observations suggested that F3, but not IR or F3 + IR, caused a significant increase in the relative level of Ki-67 in the nucleoplasm (and therefore the nucleus), and that IR antagonised the effect of F3 on Ki-67 when U2OS cells were exposed to F3 + IR.

3.3. Discussion

To analyse the effects on the nucleolus of F3, IR, or F3 + IR, fluorescent imaging of the nucleolar proteins NCL, NPM, and Ki-67 was performed using wild-type $p53^{+/+}$ U2OS cells. F3 was found to cause an increase in the area of the nucleolus (as measured by NCL fluorescence) without altering the number of nucleoli inside the nucleus of U2OS cells. This contrasts with the highly selective Pol I inhibitor CX-5461, which has been shown to cause multiple nucleoli of lymphoma cells to form a single nucleolus (Bywater*, et al.*, 2012). CX-5461 caused the relocalisation of NCL and NPM to the periphery of the nucleolus, and also reduced fibrillarin staining. Analysis and quantification of the level of NCL, NPM, and Ki-67 in the nucleus, nucleoplasm and nucleolus after exposure of U2OS cells to F3, IR, or F3 + IR was compared with untreated conditions. An incubation time of 3 h with F3 was chosen because a 3 h time-point coincided with a plateau in the cellular uptake of F3 (Cornelissen*, et al.*, 2012b), while 15 min incubation after exposure to IR was chosen because it coincided with the most pronounced change in the nucleolar proteome in response to exposure

to IR (at least for wild-type $p53^{+/+}$ WS-1 cells) (Moore*, et al.*, 2011). U2OS cells were chosen because of their wild-type $p53^{+/+}$ status, since wild-type p53 is considered necessary for the reorganisation of the nucleolar proteome (Boisvert and Lamond, 2010). The distribution of NCL, NPM, and Ki-67 between the nucleolus and the nucleoplasm was also successfully quantified. This methodology was adapted from fluorescence imaging and proteomic approaches which have characterised changes in the nucleolar proteome due to exposure of WS-1 cells to UV and IR (Moore*, et al.*, 2011). Observations of the levels of NCL and NPM in U2OS cells exposed to F3, IR, or F3 + IR support the assertion that the nucleolus is a dynamic structure, the components of which undergo complex reorganisations when exposed to different types of cellular stress. A summary of the effects caused by exposure of U2OS cells to F3, IR, or F3 + IR on the nucleolar proteins NCL, NPM, and Ki-67 is shown in Figure 3.6.

NCL is a conserved multifunctional phosphoprotein that is highly concentrated in the nucleolus. The nucleolar localisation of NCL may depend on the ability of the acidic, RNA-binding, and GAR/RGG domains of NCL to transiently interact with rDNA, pre-rRNA, r-proteins, and snoRNPs in the nucleolus (Bouvet*, et al.*, 1998; Creancier*, et al.*, 1993; Ginisty*, et al.*, 1998; Lapeyre*, et al.*, 1986; Schmidt-Zachmann and Nigg, 1993). NCL has also been proposed to bind and stabilise G-quadruplex structures in rDNA to enhance the rate of Pol I transcription (Hanakahi*, et al.*, 1999). An RNA-binding domain allows NCL to associate with pre-rRNA with a K_d of 5 to 100 nM (Ghisolfi-Nieto*, et al.*, 1996; Herrera and Olson, 1986), and the C-terminal GAR/RGG domain also confers rRNA-binding and interacts with r-proteins (Bouvet*, et al.*, 1998; Ghisolfi*, et al.*, 1992; Heine*, et al.*, 1993). NCL-mediated nuclear translocation of F3 peptide may be dependent on a conserved bipartite NLS present in NCL and transient

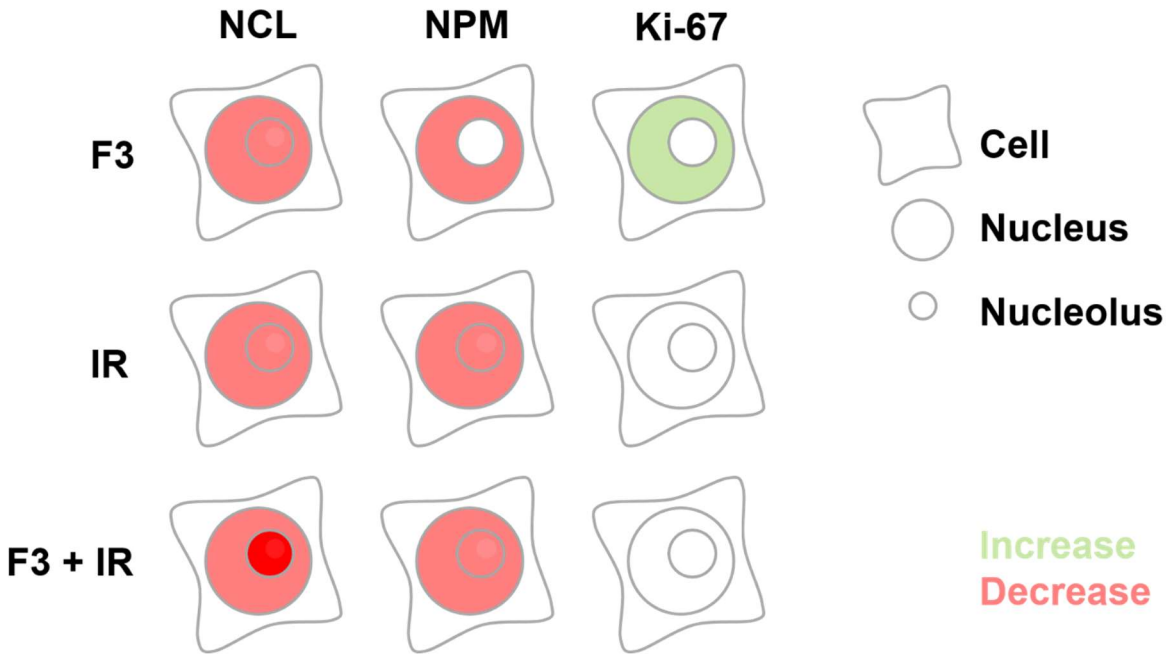

Figure 3.6. **Summary of the effects caused after exposure of U2OS cells to F3, IR, or F3 + IR on the nucleolar proteins NCL, NPM, and Ki-67**

interactions with nucleolar factors.

Reduction in the level of NCL in the nucleoplasm and the nucleolus due to exposure of U2OS cells to F3, IR, or F3 + IR, may impact upon several important cellular processes, including the transcription of rDNA, rRNA maturation, chromatin remodelling, histone chaperone activity, ribosome assembly and nucleo-cytoplasmic transport (Ginisty*, et al.*, 1999; Mongelard and Bouvet, 2007; Srivastava and Pollard, 1999). NCL binds to G-quadruplex structures in rDNA (Drygin*, et al.*, 2009) and interacts through its RRM motif with pre-rRNA in a U3 snoRNA-dependent manner to enhance Pol I transcription and pre-rRNA processing, respectively (Allain*, et al.*, 2000; Ginisty*, et al.*, 1998; Ginisty*, et al.*, 2000). During pre-rRNA processing, NCL binds to a stem-loop structure in newly transcribed pre-rRNA and acts as a chaperone that induces correct folding of pre-rRNA (Allain*, et al.*, 2000; Serin*, et al.*, 1996) and catalyses its cleavage (Ginisty*, et al.*, 1998; Ginisty*, et al.*, 2000). NCL may also play a role in the assembly and nucleo-cytoplasmic transport of ribosomal subunits due to its affinity for r-proteins (Bouvet*, et al.*, 1998; Xue and Melese, 1994). Therefore, reduction in the level of NCL in the nucleolus due to exposure of U2OS cells to F3, IR, or F3 + IR may reduce rRNA transcription, processing and assembly into r-subunits.

RNA interference (RNAi) to reduce *NCL* gene expression inhibits Pol I transcription (Ma*, et al.*, 2007; Rickards*, et al.*, 2007; Ugrinova*, et al.*, 2007). Reduction in the level of NCL has been found to correlate with the inhibition of Pol I transcription of rDNA (Rickards*, et al.*, 2007), while decrease in NCL levels may alter pre-rRNA processing (Cong*, et al.*, 2014b; Roger*, et al.*, 2003). Reduction in the level of NCL in the nucleolus may therefore inhibit Pol I transcription and processing.

NCL mediates the remodelling of rDNA-containing chromatin. Although NCL has also been shown to act as a transcriptional repressor (Yang*, et al.*, 1994), NCL plays a role

in enhancing Pol I transcription by mediating chromatin decondensation by binding to histone H1 via its N-terminus (Erard*, et al.*, 1988; Kharrat*, et al.*, 1991) and by binding and stabilising G-quadruplex structures on the non-template strand in rDNA (Drygin*, et al.*, 2009). The FACT-like activity of NCL, which has been implicated in the remodelling of chromatin containing nucleosomes comprising the histone variant macroH2A1, but not H2ABbd, may facilitate Pol I transcription by dissociation of the H2A-H2B dimer (Angelov*, et al.*, 2006). Depletion of NCL induces the recruitment of macroH2A1 at the rDNA promoter, repressing rRNA transcription (Cong*, et al.*, 2014b). Increased expression of NCL increases H3K9me2, but reduces H3K4me3 marks in rDNA genes (Cong*, et al.*, 2014a), switching rDNA genes from a transcriptionally active to transcriptionally silent state (Grummt and Pikaard, 2003). However, reductions in the level of NCL lead to increased H2K9me2 and decreased H4K12Ac (Cong*, et al.*, 2014a), and may cause the recruitment of macroH2A1 to the rDNA promoter, thereby reducing Pol I transcription.

In addition to rRNA synthesis, reduction in the level of NCL in the nucleus could also alter the rate of transcription of mRNAs (Abdelmohsen*, et al.*, 2011; Serin*, et al.*, 1996). NCL binds to the 5' untranslated region (UTR) of *TP53* mRNA, thereby repressing the translation of p53 mRNA in response to DNA damage (Takagi*, et al.*, 2005). Reduction in the level of NCL levels could therefore enhance the translation of p53 in the context of cellular stress, such as DNA damage, triggering DNA damage repair or apoptosis (Lane, 1992). Interestingly, NCL has been found to inhibit oxidative stress-induced apoptosis by downregulating Bax and was suggested to potentially stabilise *BCL-2* mRNA (Sengupta*, et al.*, 2004; Zhang*, et al.*, 2010), which encodes an anti-apoptotic protein overexpressed by leukaemia cells (Willimott and Wagner, 2010). NCL also positively regulates the biogenesis of the microRNAs miR-15a and miR-16 (which both

negatively regulate NCL and BCL-2) (Pickering*, et al.*, 2011). Nuclear and cytoplasmic localisation of NCL coupled with reduced levels of miR-15a and miR-16 (and increased levels of BCL-2) drive chronic lymphocytic leukaemia (Otake*, et al.*, 2007). miR-15a and miR-16 reduce the translation of *BCL-2* mRNA by promoting its degradation after binding to its 3' UTR. Therefore, reductions in NCL levels may reduce the rate of p53 mRNA translation, destabilise *BCL-2* mRNA and drive an apoptotic response.

Redistribution of NCL from the nucleolus to the nucleoplasm due to exposure of wild-type $p53^{+/+}$ U2OS cells to F3, IR, or F3 + IR is consistent with reports that NCL is mobilised form the nucleolus to the nucleoplasm in a wild-type p53-dependent manner following IR or camptothecin (Daniely*, et al.*, 2002). The reduction of NCL in the nucleus after exposure of U2OS cells to F3, IR, or F3 + IR may reflect the redistribution of NCL from the nucleus to the cytoplasm. Cytoplasmic and membrane levels of NCL were not measured during fluorescence imaging, because NCL was not visible in the cytoplasm or at the cell membrane, presumably due to the dilution effect caused by the larger volume of the cytoplasm and the cell membrane relative to the nucleus. However, the N-terminal domain of NCL does confer nucleo-cytoplasmic shuttling activity (Schmidt-Zachmann*, et al.*, 1993). Phosphorylation of the N-terminal domain by $p34^{cdc2}$ (also known as Cdk1) promotes the redistribution of NCL from the nucleus to the cytoplasm, while dephosphorylation redistributes NCL from the cytoplasm to the nucleus (Schwab and Dreyer, 1997). In the cytoplasm, NCL binds to mRNAs and influences their stability (as described above), while at the cell membrane NCL acts as a Ca^{2+}-dependent cell surface receptor that shuttles extracellular ligands via active transport (Hovanessian*, et al.*, 2010). Translocation of NCL to the cell membrane promotes ligand binding and triggers Ca^{2+} entry into cells (Losfeld*, et al.*, 2009). If NCL were found to relocalise to the cytoplasm and cell membrane in response to exposure

to F3, IR, or F3 + IR, NCL may act to influence mRNA stability and facilitate ligand internalisation.

Similar to NCL, a pronounced reduction in the levels of NPM in the nucleolus of U2OS cells occurred 15 min after exposure to F3, IR, or F3 + IR. This was comparable to the 'rapid' IR-induced changes in the nucleolar proteome at 15 min post-exposure in MS-SILAC experiments using WS-1 cells exposed to IR, but was distinct from the slight reductions in NPM levels in the nucleolus at 6 h after exposure of WS-1 cells to IR that were reported in Moore *et al*. (2011). Thus, the reduction in the levels of NPM in the nucleolus of U2OS cells exposed to IR was consistent with 'rapid' IR-induced changes in the nucleolar proteome, although the possibility that the response of NPM in the nucleolus at 6 h after exposure of U2OS cells to IR may differ from WS-1 cells cannot be excluded. The redistribution of NPM from the nucleolus to the nucleoplasm after exposure of U2OS cells to F3, IR, or F3 + IR adds to reports that show that NPM relocalises from the nucleolus to the nucleoplasm after exposure of cells to actinomycin D (Liu and Yung, 1999) and UVC (Al-Baker*, et al.*, 2005).

NPM possesses histone chaperone activities and belongs to the nucleoplasmin/nucleophosmin family of nuclear chaperones (Frehlick*, et al.*, 2007). The core-domain at the N-terminus of NPM contains an acidic tract responsible for oligomerisation and chaperone activity (Hingorani*, et al.*, 2000). NPM aids the CENP-A complex in the replacement of histone H3 in centromeric nucleosomes (Foltz*, et al.*, 2009; Foltz*, et al.*, 2006), preferentially binds to histone $(H3\text{-}H4)_2$ tetramers and transfers histones to 'naked' DNA to promote chromatin condensation (Okuwaki*, et al.*, 2001a) or decondensation (Okuwaki*, et al.*, 2001b). Reductions in the level of NPM in the nucleolus and the nucleoplasm caused by F3, IR, or F3 + IR may therefore alter chromatin compaction. This mechanism provides a rationale for combining F3 with

^{111}In, since chromatin remodelling has been shown to radiosensitise malignant cells to Auger electron emitters, because DNA double-strand break induction is affected by the structure of chromatin. Indeed, the histone deacetylase inhibitor suberoyl anilide hydroxamic acid (SAHA; vorinostat) increases the number of γH2AX foci induced by ^{111}In-labelled growth factors that translocate to the nucleus of growth factor receptor-positive breast carcinoma (MDA-MB-468) cells (Terry and Vallis, 2012).

In addition to chromatin remodelling, NPM controls the transcriptional activation of rDNA genes (Murano*, et al.*, 2008). NPM associates with rDNA chromatin to control the rate of Pol I transcription. Knock-down of NPM reduces the rate of Pol I transcription, while expression of a dominant-negative form of NPM (B23ΔC) that lacked its histone chaperone activity reduces the rate of Pol I transcription and cell proliferation (Murano*, et al.*, 2008). NPM drives transcription by inhibiting the activity of hexamethylene bis-acetamide inducible 1, a negative regulator of Pol II (Gurumurthy*, et al.*, 2008), but blocks lysine acetyltransferase (GN5)-dependent acetylation of chromatin (Zou*, et al.*, 2008) and enhances acetylation-dependent transcription (Swaminathan*, et al.*, 2005). Thus, F3-mediated reductions in the level of NPM may affect Pol I and II transcription.

The localisation of NPM in the nucleolus is correlated with Pol I transcription (Murano*, et al.*, 2008) and in the nucleolus NPM is involved in processing of pre-rRNA (Savkur and Olson, 1998). During pre-rRNA processing, NPM binds the second internal transcribed spacer (ITS2) of pre-rRNA and mediates the production of the 28S rRNA. Reductions in the level of NPM may inhibit the production of the 28S rRNA, leading to the accumulation of the 32S rRNA intermediate. NPM also binds to mRNA, but, unlike NCL which causes pleiotropic effects on mRNA stabilisation, binding of NPM to the mRNA for the chicken *ccn2* gene causes its degradation (Mukudai*, et al.*, 2008). Thus,

reductions in the level of NPM and NCL may produce pleiotropic effects on mRNA stability depending on the target mRNA.

The chaperone activity of NPM inhibits protein aggregation and promotes protein renaturation that exposes hydrophobic regions due to interactions between NPM and substrates (Szebeni and Olson, 1999). The chaperone activity of NPM depends on its nuclear localisation and nuclear export signals, which confer its ability to shuttle between the nucleus and the cytoplasm and to mediate the transport of other proteins through the nuclear pore complex (Borer*, et al.*, 1989; Szebeni*, et al.*, 1997; Wang*, et al.*, 2005; Yu*, et al.*, 2006). NPM is required for the nuclear export of the r-protein RPL5 (Yu*, et al.*, 2006) and the near-mature 40S and 60S r-subunits (Maggi*, et al.*, 2008). NPM also influences the nucleolar localisation and/or stability of the tumour suppressor ARF (Colombo*, et al.*, 2005; Kuo*, et al.*, 2004) and the cell cycle inhibitor p21 (Xiao*, et al.*, 2009). Therefore, reductions in the level of NPM may inhibit the nucleo-cytoplasmic transport of ribosomes and influence the stability of ARF, p53, and p21.

Interestingly, NPM expression has been reported to confer cellular survival after exposure to UV (Wu*, et al.*, 2002a; Wu*, et al.*, 2002b), IR (Dalenc*, et al.*, 2002), hypoxia (Li*, et al.*, 2004), and actinomycin D (Yao*, et al.*, 2010). NPM binds to the protein kinase PKR and inhibits its pro-apoptotic activity, but NPM is expressed at low levels in mouse embryonic fibroblasts and Fanconi-anemia derived lymphoblasts (Pang*, et al.*, 2003). However, reports suggest that NPM prevents the pro-apoptotic accumulation of p53 in mitochondria in cells treated with doxycyclin (Dhar and St Clair, 2009), and yet drives cytochrome-C release and apoptosis by binding to Bax (Kerr*, et al.*, 2007). In U2OS cells, down-regulation of NPM using RNAi reduces p53 stability following exposure to UV or doxycyclin (Colombo*, et al.*, 2002). NPM regulates p53 stability by

binding to MDM2, inhibiting its E3 ligase activity in response to UV (Kurki*, et al.*, 2004). NPM interacts with ARF via its homodimerisation domain (Itahana*, et al.*, 2003), ARF sequesters MDM2 in the nucleolus and inhibits MDM2's E3 ligase activity by binding to its central C4 zinc finger domain-containing acidic region (Sherr and Weber, 2000; Tao and Levine, 1999; Weber*, et al.*, 1999). NPM also activates p53 in the nucleoplasm independent of inducing the nucleolar sequestration of MDM2 (Korgaonkar*, et al.*, 2002; Llanos*, et al.*, 2001).

Oligomeration of NPM drives nucleolar accumulation of ARF. Phosphorylation of NPM on Ser-48 by AKT has been shown to disrupt NPM oligomer formation and promote an interaction with ARF in the nucleoplasm that prevents ARF from inhibiting MDM2's E3 ligase activity (Hamilton*, et al.*, 2014). However, the redistribution of NPM from the nucleolus to the nucleoplasm may not reduce ARF-dependent inhibition of MDM2's E3 ligase activity, if the NPM molecule to which ARF is bound has not been phosphorylated by AKT (Hamilton*, et al.*, 2014). Though most of ARF is bound to NPM, a large proportion of NPM is not bound to ARF (Bertwistle*, et al.*, 2004), and therefore F3-mediated reductions in the levels of NPM, or redistribution of NPM from the nucleolus to the nucleoplasm, may not necessarily impact on ARF-dependent p53 stabilisation, although it may reduce the level of NPM that is available to be phosphorylated by AKT (phosphorylation of NPM by AKT has been linked to the radioresistance of bladder carcinoma (T24) cells to IR) (Hamilton*, et al.*, 2014).

Ki-67 is not known to translocate from the nucleolus to the nucleoplasm following exposure to IR, although the level of Ki-67 does become reduced in the nucleolus following Pol I transcription inhibition due to exposure to Actinomycin D (Andersen*, et al.*, 2005). Ki-67 is known to become reduced in the nucleolus after exposure of cells to UV (Al-Baker*, et al.*, 2004). Ki-67 is not known to interact with NCL or NPM. Like

NCL and NPM, however, Ki-67 is localised in the Ag-NOR region of the dense fibrillar component (DFC) of the nucleolus during interphase (Braun*, et al.*, 1988; Kill, 1996; Verheijen*, et al.*, 1989), although a portion of Ki-67 also surrounds the Ag-NOR regions (Lorenzato*, et al.*, 2000). The total amount of Ki-67 protein in the nucleolus increases during S-phase (Bruno and Darzynkiewicz, 1992; Endl*, et al.*, 1997). During mitosis, $p34^{cdc2}$ in complex with cyclin B controls the phosphorylation and dephosphorylation of Ki-67 (Endl and Gerdes, 2000; MacCallum and Hall, 1999). Cytoplasmic complexes containing hyperphosphorylated Ki-67 can form throughout mitosis (MacCallum and Hall, 1999), possibly in pre-nucleolar bodies (PNBs). Ki-67 expression in G_1-phase is typified by the presence of Ki-67 in the nucleolus as well as numerous small foci within the nucleoplasm (Bridger, 1998). The amount of Ki-67 in the nucleoplasm decreases as cells progress through interphase (Bridger, 1998). Disruption of the nucleolus with 5,6-dichloro-1-β-D-ribofuranosylbenzimidazole increases nucleoplasmic levels of Ki-67, which associates with centromeres and regions of satellite DNA (Bridger, 1998). Increased nucleoplasmic levels of Ki-67 due to exposure of U2OS cells to F3 may therefore reflect disruption of the nucleolus and accumulation of cells in early G1-phase.

In summary, F3 has been shown to increase the size of the nucleolus. F3, IR, or F3 + IR reduced the level of NCL and NPM in the nucleoplasm and the nucleolus, and redistributed both proteins from the nucleolus to the nucleoplasm of U2OS cells. In contrast, F3 increased the level of Ki-67 in the nucleoplasm. Future research should focus on characterising the reorganisation of the nucleolar proteome after exposure of U2OS cells to F3.

Chapter 4. The radiotoxicity of ^{111}In-DTPA-F3

4.1. Introduction

In 2009, Drecoll *et al*. (2009) showed that a dimeric form of F3 radiolabelled with the alpha particle-emitter ^{213}Bi (^{213}Bi-DTPA-[F3]$_2$) reduced the survival of MDA-MB-435, MIAPACA, OVCAR-3, EMT-6 and CMT-93 cells (Drecoll*, et al.*, 2009). In SCID mice bearing MDA-MB-435-luc xenografts, ^{213}Bi-DTPA-[F3]$_2$ inhibited tumour growth and increased the mean survival time of the mice (Drecoll*, et al.*, 2009). Essler *et al*. (2012) also radiolabelled monomeric F3 with ^{213}Bi (^{213}Bi-DTPA-F3) and ^{225}Ac (^{225}Ac-DTPA-F3) and showed that ^{225}Ac-DOTA-F3 was approximately 1000 fold more radiotoxic to breast carcinoma (EMT6) cells than ^{213}Bi-DTPA-F3 (Essler*, et al.*, 2012). Interestingly, a 1000 fold greater concentration of radioactivity of ^{213}Bi-DTPA-F3 compared to ^{225}Ac-DOTA-F3 did not produce significantly different mean survival of SCID mice bearing MDA-MB-435-luc xenografts (Essler*, et al.*, 2012). Vallon *et al.* (2012) demonstrated that the efficacy of ^{213}Bi-DTPA-F3 on the survival of OVCAR-3 cells was enhanced when administered in combination with paclitaxel (60 ng/mL), except at the highest concentration of 750 kBq/ml (Vallon*, et al.*, 2012). The *in vitro* toxicity of ^{213}Bi-DTPA-F3 and paclitaxel translated into inhibition of tumour growth and extension of survival of SCID mice bearing OVCAR-3-luc xenografts (Vallon*, et al.*, 2012). Thus, F3 has been shown to be therapeutically effective when radiolabelled with ^{225}Ac and ^{213}Bi.

F3 has also been radiolabelled with the Auger electron-emitter ^{111}In. ^{111}In-labelled F3 (^{111}In-BnDTPA-F3) was reported in Cornelissen *et al*. (2012) to induce γH2AX foci in MDA-MB-231/H2N cells in a dose-dependent manner and also in a manner that is linearly dependent on specific activity (Spearman R = 0.99; P = 0.0028) (Cornelissen*,*

et al., 2012b). Exposure of MDA-MB-231/H2N cells to ^{111}In-BnDTPA-F3 reduced the clonogenic survival of MDA-MB-231/H2N cells *in vitro* ($P < 0.001$) (Cornelissen*, et al.*, 2012b). In athymic mice bearing MDA-MB-231/H2N xenografts, ^{111}In-BnDTPA-F3 significantly inhibited tumour growth ($P = 0.0073$) and produced a significant increase in survival ($P = 0.0174$). Thus, F3 peptide radiolabelled with ^{111}In has been shown to be an effective Auger electron-emitting radiotherapeutic agent.

The main aims of the work presented in this chapter were to investigate if F3 radiolabelled with ^{111}In (^{111}In-DTPA-F3) is significantly radiotoxic to a wide range of malignant cell lines. Following on from the work in Cornelissen *et al*. (2012b), which showed that ^{111}In-BnDTPA-F3 was more radiotoxic to MBA-MD-231/H2N cells compared to non-radiolabelled BnDTPA-F3 and ^{111}In chloride, it was hypothesised that ^{111}In-DTPA-F3 would be more radiotoxic compared to non-radioactive (DTPA, F3, DTPA-F3) and radioactive (^{111}In chloride, ^{111}In-DTPA, ^{111}In + F3) controls to a range of malignant cell lines. In order to demonstrate that to cause cell kill ^{111}In is required to be attached to F3, clonogenic survival assays were performed using a wide range of malignant cell lines. It was hypothesised that differences in the level of cell kill between different malignant cell lines that were produced by a similar concentration of ^{111}In-DTPA-F3 may be related to differences in the radiosensitivity of the malignant cell lines to external γ-radiation. To show if radiosensitivity to external γ-radiation determines the level of cell kill produced by ^{111}In-DTPA-F3, clonogenic assays and Spearman correlations were performed to assess if there was a correlation between the level of cell kill produced by ^{111}In-DTPA-F3 and the LD37 or the surviving fraction of a range of malignant cell lines following a range of doses of γ-radiation. It was also hypothesised that differences in the level of cell kill between different malignant cell lines that are produced by a similar concentration of ^{111}In-DTPA-F3 may be related to

the level of DNA double-strand breaks induced by a constant concentration of ^{111}In-DTPA-F3. To show if the level of DNA double-strand breaks induced by a constant concentration of ^{111}In-DTPA-F3 determines the level of cell kill produced by ^{111}In-DTPA-F3, γH2AX assays and Spearman correlations were performed to assess if there was a correlation between the level of cell kill produced by ^{111}In-DTPA-F3 and the level of γH2AX foci induced by ^{111}In-DTPA-F3 in a range of malignant cell lines.

4.2. Results

4.2.1. The radiosynthesis of ^{111}In-DTPA-F3

A simplified diagram of the radiosynthesis of ^{111}In-DTPA-F3 is shown in Figure 4.1. DTPA was conjugated to F3 peptide and the DTPA conjugation rate was determined. Figure 4.2.A shows the separation of DTPA-F3 from DTPA; the purity of the fractions was validated in Figure 4.2.B. The conjugation rate was 0.50±0.00 and the construct contained a ratio of DTPA-to-F3 of 0.75±0.00:1 (DTPA/F3 ratio). The mean molecular weight of DTPA-F3 was 3,700 Da. To radiolabel DTPA-F3, 22.17 MBq of ^{111}In chloride (in 0.02 M of H.Cl) was added per nmol of DTPA-F3, forming ^{111}In-DTPA-F3. Figure 4.3 shows the radiolabelling efficiency of ^{111}In-DTPA-F3 (97.1%), which was determined using instant thin layer chromatography.

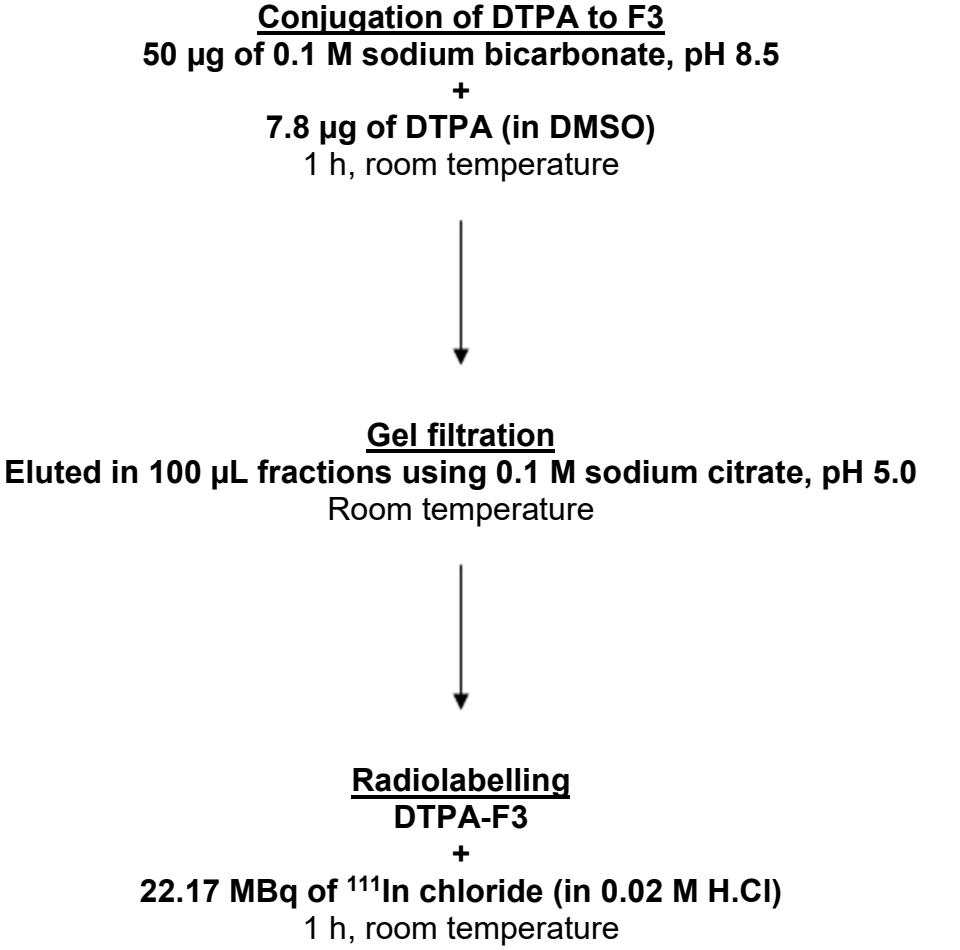

Figure 4.1. Diagram of the radiosynthesis of ^{111}In-DTPA-F3

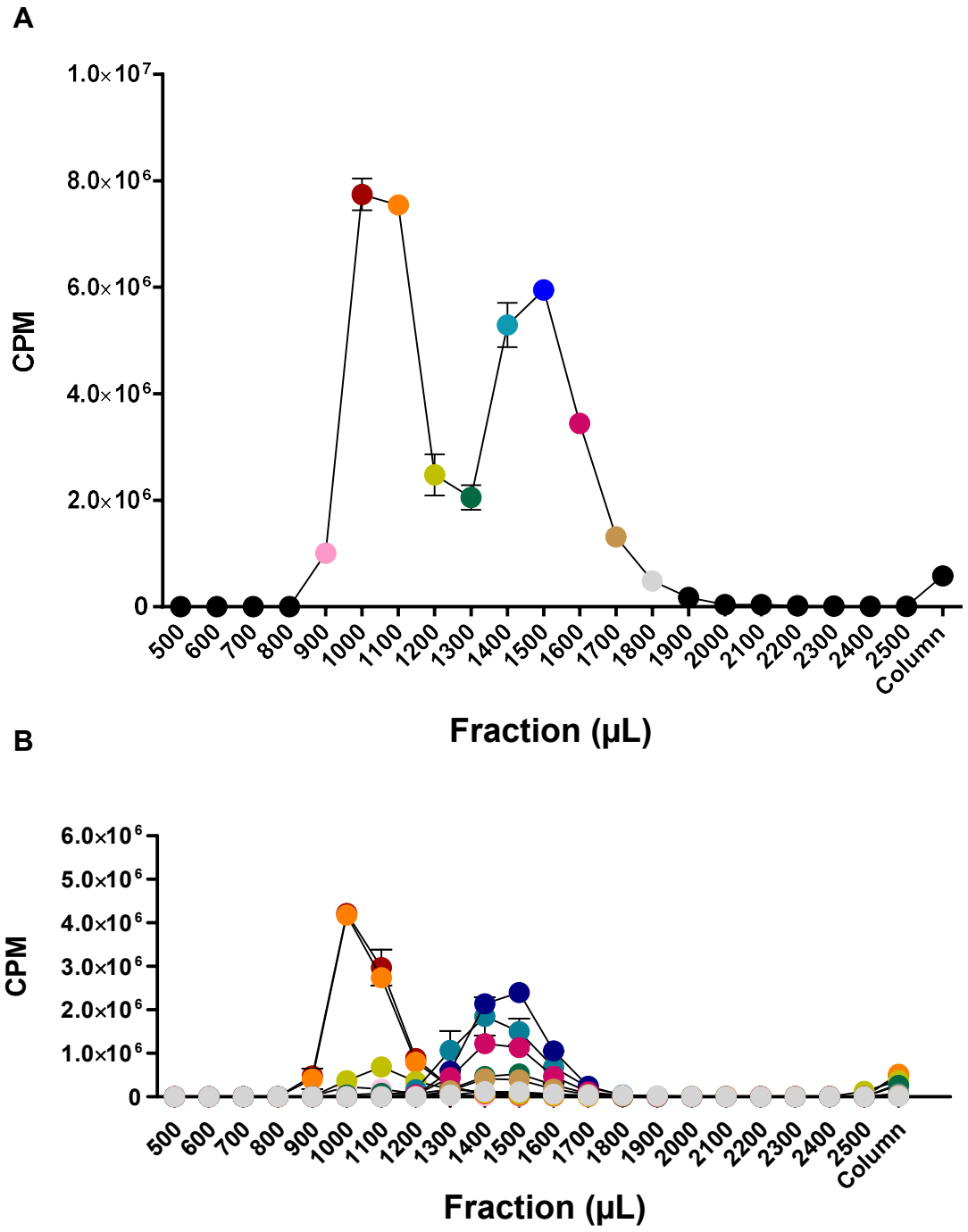

Figure 4.2. Separation of DTPA-F3 from DTPA

Gel filtration was used to separate ^{111}In-labelled DTPA-F3 (fractions 900–1200 µL) from ^{111}In-labelled DTPA (fractions 1300–2500 µL plus column). (B) Validation of the purity of fractions 900–1200 µL (^{111}In-DTPA-F3) versus fractions 1300–1800 µL (^{111}In-DTPA). The colour coding shown in (B) is used to identify fractions from (A). Values show mean ± SEM, n = 3. CPM, counts per minute.

Figure 4.3. Radiolabelling efficiency of ^{111}In-DTPA-F3

ITLC strips measured by autoradiography showing the displacement of (1) ^{111}In chloride and (2) ^{111}In-DTPA from the spotting site, while (3) ^{111}In-DTPA-F3 was retained at the spotting site (arrow) due to interaction between F3 and the ITLC strip. Values show radiolabelling efficiency (%).

4.2.2. The radiotoxicity of ^{111}In-DTPA-F3

To investigate the radiotoxicity of ^{111}In-DTPA-F3 on a wide range of malignant cell lines, clonogenic assays were used to determine the effect of ^{111}In-DTPA-F3 on the clonogenic survival of breast carcinoma (MCF7, MDA-MB-231/H2N), colon carcinoma (HCT116), melanoma (MDA-MB-435), non-small cell lung cancer (H322), and osteosarcoma (U2OS) cells. These cell lines were exposed for 3 h to 0.1 μM of ^{111}In-DTPA-F3 (22.17 MBq/nmol) or equimolar amounts of a complete set of controls, which included the chelator (DTPA), the vector (F3), the chelator attached to the vector (DTPA-F3), the radionuclide (^{111}In chloride), the radionuclide attached to the chelator (^{111}In-DTPA), and the radionuclide unattached to the vector (^{111}In chloride + F3). An untreated group was also included for comparison. The results from these experiments are shown in Figure 4.4 and Table 4.1 and they suggested that ^{111}In-DTPA-F3 was significantly radiotoxic to five malignant cell lines. In order of reducing radiosensitivity to ^{111}In-DTPA-F3 these were, MCF7, HCT116, MDA-MB-231/H2N, H322 and MDA-MB-435 cells. ^{111}In-DTPA-F3 was not significantly radiotoxic to U2OS cells.

The clonogenic survival of the MCF7 cells was significantly reduced on exposure to ^{111}In-DTPA-F3 compared to the untreated group ($P = 0.0085$) (Figure 4.4.A). The reduction in clonogenic survival that was caused by ^{111}In-DTPA-F3 was also significant in comparison to DTPA ($P = 0.0272$), F3 ($P = 0.0137$) and DTPA-F3 ($P = 0.0037$). The surviving fraction on exposure to ^{111}In chloride was significantly less than DTPA-F3 ($P = 0.0312$). However, none of the controls significantly reduced the survival of the MCF7 cells compared to the untreated group.

The clonogenic survival of the HCT116 cells was significantly reduced on exposure to ^{111}In-DTPA-F3 compared to the untreated group ($P = 0.0094$) (Figure 4.4.B). The

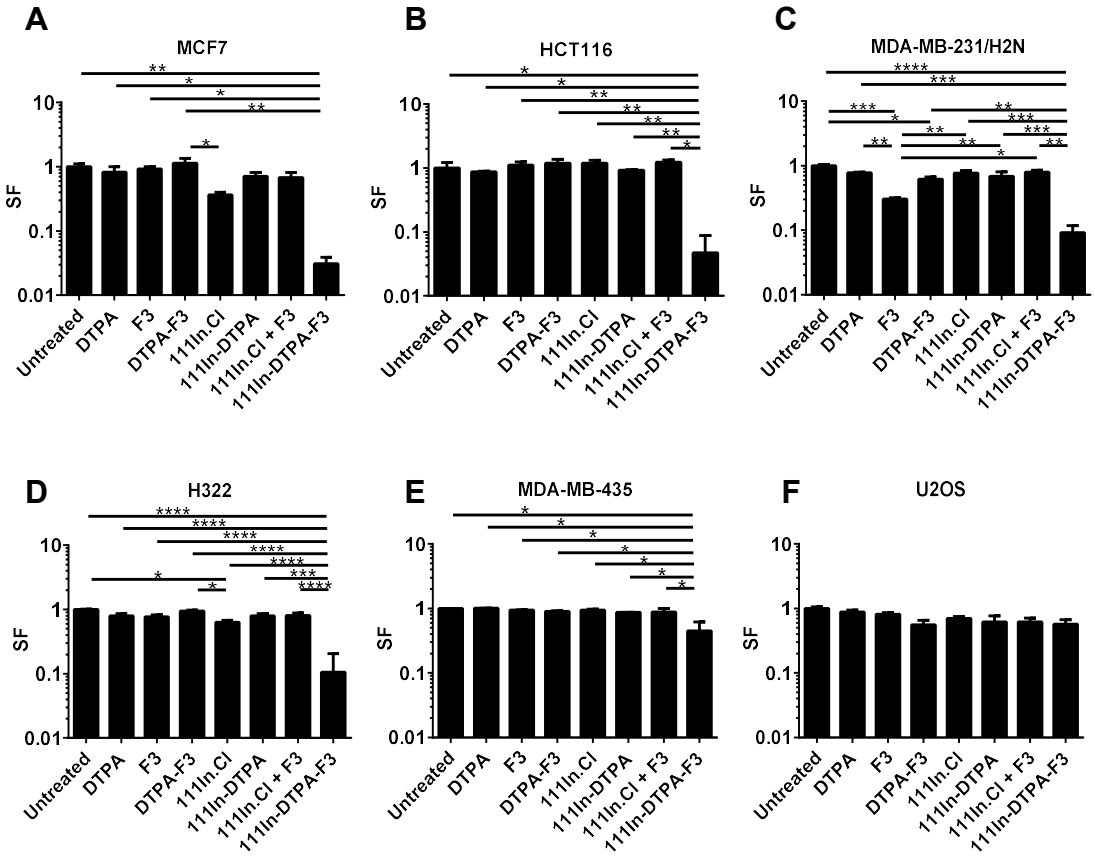

Figure 4.4. Clonogenic survival of malignant cells exposed to ^{111}In-DTPA-F3 or an equimolar control

Clonogenic survival of (A) MCF7, (B) HCT116, (C) MDA-MB-231/H2N, (D) H322, (E) MDA-MB-435, and (F) U2OS cells exposed for 3 h to 0.1 μM of ^{111}In-DTPA-F3 (22.17 MBq/nmol) or an equimolar control (^{111}In chloride + F3, ^{111}In-DTPA, ^{111}In chloride, DTPA-F3, F3 or DTPA), in comparison to an untreated group. Values show mean surviving fraction ± SEM, n = 2–3. SF, surviving fraction. GraphPad Prism 6 software was used to test if the data followed a Gaussian distribution using a D'Agostino-Pearson omnibus test. Despite the data not following a Gaussian distribution, means were compared using an ordinary one-way ANOVA comparing each mean with every other mean (Tukey; 95% confidence interval) with multiplicity adjusted P values (Tukey post-hoc test). This was because an ordinary one-way ANOVA is relatively robust for non-normal data and a non-parametric Kruskal-Wallis one-way ANOVA is not robust for small sample sizes of n < 7. *, P < 0.05, **, P < 0.01, ***, P < 0.001, ****, P < 0.0001.

	Untreated	DTPA	F3	DTPA-F3	^{111}In chloride	^{111}In-DTPA	^{111}In chloride + F3	^{111}In-DTPA-F3
MCF7	1.00±0.12	0.82±0.18	0.93±0.07	1.14±0.21	0.36±0.04	0.71±0.11	0.68±0.14	0.03±0.01
HCT116	1.00±0.22	0.87±0.03	1.11±0.13	1.19±0.17	1.19±0.14	0.92±0.02	1.23±0.10	0.05±0.04
MDA-MB-231/H2N	1.00±0.04	0.78±0.02	0.30±0.01	0.62±0.05	0.76±0.08	0.69±0.12	0.79±0.06	0.09±0.03
H322	1.00±0.01	0.80±0.06	0.77±0.06	0.95±0.04	0.64±0.05	0.80±0.07	0.81±0.07	0.11±0.10
MDA-MB-435	1.00±0.00	1.01±0.00	0.94±0.01	0.90±0.02	0.95±0.03	0.87±0.00	0.88±0.12	0.45±0.17
U2OS	1.00±0.06	0.88±0.07	0.82±0.04	0.56±0.09	0.70±0.05	0.62±0.14	0.62±0.09	0.57±0.10

Table 4.1. Surviving fraction of malignant cell lines exposed to ^{111}In-DTPA-F3 or an equimolar control

Clonogenic survival of MCF7, HCT116, MDA-MB-231/H2N, H322, MDA-MB-435, and U2OS cells exposed for 3 h to 0.1 μM of ^{111}In-DTPA-F3 (22.17 MBq/nmol) or an equimolar control (^{111}In chloride + F3, ^{111}In-DTPA, ^{111}In chloride, DTPA-F3, F3 or DTPA), in comparison to an untreated group. Values show mean surviving fraction ± SEM, n = 2–3.

reduction in clonogenic survival that was caused by ^{111}In-DTPA-F3 was also significant in comparison to DTPA (P = 0.0227), F3 (P = 0.0047), DTPA-F3 (P = 0.0029), ^{111}In chloride (P = 0.0031), ^{111}In-DTPA (P = 0.0159) and ^{111}In chloride + F3 (P = 0.0024). None of the controls produced surviving fractions that were significantly different from each other, nor did they significantly reduce the survival of the HCT116 cells compared to the untreated group.

The clonogenic survival of the MDA-MB-231/H2N cells was significantly reduced on exposure to ^{111}In-DTPA-F3 compared to the untreated group (P < 0.0001) (Figure 4.4.C). The reduction in clonogenic survival that was caused by ^{111}In-DTPA-F3 was also significant in comparison to DTPA (P = 0.0006), DTPA-F3 (P = 0.0036), ^{111}In chloride (P = 0.0007), ^{111}In-DTPA (P = 0.0016) and ^{111}In chloride + F3 (P = 0.0005). The surviving fraction on exposure to F3 was significantly less than DTPA (P = 0.0073), ^{111}In chloride (P = 0.0089), ^{111}In-DTPA (P = 0.0248) and ^{111}In chloride + F3 (P = 0.0060). However, none of the controls, with the exception of F3 (P = 0.006) and DTPA-F3 (P = 0.0271), significantly reduced the survival of the MDA-MB-231/H2N cells compared to the untreated group.

The clonogenic survival of the H322 cells was significantly reduced on exposure to ^{111}In-DTPA-F3 compared to the untreated group (P < 0.0001) (Figure 4.4.D). The reduction in clonogenic survival that was caused by ^{111}In-DTPA-F3 was also significant in comparison to DTPA (P < 0.0001), F3 (P < 0.0001), DTPA-F3 (P < 0.0001), ^{111}In chloride (P < 0.0001), ^{111}In-DTPA (P < 0.0001) and ^{111}In chloride + F3 (P < 0.0001). The surviving fraction on exposure to ^{111}In chloride was significantly less than DTPA-F3 (P = 0.0449) and the untreated group (P = 0.0138). Except for ^{111}In chloride, none of the controls produced surviving fractions that were significantly different from each

other, nor did they significantly reduce the survival of the H322 cells compared to the untreated group.

The clonogenic survival of the MDA-MB-435 cells was significantly reduced on exposure to ^{111}In-DTPA-F3 compared to the untreated group ($P = 0.0109$) (Figure 4.4.E). The reduction in clonogenic survival that was caused by ^{111}In-DTPA-F3 was also significant in comparison to DTPA ($P = 0.0100$), F3 ($P = 0.0214$), DTPA-F3 ($P = 0.0347$), ^{111}In chloride ($P = 0.0197$), ^{111}In-DTPA ($P = 0.0476$) and ^{111}In chloride + F3 ($P = 0.0412$). None of the controls produced surviving fractions that were significantly different from each other, nor did they significantly reduce the survival of the MDA-MB-435 cells compared to the untreated group.

Together, these results suggested that it was necessary for ^{111}In to be attached to the F3 to cause radiotoxicity to the HCT116, MCF7 and MDA-MB-435 cells. Although F3 and DTPA-F3 were slightly toxic to MDA-MB-231/H2N cells and ^{111}In chloride was slightly toxic to H322 cells, ^{111}In-DTPA-F3 still caused the greatest level of toxicity to both of these cell lines. Thus, ^{111}In-DTPA-F3 caused 17 fold, 12 fold, 3 fold, 6 fold, and 2 fold greater toxicity to the HCT116, MCF7, MDA-MB-231/H2N, H322, and MDA-MB-435 cells than the most toxic equimolar control that each cell line was exposed to, respectively.

In contrast, the clonogenic survival of the U2OS cells was not significantly reduced on exposure to ^{111}In-DTPA-F3 (Figure 4.4.F). None of the controls produced surviving fractions that were significantly different from each other, nor did they significantly reduce the survival of the U2OS cells compared to the untreated group. This suggested that, unlike the other malignant cell lines, the U2OS cells were not significantly radiosensitive to ^{111}In-DTPA-F3.

Thus, the significant effect of 0.1 μM of ^{111}In-DTPA-F3 (22.17 MBq/nmol) on the surviving fraction of the malignant cell lines was highly variable (19 fold range in surviving fraction) and produced levels of cell kill for MCF7, HCT116, MDA-MB-231/H2N, H322, MDA-MB-435 and U2OS cells of 97%, 95%, 91%, 89%, 55% and 43%, respectively.

4.2.3. No correlation between the radiotoxicity of ^{111}In-DTPA-F3 and cellular radiosensitivity to external γ-radiation

Clonogenic assays revealed that ^{111}In-DTPA-F3 produced variable levels of cell kill (19 fold range in surviving fraction) of MCF7, HCT116, MDA-MB-231/H2N, H322, MDA-MB-435 and U2OS cells. The range in the level of cell kill produced by ^{111}In-DTPA-F3 may have been related to differences in the cellular radiosensitivity of each malignant cell line to ionising radiation. It was therefore hypothesised that the range in the level of cell kill produced by ^{111}In-DTPA-F3 may correlate with differences in cellular radiosensitivity to external γ-radiation.

To compare the level of cell kill produced by ^{111}In-DTPA-F3 to cellular radiosensitivity to external γ-radiation, clonogenic assays exposing MCF7, HCT116, MDA-MB-231/H2N, H322, MDA-MB-435 and U2OS cells to a range of doses from 0 to 10 Gy of γ-rays (^{137}Cs irradiator) were used to produce linear quadratic survival curves to determine cellular radiosensitivity to external γ-radiation (Figure 4.5.A–F). In order of descending radiosensitivity, the LD_{37} (the dose of external γ-radiation in Gy that resulted in a surviving fraction of 0.37) for the HCT116, MCF7, MDA-MB-435, U2OS, MDA-MB-231/H2N, and H322 cell lines was 2.43, 2.89, 4.36, 4.44, 4.58 and 5.49 Gy,

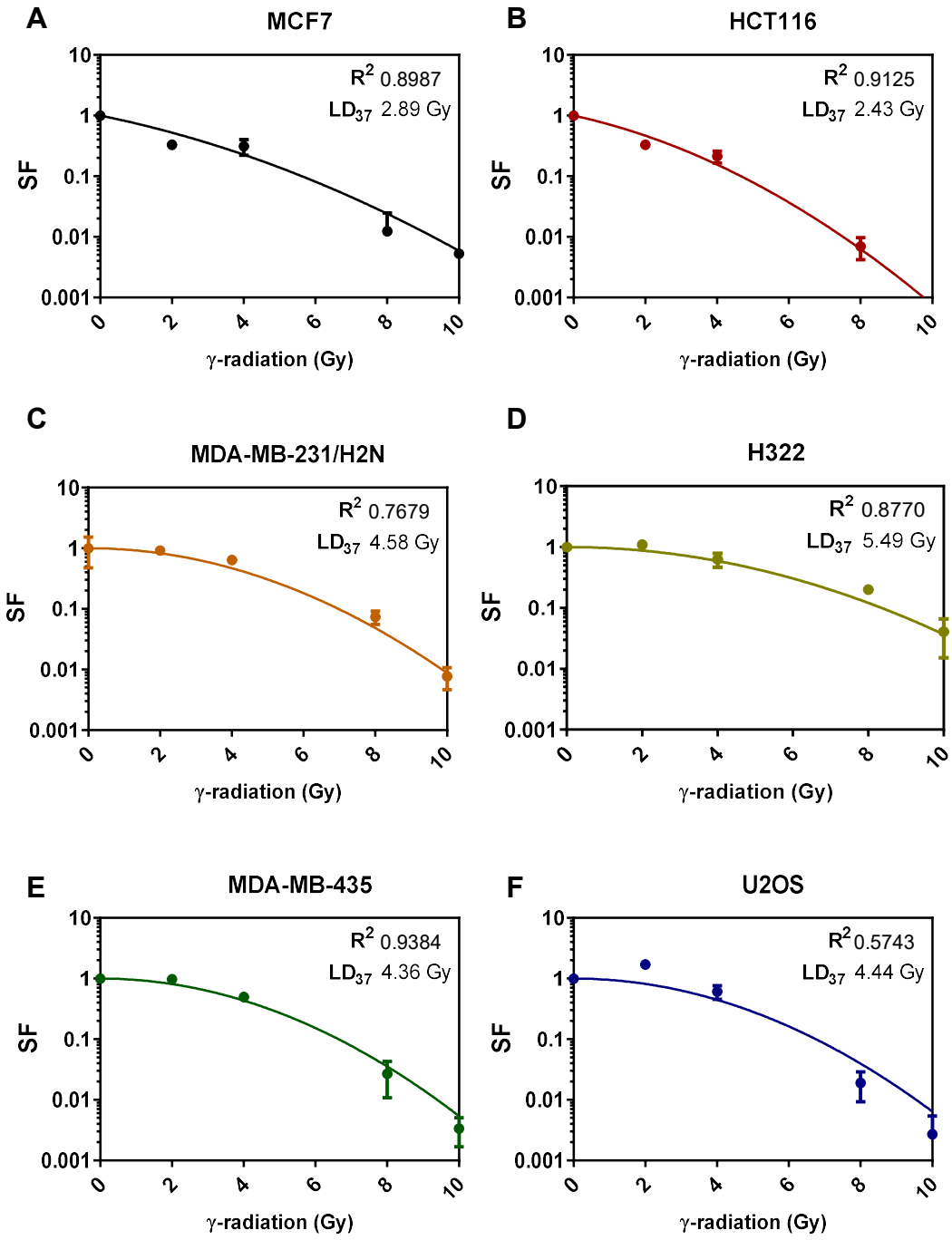

Figure 4.5. Cellular radiosensitivity of malignant cells to external γ-radiation

Linear quadratic survival curves for (A) MCF7, (B) HCT116, (C) MDA-MB-231/H2N, (D) H322, (E) MDA-B-435 and (F) U2OS. Values show mean surviving fraction ± SEM, n = 3. SF, surviving fraction. GraphPad Prism 6 software was used to fit a linear quadratic curve (to a surviving fraction which was transformed by taking the natural log of the surviving fraction): Y=Exp(-{a*X+b*X^2}), where Y is the surviving fraction, X is the dose in Gy, a is the α component and b is the β component of cell kill. Then, a and b values were used to fit a linear quadratic curve to the non-transformed data for surviving fraction (shown). A D'Agostino-Pearson omnibus test found that the residuals of the linear quadratic curves followed a Gaussian distribution. The R^2 for the linear quadratic curve and the LD_{37} are also shown.

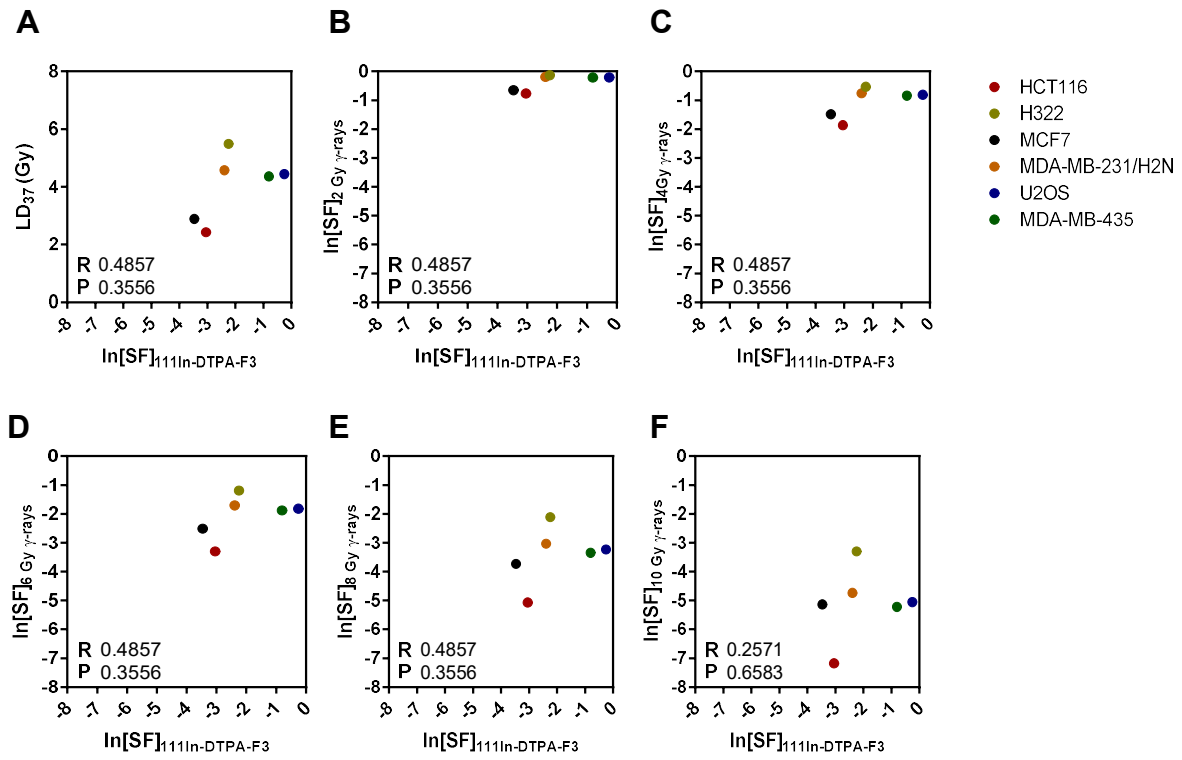

Figure 4.6. No correlation between the level of cell kill produced by ^{111}In-DTPA-F3 and cellular radiosensitivity to external γ-radiation

(A) Scatterplot showing the ln[SF]$_{^{111}\text{In-DTPA-F3}}$ (natural log of the surviving fraction due to a 3 h exposure to 0.1 μM of ^{111}In-DTPA-F3 (22.17 MBq/nmol)) on the *x axis* (values show mean, n = 2–3) against the LD_{37} for external γ-radiation on the *y axis* (LD_{37} calculated from linear quadratic curves from Figure 4.2). (B–F) Scatterplots showing the ln[SF]$_{^{111}\text{In-DTPA-F3}}$ (natural log of the surviving fraction due to a 3 h exposure to 0.1 μM of ^{111}In-DTPA-F3 (22.17 MBq/nmol)) on the *x axis* (values show mean, n = 2–3) against the ln[SF]$_{2/4/6/8/10\ \text{Gy γ-rays}}$ (natural log of the surviving fraction due to exposure to (B) 2, (C) 4, (D) 6, (E) 8 or (F) 10 Gy of external γ-radiation) on the *y axis* (SF calculated from linear quadratic curves from Figure 4.2). GraphPad Prism 6 software was used to test if the data followed a Gaussian distribution using a D'Agostino-Pearson omnibus test. Since the data did not follow a Gaussian distribution, a nonparametric Spearman correlation (95% confidence interval) with two-tailed P values (shown) was used. R, Spearman R.

respectively. This suggested that cellular radiosensitivity as measured by the LD_{37} to external γ-radiation ranged 2.3 fold.

To assess whether there was a correlation between the level of cell kill produced by ^{111}In-DTPA-F3 and cellular radiosensitivity to external γ-radiation, scatterplots were produced showing the natural logarithm of the surviving fraction after exposure to ^{111}In-DTPA-F3 on the *x axis* against either the LD_{37} for external γ-radiation or the natural logarithm of the surviving fraction after exposure to a range of doses of external γ-radiation on the *y axis* (Figure 4.6.A–F). Non-parametric Spearman correlations showed that there was no correlation between surviving fraction after exposure to ^{111}In-DTPA-F3 and the LD_{37} for external γ-radiation (Spearman R, 0.4857; P, 0.3556). There was also no correlation between surviving fraction after exposure to ^{111}In-DTPA-F3 and surviving fraction after exposure to 2 (Spearman R, 0.4857; P, 0.3556), 4 (Spearman R, 0.4857; P, 0.3556), 6 (Spearman R, 0.4857; P, 0.3556), 8 (Spearman R, 0.4857; P, 0.3556) or 10 (Spearman R, 0.2571; P, 0.6583) Gy of external γ-radiation. Together, this suggested that the level of cell kill produced by ^{111}In-DTPA-F3 was not related to differences in cellular radiosensitivity to external γ-radiation.

4.2.4. No correlation between the level of cell kill produced by ^{111}In-DTPA-F3 and the induction of γH2AX by ^{111}In-DTPA-F3

To determine whether ^{111}In-DTPA-F3 causes the formation of γH2AX foci, malignant cell lines were exposed to ^{111}In-DTPA-F3 or a control lacking F3 (^{111}In-DTPA). MDA-MB-435, U2OS, MDA-MB-231/H2N, HCT116 and MCF7 cells were exposed to 1 μM of ^{111}In-DTPA-F3 (22.17 MBq/nmol) or an equimolar amount of ^{111}In-DTPA for 0, 3 or 6 h. After fixation, cells were immunochemically stained for γH2AX and γH2AX foci were quantified (Figure 4.7 shows a schematic of the detection and quantification of

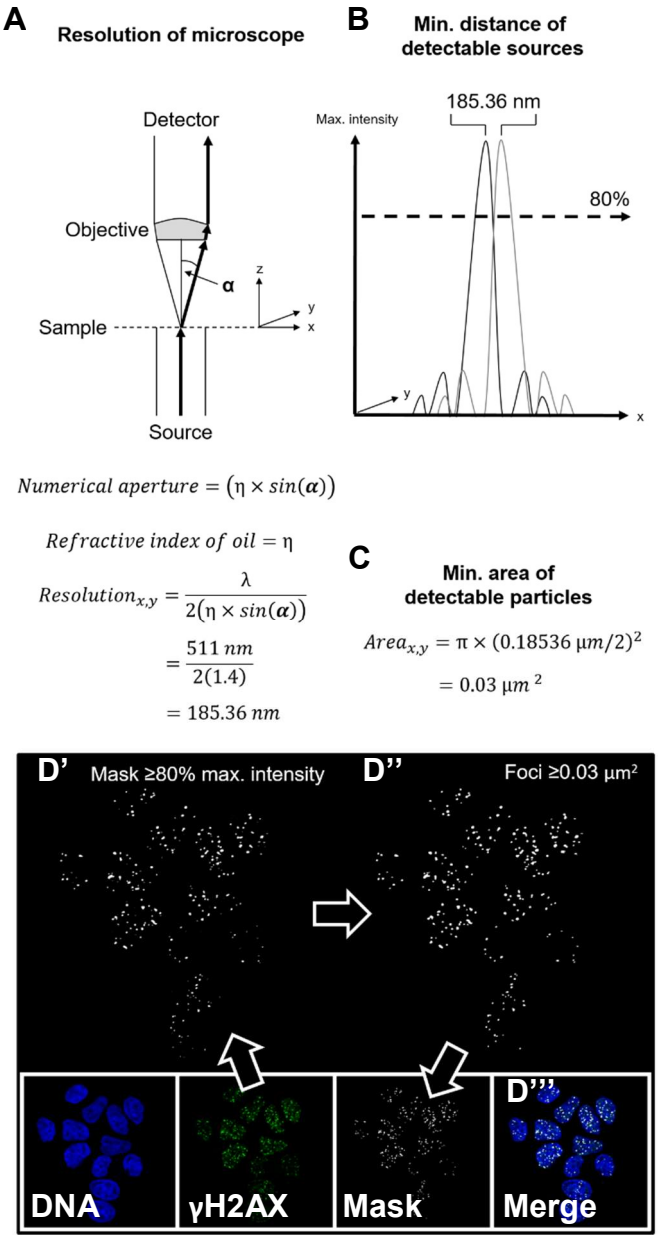

Figure 4.7. Schematic of the quantification of γH2AX foci

Only γH2AX foci with an area of ≥0.03 µm² were quantified. (A) The resolution$_{x,y}$ of the 63x objective determined the distance (185 nm) at which separate sources of light could be detected by the confocal microscope. (B) At 185 nm apart, two airy discs are indistinguishable below ~80% maximum intensity, since at this intensity the valley between the two airy discs meets. (C) Because the radius of the airy discs at 80% maximum intensity is also 185 nm, the minimum detectable area of γH2AX foci was calculated to be 0.03 µm². Thus, (D') a mask with 80% threshold (showing γH2AX foci as maxima) was created from an image of immunochemically stained γH2AX; (D'') foci <0.03 µm² were excluded from the mask; and (D''') the number of γH2AX foci (or maxima) per cell was counted using the merged image.

γH2AX foci). Figures 4.8–4.12 show the results from the fluorescence imaging experiments in which exposure of the malignant cell lines to ^{111}In-DTPA-F3 induced more γH2AX foci compared to ^{111}In-DTPA.

MDA-MB-435 cells contained basal levels of γH2AX foci that increased following exposure to ^{111}In-DTPA-F3 and ^{111}In-DTPA (Figure 4.8.A). The absolute number of γH2AX foci per cell after a 3 or 6 h exposure to ^{111}In-DTPA-F3 versus ^{111}In-DTPA was 8.31±0.81 versus 5.38±0.50 (P = 0.0113) and 15.82±1.43 versus 9.30±0.89 (P = 0.0004) foci per cell, respectively (Figure 4.8.B). The number of additional γH2AX foci over the basal levels after a 3 or 6 h exposure to ^{111}In-DTPA-F3 versus ^{111}In-DTPA (i.e. the number of foci counted at 3 or 6 h minus the number of foci counted at 0 h) was 1.27±0.81 versus 0.22±0.50 and 8.78±1.41 versus 4.14±0.89 (P = 0.0029) foci per cell, respectively (Figure 4.8.C).

U2OS cells contained basal levels of γH2AX foci that increased following exposure to ^{111}In-DTPA-F3 and ^{111}In-DTPA (Figure 4.9.A). The absolute number of γH2AX foci per cell after a 3 or 6 h exposure to ^{111}In-DTPA-F3 versus ^{111}In-DTPA was 14.07±1.38 versus 10.12±0.91 (P = 0.0098) and 20.33±1.37 versus 15.34±0.95 (P = 0.0061) foci per cell, respectively (Figure 4.9.B). The number of additional γH2AX foci after a 3 or 6 h exposure to ^{111}In-DTPA-F3 versus ^{111}In-DTPA was 14.07±1.38 versus 10.00±0.91 (P = 0.0061) and 20.33±1.37 versus 13.53±1.27 (P = 0.0026) foci per cell, respectively (Figure 4.9.C).

MDA-MB-231/H2N cells contained basal levels of γH2AX foci that increased following exposure to ^{111}In-DTPA-F3 and ^{111}In-DTPA (Figure 4.10.A). The absolute number of γH2AX foci per cell after a 3 or 6 h exposure to ^{111}In-DTPA-F3 versus ^{111}In-DTPA was 11.45±1.30 versus 5.98±0.63 (P < 0.0001) and 10.44±0.74 versus 8.84±0.70 foci per cell, respectively (Figure 4.10.B). The number of additional γH2AX foci after a 3 or 6

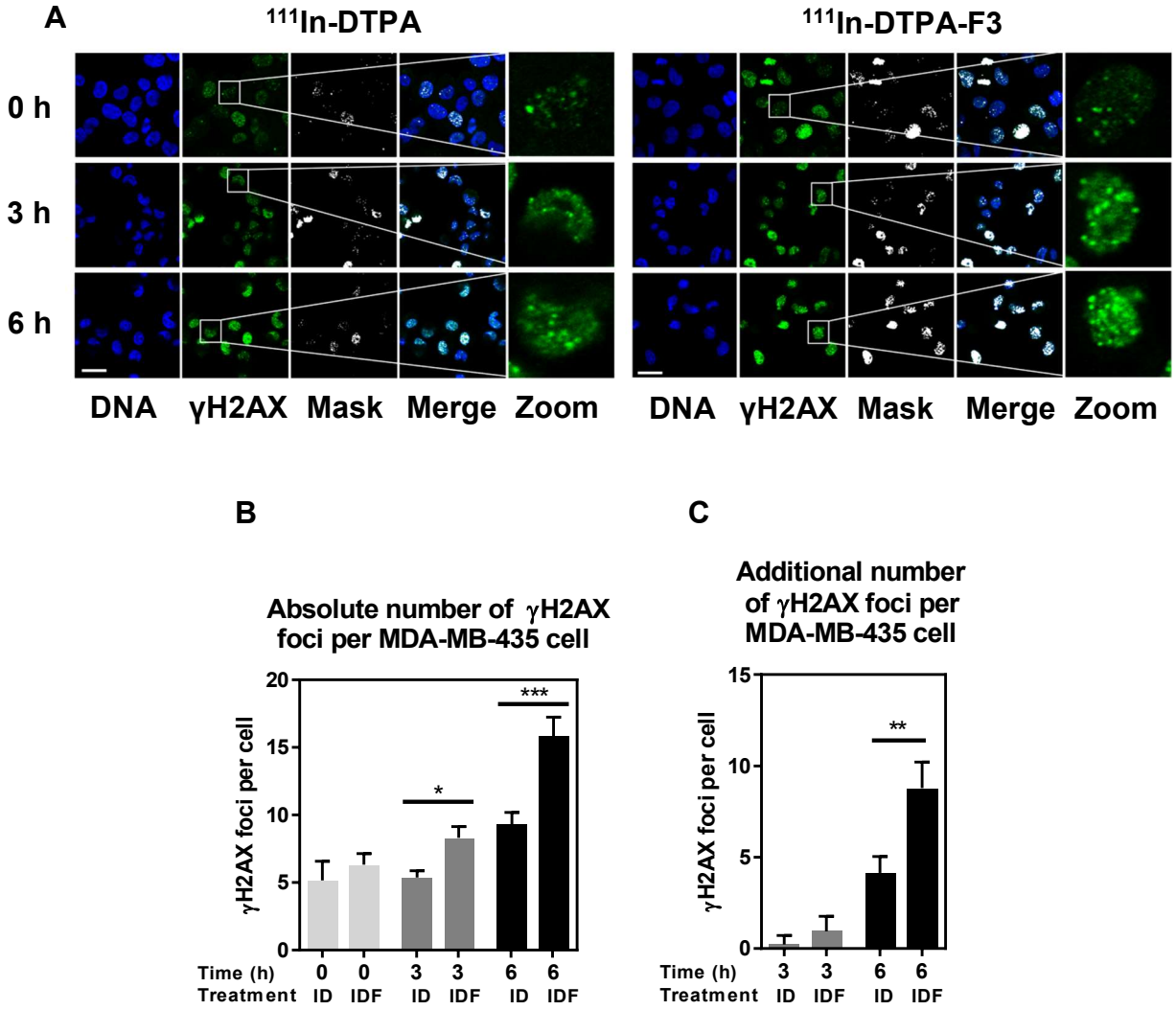

Figure 4.8. Levels of γH2AX foci per MDA-MB-435 cell after exposure to ^{111}In-DTPA-F3 or ^{111}In-DTPA

(A) Fluorescence images of immunocytochemically stained γH2AX in MDA-MB-435 cells exposed to ^{111}In-DTPA versus ^{111}In-DTPA-F3 for 0, 3, or 6 h. Scale, 20 μm. Quantification of (B) the absolute number of γH2AX foci per cell at 0, 3, or 6 h after exposure to ^{111}In-DTPA versus ^{111}In-DTPA-F3, or (C) the additional number of γH2AX foci per cell at 0, 3, or 6 h after exposure to ^{111}In-DTPA versus ^{111}In-DTPA-F3. ID, ^{111}In-DTPA. IDF, ^{111}In-DTPA-F3. Values show mean foci per cell ± SEM, n = 17–50. GraphPad Prism 6 software was used to test if the data followed a Gaussian distribution using a D'Agostino-Pearson omnibus test. Since the data did not follow a Gaussian distribution, differences between means for ^{111}In-DTPA versus ^{111}In-DTPA-F3 were compared at each time point using unpaired Mann-Whitney tests (95% confidence interval) with two-tailed P values. *, $P < 0.05$; **, $P < 0.01$; ***, $P < 0.001$.

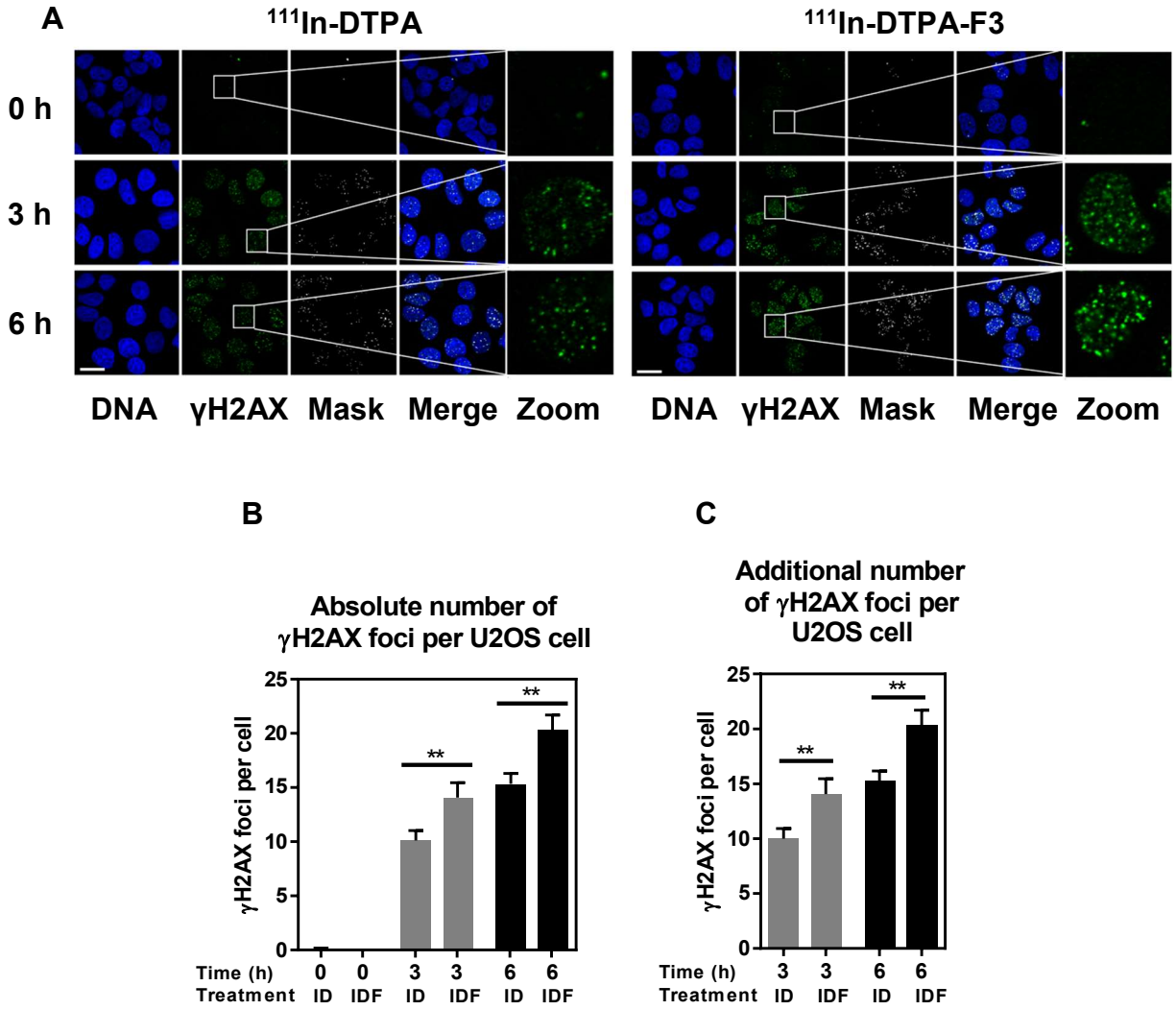

Figure 4.9. Levels of γH2AX foci per U2OS cell after exposure to ^{111}In-DTPA-F3 or ^{111}In-DTPA

(A) Fluorescence images of immunocytochemically stained γH2AX in U2OS cells exposed to ^{111}In-DTPA versus ^{111}In-DTPA-F3 for 0, 3, or 6 h. Scale, 20 μm. Quantification of (B) the absolute number of γH2AX foci per cell at 0, 3, or 6 h after exposure to ^{111}In-DTPA versus ^{111}In-DTPA-F3, or (C) the additional number of γH2AX foci per cell at 0, 3, or 6 h after exposure to ^{111}In-DTPA versus ^{111}In-DTPA-F3. ID, ^{111}In-DTPA. IDF, ^{111}In-DTPA-F3. Values show mean foci per cell ± SEM, n = 25–50. GraphPad Prism 6 software was used to test if the data followed a Gaussian distribution using a D'Agostino-Pearson omnibus test. Since the data did not follow a Gaussian distribution, differences between means for ^{111}In-DTPA versus ^{111}In-DTPA-F3 were compared at each time point using unpaired Mann-Whitney tests (95% confidence interval) with two-tailed P values. **, $P < 0.01$.

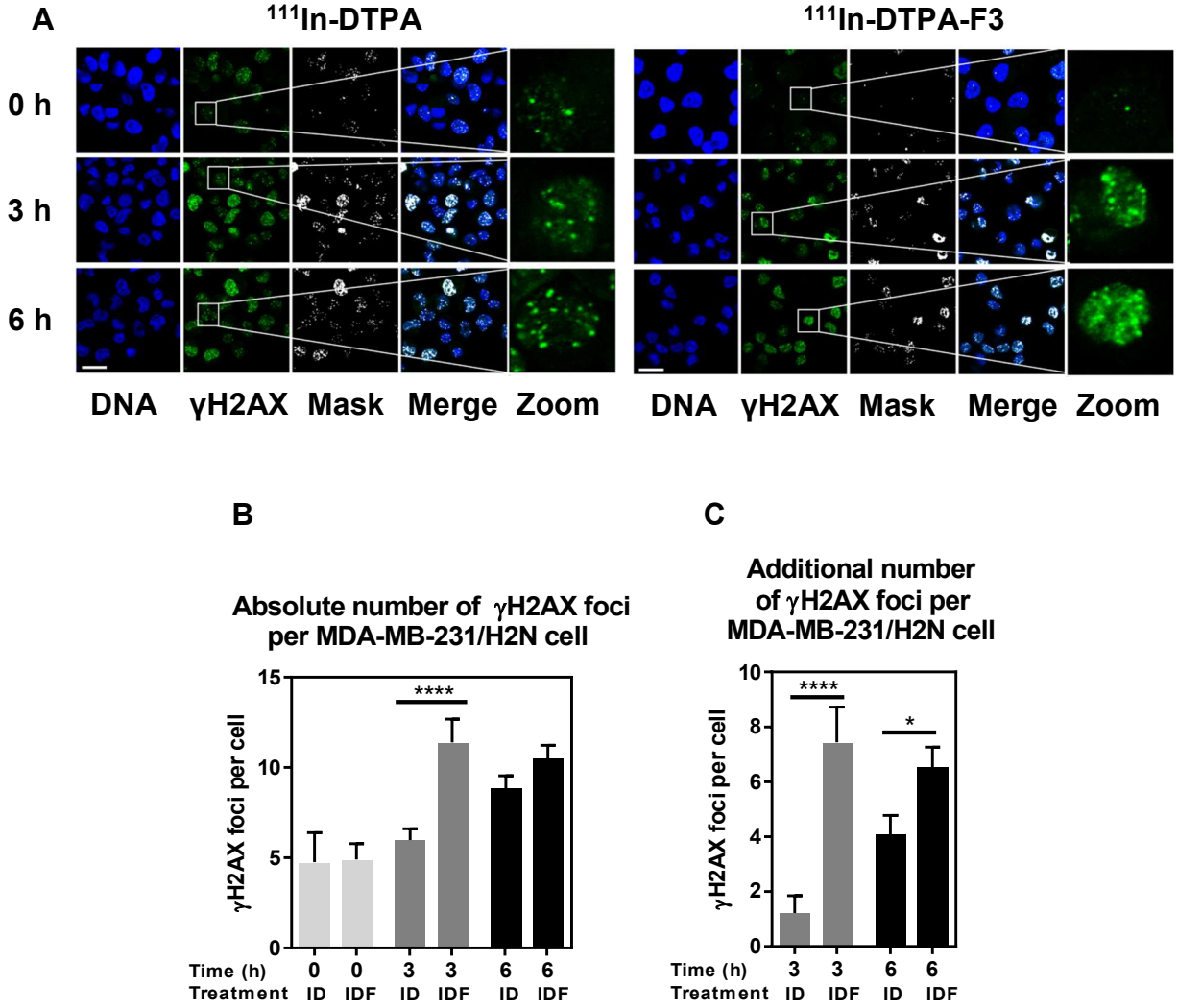

Figure 4.10. Levels of γH2AX foci per MDA-MB-231/H2N cell after exposure to ^{111}In-DTPA-F3 or ^{111}In-DTPA

(A) Fluorescence images of immunocytochemically stained γH2AX in MDA-MB-231/H2N cells exposed to ^{111}In-DTPA versus ^{111}In-DTPA-F3 for 0, 3, or 6 h. Scale, 20 μm. Quantification of (B) the absolute number of γH2AX foci per cell at 0, 3, or 6 h after exposure to ^{111}In-DTPA versus ^{111}In-DTPA-F3, or (C) the additional number of γH2AX foci per cell at 0, 3, or 6 h after exposure to ^{111}In-DTPA versus ^{111}In-DTPA-F3. ID, ^{111}In-DTPA. IDF, ^{111}In-DTPA-F3. Values show mean foci per cell ± SEM, n = 25–50. GraphPad Prism 6 software was used to test if the data followed a Gaussian distribution using a D'Agostino-Pearson omnibus test. Since the data did not follow a Gaussian distribution, differences between means for ^{111}In-DTPA versus ^{111}In-DTPA-F3 were compared at each time point using unpaired Mann-Whitney tests (95% confidence interval) with two-tailed P values. *, $P < 0.05$; ****, $P < 0.0001$.

h exposure to ^{111}In-DTPA-F3 versus ^{111}In-DTPA was 7.49±1.30 versus 1.10±0.69 ($P < 0.0001$) and 6.48±0.74 versus 3.99±0.71 ($P = 0.0275$) foci per cell, respectively (Figure 4.10.C).

HCT116 cells contained basal levels of γH2AX foci that increased following exposure to ^{111}In-DTPA-F3 and ^{111}In-DTPA (Figure 4.11.A). The absolute number of γH2AX foci per cell after a 3 or 6 h exposure to ^{111}In-DTPA-F3 versus ^{111}In-DTPA was 10.09±1.09 versus 6.60±0.95 ($P = 0.0123$) and 10.48±0.72 versus 9.78±0.70 foci per cell, respectively (Figure 4.11.B). The number of additional γH2AX foci after a 3 or 6 h exposure to ^{111}In-DTPA- F3 versus ^{111}In-DTPA was 8.61±1.09 versus 4.28±0.95 ($P = 0.0013$) and 9.00±0.72 versus 7.46±0.70 foci per cell, respectively (Figure 4.11.C).

MCF7 cells contained basal levels of γH2AX foci that were increased following exposure to ^{111}In-DTPA-F3 and ^{111}In-DTPA (Figure 4.12.A). The absolute number of γH2AX foci per cell after a 3 or 6 h exposure to ^{111}In-DTPA-F3 versus ^{111}In-DTPA was 13.50±1.32 versus 11.88±1.32 and 17.13±1.41 versus 12.18±1.22 ($P = 0.0206$) foci per cell, respectively (Figure 4.12.B). The number of additional γH2AX foci after a 3 or 6 h exposure to ^{111}In-DTPA-F3 versus ^{111}In-DTPA was 12.94±1.32 versus 11.78±1.22 and 16.57±1.41 versus 11.48±1.32 ($P = 0.0424$) foci per cell, respectively (Figure 4.12.C).

The absolute number of γH2AX foci per cell at 3 h exposure of MDA-MB-435 ($P = 0.0113$), U2OS ($P = 0.0098$), MDA-MB-231/H2N ($P < 0.0001$) and HCT116 ($P = 0.0123$) cells to ^{111}In-DTPA-F3 was significantly greater than ^{111}In-DTPA. For MDA-MB-435 ($P = 0.0004$), and U2OS ($P = 0.0061$) cells, the absolute number of γH2AX foci per cell after exposure to ^{111}In-DTPA-F3 was also significantly greater than ^{111}In-DTPA at 6 h. The absolute number of γH2AX foci per MCF7 cell after exposure to ^{111}In-DTPA-F3 became significantly greater than ^{111}In-DTPA at 6 h ($P = 0.0206$).

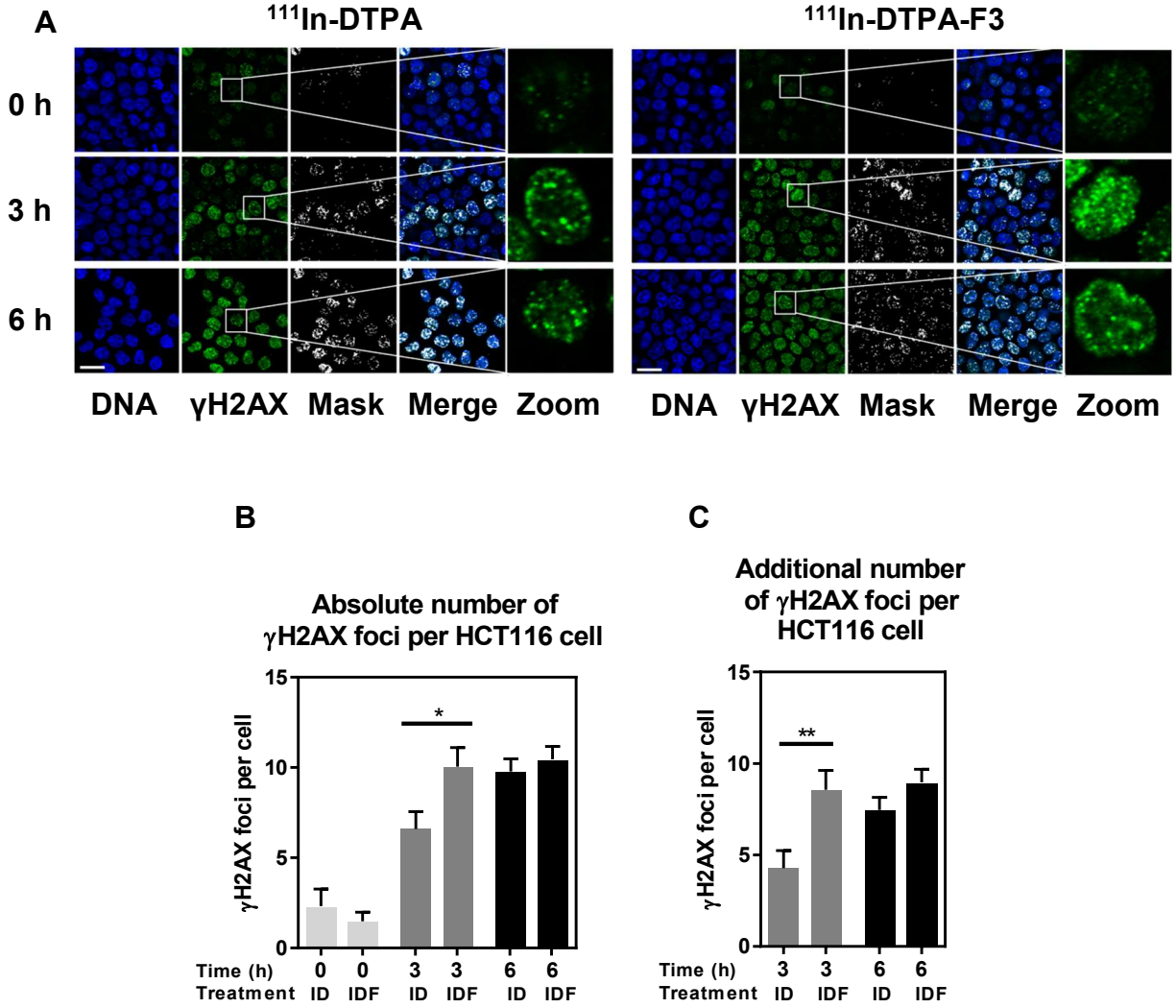

Figure 4.11. Levels of γH2AX foci per HCT116 cell after exposure to ^{111}In-DTPA-F3 or ^{111}In-DTPA

(A) Fluorescence images of immunocytochemically stained γH2AX in HCT116 cells exposed to ^{111}In-DTPA versus ^{111}In-DTPA-F3 for 0, 3, or 6 h. Scale, 20 μm. Quantification of (B) the absolute number of γH2AX foci per cell at 0, 3, or 6 h after exposure to ^{111}In-DTPA versus ^{111}In-DTPA-F3, or (C) the additional number of γH2AX foci per cell at 0, 3, or 6 h after exposure to ^{111}In-DTPA versus ^{111}In-DTPA-F3. ID, ^{111}In-DTPA. IDF, ^{111}In-DTPA-F3. Values show mean foci per cell ± SEM, n = 25–50. GraphPad Prism 6 software was used to test if the data followed a Gaussian distribution using a D'Agostino-Pearson omnibus test. Since the data did not follow a Gaussian distribution, differences between means for ^{111}In-DTPA versus ^{111}In-DTPA-F3 were compared at each time point using unpaired Mann-Whitney tests (95% confidence interval) with two-tailed P values. *, $P < 0.05$; **, $P < 0.01$.

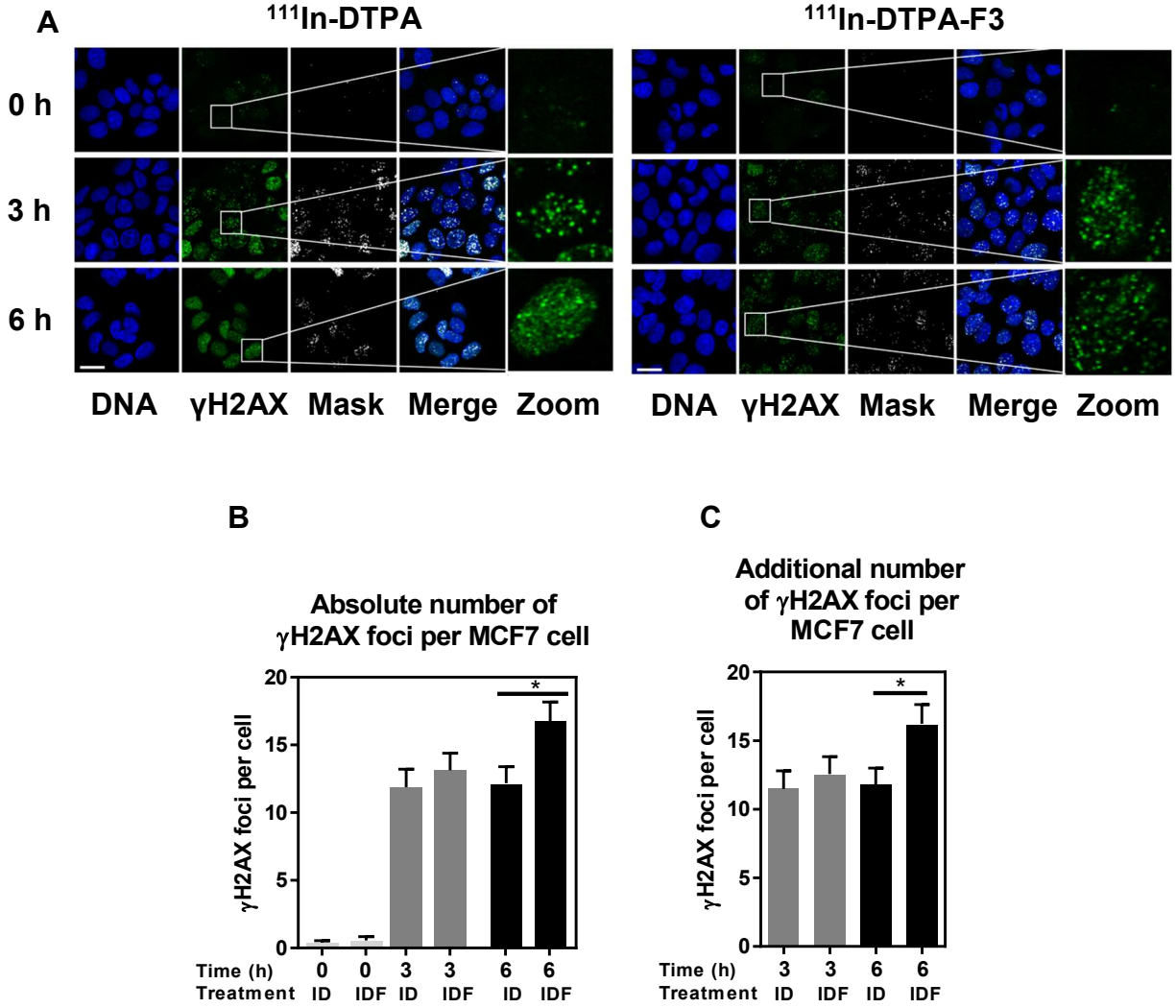

Figure 4.12. Levels of γH2AX foci per MCF7 cell after exposure to ^{111}In-DTPA-F3 or ^{111}In-DTPA

(A) Fluorescence images of immunocytochemically stained γH2AX in MCF7 cells exposed to ^{111}In-DTPA versus ^{111}In-DTPA-F3 for 0, 3, or 6 h. Scale, 20 μm. Quantification of (B) the absolute number of γH2AX foci per cell at 0, 3, or 6 h after exposure to ^{111}In-DTPA versus ^{111}In-DTPA-F3, or (C) the additional number of γH2AX foci per cell at 0, 3, or 6 h after exposure to ^{111}In-DTPA versus ^{111}In-DTPA-F3. ID, ^{111}In-DTPA. IDF, ^{111}In-DTPA-F3. Values show mean foci per cell ± SEM, n = 25–50. GraphPad Prism 6 software was used to test if the data followed a Gaussian distribution using a D'Agostino-Pearson omnibus test. Since the data did not follow a Gaussian distribution, differences between means for ^{111}In-DTPA versus ^{111}In-DTPA-F3 were compared at each time point using unpaired Mann-Whitney tests (95% confidence interval) with two-tailed P values. *, $P < 0.05$.

In comparison, the additional number of γH2AX foci per cell at 3 h exposure of U2OS ($P = 0.0061$), MDA-MB-231/H2N ($P < 0.0001$) and HCT116 ($P = 0.0030$) cells to ^{111}In-DTPA-F3 was significantly greater than ^{111}In-DTPA. For U2OS ($P = 0.0026$) and MDA-MB-231/H2N ($P = 0.0275$) cells, the number of additional γH2AX foci per cell after exposure to ^{111}In-DTPA-F3 was also significantly greater than ^{111}In-DTPA at 6 h. The absolute number of γH2AX foci per cell after exposure to ^{111}In-DTPA-F3 became significantly greater than ^{111}In-DTPA for MDA-MB-435 ($P = 0.0029$) and MCF7 ($P = 0.0424$) cells at 6 h.

To assess whether there was a correlation between the level of cell kill produced by ^{111}In-DTPA-F3 and the induction of γH2AX foci by ^{111}In-DTPA-F3, scatterplots were produced showing the natural logarithm of the surviving fraction after exposure to ^{111}In-DTPA-F3 on the *x axis* against the absolute number of γH2AX foci or additional number of γH2AX foci on the *y axis* (Figure 4.13.A–D). Non-parametric Spearman correlations showed that there was no correlation between surviving fraction after 3 h exposure to ^{111}In-DTPA-F3 and the absolute number of γH2AX foci at 3 h (Spearman R, 0.1000; P, 0.9500) or 6 h (Spearman R, 0.3000; P, 0.6833) after exposure to ^{111}In-DTPA-F3. Similarly, non-parametric Spearman correlations showed that there was no correlation between surviving fraction after 3 h exposure to ^{111}In-DTPA-F3 and the additional number of γH2AX foci at 3 h (Spearman R, 0.0; P, > 0.9999) or 6 h (Spearman R, 0.1000; P, 0.9500) after exposure to ^{111}In-DTPA-F3.

4.3. Discussion

In this Chapter, ^{111}In-DTPA-F3 was successfully radiosynthesised and the radiotoxicity of ^{111}In-DTPA-F3 was investigated using a wide range of malignant cell lines. The

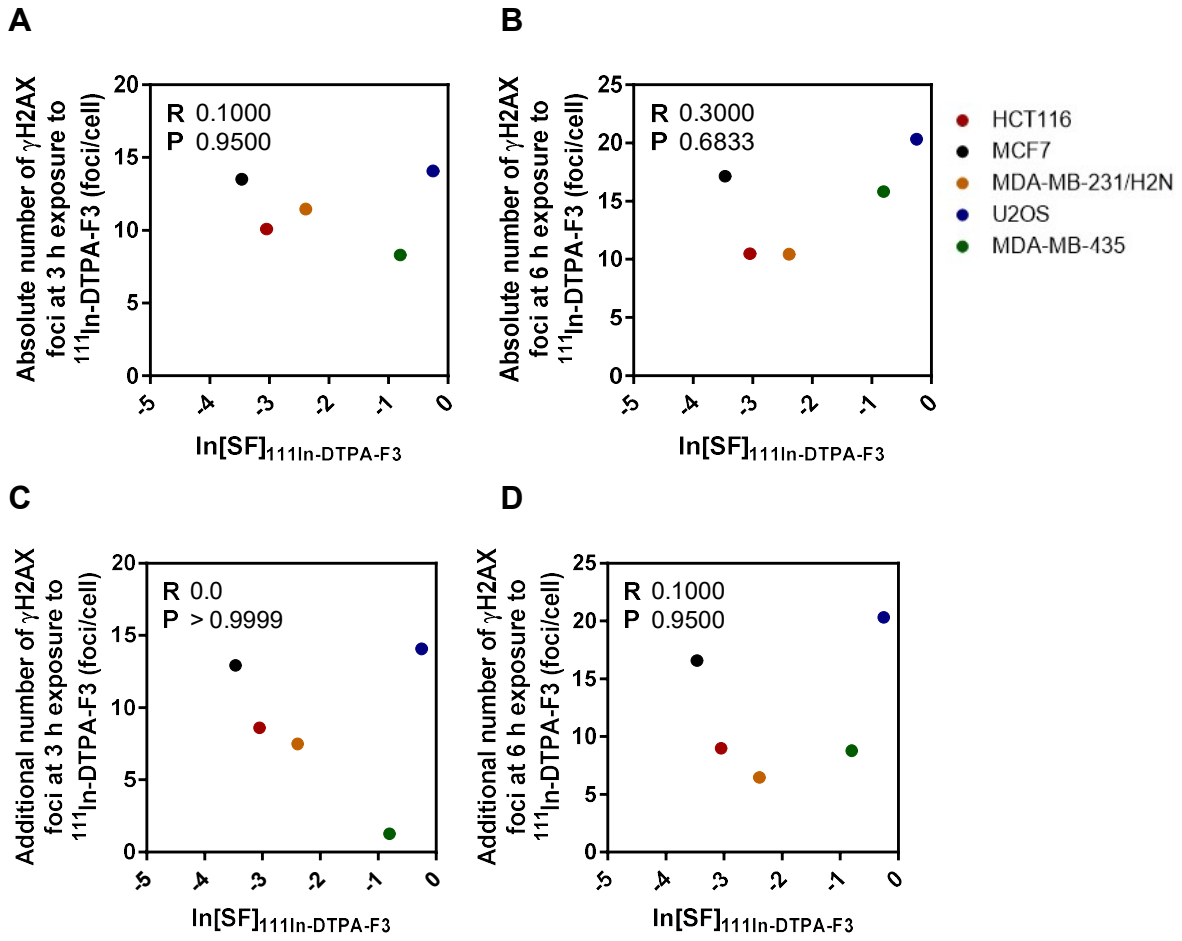

Figure 4.13. No correlation between the level of cell kill produced by ^{111}In-DTPA-F3 and the induction of γH2AX foci by ^{111}In-DTPA-F3

(A–B) Histograms showing the $\ln[SF]_{^{111}\text{In-DTPA-F3}}$ (natural log of the surviving fraction due to a 3 h exposure to 0.1 μM of ^{111}In-DTPA-F3 (22.17 MBq/nmol)) on the *x axis* (values show mean, n = 2–3) and the absolute number of γH2AX foci at (A) 3 h or (B) 6 h after exposure to 1 μM of ^{111}In-DTPA-F3 on the *y axis* (values show mean, n = 17–50). (C–D) Histograms showing the $\ln[SF]_{^{111}\text{In-DTPA-F3}}$ (natural log of the surviving fraction due to a 3 h exposure to 0.1 μM of ^{111}In-DTPA-F3 (22.17 MBq/nmol)) on the *x axis* (values show mean, n = 2–3) and the number of additional γH2AX foci at (C) 3 h or (D) 6 h after exposure to 1 μM of ^{111}In-DTPA-F3 (22.17 MBq/nmol)] on the y axis (values show mean, n = 17–50). GraphPad Prism 6 software was used to test if the data followed a Gaussian distribution using a D'Agostino-Pearson omnibus test. Since the data did not follow a Gaussian distribution, a nonparametric Spearman correlation (95% confidence interval) with two-tailed P values (shown) was used. R, Spearman R.

effect of 0.1 μM of ^{111}In-DTPA-F3 (22.17 MBq/nmol) on the surviving fraction of the malignant cell lines was highly variable (19 fold range in surviving fraction). Exposure of MDA-MB-435 cells for 3 h to a concentration of ^{111}In-DTPA-F3 (22.17 MBq/nmol) of 0.1 μM (based on an average molecular weight of DTPA-F3 of 3,700 Da with a DTPA:F3 ratio of 0.75:1) produced a level of cell kill of 55%. Drecoll *et al.* (2012) reported that a concentration of ^{213}Bi-DTPA-$[F3]_2$ (80.97 MBq/nmol) of 1.47 nM (based on an average molecular weight of DTPA-$[F3]_2$ of 7,221 Da with a DTPA:$[F3]_2$ ratio of 1:1) produced a level of cell kill of 50% after exposure of MDA-MB- 435 cells for 3 days. A level of cell kill of 55% was therefore achieved with a concentration of ^{111}In-DTPA-F3 that was 68 fold greater than the concentration of ^{213}Bi-DTPA-$[F3]_2$ that produced the 50% cell kill of MDA-MB-435 cells that was reported in Drecoll *et al*. (2009). However, it should be noted that the specific activity and incubation time of ^{111}In-DTPA-F3 was approximately 3.65 and 24 fold less than the specific activity and incubation time of ^{213}Bi-DTPA-$[F3]_2$ (Drecoll*, et al.*, 2009).

Although ^{213}Bi-DTPA-$[F3]_2$ was reported in Drecoll *et al*. (2009) to significantly reduce the colony forming potential of MDA-MB-435 cells, DTPA-$[F3]_2$ did not significantly reduce colony forming potential (Drecoll*, et al.*, 2009). The differential effect of ^{111}In-DTPA-F3 versus DTPA-F3 on the clonogenic survival of MDA-MB-435 cells was similar to the differential effect of ^{213}Bi-DTPA-$[F3]_2$ and DTPA-$[F3]_2$ (Drecoll*, et al.*, 2009). Further, Reilly *et al*. (2000) showed that, although ^{111}In-DTPA-EGF was significantly radiotoxic to EGFR-overexpressing MDA-MB-435 cells, ^{111}In-DTPA had no effect on cell survival. The differential effect of ^{111}In-DTPA-F3 versus ^{111}In-DTPA on the clonogenic survival of MDA-MB-435 cells was similar to the differential effect of ^{111}In-DTPA-EGF versus ^{111}In-DTPA (Reilly*, et al.*, 2000). Together, these data suggested that F3 (in monomeric or dimeric form) is required to be radiolabelled with

a short range particle-emitter and that a short range particle-emitter is required to be linked to F3 to cause anti-cancer effects *in vitro*.

The level of cell kill produced by 0.1 μM of ^{111}In-DTPA-F3 (22.17 MBq/nmol) after exposure of MDA-MB-231/H2N cells for 3 h (91% cell kill) was similar to the level of cell kill produced by 3 μM of ^{111}In-BnDTPA-F3 (20.6 MBq/nmol) after exposure of MDA-MB-231/H2N cells for 24 h (90% cell kill) that was reported in Cornelissen *et al*. (2012b). The number of moieties of chelator attached per molecule of F3 was similar, 0.75:1 (DPTA:F3) for ^{111}In-DTPA-F3 and 0.9:1 (BnDTPA:F3) for ^{111}In-BnDTPA-F3 (Cornelissen*, et al.*, 2012b). Therefore, the ability of ^{111}In-DTPA-F3 versus ^{111}In-BnDTPA-F3 to bind to the receptor NCL could not be expected to differ significantly due to excess conjugation of chelator to the ε-amine groups on side chains of lysines (bold) or the N-terminus of F3 (**K**DEPQRRSARLSA**K**PAPP**K**PEP**K**P**KK**APA**KK**). However, it is also possible that the maximum level of cell kill of MDA-MB-231/H2N cells that can be produced by ^{111}In-labelled F3 is approximately 90%, possibly due to heterogeneity of expression of cell membrane NCL that enables ~10% of MDA-MB-231/H2N cells to escape being targeted by ^{111}In-labelled F3. It should also be noted that the method of exposing the MDA-MB-231/H2N cells to ^{111}In-DTPA-F3 differed from the method reported in Cornelissen *et al.* (2012b) for exposing MDA-MB-231/H2N cells to ^{111}In-BnDTPA-F3. In Cornelissen *et al.* (2012b), cells exposed to ^{111}In-BnDTPA-F3 were suspended in aliquots, while cells exposed to ^{111}In-DTPA-F3 had adhered to 96 well plates. The adherence of cells to 96-well pates may have enhanced the level of cell kill produced by ^{111}In-DTPA-F3, as adherent cells would not have become aggregated due to the sedimentation of cells from suspension over the 3 h time period, and may therefore have been more efficient as a cell population at taking up and internalising ^{111}In-DTPA-F3. In contrast, suspension cells exposed to

^{111}In-BnDTPA-F3 may have aggregated as the cells sedimented from suspension over the 24 h time period and may therefore have been less efficient as a cell population at taking up and internalising ^{111}In-BnDTPA-F3. It is therefore hypothesised that, despite MDA-MB-231/H2N cells being exposed for an 8 fold greater incubation time to a 30 fold higher concentration of ^{111}In-BnDTPA-F3 (Cornelissen*, et al.*, 2012b), similar levels of cell kill were produced by ^{111}In-DTPA-F3 and ^{111}In-BnDTPA-F3 due to heterogeneity of expression of cell membrane NCL and differences in the method of the clonogenic assay.

The level of cell kill produced by ^{111}In-DTPA-F3 was 97%, 95%, 91%, 89%, 55% and 43% for MCF7, HCT116, MDA-MB-231/H2N, H322, MDA-MB-435 and U2OS cells, respectively. The LD_{37} after exposure of these cell lines to external γ-radiation ranged by 2.3 fold. The level of cell kill produced by ^{111}In-DTPA-F3 was not found to correlate with cellular radiosensitivity, either using the LD_{37} for external γ-radiation or the surviving fraction after exposure to 2, 4, 6, 8 or 10 Gy of external γ-radiation. However, it should be noted that it cannot be excluded that a correlation could still be found with a larger sample size that tests a greater number of cell lines.

Cornelissen *et al.* (2012b) reported that exposure of MDA-MB-231/H2N cells with up to 5 μM of ^{111}In-BnDTPA-F3 (20.6 MBq/nmol) for 2 or 24 h caused the induction of γH2AX foci in a dose-dependent manner and also in a manner that was linearly dependent on specific activity (Spearman R, 0.99; P, 0.0028) (Cornelissen*, et al.*, 2012b). 1 μM of ^{111}In-DTPA-F3 (22.17 MBq/nmol) also induced γH2AX foci. The absolute number of γH2AX foci per cell at 3 or 6 h exposure of malignant cells to ^{111}In-DTPA-F3 was significantly greater than ^{111}In-DTPA. Similarly, the additional number (over baseline levels) of γH2AX foci per cell at 3 or 6 h exposure of malignant cells to ^{111}In-DTPA-F3 was significantly greater than ^{111}In-DTPA.

However, the level of cell kill produced by ^{111}In-DTPA-F3 was not found to correlate with the absolute number of γH2AX foci or additional number of γH2AX foci that were present at 3 or 6 h exposure of malignant cell lines to ^{111}In-DTPA-F3. The induction of DNA double-strand breaks did therefore not determine the level of cell kill of malignant cell lines exposed to ^{111}In-DTPA-F3, despite evidence in Cornelissen *et al.* (2012b) that the induction of γH2AX foci in MDA-MB-231/H2N cells was dependent on concentration and specific activity of ^{111}In-BnDTPA-F3. Radiation dose-dependent ^{123}I-labelled oestrogen-induced DNA double-strand breaks, single-strand breaks and chromosome aberrations have also previously been correlated with survival (Schwartz*, et al.*, 1996). However, these correlations were demonstrated for a range of doses using a single cell line as opposed to a range of different cancer cell lines. It should be noted however that it cannot be ruled out that a higher number of data points could make it possible to find a correlation between the level of cell kill and the number of γH2AX foci induced by ^{111}In-DTPA-F3. Nevertheless, these data suggested that 1) DNA double-strand breaks induced by ^{111}In-DTPA-F3 resulted in different levels of cytotoxicity in different cells lines (possibly due to different rates of DNA repair) and/or 2) DNA double-strand breaks were not the only type of damage that caused cell death, but were nonetheless caused as a consequence of exposure of malignant cells to ^{111}In-DTPA-F3.

MacPhail *et al*. (2003) measured the rate of induction of γH2AX following a range of doses of external X-radiation (0–8 Gy). After normalising for basal γH2AX levels, no correlation was found between the rate of γH2AX induction and the cellular radiosensitivity of seven cell lines (WiDr, V79, DU145, SiHa, U87, WIL-2NS and HT144) exposed to external X-radiation, using the surviving fraction at 2 Gy. Further, Banáth *et al*. (2004) found no correlation between the rate of γH2AX induction and the

cellular radiosensitivity of six cell lines (HeLa, Caski, MS751, CC3A, SW756 and SiHa) exposed to external X-radiation (Banath*, et al.*, 2004). MacPhail *et al*. (2003) and Olive and Banáth (2004) also studied the correlation between the radiosensitivity to external X-rays and the rate of loss of γH2AX (loss half-time), which reflects the rate of repair of γH2AX foci. The rate of repair of γH2AX foci was found to correlate with cellular radiosensitivity to external X-rays. In 10 cell lines (V79, CHO-K1, SiHa, WiDr, DU145, WIL-2NS, HT144, HCC1937, U87), SiHa xenografts and normal mouse tissues, a longer γH2AX loss half-time was correlated with greater cellular radiosensitivity to external X-rays (R^2, ~0.66) (MacPhail*, et al.*, 2003; Olive and Banath, 2004). The same relationship was found by Banáth *et al*. (2004) for 13 p53 wild-type cell lines (HCC1937, HT144, AT3B1, TK6, U87, HFL1, 48BR, H-tert, HCT116, HF1, A549 and HUVEC) and six p53 deficient cell lines (HCT116, WiDr, Du145, M059K, M059J and Wil2NS) (R^2, 0.75) (Banath*, et al.*, 2004). In a similar study, Taneja *et al*. (2004) studied the radiosensitivity of head and neck cancer (SQ-20B and SCC-61) cells exposed to external γ-radiation and found that the more radiosensitive of the two cell lines (SCC-61) had a slower rate of repair of γH2AX foci after exposure to 3 Gy of external γ-radiation compared to the more radioresistant cell line (SQ-20B) (Taneja*, et al.*, 2004). It would therefore be interesting to investigate the relationship between the radiotoxicity of ^{111}In-DTPA-F3 and the rate of repair of γH2AX foci induced by ^{111}In-DTPA-F3 and external γ-radiation.

In summary, the radiotoxicity of ^{111}In-DTPA-F3 has been shown to vary (19 fold range in surviving fraction) depending on the malignant cell line, but the level of cell kill produced by ^{111}In-DTPA-F3 was not related to cellular radiosensitivity to external γ-radiation nor to the level of γH2AX foci induced by ^{111}In-DTPA-F3. Nevertheless, ^{111}In-DTPA-F3 is a promising Auger electron-emitting radiopharmaceutic agent for the

treatment of a wide range of malignant cells. Future research should focus on characterising the radiotoxicity of ^{111}In-DTPA-F3 on a wider range of malignant cell lines and its relationship with the rate of repair of γH2AX foci.

Chapter 5. The internalisation of ^{111}In-DTPA-F3

5.1. Introduction

^{111}In-labelled F3 (^{111}In-DTPA-F3) was found, as described in Chapter 4, to produce variable levels of cell kill (19 fold range in surviving fraction) to breast carcinoma (MCF7, MDA-MB-231/H2N), colon carcinoma (HCT116), melanoma (MDA-MB-435) and non-small cell lung cancer (H322) cells *in vitro*. However, ^{111}In-DTPA-F3 was not found to be significantly radiotoxic to osteosarcoma (U2OS) cells. The radiotoxicity of ^{111}In-DTPA-F3 was not ascribed to cellular radiosensitivity to external γ-radiation nor to the ability of ^{111}In-DTPA-F3 to induce γH2AX foci.

The main aims of the work presented in this chapter were to investigate the spatial localisation of ^{111}In-DTPA-F3 inside a wide range of malignant cell lines. In 2012, Cornelissen *et al.* (2012b) reported that fluorescein-labelled F3 (FITC-F3) colocalised with nucleolin (NCL) in the nucleolus of MDA-MB-231/H2N cells *in vitro* (Cornelissen*, et al.*, 2012b). It was hypothesised that the mechanism underpinning the cell kill produced by ^{111}In-DTPA-F3 involved the accumulation of radioactivity in the nucleolus of the malignant cells. To attribute the accumulation of radioactivity in the nucleolus to the cell kill produced by ^{111}In-DTPA-F3, a fractionation protocol was validated and the membrane, cytoplasm, nucleoplasm and nucleolus fractions of the malignant cells was isolated (internalisation assay). The internalisation assay was utilised to measure the amount of radioactivity in the membrane, cytoplasm, nucleoplasm and nucleolus fractions of malignant cell lines exposed to ^{111}In-DTPA-F3 or a non-radiotoxic control that lacked F3 (^{111}In-DTPA). To show the localisation of ^{111}In-DTPA-F3 between the intracellular compartments the data from the internalisation assays was presented as

the percentage of cell-bound radioactivity, while the absolute amount of radioactivity expressed in mBq/cell was also calculated to show the differences in the level of uptake in the intracellular compartments between a range of malignant cell lines. It was hypothesised that higher levels of radioactivity would be detected in the nucleolus of cells exposed to ^{111}In-DTPA-F3 compared to equimolar amounts of ^{111}In-DTPA. To show that there was an increase in the level of radioactivity in the nucleolus, and to attribute the mechanism underpinning the cell kill produced by ^{111}In-DTPA-F3 to the delivery of radioactivity to the nucleolus, the ratio of the amount of radioactivity in the subcellular compartments after exposure of cells to ^{111}In-DTPA-F3 or ^{111}In-DTPA (^{111}In-DTPA-F3:^{111}In-DTPA ratio) was calculated. It was hypothesised that the mean absorbed radiation dose in the nucleolus may be relatively high due to its relatively small volume. To model the level of radiation dose deposited in the membrane, cytoplasm, nucleoplasm and nucleolus, fluorescence microscopy was used to quantify the volumes of these intracellular compartments for a range of malignant cell lines. Then, concentric single cell models, comprising membrane, cytoplasm, nucleoplasm and nucleolus, were generated; these single cell models were used by Dr Nadia Falzone to calculate S-values. S-values were used with data from internalisation experiments to calculate the mean absorbed radiation dose in the membrane, cytoplasm, nucleoplasm and nucleolus of the malignant cell lines. It was hypothesised that higher levels of mean absorbed radiation dose would be deposited in the nucleolus of cells exposed to ^{111}In-DTPA-F3 compared to ^{111}In-DTPA. To show that there was shift in the level of mean absorbed radiation dose to the nucleolus, the ratio of the mean absorbed radiation dose in the subcellular compartments after exposure of cells to ^{111}In-DTPA-F3 or ^{111}In-DTPA (^{111}In-DTPA-F3:^{111}In-DTPA ratio) was calculated. It was then hypothesised that there may be a relationship between the level

of cell kill produced by ^{111}In-DTPA-F3 and either the percentage of cell-bound radioactivity (spatial distribution-dependent), the absolute amount of radioactivity (internalisation rate-dependent), or the mean absorbed radiation dose (intracellular compartment volume-dependent) deposited in the intracellular compartments of the malignant cells by ^{111}In-DTPA-F3. Spearman correlations were performed to show if the percentage of cell-bound radioactivity, the absolute amount of radioactivity, or the mean absorbed radiation dose deposited in the intracellular compartments of the malignant cells by ^{111}In-DTPA-F3 determined the level of cell kill produced by ^{111}In-DTPA-F3. Finally, it was hypothesised that there may be a relationship between the volume of the intracellular compartments of the malignant cell lines and the number of γH2AX foci produced by ^{111}In-DTPA-F3 or the level of cell kill produced by ^{111}In-DTPA-F3. Spearman correlations were performed to show if the number of γH2AX foci produced by ^{111}In-DTPA-F3 or the level of cell kill produced by ^{111}In-DTPA-F3 was determined by the volume of the intracellular compartments of the malignant cell lines.

5.2. Results

5.2.1. ^{111}In-DTPA-F3 targets the nucleolus

To assess the uptake of radioactivity in the membrane, cytoplasm, nucleoplasm and nucleolus of malignant cells exposed to ^{111}In-DTPA-F3 or an equimolar control lacking F3 (^{111}In-DTPA), the malignant cell lines (MCF7, HCT116, MDA-MB-231/H2N, H322, MDA-MB-435 and U2OS cells) were exposed for 3 h to 1 μM of ^{111}In-DTPA-F3 (22.17 MBq/nmol) or an equimolar amount of a control lacking F3 (^{111}In-DTPA), before being fractionated as per the internalisation assay (see the internalisation assay schematic

in Figure 5.1). Figure 5.2 shows the validation of the separation of the cytoplasm, nucleoplasm and nucleolus fractions for each malignant cell line. Table 5.1 and Figures 5.3–5.8 show the percentage of radioactivity that became cell-bound (%), and the proportion of cell-bound radioactivity (%) that was associated with the membrane, cytoplasm, nucleus, nucleoplasm or nucleolus, after exposure of MCF7, HCT116, MDA-MB-231/H2N, H322, MDA-MB-435 and U2OS cells to ^{111}In-DTPA-F3 or ^{111}In-DTPA. A D'Agostino-Pearson omnibus test indicated that these data did not follow a Gaussian distribution. Therefore, differences between ^{111}In-DTPA-F3 versus ^{111}In-DTPA were compared using an unpaired Mann-Whitney (M-W) test with two-tailed P values. However, the non-parametric, unpaired M-W test has little statistical power and will never produce a two-tailed P value of less than 0.1 for a sample size of 3 or less. A P value of 0.1 was therefore taken, with a moderate level of confidence, as indication that data for ^{111}In-DTPA-F3 and ^{111}In-DTPA were not similar. In conjunction, parametric, unpaired T-tests with Welch's correction for unequal standard deviations were also performed. A two-tailed P value of <0.5 was taken, with a moderate level of confidence, as indication that data for ^{111}In-DTPA-F3 and ^{111}In-DTPA were not similar. Where both the M-W and T-test produced P values that were significant then this was taken with a higher degree of confidence that the data for ^{111}In-DTPA-F3 and ^{111}In-DTPA were not similar.

The percentage of cell-bound ^{111}In-DTPA-F3 was similar to ^{111}In-DTPA, with the exception that a lower level of cell-bound ^{111}In-DTPA-F3 was associated with the HCT116 cells compared to ^{111}In-DTPA (M-W test, P = 0.1000; T-test, P = 0.0125) (Figure 5.3). The proportion of cell-bound ^{111}In-DTPA-F3 that was associated with the membrane (Figure 5.4), cytoplasm (Figure 5.5), nucleus (Figure 5.6) and nucleoplasm (Figure 5.7) of the malignant cells was also similar to ^{111}In-DTPA, with the exceptions

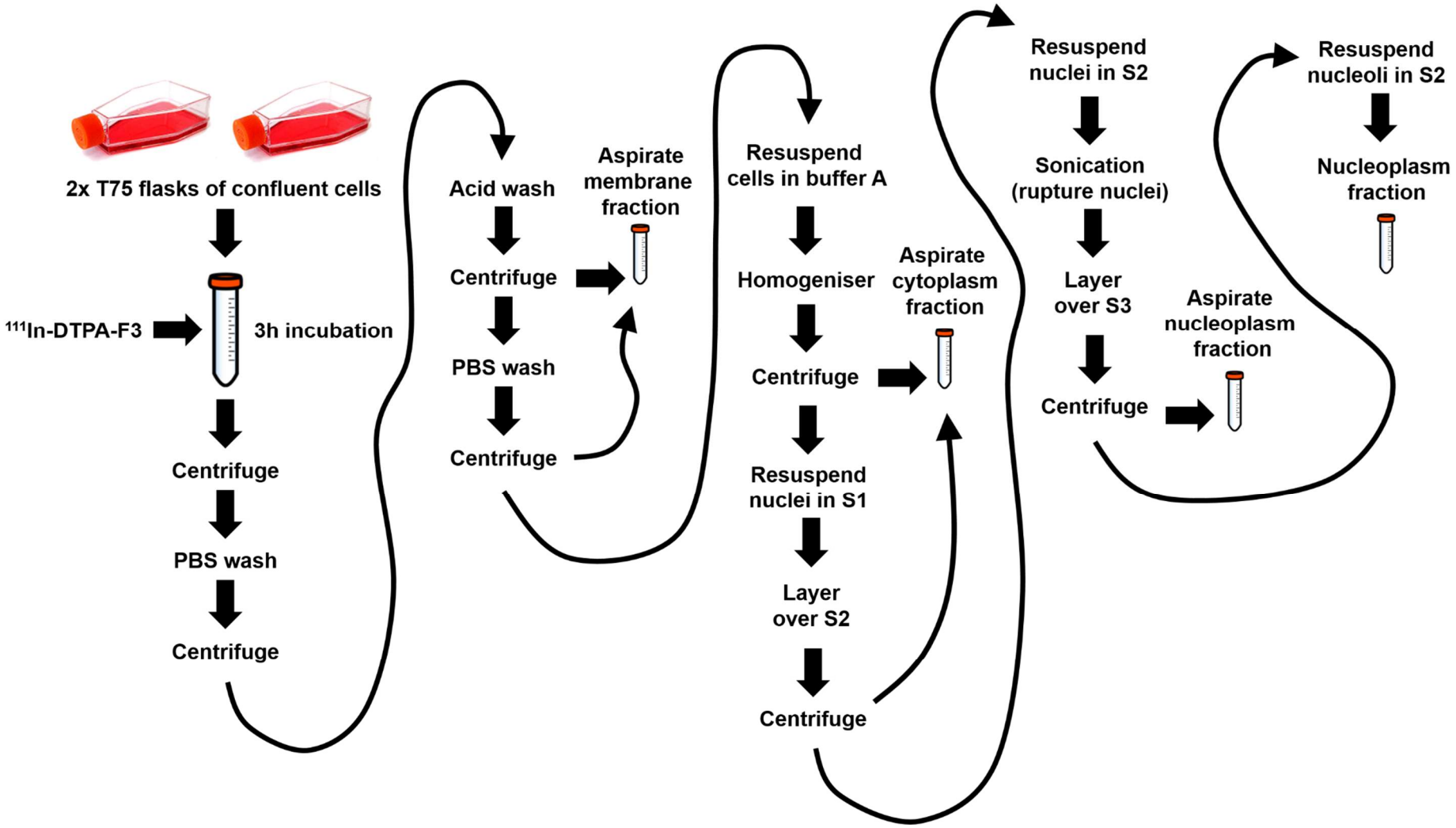

Figure 5.1. Separation of the cytoplasm, nucleoplasm, and nucleolus fractions of malignant cell lines

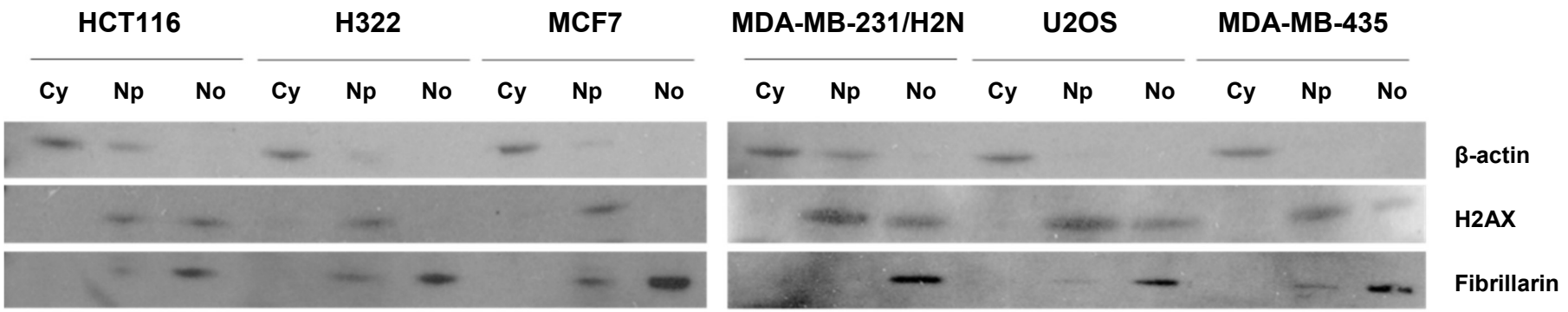

Figure 5.2. Separation of the cytoplasm, nucleoplasm, and nucleolus fractions of malignant cell lines

β-actin was used as a cytoplasmic marker, H2AX as a nuclear marker, and fibrillarin as a nucleolar marker. Cy, cytoplasm fraction; Np, nucleoplasm fraction; No, nucleolus fraction. 12.5 μg of protein loaded per sample.

	^{111}In-DTPA-F3						^{111}In-DTPA					
	% cell-bound	Proportion of cell-bound (%)					% cell-bound	Proportion of cell-bound (%)				
		Me	Cy	Nu	Np	No		Me	Cy	Nu	Np	No
MCF7	0.39 ±0.08	53.79 ±4.61	40.46 ±3.61	5.74 ±1.06	5.52 ±1.05	**0.22 ±0.02**	0.56 ±0.12	60.29 ±5.27	36.21 ±4.54	3.50 ±0.77	3.41 ±0.77	**0.08 ±0.00**
HCT116	**0.78 ±0.05**	73.95 ±0.67	20.04 ±1.12	**6.01 ±0.52**	**5.42 ±0.39**	**0.59 ±0.30**	**1.16 ±0.01**	78.20 ±7.50	18.31 ±7.49	**3.49 ±0.13**	**3.39 ±0.10**	**0.10 ±0.03**
MDA-MB-231/H2N	1.36 ±0.13	69.05 ±2.16	25.93 ±2.03	5.02 ±0.12	3.79 ±0.25	1.23 ±0.13	1.86 ±0.10	69.25 ±2.51	27.84 ±2.44	2.91 ±0.07	2.42 ±0.14	0.50 ±0.07
H322	0.51 ±0.02	**72.41 ±094**	**23.19 ±0.85**	4.40 ±0.55	4.14 ±0.52	**0.27 ±0.01**	0.54 ±0.14	**62.05 ±4.25**	**35.40 ±4.36**	2.55 ±0.67	2.48 ±0.66	**0.07 ±0.02**
MDA-MB-435	0.78 ±0.05	70.65 ±0.82	24.46 ±1.32	4.88 ±0.52	3.80 ±0.50	1.07 ±0.13	0.69 ±0.10	67.20 ±2029	28.52 ±1.97	4.28 ±0.36	3.53 ±0.30	0.75 ±0.11
U2OS	0.90 ±0.11	78.98 ±1.99	**17.49 ±1.42**	3.53 ±0.56	2.96 ±0.56	0.57 ±0.16	0.83 ±0.06	75.64 ±0.29	**22.01 ±0.30**	2.35 ±0.22	2.12 ±0.26	0.23 ±0.04

Table 5.1. Proportion of cell-bound radioactivity in the membrane, cytoplasm, nucleus, nucleoplasm, and nucleolus of malignant cells exposed to ^{111}In-DTPA-F3 or ^{111}In-DTPA

Proportion of cell-bound radioactivity (%) in the membrane, cytoplasm, nucleus, nucleoplasm, and nucleolus of MCF7, HCT116, MDA-MB-231/H2N, H322, MDA-MB-435, and U2OS cells exposed for 3 h to 1 μM of ^{111}In-DTPA-F3 (22.17 MBq/nmol) or an equimolar amount of ^{111}In-DTPA. Percentage radioactivity that became cell-bound (% cell-bound) was calculated by combining the radioactivity associated with the membrane, cytoplasm, nucleoplasm and nucleolus (radioactivity associated with the cell) and dividing this by the total amount of radioactivity to which the cells were exposed (22.17 MBq in 1 mL). Proportion of cell-bound radioactivity was calculated by dividing the radioactivity associated with the membrane, cytoplasm, nucleoplasm or nucleolus by the radioactivity associated with the cell. Proportion of cell-bound radioactivity associated with the nucleus was calculated by combining the proportion of cell-bound radioactivity associated with the nucleoplasm and nucleolus. Values show mean percentage ± SEM, n = 2–3. Me, membrane; Cy, cytoplasm; Nu, nucleus; Np, nucleoplasm; No, nucleolus. Using GraphPad Prism 6, data for ^{111}In-DTPA-F3 versus ^{111}In-DTPA was compared using an unpaired Mann-Whitney test (two-tailed P values) and T-tests with Welch's correction for unequal standard deviations (two-tailed P values). Bold values, significance.

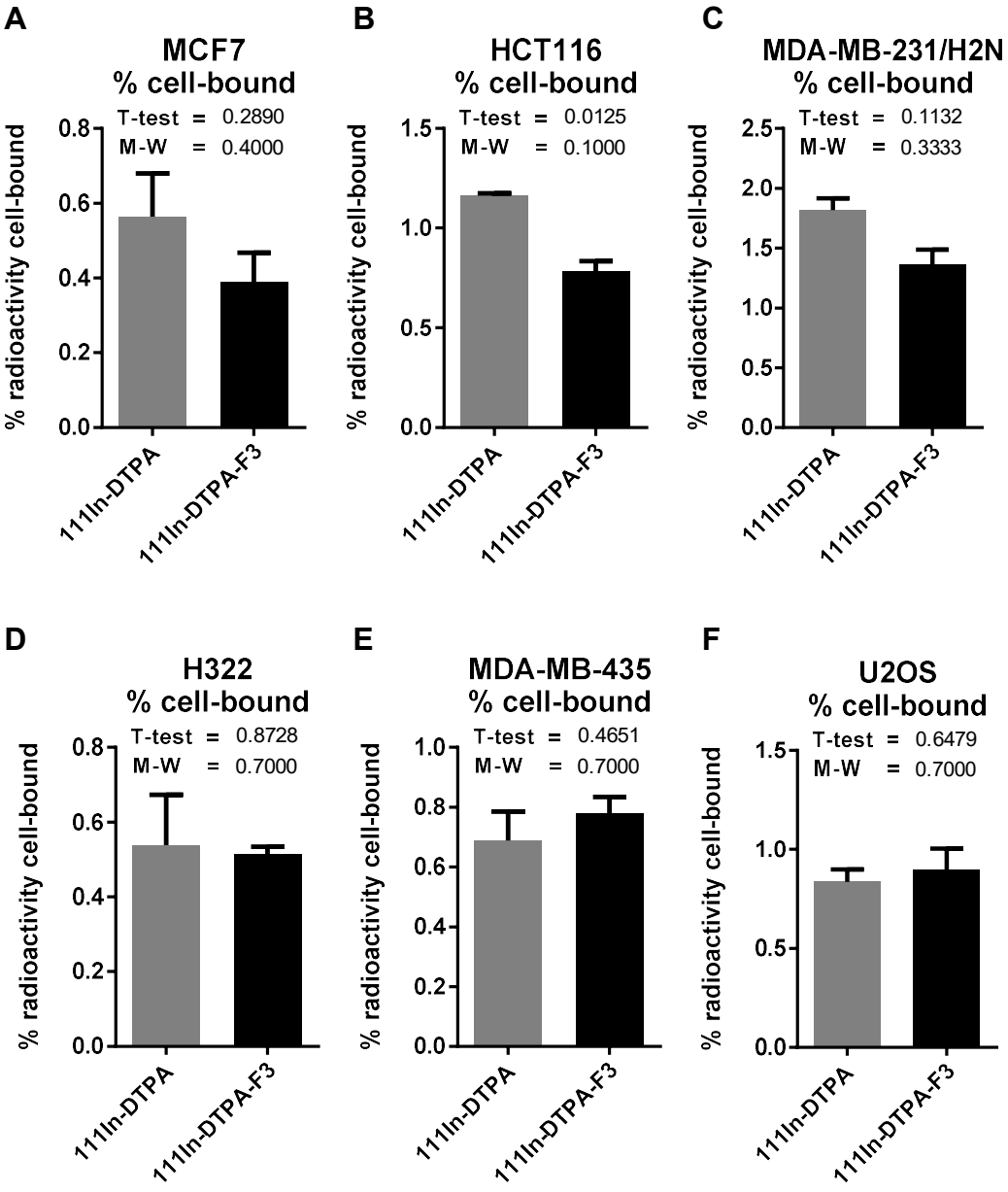

Figure 5.3. Percentage of radioactivity that became cell-bound after exposure of malignant cells to ^{111}In-DTPA-F3 or ^{111}In-DTPA

Percentage of radioactivity that became cell-bound (%) after exposure of (A) MCF7, (B) HCT116, (C) MDA-MB-231/H2N, (D) H322, (E) MDA-MB-435, and (F) U2OS cells for 3 h to 1 μM of ^{111}In-DTPA-F3 (22.17 MBq/nmol) or an equimolar amount of ^{111}In-DTPA. Values show mean percentage radioactivity cell-bound ± SEM, n = 2–3.GraphPad Prism 6 software was used to test if the data followed a Gaussian distribution using a D'Agostino-Pearson omnibus test. Since the data did not follow a Gaussian distribution, means were compared using unpaired Mann-Whitney (M-W) tests with two-tailed P values. However, the unpaired, two-tailed M-W test has little statistical power and will never produce a P value of less than 0.1 for a sample size of 3 or less. Therefore, parametric T-tests with Welch's correction for unequal standard deviations (two-tailed P values) were also performed.

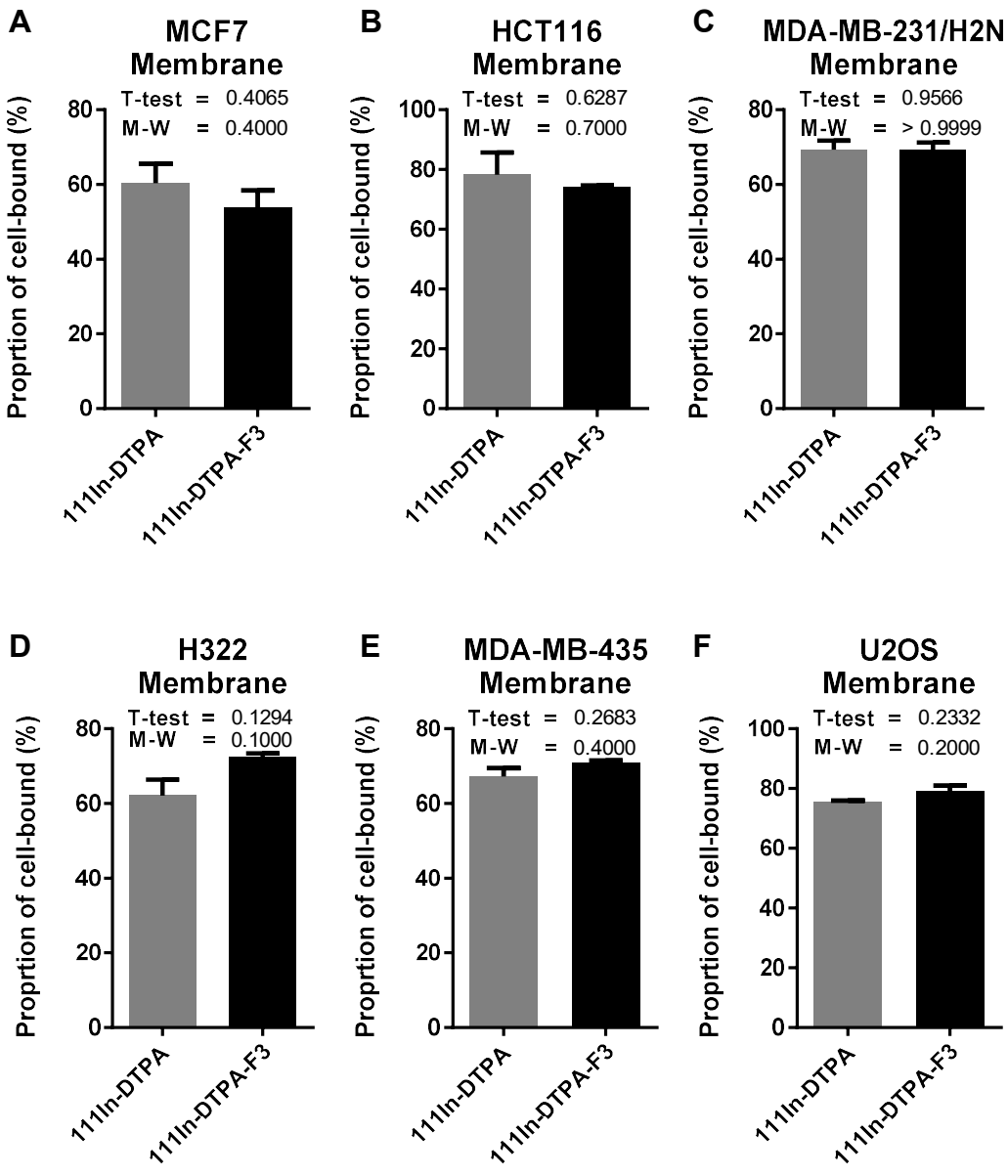

Figure 5.4. Proportion of cell-bound radioactivity associated with the membrane of malignant cells after exposure to ^{111}In-DTPA-F3 or ^{111}In-DTPA

Proportion of cell-bound radioactivity (%) associated the membrane of (A) MCF7, (B) HCT116, (C) MDA-MB-231/H2N, (D) H322, (E) MDA-MB-435, and (F) U2OS cells exposed for 3 h to 1 μM of ^{111}In-DTPA-F3 (22.17 MBq/nmol) or an equimolar amount of ^{111}In-DTPA. Values show mean proportion of cell-bound radioactivity ± SEM, n = 2–3. GraphPad Prism 6 software was used to test if the data followed a Gaussian distribution using a D'Agostino-Pearson omnibus test. Since the data did not follow a Gaussian distribution, means were compared using unpaired Mann-Whitney (M-W) tests with two-tailed P values. However, the unpaired, two-tailed M-W test has little statistical power and will never produce a P value of less than 0.1 for a sample size of 3 or less. Therefore, parametric T-tests with Welch's correction for unequal standard deviations (two-tailed P values) were also performed.

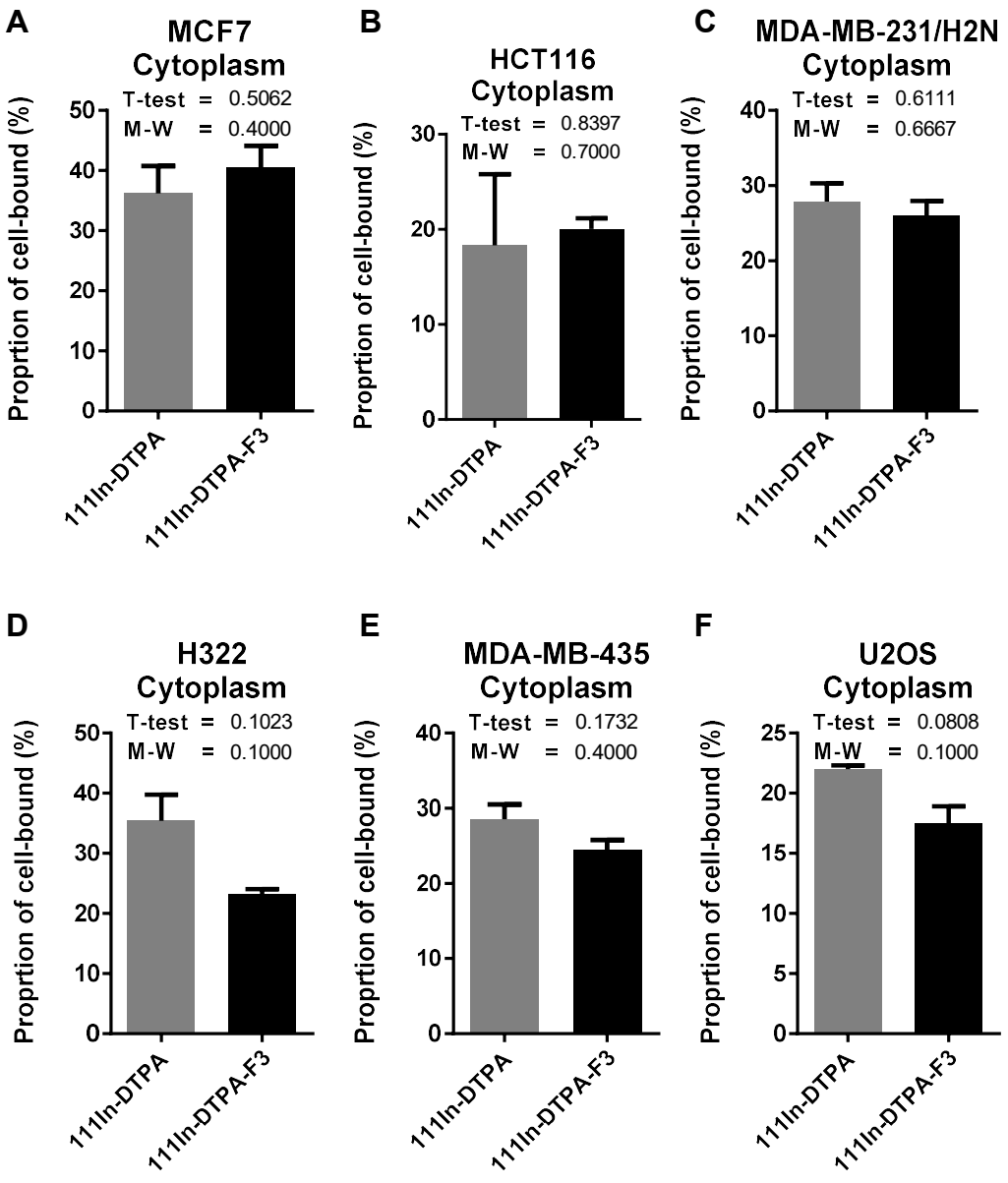

Figure 5.5. Proportion of cell-bound radioactivity associated with the cytoplasm of malignant cells after exposure to ^{111}In-DTPA-F3 or ^{111}In-DTPA

Proportion of cell-bound radioactivity (%) associated the cytoplasm of (A) MCF7, (B) HCT116, (C) MDA-MB-231/H2N, (D) H322, (E) MDA-MB-435, and (F) U2OS cells exposed for 3 h to 1 μM of ^{111}In-DTPA-F3 (22.17 MBq/nmol) or an equimolar amount of ^{111}In-DTPA. Values show mean proportion of cell-bound radioactivity ± SEM, n = 2–3. GraphPad Prism 6 software was used to test if the data followed a Gaussian distribution using a D'Agostino-Pearson omnibus test. Since the data did not follow a Gaussian distribution, means were compared using unpaired Mann-Whitney (M-W) tests with two-tailed P values. However, the unpaired, two-tailed M-W test has little statistical power and will never produce a P value of less than 0.1 for a sample size of 3 or less. Therefore, parametric T-tests with Welch's correction for unequal standard deviations (two-tailed P values) were also performed.

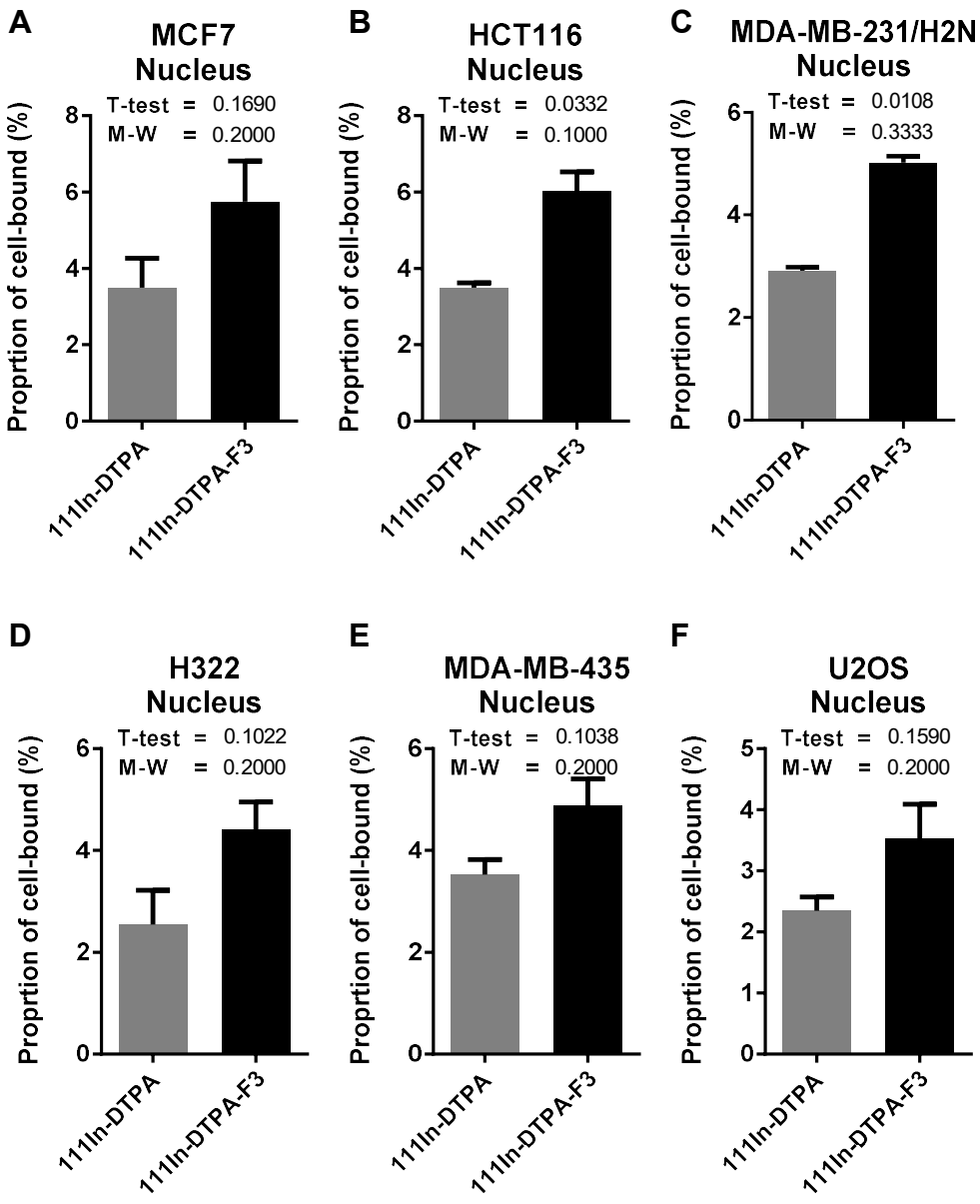

Figure 5.6. Proportion of cell-bound radioactivity associated with the nucleus of malignant cells after exposure to ^{111}In-DTPA-F3 or ^{111}In-DTPA

Proportion of cell-bound radioactivity (%) associated the nucleus of (A) MCF7, (B) HCT116, (C) MDA-MB-231/H2N, (D) H322, (E) MDA-MB-435, and (F) U2OS cells exposed for 3 h to 1 μM of ^{111}In-DTPA-F3 (22.17 MBq/nmol) or an equimolar amount of ^{111}In-DTPA. The proportion of cell-bound radioactivity associated with the nucleus was calculated by combining the proportion of cell-bound radioactivity associated with the nucleoplasm and nucleolus. Values show mean proportion of cell-bound radioactivity ± SEM, n = 2–3. GraphPad Prism 6 software was used to test if the data followed a Gaussian distribution using a D'Agostino-Pearson omnibus test. Since the data did not follow a Gaussian distribution, means were compared using unpaired Mann-Whitney (M-W) tests with two-tailed P values. However, the unpaired, two-tailed M-W test has little statistical power and will never produce a P value of less than 0.1 for a sample size of 3 or less. Therefore, parametric T-tests with Welch's correction for unequal standard deviations (two-tailed P values) were also performed.

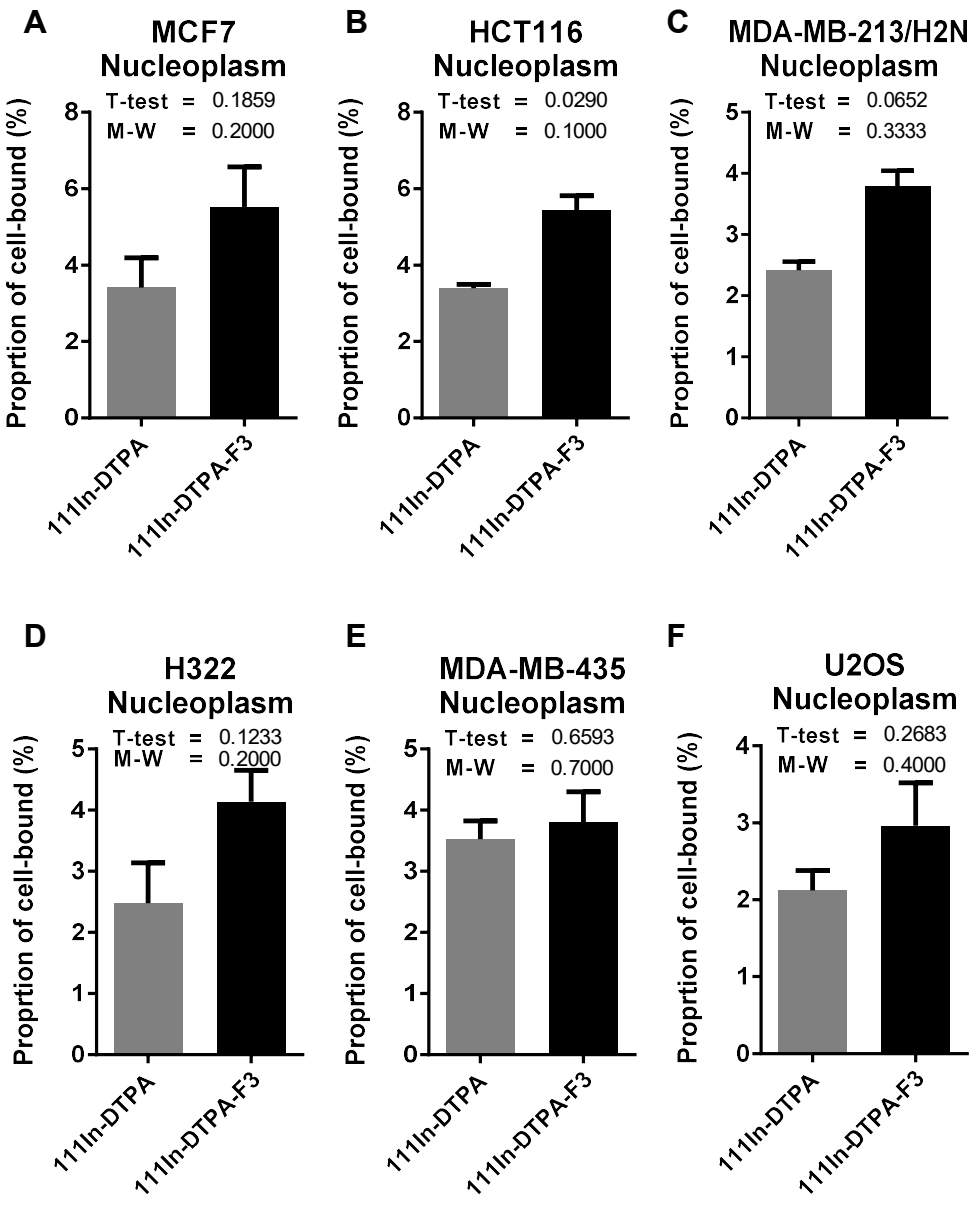

Figure 5.7. Proportion of cell-bound radioactivity associated with the nucleoplasm of malignant cells after exposure to ^{111}In-DTPA-F3 or ^{111}In-DTPA

Proportion of cell-bound radioactivity (%) associated the nucleoplasm of (A) MCF7, (B) HCT116, (C) MDA-MB-231/H2N, (D) H322, (E) MDA-MB-435, and (F) U2OS cells exposed for 3 h to 1 μM of ^{111}In-DTPA-F3 (22.17 MBq/nmol) or an equimolar amount of ^{111}In-DTPA. Values show mean proportion of cell-bound radioactivity ± SEM, n = 2–3. GraphPad Prism 6 software was used to test if the data followed a Gaussian distribution using a D'Agostino-Pearson omnibus test. Since the data did not follow a Gaussian distribution, means were compared using unpaired Mann-Whitney (M-W) tests with two-tailed P values. However, the unpaired, two-tailed M-W test has little statistical power and will never produce a P value of less than 0.1 for a sample size of 3 or less. Therefore, parametric T-tests with Welch's correction for unequal standard deviations (two-tailed P values) were also performed.

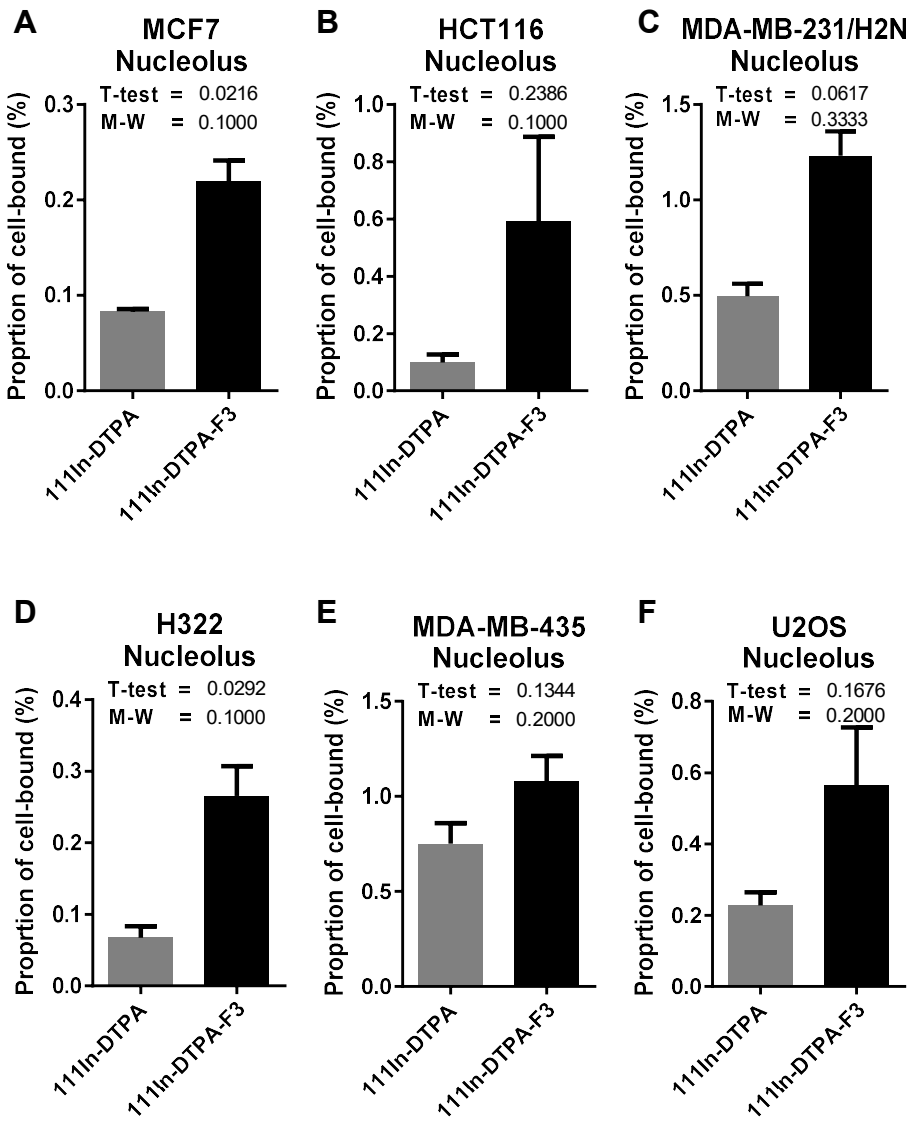

Figure 5.8. Proportion of cell-bound radioactivity associated with the nucleolus of malignant cells after exposure to ^{111}In-DTPA-F3 or ^{111}In-DTPA

Proportion of cell-bound radioactivity (%) associated the nucleolus of (A) MCF7, (B) HCT116, (C) MDA-MB-231/H2N, (D) H322, (E) MDA-MB-435, and (F) U2OS cells exposed for 3 h to 1 μM of ^{111}In-DTPA-F3 (22.17 MBq/nmol) or an equimolar amount of ^{111}In-DTPA. Values show mean proportion of cell-bound radioactivity ± SEM, n = 2–3. GraphPad Prism 6 software was used to test if the data followed a Gaussian distribution using a D'Agostino-Pearson omnibus test. Since the data did not follow a Gaussian distribution, means were compared using unpaired Mann-Whitney (M-W) tests with two-tailed P values. However, the unpaired, two-tailed M-W test has little statistical power and will never produce a P value of less than 0.1 for a sample size of 3 or less. Therefore, parametric T-tests with Welch's correction for unequal standard deviations (two-tailed P values) were also performed.

that a lower proportion of cell-bound ^{111}In-DTPA-F3 was associated with the membrane of the H322 cells compared to ^{111}In-DTPA (M-W test, P = 0.1000; T-test, P=0.1294); a lower proportion of cell-bound ^{111}In-DTPA-F3 was associated with the cytoplasm of the H322 (M-W test, P = 0.1000; T-test, P = 0.1023) and U2OS (M-W test, P = 0.1000; T-test, P = 0.0808) cells compared to ^{111}In-DTPA; and a higher proportion of cell-bound ^{111}In-DTPA-F3 was associated with the nucleus (M-W test, P = 0.1000; T-test, P = 0.0332) and nucleoplasm (M-W test, P = 0.1000; T-test, P = 0.0290) of the HCT116 cells compared to ^{111}In-DTPA.

However, there was a trend of a higher level of cell-bound ^{111}In-DTPA-F3 associated with the nucleolus of malignant cells compared to ^{111}In-DTPA (Figure 5.9). A higher level of cell-bound ^{111}In-DTPA-F3 was associated with the nucleolus of the MCF7 (M-W test, P = 0.1000; T-test, P = 0.0216), HCT116 (M-W test, P = 0.1000; T-test, P = 0.2386) and H322 (M-W test, P = 0.1000; T-test, P = 0.0292) cells compared to ^{111}In-DTPA; although the proportion of cell-bound ^{111}In-DTPA-F3 associated with the nucleolus of the MDA-MB-231/H2N, MDA-MB-435 and U2OS cells was not statistically significantly different from ^{111}In-DTPA. Nevertheless, this evidence supported the hypothesis that ^{111}In-DTPA-F3 targeted the nucleolus of the malignant cells.

Further analysis of the fraction in which there had been greater uptake of ^{111}In-DTPA-F3 compared to ^{111}In-DTPA, was carried out by calculating the ^{111}In-DTPA-F3-to-^{111}In-DTPA ratio (^{111}In-DTPA-F3/^{111}In-DTPA ratio) for the percentage of radioactivity that became cell-bound (% cell-bound radioactivity) and for the proportion of cell-bound radioactivity associated with the membrane, cytoplasm, nucleus, nucleoplasm and nucleolus. Table 5.2 and Figure 5.10 show the ^{111}In-DTPA-F3/^{111}In-DTPA ratio (a measure of the fold-change in radioactivity due to the incorporation of F3 into ^{111}In-DTPA) for % cell-bound radioactivity and for the proportion of cell-bound radioactivity

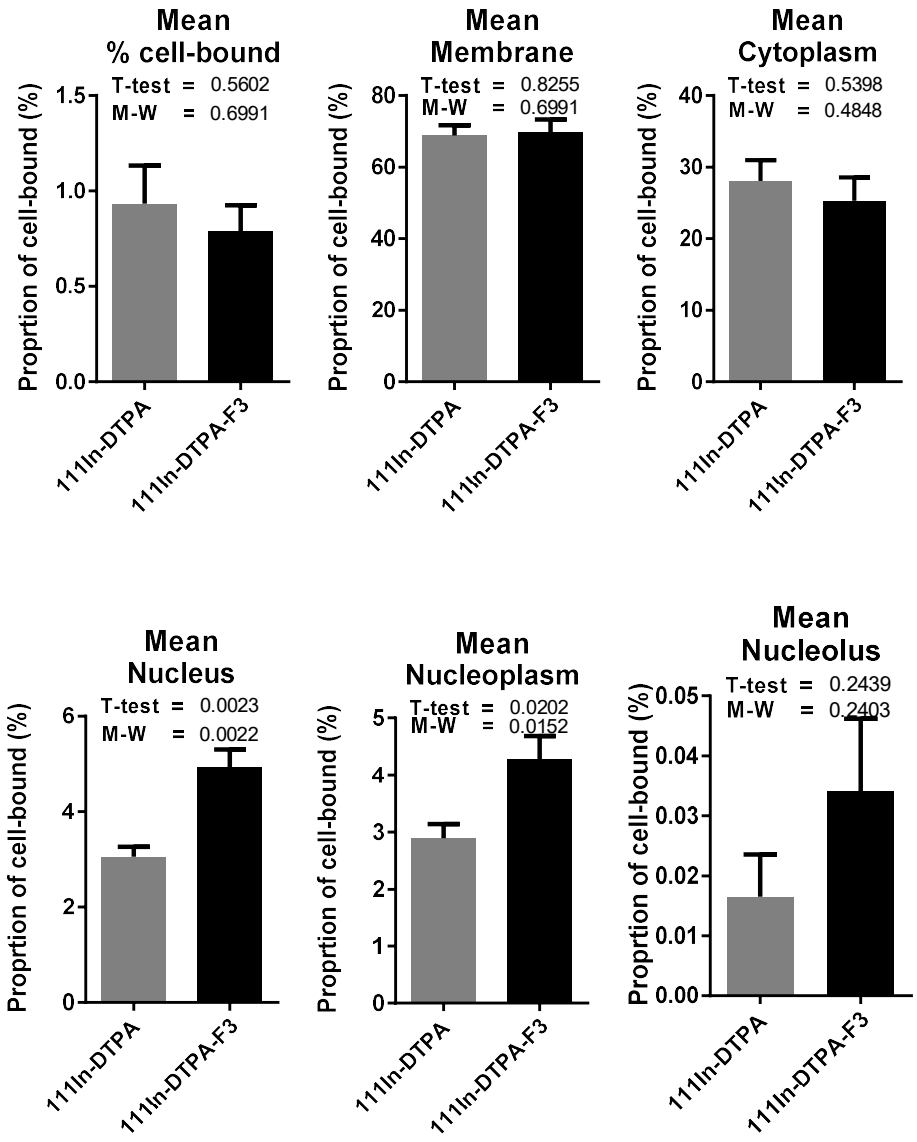

Figure 5.9. Mean percentage of radioactivity that became cell-bound and mean proportion of cell-bound radioactivity associated with malignant cells after exposure to ^{111}In-DTPA-F3 or ^{111}In-DTPA

Proportion of cell-bound radioactivity (%) associated the nucleolus of (A) MCF7, (B) HCT116, (C) MDA-MB-231/H2N, (D) H322, (E) MDA-MB-435, and (F) U2OS cells exposed for 3 h to 1 μM of ^{111}In-DTPA-F3 (22.17 MBq/nmol) or an equimolar amount of ^{111}In-DTPA. Values show mean proportion of cell-bound radioactivity ± SEM, n = 2–3. GraphPad Prism 6 software was used to test if the data followed a Gaussian distribution using a D'Agostino-Pearson omnibus test. Since the data did not follow a Gaussian distribution, means were compared using unpaired Mann-Whitney (M-W) tests with two-tailed P values. However, the unpaired, two-tailed M-W test has little statistical power and will never produce a P value of less than 0.1 for a sample size of 3 or less. Therefore, parametric T-tests with Welch's correction for unequal standard deviations (two-tailed P values) were also performed.

	Fold-change in % cell-bound	Fold-change in proportion of cell-bound (%)				
		Membrane	Cytoplasm	Nucleus	Nucleoplasm	Nucleolus
MCF7	0.77±0.24	0.91±0.11	1.17±0.22	1.79±0.46	1.77±0.47	2.67±0.34
HCT116	0.68±0.05	0.96±0.07	2.34±1.53	1.17±0.20	1.61±0.16	7.24±3.87
MDA-MB-231/H2N	0.75±0.03	1.00±0.07	0.95±0.16	1.73±0.08	1.58±0.19	2.56±0.59
H322	1.05±0.19	1.18±0.07	0.68±0.11	2.12±0.78	2.05 ±0.75	4.33±1.22
MDA-MB-435	1.17±0.17	1.05±0.05	0.87±0.09	1.41±0.22	1.11±0.21	1.46±0.15
U2OS	1.07±0.08	1.04±0.03	0.80±0.07	1.48±0.11	1.37±0.13	2.58±0.90
Mean	**0.91±0.08**	**1.02±0.04**	**1.13±0.25**	**1.71±0.10**	**1.58±0.13**	**3.47±0.84**

Table 5.2. Fold-change in % cell-bound radioactivity and the fold-change in the proportion of cell-bound radioactivity associated with the cell, membrane, cytoplasm, nucleus, nucleoplasm and nucleolus of malignant cells due to the incorporation of F3 into ^{111}In-DTPA

Fold-change in (A) % cell-bound radioactivity (^{111}In-DTPA-F3/^{111}In-DTPA ratio) and the fold-change in the proportion of radioactivity associated with the (B) membrane, (C) cytoplasm, (D) nucleus, (E) nucleoplasm and (F) nucleolus of MCF7, HCT116, MDA-MB-231/H2N, H322, MDA-MB-435, and U2OS cells exposed for 3 h to 1 μM of ^{111}In-DTPA-F3 (22.17 MBq/nmol) or an equimolar amount of ^{111}In-DTPA, due to the incorporation of F3 into ^{111}In-DTPA. ^{111}In-DTPA-F3/^{111}In-DTPA ratios were calculated by dividing the proportion of cell-bound radioactivity associated with the membrane, cytoplasm, nucleoplasm or nucleolus after exposure to ^{111}In-DTPA-F3 by the proportion of cell-bound radioactivity in the same fraction after exposure to ^{111}In-DTPA. ^{111}In-DTPA-F3/^{111}In-DTPA ratios for % cell-bound radioactivity were calculated in a similar manner after dividing the total amount of radioactivity the cells were exposed to by the total radioactivity from the membrane, cytoplasm, nucleoplasm and nucleolus; while ^{111}In-DTPA-F3/^{111}In-DTPA ratios for the proportion of cell-bound radioactivity in the nucleus were calculated after combining the proportion of cell-bound radioactivity from the nucleoplasm and nucleolus. Values show fold-change ± SEM, n = 2–3.

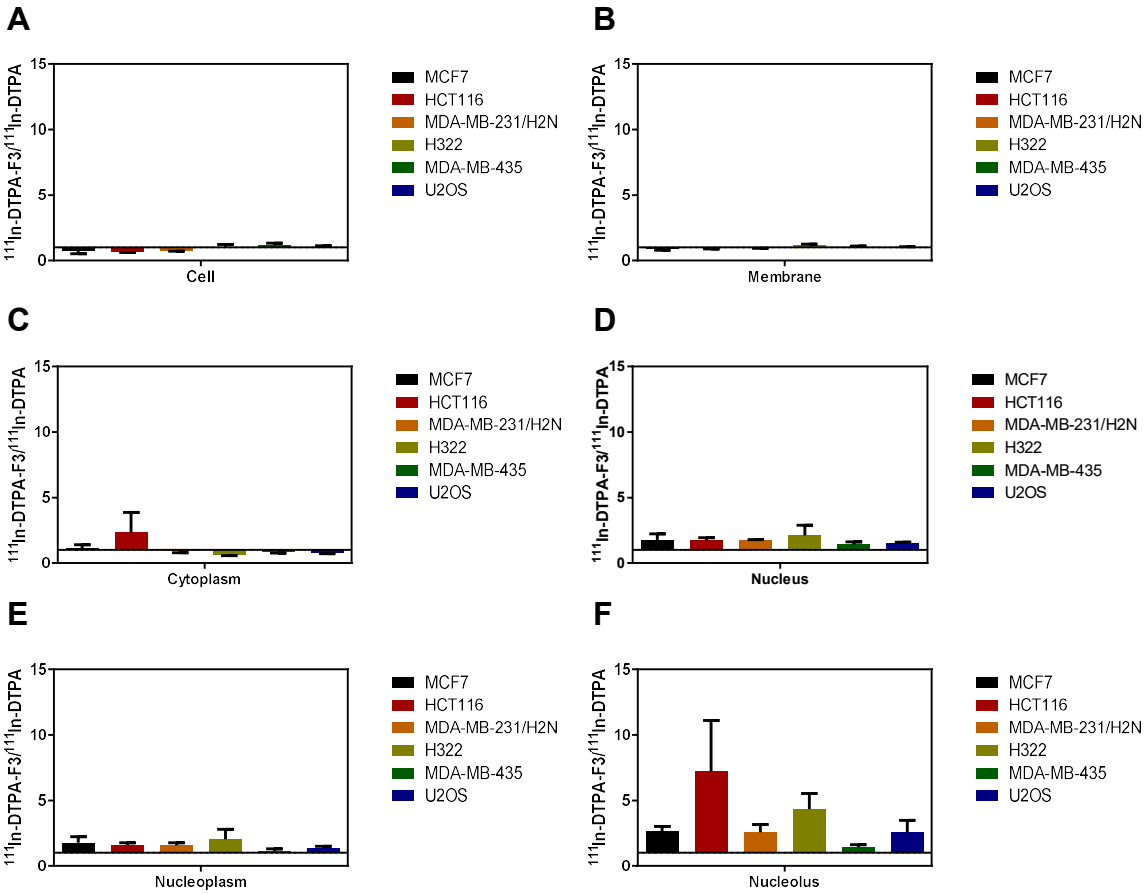

Figure 5.10. Fold-change in % cell-bound radioactivity and the fold-change in the proportion of cell-bound radioactivity associated with the cell, membrane, cytoplasm, nucleus, nucleoplasm and nucleolus of malignant cells due to the incorporation of F3 into ^{111}In-DTPA

Fold-change in (A) % cell-bound radioactivity (^{111}In-DTPA-F3/^{111}In-DTPA ratio) and the fold-change in the proportion of radioactivity associated with the (B) membrane, (C) cytoplasm, (D) nucleus, (E) nucleoplasm and (F) nucleolus of MCF7, HCT116, MDA-MB-231/H2N, H322, MDA-MB-435, and U2OS cells exposed for 3 h to 1 μM of ^{111}In-DTPA-F3 (22.17 MBq/nmol) or an equimolar amount of ^{111}In-DTPA, due to the incorporation of F3 into ^{111}In-DTPA. ^{111}In-DTPA-F3/^{111}In-DTPA ratios were calculated by dividing the proportion of cell-bound radioactivity associated with the membrane, cytoplasm, nucleoplasm or nucleolus after exposure to ^{111}In-DTPA-F3 by the proportion of cell-bound radioactivity in the same fraction after exposure to ^{111}In-DTPA. ^{111}In-DTPA-F3/^{111}In-DTPA ratios for % cell-bound radioactivity were calculated in a similar manner after dividing the total amount of radioactivity the cells were exposed to by the total radioactivity from the membrane, cytoplasm, nucleoplasm and nucleolus; while ^{111}In-DTPA-F3/^{111}In-DTPA ratios for the proportion of cell-bound radioactivity in the nucleus were calculated after combining the proportion of cell-bound radioactivity from the nucleoplasm and nucleolus. Values show fold-change ± SEM, n = 2–3.

associated with the membrane, cytoplasm, nucleus, nucleoplasm and nucleolus of MCF7, HCT116, MDA-MB-231/H2N, H322, MDA-MB-435 and U2OS cells. A trend emerged, as shown in Figure 5.10.F, that showed that the ^{111}In-DTPA-F3/^{111}In-DTPA ratio was highest in the nucleolus, suggesting that ^{111}In-DTPA-F3 was transported to the nucleolus at a higher rate compared to ^{111}In-DTPA. Figure 5.11 shows the mean ^{111}In-DTPA-F3/^{111}In-DTPA ratio (i.e., an average of the ^{111}In-DTPA-F3/^{111}In-DTPA ratios for the six malignant cell lines, n = 6) for % cell-bound radioactivity and for the proportion of cell-bound radioactivity associated with the membrane, cytoplasm, nucleus, nucleoplasm and nucleolus. A D'Agostino-Pearson omnibus test indicated that these data did not follow a Gaussian distribution. Therefore, differences between the mean ^{111}In-DTPA-F3/^{111}In-DTPA ratios and a hypothetical value of 1 (i.e., unity) were compared using a non-parametric Wilcoxon signed-rank test. A parametric one-sample T-tests was also performed and a P value of <0.05 was taken with a moderate level of confidence that the mean ^{111}In-DTPA-F3/^{111}In-DTPA ratios was not similar to unity. The ^{111}In-DTPA-F3/^{111}In-DTPA ratio for the proportion of cell-bound radioactivity associated with the nucleus (Wilcoxon, P = 0.0313; T-test, P = 0.0001), nucleoplasm (Wilcoxon, P = 0.0.0313; T-test, P = 0.0029) and nucleolus (Wilcoxon, P = 0.0313; T-test, P = 0.0209) was significantly different from unity (1). The ^{111}In-DTPA-F3/^{111}In-DTPA ratio for the proportion of cell-bound radioactivity associated with the nucleolus was greatest than that of all other intracellular compartments, and was significantly different from that for % cell-bound radioactivity (P = 0.0017) and for the proportion of cell-bound radioactivity in the membrane (P = 0.0137) and cytoplasm (P = 0.021). The ^{111}In-DTPA-F3/^{111}In-DTPA ratio for the proportion of cell-bound radioactivity associated with the nucleus was also significantly different from that for % cell-bound radioactivity (P = 0.0423). Together, this suggested that ^{111}In-DTPA-F3 was

Wilcoxon signed-rank test (significantly different from unity)

Cell	Membrane	Cytoplasm	Nucleus	Nucleoplasm	Nucleolus
0.3125	> 0.9999	0.3125	0.0313	0.0313	0.0313

One-sample T-test (significantly different from unity)

Cell	Membrane	Cytoplasm	Nucleus	Nucleoplasm	Nucleolus
0.2013	0.6945	0.2638	0.0001	0.0029	0.0209

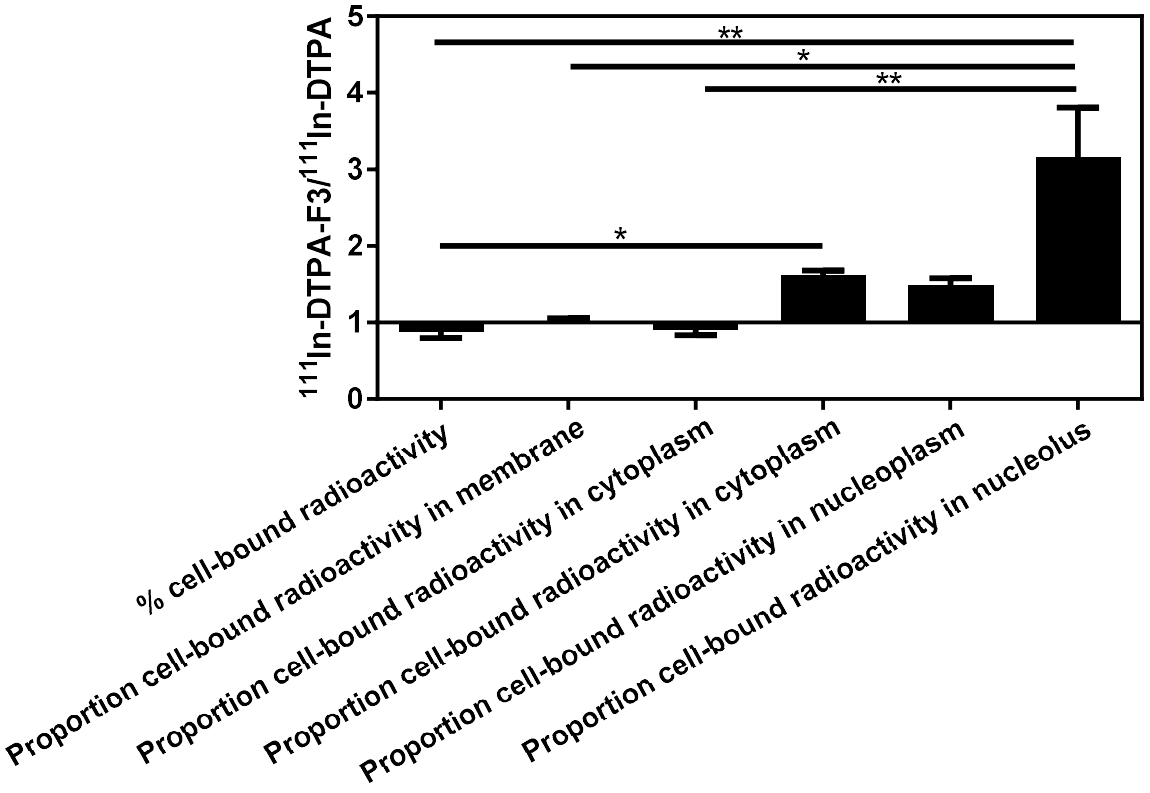

Figure 5.11. Mean fold-change in radioactivity associated with the cell, membrane, cytoplasm, nucleus, nucleoplasm and nucleolus of malignant cells due to the incorporation of F3 into ^{111}In-DTPA

Mean fold-change in radioactivity (mean ^{111}In-DTPA-F3/^{111}In-DTPA ratio) associated with the cell, membrane, cytoplasm, nucleus, nucleoplasm and nucleolus of MCF7, HCT116, MDA-MB-231/H2N, H322, MDA-MB-435, and U2OS cells exposed for 3 h to 1 μM of ^{111}In-DTPA-F3 (22.17 MBq/nmol) or an equimolar amount of ^{111}In-DTPA, due to the incorporation of F3 into ^{111}In-DTPA. Mean ^{111}In-DTPA-F3/^{111}In-DTPA ratios were calculated by taking the average of ^{111}In-DTPA-F3/^{111}In-DTPA ratios of MCF7, HCT116, MDA-MB-231/H2N, H322, MDA-MB-435, and U2OS cells (see Table 5.2). Values show mean fold-change ± SEM, n = 6. GraphPad Prism 6 software was used to test if the data followed a Gaussian distribution using a D'Agostino-Pearson omnibus test. Since the data did not follow a Gaussian distribution, medians were compared to a hypothetical value of 1 using non-parametric Wilcoxon signed-rank test. Nevertheless, parametric one-sample T-tests were also performed to test if means were significantly different from 1. A non-parametric Kruskal-Wallis one-way ANOVA with multiplicity adjusted P values (Dunn's post-hoc test) was also performed. *, $P < 0.05$; **, $P < 0.01$.

transported to the nucleolus at a higher rate compared to ^{111}In-DTPA. Along with the clonogenic survival data (Chapter 4, Figure 4.4) that showed that ^{111}In-DTPA-F3, but not ^{111}In-DTPA, was significantly radiotoxic to the malignant cell lines (except for U2OS cells which were not radiosensitive to ^{111}In-DTPA-F3), this suggested that the transportation of ^{111}In-DTPA-F3 to the nucleolus was likely to be responsible for the radiotoxicity of ^{111}In-DTPA-F3.

Table 5.3 and Figures 5.12–5.17 show the amount of radioactivity (mBq/cell) that was associated with the cell, membrane, cytoplasm, nucleus, nucleoplasm and nucleolus of MCF7, HCT116, MDA-MB-231/H2N, H322, MDA-MB-435 and U2OS cells exposed to ^{111}In-DTPA-F3 or ^{111}In-DTPA. The level of radioactivity that was associated with the malignant cells after exposure to ^{111}In-DTPA-F3 was similar to ^{111}In-DTPA, with the exception that a lower level of radioactivity was associated with the HCT116 cells after exposure to ^{111}In-DTPA-F3 compared to ^{111}In-DTPA (M-W test, P = 0.1000; T-test, P = 0.0125) (Figure 5.12). The level of radioactivity that was associated with the membrane (Figure 5.13), cytoplasm (Figure 5.14), nucleus (Figure 5.15) and nucleoplasm (Figure 5.16) of the malignant cells after exposure to ^{111}In-DTPA-F3 was also similar to ^{111}In-DTPA, with the exceptions that a lower level of radioactivity was associated with the membrane of the HCT116 cells after exposure to ^{111}In-DTPA-F3 compared to ^{111}In-DTPA (M-W test, P = 0.1000; T-test, P = 0.0665); a lower level of radioactivity was associated with the cytoplasm of the MCF7 cells after exposure to ^{111}In-DTPA-F3 compared to ^{111}In-DTPA (M-W test, P = 0.1000; T-test, P = 0.1179); a higher level of radioactivity was associated with the nucleus of the H322 (M-W test, P = 0.1000; T-test, P = 0.0274) and U2OS (M-W test, P = 0.1000; T-test, P = 0.0155) cells after exposure to ^{111}In-DTPA-F3 compared to ^{111}In-DTPA; and a higher level of radioactivity was associated with the nucleoplasm of the H322 cells after exposure to

	^{111}In-DTPA-F3 (mBq/cell)						^{111}In-DTPA (mBq/cell)					
	Cell	**Me**	**Cy**	**Nu**	**Np**	**No**	**Cell**	**Me**	**Cy**	**Nu**	**Np**	**No**
MCF7	1.378 ±0.274	0.764 ±0.219	**0.539 ±0.059**	0.075 ±0.010	0.072 ±0.010	**0.003 ±0.000**	1.994 ±0.410	1.245 ±0.373	**0.685 ±0.040**	0.064 ±0.005	0.062 ±0.006	**0.002 ±0.000**
HCT116	**3.062 ±0.194**	**2.262 ±0.125**	0.617 ±0.069	0.183 ±0.014	0.166 ±0.017	**0.017 ±0.007**	**4.532 ±0.051**	**3.551 ±0.384**	0.822 ±0.334	0.158 ±0.006	0.154 ±0.005	**0.004 ±0.001**
MDA-MB-231/H2N	5.034 ±0.475	3.465 ±0.219	1.315 ±0.226	0.253 ±0.030	0.192 ±0.031	0.061 ±0.001	6.732 ±0.373	4.671 ±0.428	1.865 ±0.060	0.196 ±0.006	0.162 ±0.000	0.034 ±0.006
H322	1.702 ±0.067	1.234 ±0.063	0.394 ±0.014	**0.074 ±0.007**	**0.070 ±0.007**	**0.005 ±0.001**	1.784 ±0.448	1.100 ±0.261	0.645 ±0.205	**0.039 ±0.003**	**0.038 ±0.0034**	**0.001 ±0.000**
MDA-MB-435	6.336 ±0.441	4.479 ±0.337	1.547 ±0.117	0.310 ±0.042	0.240 ±0.033	**0.070 ±0.013**	5.594 ±0.779	3.775 ±0.596	1.580 ±0.178	0.239 ±0.037	0.198 ±0.035	**0.041 ±0.003**
U2OS	8.253 ±0.981	6.535 ±0.864	1.432 ±0.169	**0.287 ±0.050**	0.237 ±0.040	0.049 ±0.017	7.681 ±0.583	5.807 ±0.420	1.693 ±0.145	**0.181 ±0.026**	0.163 ±0.027	0.018 ±0.003

Table 5.3. Radioactivity associated with the cell, membrane, cytoplasm, nucleus, nucleoplasm, and nucleolus of malignant cells exposed to ^{111}In-DTPA-F3 or ^{111}In-DTPA

Radioactivity (mBq/cell) associated with the cell, membrane, cytoplasm, nucleus, nucleoplasm, and nucleolus of MCF7, HCT116, MDA-MB-231/H2N, H322, MDA-MB-435, and U2OS cells exposed for 3 h to 1 μM of ^{111}In-DTPA-F3 (22.17 MBq/nmol) or an equimolar amount of ^{111}In-DTPA. Radioactivity associated with the cell was calculated by combining the radioactivity associated with the membrane, cytoplasm, nucleoplasm and nucleolus. Radioactivity associated with the nucleus was calculated by combining the radioactivity associated with the nucleoplasm and nucleolus. Values show mean radioactivity ± SEM, n = 2–3. Me, membrane; Cy, cytoplasm; Nu, nucleus; Np, nucleoplasm; No, nucleolus. Using GraphPad Prism 6, data for ^{111}In-DTPA-F3 versus ^{111}In-DTPA was compared using an unpaired Mann-Whitney test (two-tailed P values) and T-tests with Welch's correction for unequal standard deviations (two-tailed P values). Bold values, significance.

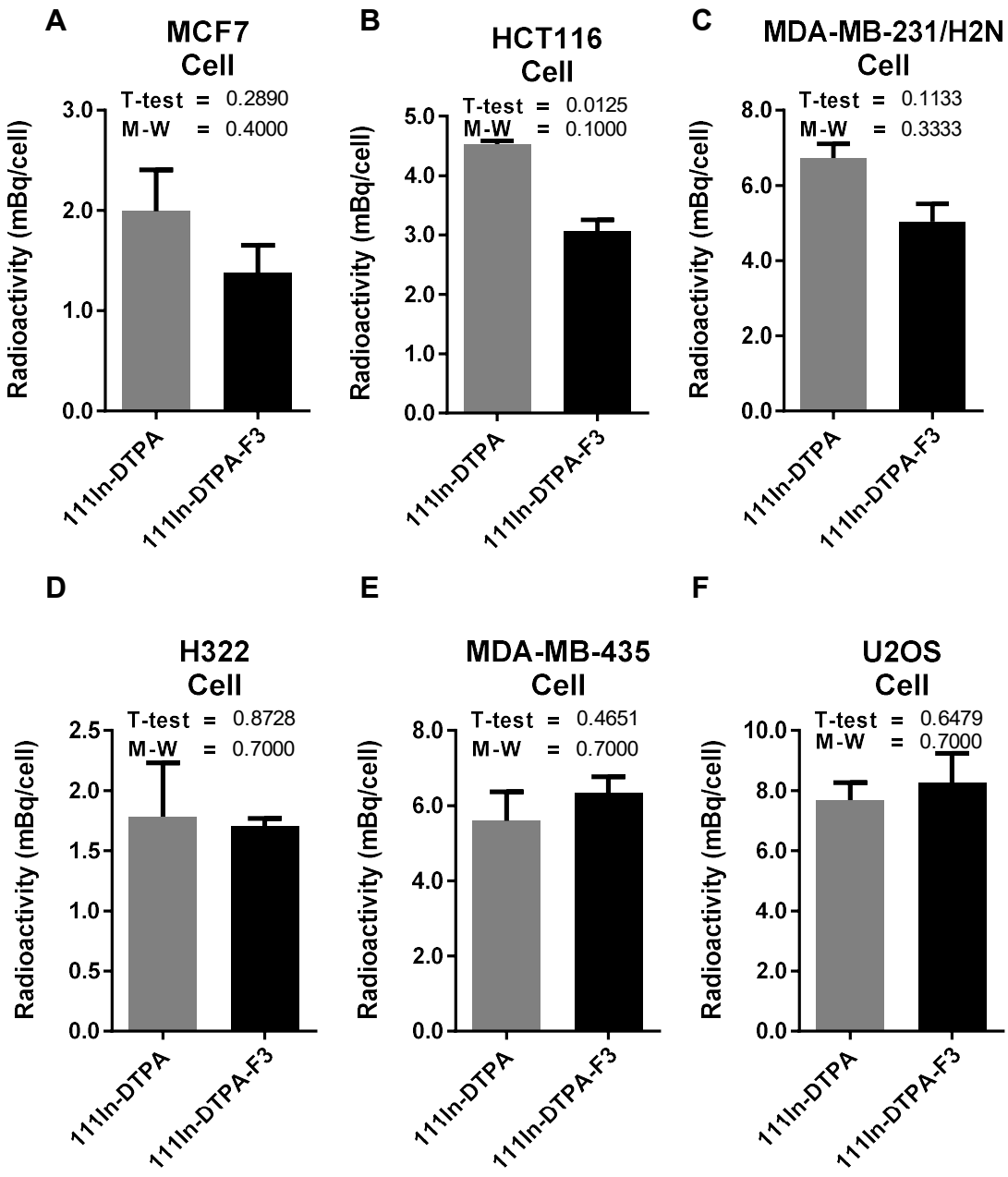

Figure 5.12. Radioactivity associated with malignant cells after exposure to ^{111}In-DTPA-F3 or ^{111}In-DTPA

Radioactivity (mBq/cell) associated with (A) MCF7, (B) HCT116, (C) MDA-MB-231/H2N, (D) H322, (E) MDA-MB-435, and (F) U2OS cells exposed for 3 h to 1 μM of ^{111}In-DTPA-F3 (22.17 MBq/nmol) or an equimolar amount of ^{111}In-DTPA. Radioactivity associated with the cell was calculated by combining the radioactivity associated with the membrane, cytoplasm, nucleoplasm and nucleolus. Values show mean radioactivity ± SEM, n = 2–3. GraphPad Prism 6 software was used to test if the data followed a Gaussian distribution using a D'Agostino-Pearson omnibus test. Since the data did not follow a Gaussian distribution, means were compared using unpaired Mann-Whitney (M-W) tests with two-tailed P values. However, the unpaired, two-tailed M-W test has little statistical power and will never produce a P value of less than 0.1 for a sample size of 3 or less. Therefore, parametric T-tests with Welch's correction for unequal standard deviations (two-tailed P values) were also performed.

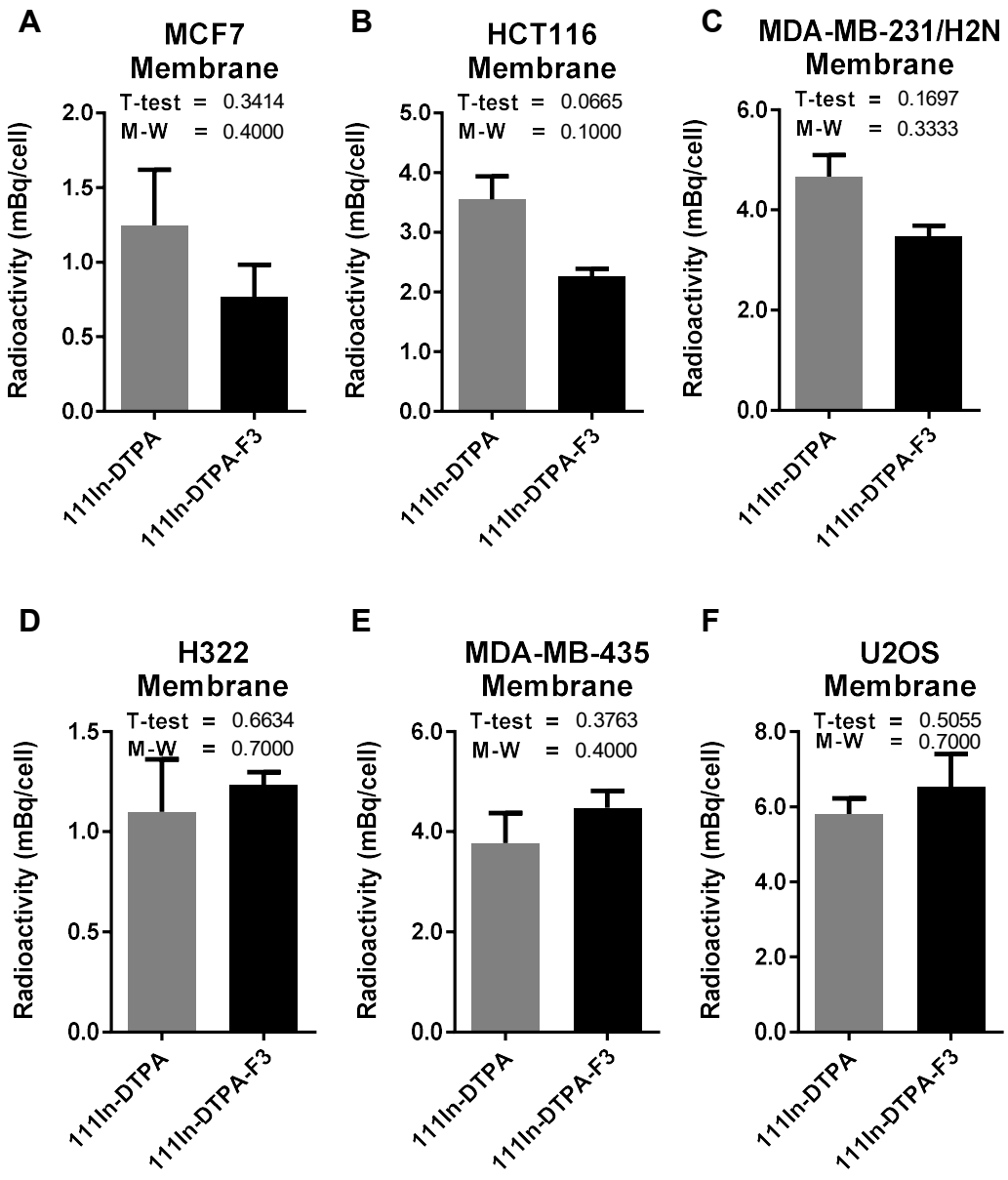

Figure 5.13. Radioactivity associated with the membrane of malignant cells after exposure to ^{111}In-DTPA-F3 or ^{111}In-DTPA

Radioactivity (mBq/cell) associated with the membrane of (A) MCF7, (B) HCT116, (C) MDA-MB-231/H2N, (D) H322, (E) MDA-MB-435, and (F) U2OS cells exposed for 3 h to 1 μM of ^{111}In-DTPA-F3 (22.17 MBq/nmol) or an equimolar amount of ^{111}In-DTPA. Values show mean radioactivity ± SEM, n = 2–3. GraphPad Prism 6 software was used to test if the data followed a Gaussian distribution using a D'Agostino-Pearson omnibus test. Since the data did not follow a Gaussian distribution, means were compared using unpaired Mann-Whitney (M-W) tests with two-tailed P values. However, the unpaired, two-tailed M-W test has little statistical power and will never produce a P value of less than 0.1 for a sample size of 3 or less. Therefore, parametric T-tests with Welch's correction for unequal standard deviations (two-tailed P values) were also performed.

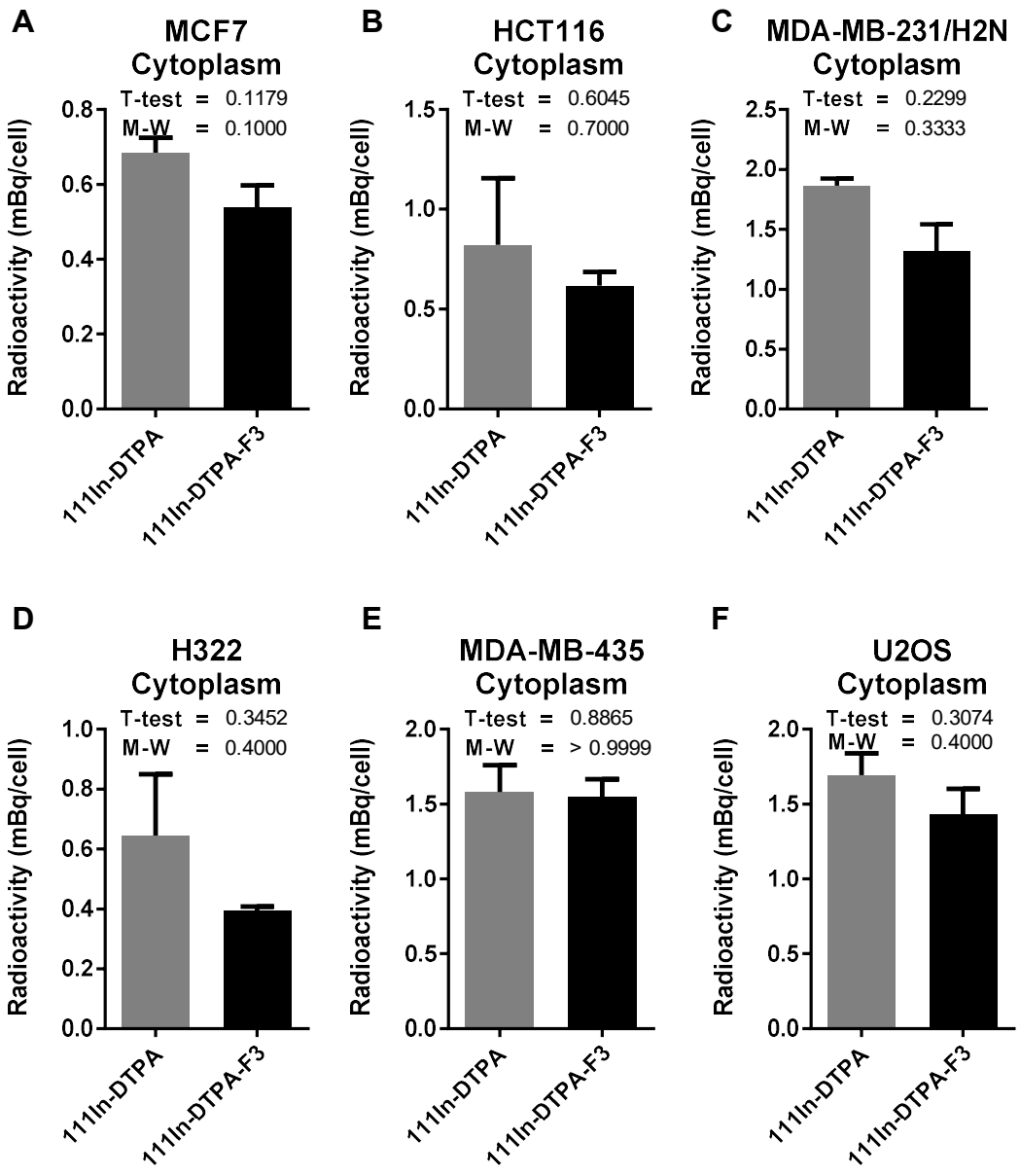

Figure 5.14. Radioactivity associated with the cytoplasm of malignant cells after exposure to ^{111}In-DTPA-F3 or ^{111}In-DTPA

Radioactivity (mBq/cell) associated with the cytoplasm of (A) MCF7, (B) HCT116, (C) MDA-MB-231/H2N, (D) H322, (E) MDA-MB-435, and (F) U2OS cells exposed for 3 h to 1 μM of ^{111}In-DTPA-F3 (22.17 MBq/nmol) or an equimolar amount of ^{111}In-DTPA. Values show mean radioactivity ± SEM, n = 2–3. GraphPad Prism 6 software was used to test if the data followed a Gaussian distribution using a D'Agostino-Pearson omnibus test. Since the data did not follow a Gaussian distribution, means were compared using unpaired Mann-Whitney (M-W) tests with two-tailed P values. However, the unpaired, two-tailed M-W test has little statistical power and will never produce a P value of less than 0.1 for a sample size of 3 or less. Therefore, parametric T-tests with Welch's correction for unequal standard deviations (two-tailed P values) were also performed.

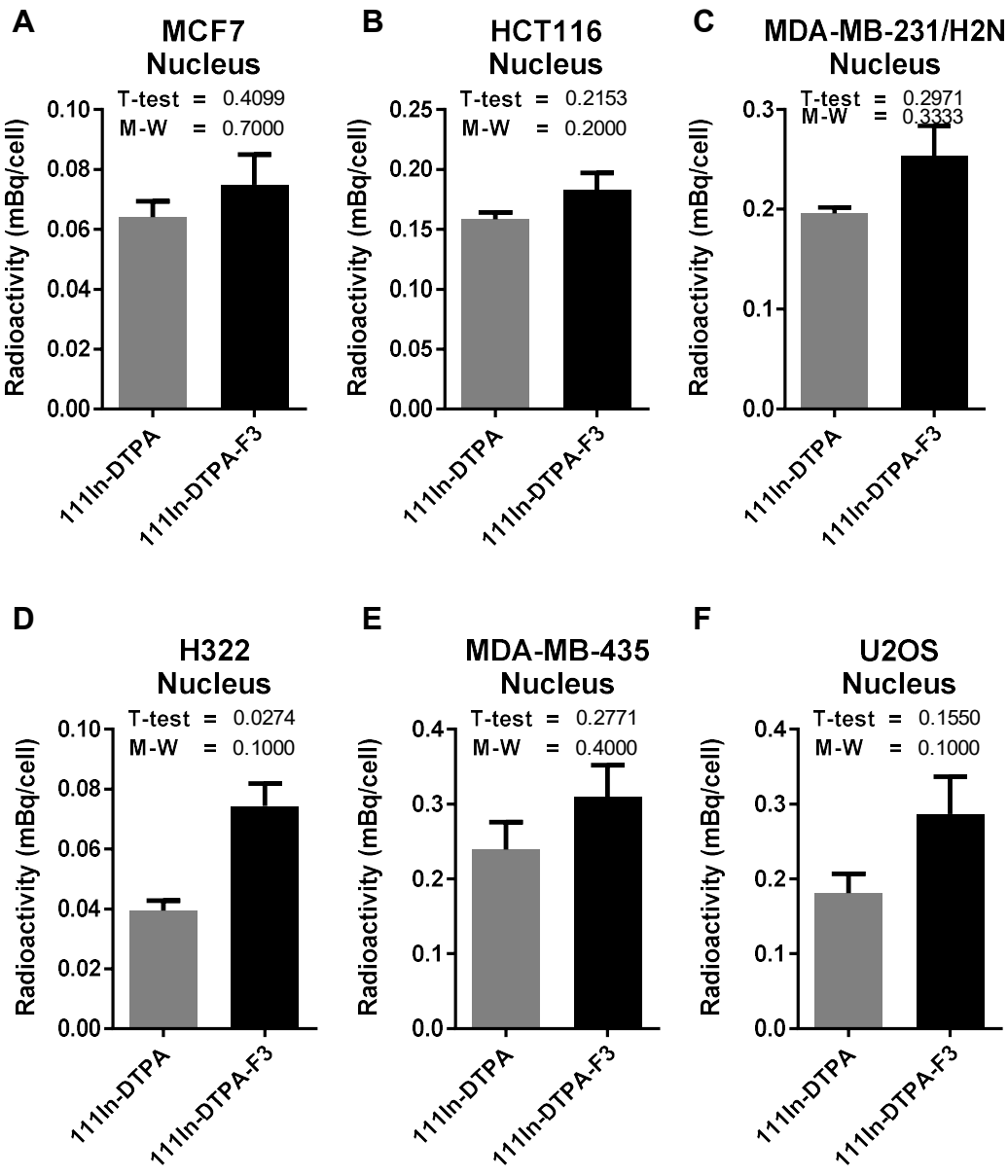

Figure 5.15. Radioactivity associated with the nucleus of malignant cells after exposure to ^{111}In-DTPA-F3 or ^{111}In-DTPA

Radioactivity (mBq/cell) associated with the nucleus of (A) MCF7, (B) HCT116, (C) MDA-MB-231/H2N, (D) H322, (E) MDA-MB-435, and (F) U2OS cells exposed for 3 h to 1 μM of ^{111}In-DTPA-F3 (22.17 MBq/nmol) or an equimolar amount of ^{111}In-DTPA. Radioactivity associated with the nucleus was calculated by combining the radioactivity associated with the nucleoplasm and nucleolus. Values show mean radioactivity ± SEM, n = 2–3. GraphPad Prism 6 software was used to test if the data followed a Gaussian distribution using a D'Agostino-Pearson omnibus test. Since the data did not follow a Gaussian distribution, means were compared using unpaired Mann-Whitney (M-W) tests with two-tailed P values. However, the unpaired, two-tailed M-W test has little statistical power and will never produce a P value of less than 0.1 for a sample size of 3 or less. Therefore, parametric T-tests with Welch's correction for unequal standard deviations (two-tailed P values) were also performed.

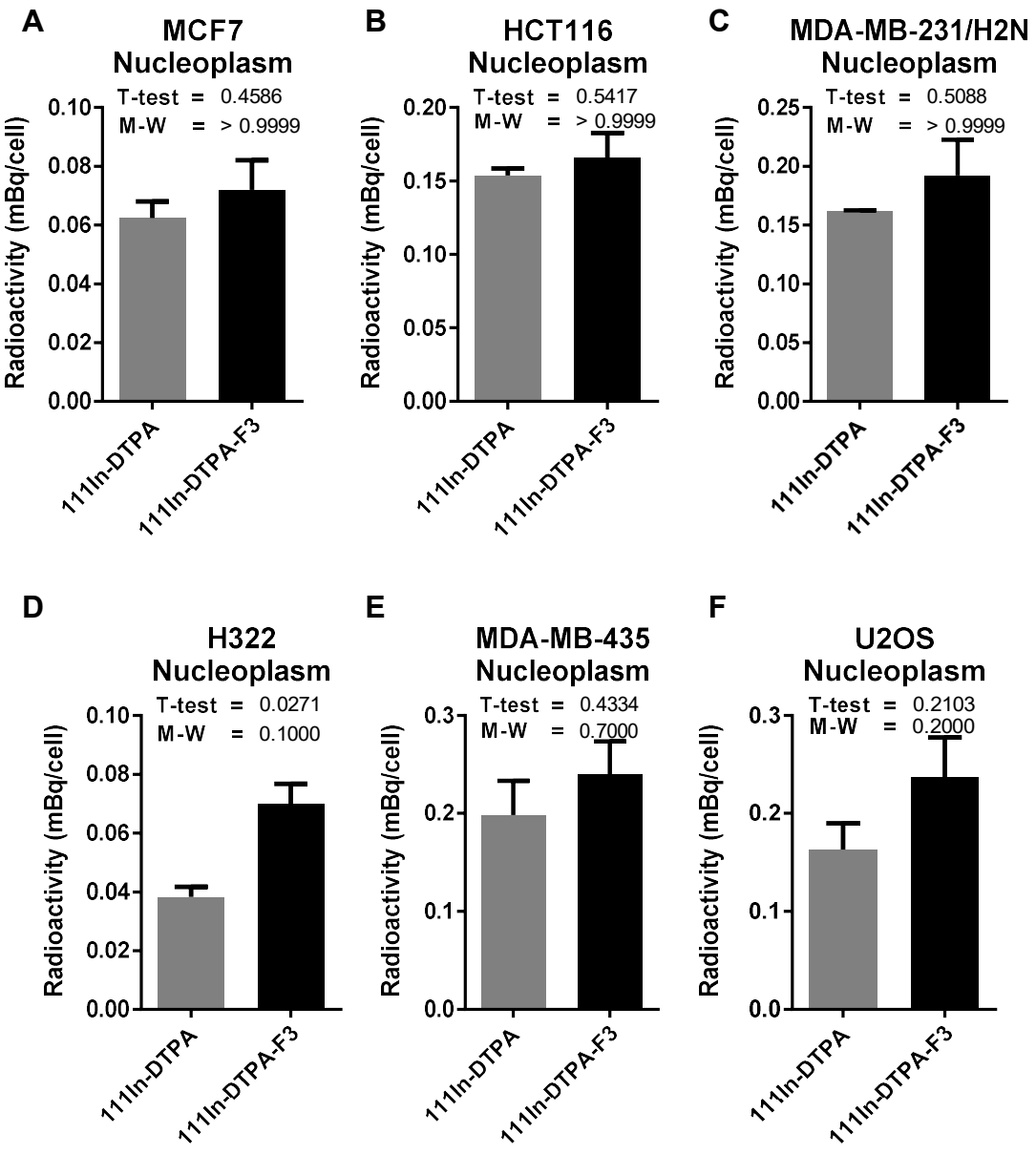

Figure 5.16. Radioactivity associated with the nucleoplasm of malignant cells after exposure to ^{111}In-DTPA-F3 or ^{111}In-DTPA

Radioactivity (mBq/cell) associated with the nucleoplasm of (A) MCF7, (B) HCT116, (C) MDA-MB-231/H2N, (D) H322, (E) MDA-MB-435, and (F) U2OS cells exposed for 3 h to 1 μM of ^{111}In-DTPA-F3 (22.17 MBq/nmol) or an equimolar amount of ^{111}In-DTPA. Values show mean radioactivity ± SEM, n = 2–3. GraphPad Prism 6 software was used to test if the data followed a Gaussian distribution using a D'Agostino-Pearson omnibus test. Since the data did not follow a Gaussian distribution, means were compared using unpaired Mann-Whitney (M-W) tests with two-tailed P values. However, the unpaired, two-tailed M-W test has little statistical power and will never produce a P value of less than 0.1 for a sample size of 3 or less. Therefore, parametric T-tests with Welch's correction for unequal standard deviations (two-tailed P values) were also performed.

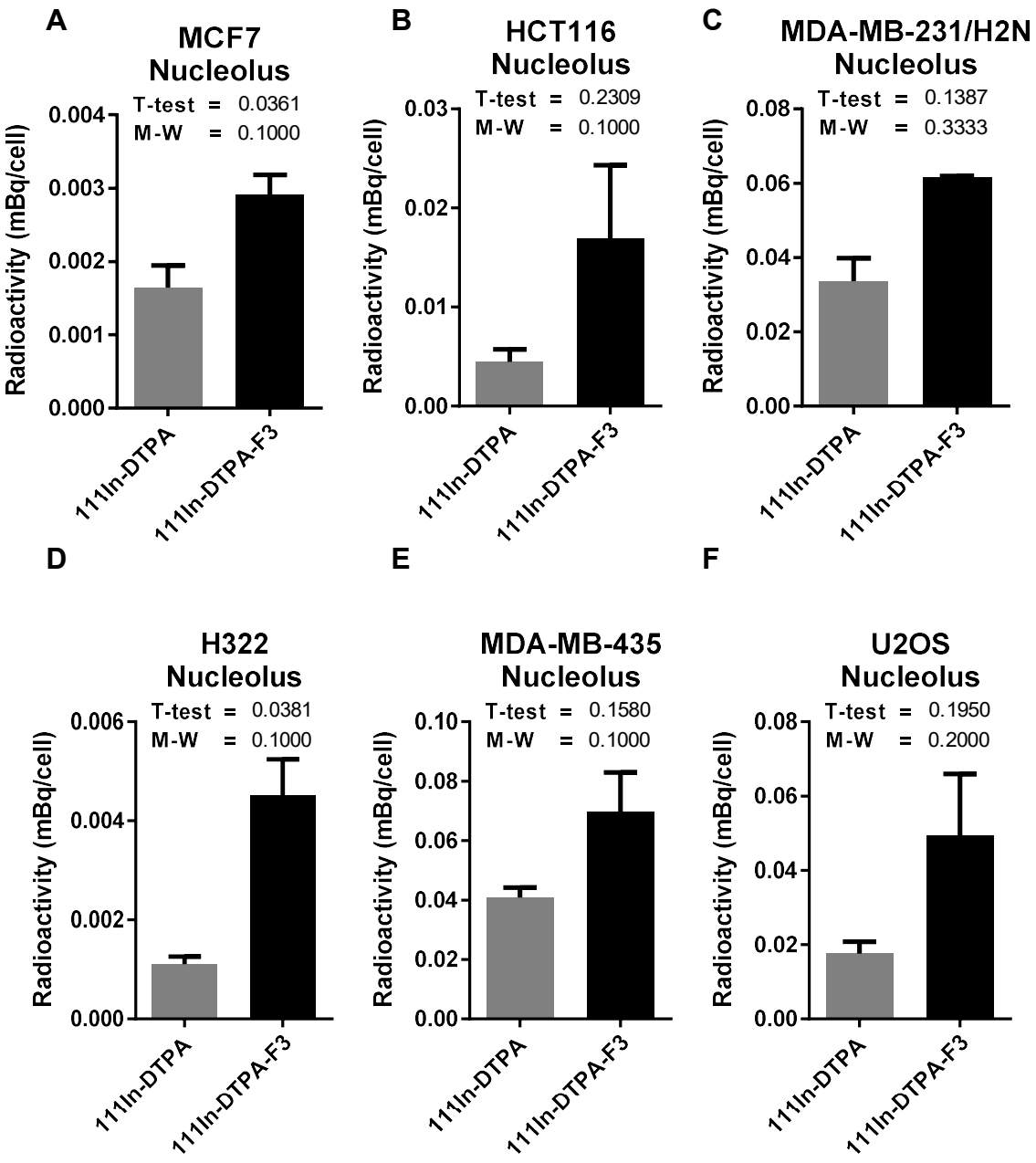

Figure 5.17. Radioactivity associated with the nucleolus of malignant cells after exposure to ^{111}In-DTPA-F3 or ^{111}In-DTPA

Radioactivity (mBq/cell) associated with the nucleolus of (A) MCF7, (B) HCT116, (C) MDA-MB-231/H2N, (D) H322, (E) MDA-MB-435, and (F) U2OS cells exposed for 3 h to 1 μM of ^{111}In-DTPA-F3 (22.17 MBq/nmol) or an equimolar amount of ^{111}In-DTPA. Values show mean radioactivity ± SEM, n = 2–3. GraphPad Prism 6 software was used to test if the data followed a Gaussian distribution using a D'Agostino-Pearson omnibus test. Since the data did not follow a Gaussian distribution, means were compared using unpaired Mann-Whitney (M-W) tests with two-tailed P values. However, the unpaired, two-tailed M-W test has little statistical power and will never produce a P value of less than 0.1 for a sample size of 3 or less. Therefore, parametric T-tests with Welch's correction for unequal standard deviations (two-tailed P values) were also performed.

^{111}In-DTPA-F3 compared to ^{111}In-DTPA (M-W test, P = 0.1000; T-test, P = 0.0271). However, there was a trend of a higher level of radioactivity in the nucleolus after exposure of malignant cells to ^{111}In-DTPA-F3 compared to ^{111}In-DTPA (Figure 5.17). A higher level of radioactivity was associated with the nucleolus of the MCF7 (M-W test, P = 0.1000; T-test, P = 0.0361), HCT116 (M-W test, P = 0.1000; T-test, P = 0.2309), H322 (M-W test, P = 0.1000; T-test, P = 0.0381) and MD-MB-435 (M-W test, P = 0.1000; T-test, P = 1580) cells after exposure to ^{111}In-DTPA-F3 compared to ^{111}In-DTPA; although the level of radioactivity associated with the nucleolus of the MDA-MB-231/H2N and U2OS cells after exposure to ^{111}In-DTPA-F3 was not statistically significantly different from ^{111}In-DTPA. Nevertheless, this evidence supported the hypothesis that ^{111}In-DTPA-F3 targeted the nucleolus of the malignant cells.

Further analysis of the fraction in which there had been greater uptake of ^{111}In-DTPA-F3 compared to ^{111}In-DTPA, was carried out by calculating the ^{111}In-DTPA-F3-to-^{111}In-DTPA ratio (^{111}In-DTPA-F3/^{111}In-DTPA ratio) of the level of radioactivity in the cell, membrane, cytoplasm, nucleus, nucleoplasm and nucleolus. Table 5.4 and Figure 5.18 show the ^{111}In-DTPA-F3/^{111}In-DTPA ratio (a measure of the fold-change in radioactivity due to the incorporation of F3 into ^{111}In-DTPA) for the cell, membrane, cytoplasm, nucleus, nucleoplasm and nucleolus of MCF7, HCT116, MDA-MB-231/H2N, H322, MDA-MB-435 and U2OS cells. A trend emerged, as shown in Figure 5.18.F, that showed that the ^{111}In-DTPA-F3/^{111}In-DTPA ratio was highest in the nucleolus.

Figure 5.19 shows the mean ^{111}In-DTPA-F3/^{111}In-DTPA ratio (i.e., an average of the ^{111}In-DTPA-F3/^{111}In-DTPA ratios for the six malignant cell lines, n = 6) for the radioactivity associated with the cell, membrane, cytoplasm, nucleus, nucleoplasm and nucleolus. The ^{111}In-DTPA-F3/^{111}In-DTPA ratio for the radioactivity associated

	Cell	Membrane	Cytoplasm	Nucleus	Nucleo-plasm	Nucleolus
MCF7	0.77±0.24	0.76±0.31	0.80±0.12	1.17±0.11	1.15±0.10	1.92±0.41
HCT116	0.68±0.05	0.66±0.10	1.43±0.84	1.17±0.14	1.09±0.15	4.53±2.12
MDA-MB-231/H2N	0.75±0.03	0.87±0.12	0.81±0.13	1.29±0.11	1.40±0.24	1.90±0.30
H322	1.05±0.19	1.22±0.22	0.74±0.22	1.92±0.30	1.87±0.29	4.08±0.25
MDA-MB-435	1.17±0.17	1.25±0.23	0.99±0.04	1.37±0.28	1.32±0.32	1.68±0.19
U2OS	1.07±0.08	1.12±0.11	0.84±0.03	1.57±0.05	1.45±0.04	2.75±0.92
Mean	**0.91±0.08**	**0.96±0.11**	**0.892±0.11**	**1.42±0.12**	**1.34±0.12**	**2.81±0.50**

Table 5.4. Fold-change in radioactivity associated with the cell, membrane, cytoplasm, nucleus, nucleplasm and nucleolus of malignant cells due to the incorporation of F3 into ^{111}In-DTPA

Fold-change in radioactivity (^{111}In-DTPA-F3/^{111}In-DTPA ratio) associated with the cell, membrane, cytoplasm, nucleus, nucleoplasm and nucleolus of MCF7, HCT116, MDA-MB-231/H2N, H322, MDA-MB-435, and U2OS cells exposed for 3 h to 1 μM of ^{111}In-DTPA-F3 (22.17 MBq/nmol) or an equimolar amount of ^{111}In-DTPA, due to the incorporation of F3 into ^{111}In-DTPA. ^{111}In-DTPA-F3/^{111}In-DTPA ratios were calculated by dividing the radioactivity associated with the membrane, cytoplasm, nucleoplasm or nucleolus after exposure to ^{111}In-DTPA-F3 by the radioactivity in the same fraction after exposure to ^{111}In-DTPA. ^{111}In-DTPA-F3/^{111}In-DTPA ratios for the cell were calculated in a similar manner after combining radioactivity from the membrane, cytoplasm, nucleoplasm and nucleolus; while ^{111}In-DTPA-F3/^{111}In-DTPA ratios for the nucleus were calculated after combining radioactivity from the nucleoplasm and nucleolus. Values show mean fold-change ± SEM, n = 2–3.

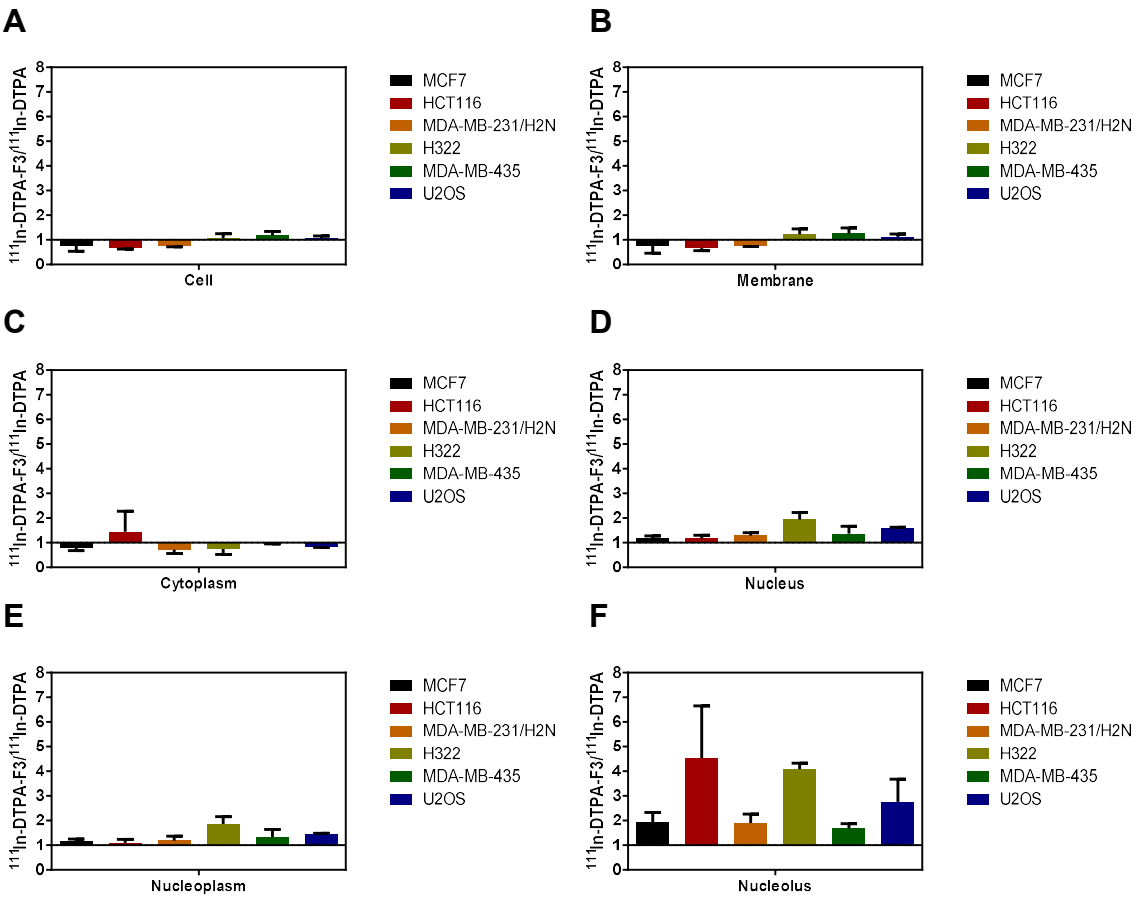

Figure 5.18. Fold-change in radioactivity associated with the cell, membrane, cytoplasm, nucleus, nucleoplasm and nucleolus of malignant cells due to the incorporation of F3 into ^{111}In-DTPA

Fold-change in radioactivity (^{111}In-DTPA-F3/^{111}In-DTPA ratio) associated with the (A) cell, (B) membrane, (C) cytoplasm, (D) nucleus, (E) nucleoplasm and (F) nucleolus of MCF7, HCT116, MDA-MB-231/H2N, H322, MDA-MB-435, and U2OS cells exposed for 3 h to 1 μM of ^{111}In-DTPA-F3 (22.17 MBq/nmol) or an equimolar amount of ^{111}In-DTPA, due to the incorporation of F3 into ^{111}In-DTPA. ^{111}In-DTPA-F3/^{111}In-DTPA ratios were calculated by dividing the radioactivity associated with the membrane, cytoplasm, nucleoplasm or nucleolus after exposure to ^{111}In-DTPA-F3 by the radioactivity in the same fraction after exposure to ^{111}In-DTPA. ^{111}In-DTPA-F3/^{111}In-DTPA ratios for the cell were calculated in a similar manner after combining radioactivity from the membrane, cytoplasm, nucleoplasm and nucleolus; while ^{111}In-DTPA-F3/^{111}In-DTPA ratios for the nucleus were calculated after combining radioactivity from the nucleoplasm and nucleolus. Values show fold-change ± SEM, n = 2–3.

Wilcoxon signed-rank test (significantly different from unity)

Cell	Membrane	Cytoplasm	Nucleus	Nucleoplasm	Nucleolus
0.3125	0.4375	0.0313	0.0313	0.0313	0.0313

One-sample T-test (significantly different from unity)

Cell	Membrane	Cytoplasm	Nucleus	Nucleoplasm	Nucleolus
0.2013	0.4210	0.0078	0.0188	0.0383	0.0125

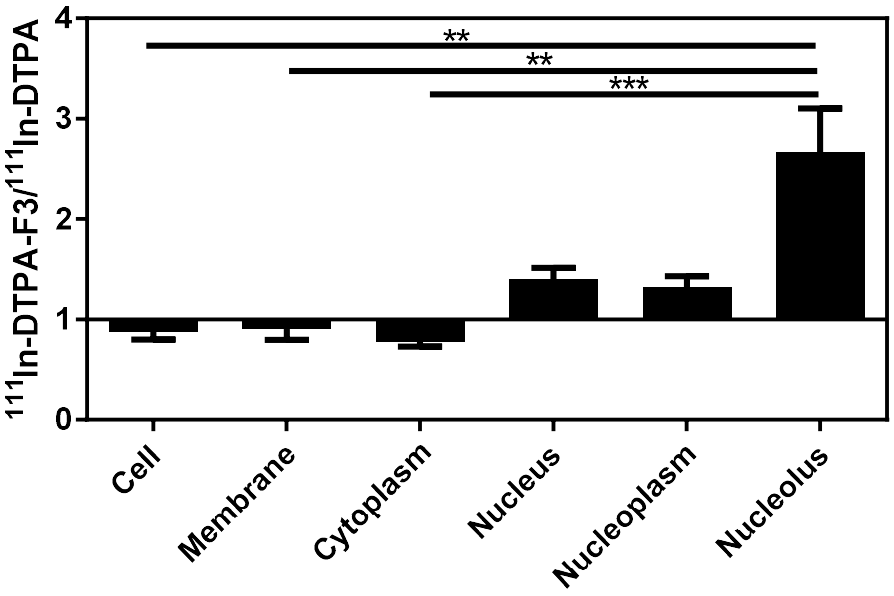

Figure 5.19. Mean fold-change in radioactivity associated with the cell, membrane, cytoplasm, nucleus, nucleoplasm and nucleolus of malignant cells due to the incorporation of F3 into ^{111}In-DTPA

Mean fold-change in radioactivity (mean ^{111}In-DTPA-F3/^{111}In-DTPA ratio) associated with the cell, membrane, cytoplasm, nucleus, nucleoplasm and nucleolus of MCF7, HCT116, MDA-MB-231/H2N, H322, MDA-MB-435, and U2OS cells exposed for 3 h to 1 μM of ^{111}In-DTPA-F3 (22.17 MBq/nmol) or an equimolar amount of ^{111}In-DTPA, due to the incorporation of F3 into ^{111}In-DTPA. Mean ^{111}In-DTPA-F3/^{111}In-DTPA ratios were calculated by taking the average of ^{111}In-DTPA-F3/^{111}In-DTPA ratios of MCF7, HCT116, MDA-MB-231/H2N, H322, MDA-MB-435, and U2OS cells (see Table 5.4). Values show mean fold-change ± SEM, n = 6. GraphPad Prism 6 software was used to test if the data followed a Gaussian distribution using a D'Agostino-Pearson omnibus test. Since the data did not follow a Gaussian distribution, medians were compared to a hypothetical value of 1 using non-parametric Wilcoxon signed-rank test. Nevertheless, parametric one-sample T-tests were also performed to test if means were significantly different from 1. A non-parametric Kruskal-Wallis one-way ANOVA with multiplicity adjusted P values (Dunn's post-hoc test) was also performed. **, $P < 0.01$; ***, $P < 0.001$.

with the cytoplasm (Wilcoxon, P = 0.0313; T-test, P = 0.0078), nucleus (Wilcoxon, P = 0.0313; T-test, P = 0.0188), nucleoplasm (Wilcoxon, P = 0.0.0313; T-test, P = 0.0383) and nucleolus (Wilcoxon, P = 0.0313; T-test, P = 0.0125) was significantly different from unity (1). The mean ^{111}In-DTPA-F3/^{111}In-DTPA ratio for the radioactivity associated with the nucleolus was greatest than that of all other intracellular compartments, and was significantly different from that for the cell (P = 0.0032), membrane (P = 0.0068) and cytoplasm (P = 0.0009).

Together, this suggested that in the nucleolus ^{111}In-DTPA-F3 was taken up at higher levels compared to ^{111}In-DTPA. Along with the clonogenic survival data (Chapter 4, Figure 4.4) that showed that ^{111}In-DTPA-F3, but not ^{111}In-DTPA, was significantly radiotoxic to the malignant cell lines (except for U2OS cells which were not radiosensitive to ^{111}In-DTPA-F3), this suggested that the localisation of ^{111}In-DTPA-F3 in the nucleolus was likely to be responsible for the radiotoxicity of ^{111}In-DTPA-F3.

5.2.2. ^{111}In-DTPA-F3 deposits radiation dose in the nucleolus

Since ^{111}In-DTPA-F3 was found to target the nucleolus, it was hypothesised that ^{111}In-DTPA-F3 would have deposited radiation dose in the nucleolus. To assess the mean absorbed radiation dose deposited in the cell, membrane, cytoplasm, nucleus, nucleoplasm and nucleolus after exposure of malignant cells to ^{111}In-DTPA-F3 or ^{111}In-DTPA, single cell models were generated for MCF7, HCT116, MDA-MB-231/H2N, H322, MDA-MB-435 and U2OS cells by measuring the volume of the cell, nucleus and nucleolus using fluorescence microscopy (see the schematic of the generation of single cell models in Figure 5.20). Z-stacks of MCF7, HCT116, MDA-MB-231/H2N, H322, MDA-MB-435 and U2OS cells showing membrane, DNA and

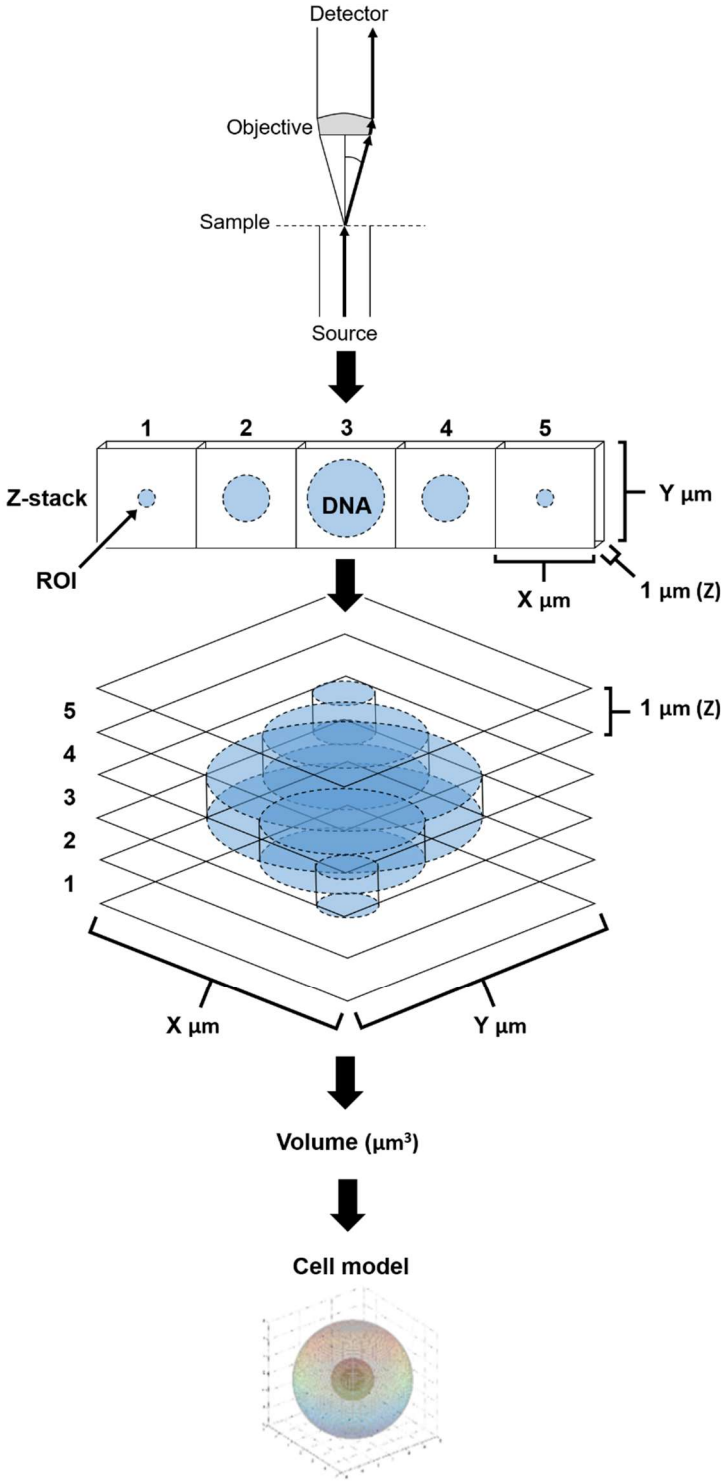

Figure 5.20. Schematic of the generation of single cell models

nucleolin (markers of the volume of the cell, nucleus and nucleolus, respectively) were used to calculate the volumes of these structures (Figure 5.21–5.23). Cell, nucleus and nucleolus volumes were used to calculate radii to generate concentric single cell models comprising the membrane, cytoplasm, nucleoplasm and nucleolus regions (Table 5.5). Concentric single cell models were used by Dr Nadia Falzone to generate S-values (Gy/Bq·sec; see Appendix Table 1.1). The cumulated radioactivity (mBq·sec/cell) in the membrane, cytoplasm, nucleoplasm and nucleolus of the malignant cells after 3 h exposure to ^{111}In-DTPA-F3 or ^{111}In-DTPA was corrected for decay of ^{111}In ($t_{½}$, 2.8 days) (Table 5.6). The cumulated radioactivity was multiplied by S-values to give the mean absorbed radiation dose deposited in the membrane, cytoplasm, nucleoplasm and nucleolus regions (mGy/cell) (Table 5.7). The mean absorbed radiation dose deposited in the malignant cells after exposure to ^{111}In-DTPA-F3 was similar to ^{111}In-DTPA, with the exception that a lower mean absorbed radiation dose was deposited in the HCT116 cells after exposure to ^{111}In-DTPA-F3 compared to ^{111}In-DTPA (M-W test, P = 0.1000; T-test, P = 0.0295) (Figure 5.24). The mean absorbed radiation dose deposited in the membrane (Figure 5.25), cytoplasm (Figure 5.26), nucleus (Figure 5.27) and nucleoplasm (Figure 5.28) of malignant cells after exposure to ^{111}In-DTPA-F3 was similar to ^{111}In-DTPA, with the exceptions that a lower mean absorbed radiation dose was deposited in the membrane (M-W test, P = 0.1000; T-test, P = 0.0035) and cytoplasm (M-W test, P = 0.1000; T-test, P =0.0147) of the HCT116 cells after exposure to ^{111}In-DTPA-F3 compared to ^{111}In-DTPA; a higher mean absorbed radiation dose was deposited in the nucleus of the H322 (M-W test, P = 0.1000; T-test, P = 0.0316) and MDA-MB-435 (M-W test, P = 0.1000; T-test, P = 0.1602) cells after exposure to ^{111}In-DTPA-F3 compared to ^{111}In-DTPA; and a higher mean absorbed radiation dose was deposited in the nucleoplasm of the

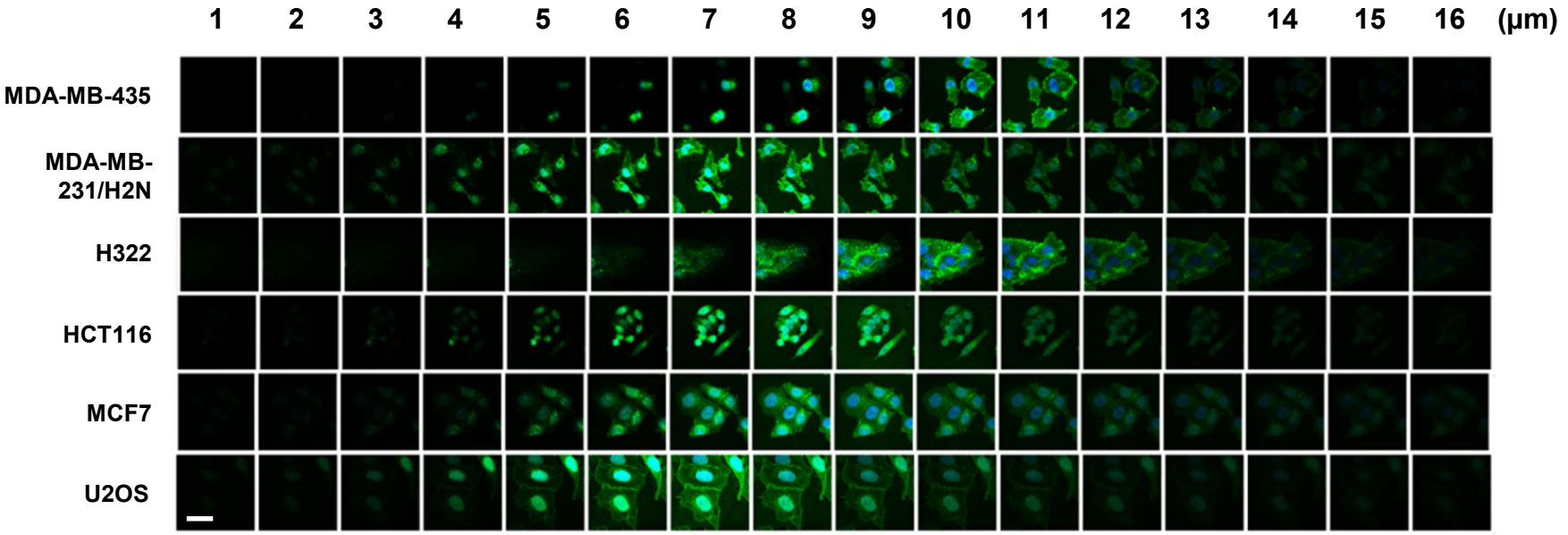

Figure 5.21. Z-stacks showing the volume of the cell and nucleus of malignant cells

Z-stacks with 1 μm intervals showing the volume of the membrane (green, AF488-WGA) and nucleus (blue, Hoechst-33342) of MDA-MB-435, MDA-MB-231/H2N, H322, HCT116, MCF7 and U2OS cells. Scale, 20 μm.

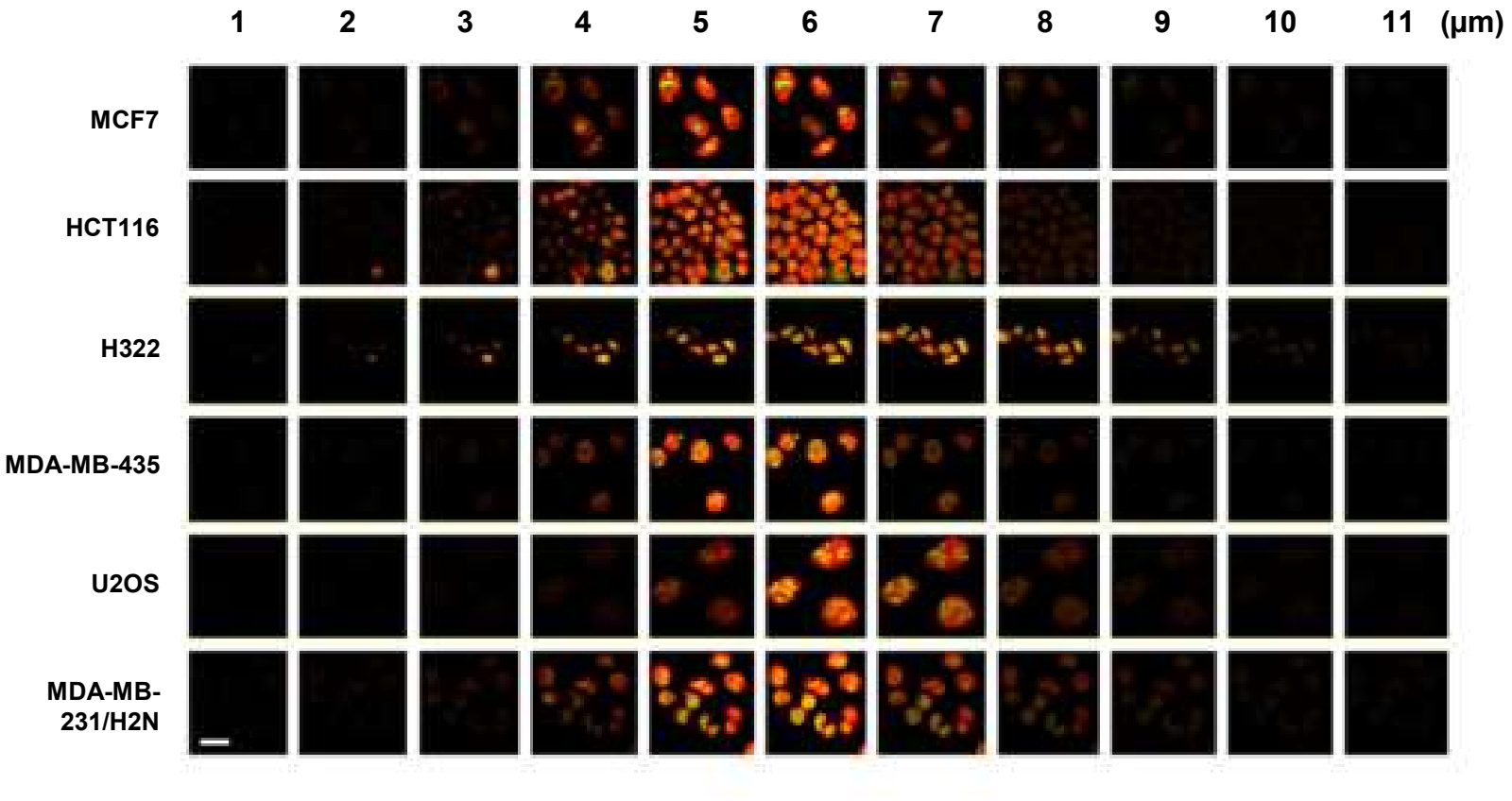

Figure 5.22. Z-stacks showing the volume of the nucleus and nucleolus of malignant cells

Z-stacks with 1 µm intervals showing the volume of the nucleus (red, Hoechst-33342) and nucleolus (green, nucleolin) of MCF7, HCT116, H322, MD-MB-435, U2OS and MDA-MB-231/H2N cells. Scale, 20 µm.

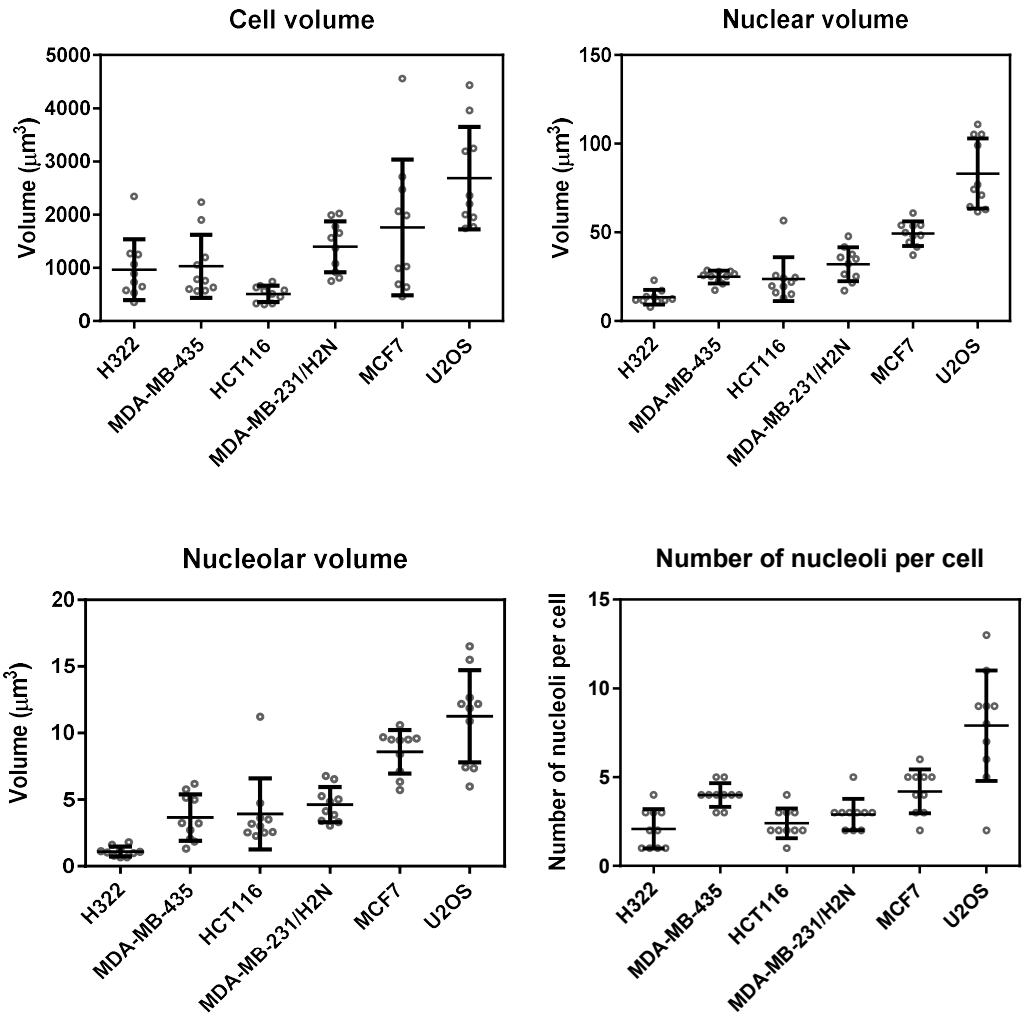

Figure 5.23. The number of nucleoli in, and the volume of the cell, nucleus, and nucleolus of malignant cell lines

The volume for the (A) cell, (B) nucleus and (C) nucleolus of malignant cell lines is given in μm^3. The volume for a hypothetical single nucleolus was calculated by combining the volumes of multiple nucleoli inside a single nucleus. (D) Number of nucleoli per cell for the malignant cell lines. Values show mean volume ± SD, n = 10.

Cell line	Cell volume (μm^3)	Nucleus volume (μm^3)	Nucleolus volume (μm^3)	Membrane radius (μm)	Cytoplasm radius (μm)	Nucleus radius (μm)	Nucleolus radius (μm)	Single cell model
MCF7	1761.12±403.05	49.28±2.18	8.59±0.52	7.110±0.557	7.102±0.557	2.27±0.03	1.27±0.03	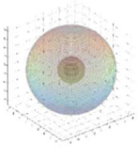
HCT116	512.471±47.801	23.67±3.90	3.92±0.84	4.918±0.160	4.910±0.160	1.75±0.08	0.95±0.05	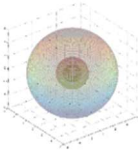
MDA-MB-231/H2N	1396.00±151.58	32.09±2.99	4.62±0.41	6.845±0.262	6.837±0.262	1.95±0.06	1.03±0.03	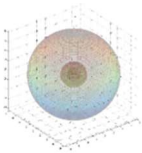
H322	966.66±181.52	13.44±1.30	1.11±0.12	5.949±0.349	5.941±0.349	1.46±0.04	0.64±0.02	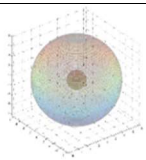
MDA-MB-435	1030.77±186.87	24.88±1.12	3.65±0.55	6.093±0.349	6.085±0.349	1.81±0.03	0.93±0.05	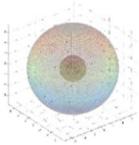
U2OS	2686.90±304.26	83.22±6.23	11.25±1.09	8.520±0.312	8.512±0.312	2.69±0.07	1.38±0.05	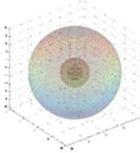

Table 5.5. Concentric single cell models of malignant cells

Volume of the cell, nucleus and nucleolus of malignant cells are given in μm^3, while radii of membrane, cytoplasm, nucleoplasm and nucleolus (calculated to generate concentric single cell models, shown) are given in μm. Values show mean ± SEM, n = 10.

	^{111}In-DTPA-F3 (mBq·sec/cell)						^{111}In-DTPA (mBq·sec/cell)					
	Cell	**Me**	**Cy**	**Nu**	**Np**	**No**	**Cell**	**Me**	**Cy**	**Nu**	**Np**	**No**
MCF7	15111 ±3008	8378 ±2404	5911 ±684	822 ±111	790 ±109	32 ±3	21872 ±4501	13657 ±4087	7512 ±440	702 ±59	684 ±61	18 ±3
HCT116	33586 ±2123	24808 ±1369	6772 ±751	2006 ±155	1819 ±182	186 ±81	49709 ±561	38955 ±4209	9020 ±3362	1734 ±65	1685 ±53	49 ±14
MDA-MB-231/H2N	55213 ±5210	38010 ±2406	14423 ±2474	2780 ±330	2106 ±335	674 ±5	73844 ±4095	51239 ±4689	20456 ±662	2148 ±67	1780 ±1	369 ±68
H322	18674 ±732	13534 ±694	4323 ±155	816 ±82	767 ±75	49 ±8	19569 ±4911	12067 ±2867	7070 ±2243	432 ±36	420 ±37	12 ±2
MDA-MB-435	69497 ±4838	49129 ±3693	16970 ±1284	3397 ±464	2635 ±365	762 ±147	61362 ±8540	41410 ±6542	17330 ±1956	2623 ±403	2175 ±382	447 ±37
U2OS	90527 ±10756	71678 ±9477	15705 ±184	3144 ±545	2603 ±440	540 ±184	84250 ±6393	63694 ±4601	18572 ±1592	1984 ±283	1792 ±295	192 ±60

Table 5.6. Cumulated radioactivity associated with malignant cells exposed to ^{111}In-DTPA-F3 or ^{111}In-DTPA

Cumulated radioactivity ($\tilde{A}_h$; mBq·sec/cell) was calculated for HCT116, MCF7, MDA-MB-321/H2N, H322, MDA-MB-435 and U2OS cells exposed for 3 h to 1 μM of ^{111}In-DTPA-F3 (22.17 MBq/nmol) or an equimolar amount of ^{111}In-DTPA, by extrapolating the radioactivity associated with the membrane, cytoplasm, nucleoplasm, or nucleolus at 3 h back to 0 h, and correcting for decay of ^{111}In (t½, 2.8 days). Cumulated radioactivity associated with the cell was calculated in a similar manner after combining the radioactivity associated with the membrane, cytoplasm, nucleoplasm, and nucleolus; while cumulated radioactivity associated with the nucleus was calculated after combining the radioactivity associated with the nucleoplasm and nucleolus. Values show mean cumulated radioactivity ± SEM, n = 2–3. Me, membrane (r_{Me}); Cy, cytoplasm (r_{Cy}); Nu, nucleus; Np, nucleoplasm (r_{Np}); No, nucleolus (r_{No}).

	^{111}In-DTPA-F3 (mGy/cell)						^{111}In-DTPA (mGy/cell)					
	Cell	**Me**	**Cy**	**Nu**	**Np**	**No**	**Cell**	**Me**	**Cy**	**Nu**	**Np**	**No**
MCF7	17.93 ±2.66	1.95 ±0.39	10.23 ±1.75	5.75 ±0.60	2.64 ±0.29	3.11 ±0.31	22.53 ±3.36	2.85 ±0.58	14.28 ±2.37	5.40 ±0.42	2.75 ±0.19	2.65 ±0.24
HCT116	**149.97 ±1.59**	**19.70 ±1.23**	**88.55 ±6.36**	41.72 ±6.59	14.85 ±0.71	26.87 ±5.96	**193.25 ±8.11**	**29.94 ±1.07**	**129.21 ±7.39**	34.10 ±2.24	15.59 ±0.79	18.52 ±18.52
MDA-MB-231/H2N	115.75 ±7.04	8.16 ±0.81	37.42 ±4.17	70.17 ±2.06	17.56 ±1.19	52.61 ±0.87	109.80 ±7.87	11.12 ±0.55	50.71 ±1.79	47.96 ±5.52	14.57 ±0.97	33.39 ±4.56
H322	36.33 ±2.88	2.29 ±0.09	9.33 ±0.33	**24.71 ±2.91**	**6.56 ±0.53**	**18.15 ±2.40**	24.85 ±4.61	2.62 ±0.70	10.86 ±2.89	**11.38 ±1.13**	**4.33 ±0.42**	**7.05 ±0.73**
MDA-MB-435	186.54 ±21.79	13.92 ±0.96	62.29 ±4.18	**110.33 ±17.00**	27.25 ±3.47	**83.08 ±13.54**	143.96 ±14.92	12.43 ±1.71	56.80 ±7.42	**74.73 ±6.69**	20.30 ±2.20	**54.43 ±4.55**
U2OS	77.09 ±12.94	8.42 ±1.01	39.05 ±4.45	29.63 ±7.55	8.21 ±1.51	21.41 ±6.06	61.67 ±4.98	7.95 ±0.60	37.91 ±2.94	15.82 ±1.54	5.70 ±0.51	10.12 ±1.15

Table 5.7. Mean absorbed radiation dose deposited in the cell, membrane, cytoplasm, nucleus, nucleoplasm, and nucleolus of malignant cells exposed to ^{111}In-DTPA-F3 or ^{111}In-DTPA

Mean absorbed radiation dose (mGy/cell) deposited in the cell, membrane, cytoplasm, nucleoplasm, and nucleolus of HCT116, MCF7, MDA-MB-321/H2N, H322, MDA-MB-435 and U2OS cells exposed for 3 h to 1 μM of ^{111}In-DTPA-F3 (22.17 MBq/nmol) or an equimolar amount of ^{111}In-DTPA, was calculated by multiplying the cumulated radioactivity associated with the membrane, cytoplasm, nucleoplasm, or nucleolus by appropriate S-values (see 7. Appendix, Table 7.1). Mean absorbed radiation dose deposited in the cell was calculated by combining the mean absorbed radiation dose deposited in the membrane, cytoplasm, nucleoplasm, and nucleolus; while the mean absorbed radiation dose deposited in the nucleus was calculated by combining the mean absorbed radiation dose deposited in the nucleoplasm and nucleolus. Values show mean absorbed radiation dose ± SEM, n = 2–3. Me, membrane; Cy, cytoplasm; Nu, nucleus; Np, nucleoplasm; No, nucleolus. GraphPad Prism 6 was used to test if the data followed a Gaussian distribution using a D'Agostino-Pearson omnibus test. Means for ^{111}In-DTPA-F3 versus ^{111}In-DTPA were compared using an unpaired Mann-Whitney test (two-tailed P values). Bold values, P = 0.1.

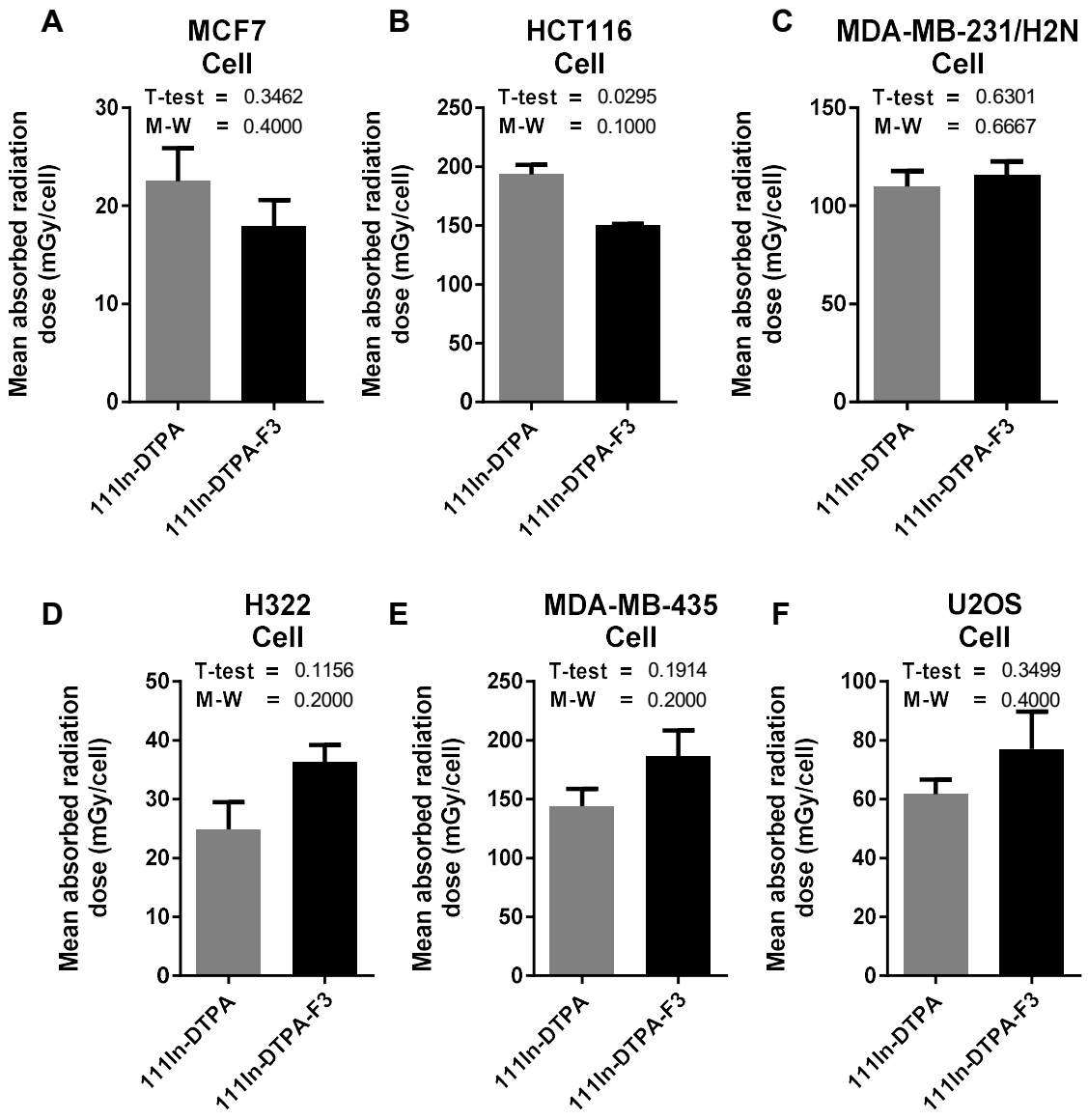

Figure 5.24. Mean absorbed radiation dose deposited in the malignant cells after exposure to ^{111}In-DTPA-F3 or ^{111}In-DTPA

Mean absorbed radiation dose (mGy/cell) deposited in (A) MCF7, (B) HCT116, (C) MDA-MB-231/H2N, (D) H322, (E) MDA-MB-435, and (F) U2OS cells exposed for 3 h to 1 μM of ^{111}In-DTPA-F3 (22.17 MBq/nmol) or an equimolar amount of ^{111}In-DTPA. Mean absorbed radiation dose deposited in the cell was calculated by combining the mean absorbed radiation dose deposited in the membrane, cytoplasm, nucleoplasm and nucleolus. Values show mean absorbed radiation dose ± SEM, n = 2–3. GraphPad Prism 6 software was used to test if the data followed a Gaussian distribution using a D'Agostino-Pearson omnibus test. Since the data did not follow a Gaussian distribution, means were compared using unpaired Mann-Whitney (M-W) tests with two-tailed P values. However, the unpaired, two-tailed M-W test has little statistical power and will never produce a P value of less than 0.1 for a sample size of 3 or less. Therefore, parametric T-tests with Welch's correction for unequal standard deviations (two-tailed P values) were also performed.

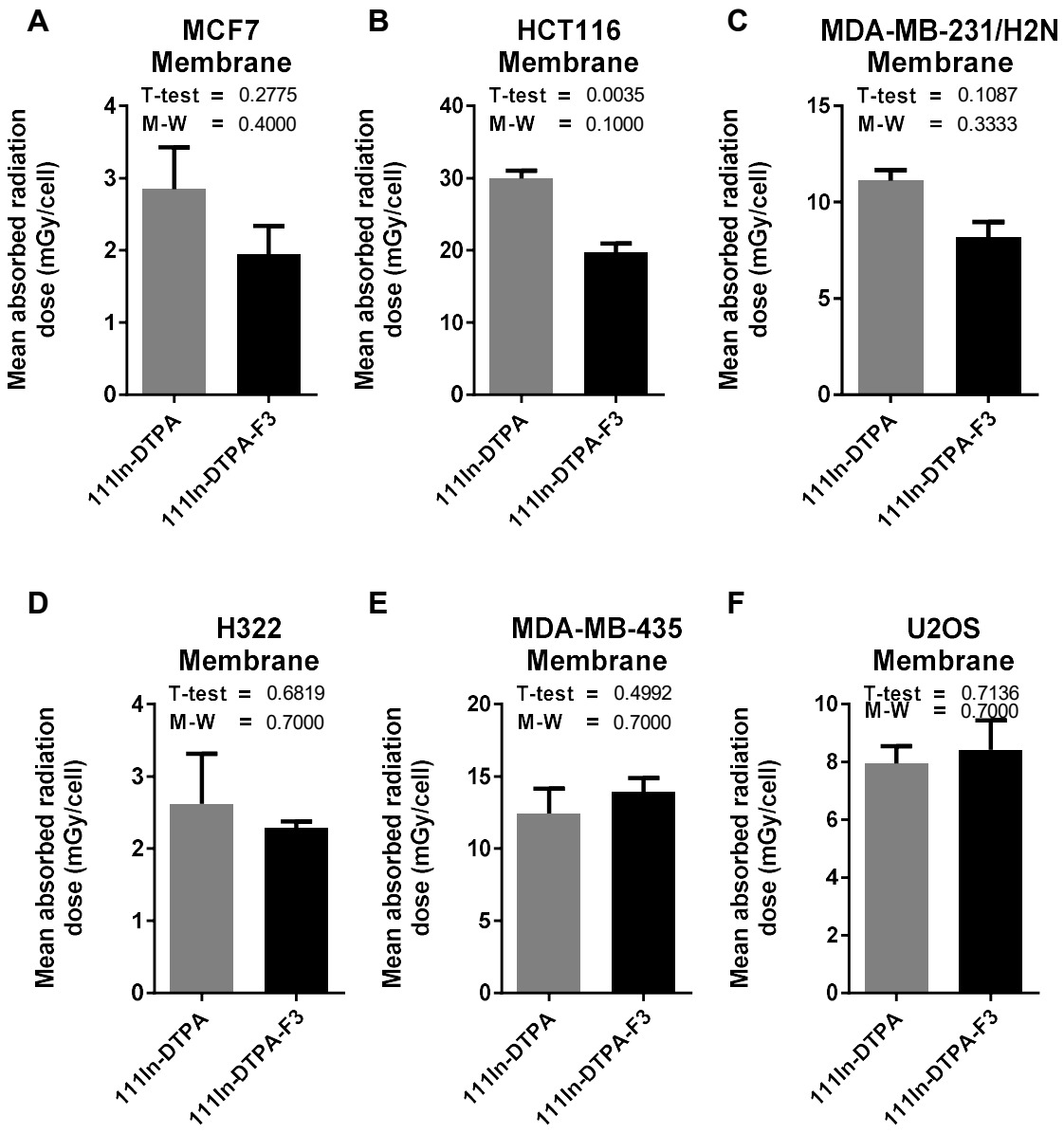

Figure 5.25. Mean absorbed radiation dose deposited in the membrane of malignant cells after exposure to ^{111}In-DTPA-F3 or ^{111}In-DTPA

Mean absorbed radiation dose (mGy/cell) deposited in the membrane of (A) MCF7, (B) HCT116, (C) MDA-MB-231/H2N, (D) H322, (E) MDA-MB-435, and (F) U2OS cells exposed for 3 h to 1 μM of ^{111}In-DTPA-F3 (22.17 MBq/nmol) or an equimolar amount of ^{111}In-DTPA. Values show mean absorbed radiation dose ± SEM, n = 2–3. GraphPad Prism 6 software was used to test if the data followed a Gaussian distribution using a D'Agostino-Pearson omnibus test. Since the data did not follow a Gaussian distribution, means were compared using unpaired Mann-Whitney (M-W) tests with two-tailed P values. However, the unpaired, two-tailed M-W test has little statistical power and will never produce a P value of less than 0.1 for a sample size of 3 or less. Therefore, parametric T-tests with Welch's correction for unequal standard deviations (two-tailed P values) were also performed.

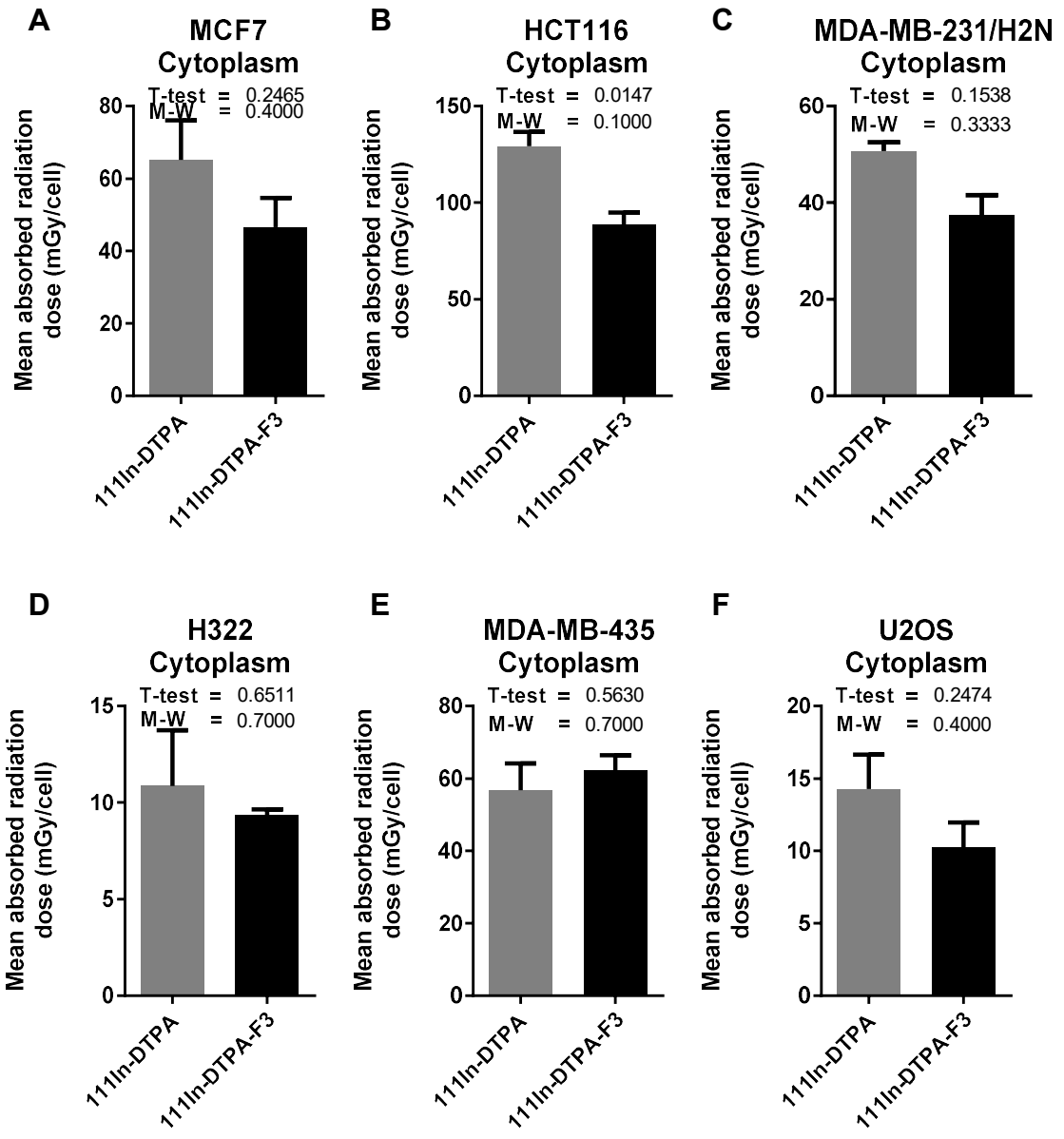

Figure 5.26. Mean absorbed radiation dose deposited in the cytoplasm of malignant cells after exposure to ^{111}In-DTPA-F3 or ^{111}In-DTPA

Mean absorbed radiation dose (mGy/cell) deposited in the cytoplasm of (A) MCF7, (B) HCT116, (C) MDA-MB-231/H2N, (D) H322, (E) MDA-MB-435, and (F) U2OS cells exposed for 3 h to 1 μM of ^{111}In-DTPA-F3 (22.17 MBq/nmol) or an equimolar amount of ^{111}In-DTPA. Values show mean absorbed radiation dose ± SEM. n = 2–3. GraphPad Prism 6 software was used to test if the data followed a Gaussian distribution using a D'Agostino-Pearson omnibus test. Since the data did not follow a Gaussian distribution, means were compared using unpaired Mann-Whitney (M-W) tests with two-tailed P values. However, the unpaired, two-tailed M-W test has little statistical power and will never produce a P value of less than 0.1 for a sample size of 3 or less. Therefore, parametric T-tests with Welch's correction for unequal standard deviations (two-tailed P values) were also performed.

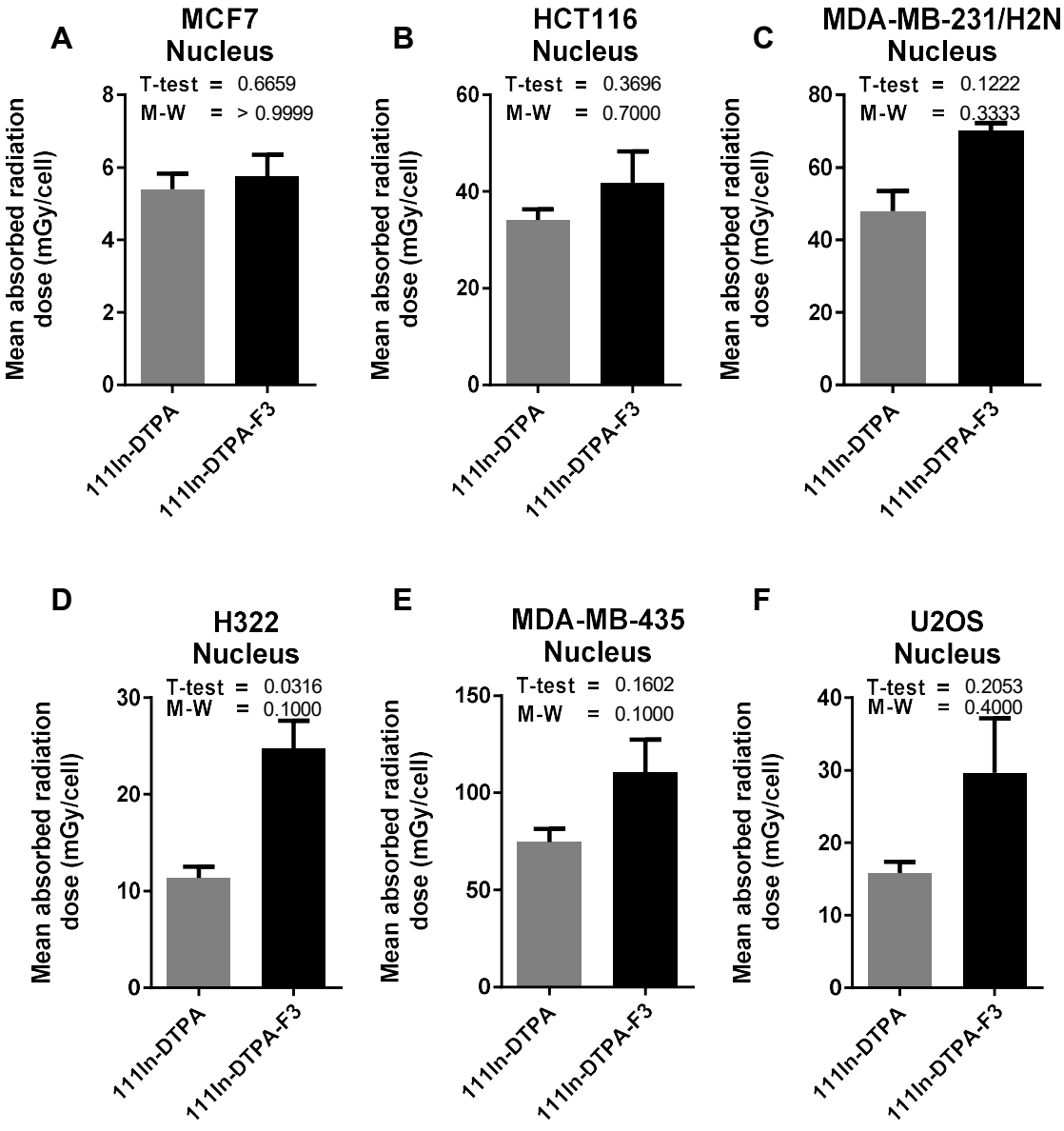

Figure 5.27. Mean absorbed radiation dose deposited in the nucleus of malignant cells after exposure to ^{111}In-DTPA-F3 or ^{111}In-DTPA

Mean absorbed radiation dose (mGy/cell) deposited in the nucleus of (A) MCF7, (B) HCT116, (C) MDA-MB-231/H2N, (D) H322, (E) MDA-MB-435, and (F) U2OS cells exposed for 3 h to 1 μM of ^{111}In-DTPA-F3 (22.17 MBq/nmol) or an equimolar amount of ^{111}In-DTPA. Mean absorbed radiation dose deposited in the nucleus was calculated by combining the mean absorbed radiation dose deposited in the nucleoplasm and nucleolus. Values show mean absorbed radiation dose ± SEM, n = 2–3. GraphPad Prism 6 software was used to test if the data followed a Gaussian distribution using a D'Agostino-Pearson omnibus test. Since the data did not follow a Gaussian distribution, means were compared using unpaired Mann-Whitney (M-W) tests with two-tailed P values. However, the unpaired, two-tailed M-W test has little statistical power and will never produce a P value of less than 0.1 for a sample size of 3 or less. Therefore, parametric T-tests with Welch's correction for unequal standard deviations (two-tailed P values) were also performed.

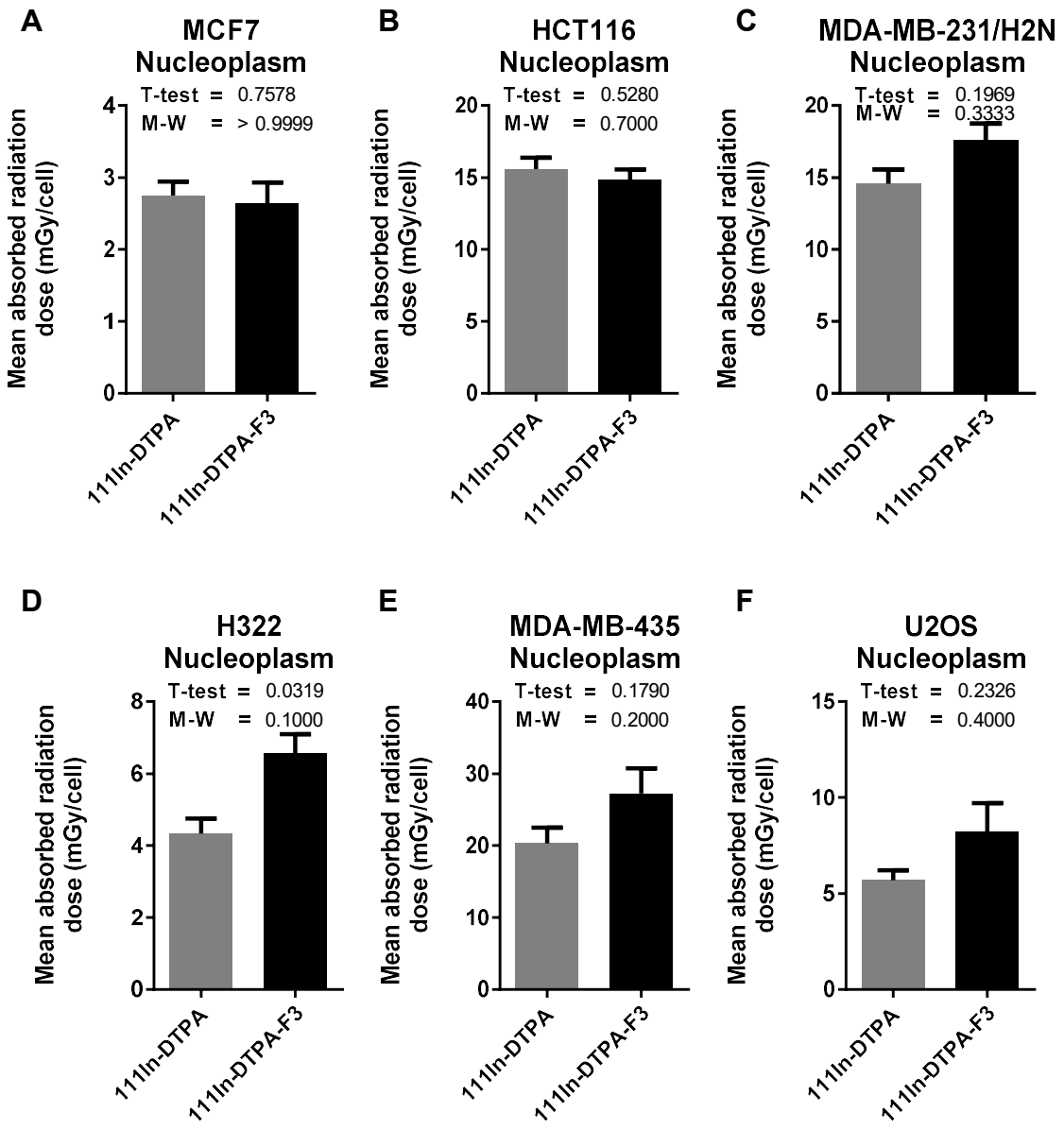

Figure 5.28. Mean absorbed radiation dose deposited in the nucleoplasm of malignant cells after exposure to ^{111}In-DTPA-F3 or ^{111}In-DTPA

Mean absorbed radiation dose (mGy/cell) deposited in the nucleoplasm of (A) MCF7, (B) HCT116, (C) MDA-MB-231/H2N, (D) H322, (E) MDA-MB-435, and (F) U2OS cells exposed for 3 h to 1 μM of ^{111}In-DTPA-F3 (22.17 MBq/nmol) or an equimolar amount of ^{111}In-DTPA. Values show mean absorbed radiation dose ± SEM, n = 2–3. GraphPad Prism 6 software was used to test if the data followed a Gaussian distribution using a D'Agostino-Pearson omnibus test. Since the data did not follow a Gaussian distribution, means were compared using unpaired Mann-Whitney (M-W) tests with two-tailed P values. However, the unpaired, two-tailed M-W test has little statistical power and will never produce a P value of less than 0.1 for a sample size of 3 or less. Therefore, parametric T-tests with Welch's correction for unequal standard deviations (two-tailed P values) were also performed.

H322 cells after exposure to ^{111}In-DTPA-F3 compared to ^{111}In-DTPA (M-W test, P = 0.1000; T-test, P = 0.0319). However, there was a trend of a higher mean absorbed radiation dose deposited in the nucleolus after exposure of malignant cells to ^{111}In-DTPA-F3 compared to ^{111}In-DTPA (Figure 5.29). The mean absorbed radiation dose deposited in the nucleolus of the H322 (M-W test, P = 0.1000; T-test, P = 0.0346) and MDA-MB-435 (M-W test, P = 0.1000; T-test, P = 0.1590) cells after exposure to ^{111}In-DTPA-F3 was higher compared to ^{111}In-DTPA; although the mean absorbed radiation dose deposited in the nucleolus of the MCF7, HCT116, MDA-MB-231/H2N and U2OS cells after exposure to ^{111}In-DTPA-F3 was not statistically significantly different from ^{111}In-DTPA. Nevertheless, these single cell models supported the hypothesis that a higher mean absorbed radiation dose could have been deposited in the nucleolus by ^{111}In-DTPA-F3 compared to ^{111}In-DTPA.

Further analysis of the region in which ^{111}In-DTPA-F3 deposited radiation dose was carried out by calculating the ^{111}In-DTPA-F3-to-^{111}In-DTPA ratio (^{111}In-DTPA-F3/^{111}In-DTPA ratio) of the level of mean absorbed radiation dose for the cell, membrane, cytoplasm, nucleus, nucleoplasm and nucleolus. Table 5.8 and Figure 5.30 show the ^{111}In-DTPA-F3/^{111}In-DTPA ratios for the level of mean absorbed radiation dose deposited in the cell, membrane, cytoplasm, nucleus, nucleoplasm and nucleolus of MCF7, HCT116, MDA-MB-231/H2N, H322, MDA-MB-435, and U2OS cells. A trend emerged, as shown in Figure 5.30, that suggested that ^{111}In-DTPA-F3 deposited higher levels of radiation dose in the nucleus, and in particular the nucleolus, compared to ^{111}In-DTPA.

Figure 5.31 shows the mean ^{111}In-DTPA-F3/^{111}In-DTPA ratio (i.e., an average of the ^{111}In-DTPA-F3/^{111}In-DTPA ratios for the six malignant cell lines, n = 6) for the mean absorbed radiation dose deposited in the cell, membrane, cytoplasm, nucleus,

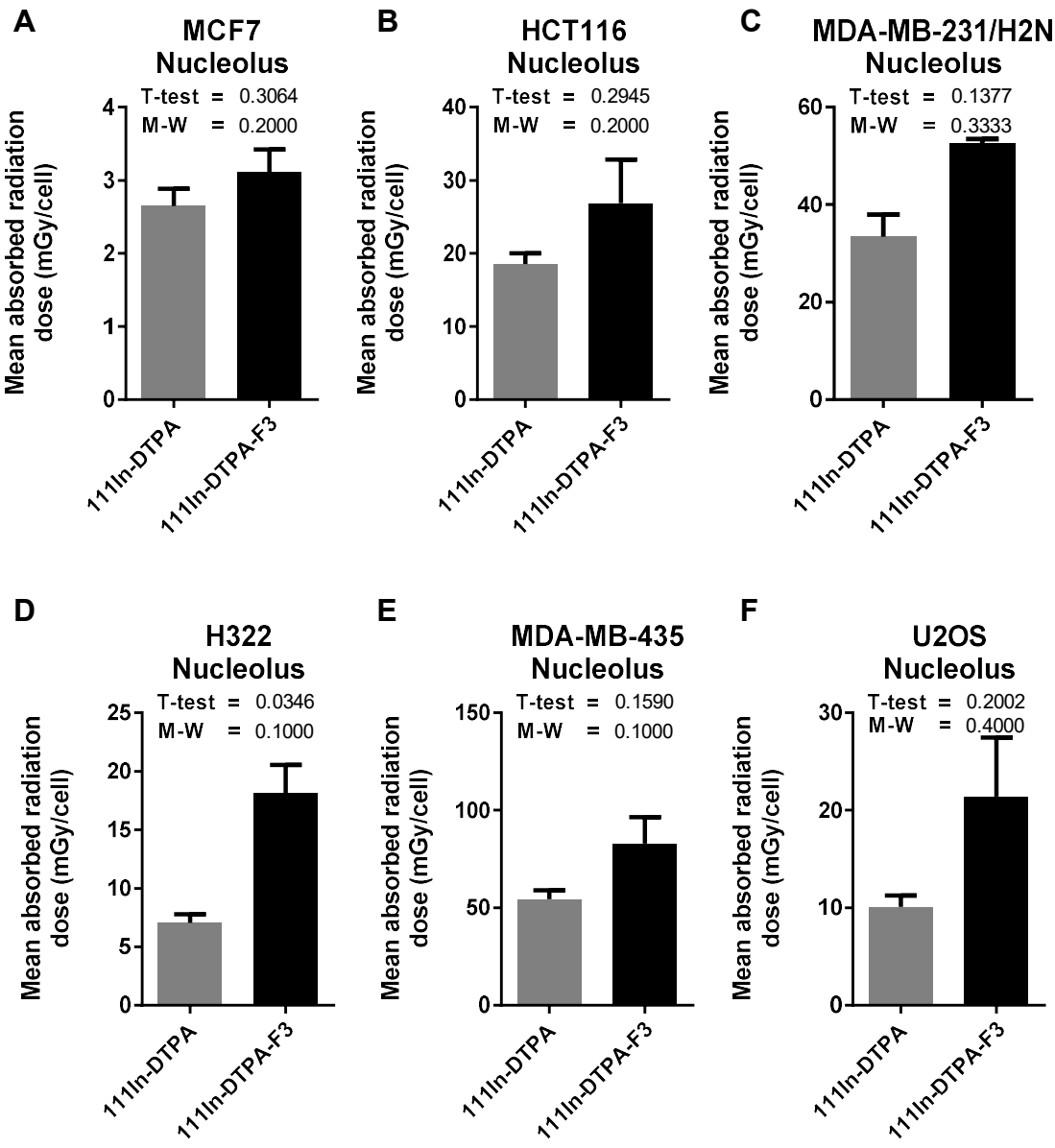

Figure 5.29. Mean absorbed radiation dose deposited in the nucleolus of malignant cells after exposure to ^{111}In-DTPA-F3 or ^{111}In-DTPA

Mean absorbed radiation dose (mGy/cell) deposited in the nucleolus of (A) MCF7, (B) HCT116, (C) MDA-MB-231/H2N, (D) H322, (E) MDA-MB-435, and (F) U2OS cells exposed for 3 h to 1 μM of ^{111}In-DTPA-F3 (22.17 MBq/nmol) or an equimolar amount of ^{111}In-DTPA. Values show mean absorbed radiation dose ± SEM, n = 2–3. GraphPad Prism 6 software was used to test if the data followed a Gaussian distribution using a D'Agostino-Pearson omnibus test. Since the data did not follow a Gaussian distribution, means were compared using unpaired Mann-Whitney (M-W) tests with two-tailed P values. However, the unpaired, two-tailed M-W test has little statistical power and will never produce a P value of less than 0.1 for a sample size of 3 or less. Therefore, parametric T-tests with Welch's correction for unequal standard deviations (two-tailed P values) were also performed.

	Cell	Membrane	Cytoplasm	Nucleus	Nucleoplasm	Nucleolus
MCF7	0.85±0.21	0.77±0.24	0.78±0.21	1.09±0.19	0.98±0.17	1.21±0.21
HCT116	0.78±0.03	0.66±0.06	0.68±0.01	1.25±0.27	0.96±0.09	1.50±0.41
MDA-MB-231/H2N	1.06±0.01	0.73±0.04	0.74±0.06	1.48±0.13	1.21±0.00	1.60±0.19
H322	1.52±0.16	0.97±0.19	0.96±0.19	2.16±0.07	1.52±0.09	2.56±0.08
MDA-MB-435	1.31±0.17	1.16±0.16	1.12±0.13	1.48±0.18	1.36±0.18	1.52±0.19
U2OS	1.23±0.11	1.05±0.79	1.03±0.06	1.82±0.34	1.42±0.14	2.05±0.47
Mean	**1.12±0.15**	**0.89±0.08**	**0.88±0.07**	**1.55±0.16**	**1.24±0.10**	**1.74±0.20**

Table 5.8. Fold-change in mean absorbed radiation dose deposited in the cell, membrane, cytoplasm, nucleus, nucleoplasm and nucleolus of malignant cells due to the incorporation of F3 into ^{111}In-DTPA

Fold-change in mean absorbed radiation dose (^{111}In-DTPA-F3/^{111}In-DTPA ratio) deposited in the cell, membrane, cytoplasm, nucleus, nucleoplasm and nucleolus of MCF7, HCT116, MDA-MB-231/H2N, H322, MDA-MB-435, and U2OS cells exposed for 3 h to 1 μM of ^{111}In-DTPA-F3 (22.17 MBq/nmol) or an equimolar amount of ^{111}In-DTPA, due to the incorporation of F3 into ^{111}In-DTPA. ^{111}In-DTPA-F3/^{111}In-DTPA ratios were calculated by dividing the mean absorbed radiation dose deposited in the membrane, cytoplasm, nucleoplasm or nucleolus after exposure to ^{111}In-DTPA-F3 by the mean absorbed radiation dose deposited in the same fraction after exposure to ^{111}In-DTPA. ^{111}In-DTPA-F3/^{111}In-DTPA ratios for the cell were calculated in a similar manner after combining the mean absorbed radiation dose deposited in the membrane, cytoplasm, nucleoplasm and nucleolus; while ^{111}In-DTPA-F3/^{111}In-DTPA ratios for the nucleus were calculated after combining the mean absorbed radiation dose deposited in the nucleoplasm and nucleolus. Values show mean fold-change ± SEM, n = 2–3.

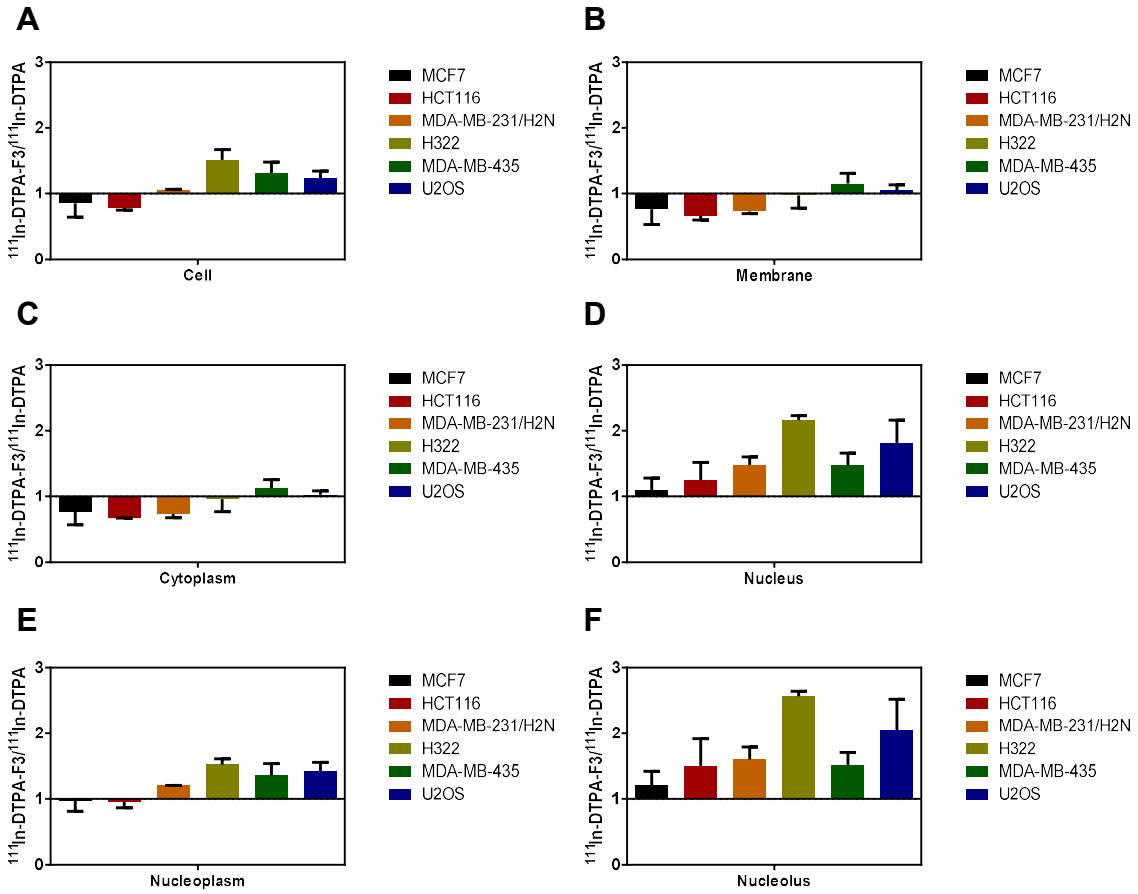

Figure 5.30. Fold-change in mean absorbed radiation dose deposited in the cell, membrane, cytoplasm, nucleus, nucleoplasm and nucleolus of malignant cells due to the incorporation of F3 into ^{111}In-DTPA

Fold-change in mean absorbed radiation dose (^{111}In-DTPA-F3/^{111}In-DTPA ratio) deposited in the (A) cell, (B) membrane, (C) cytoplasm, (D) nucleus, (E) nucleoplasm and (F) nucleolus of MCF7, HCT116, MDA-MB-231/H2N, H322, MDA-MB-435, and U2OS cells exposed for 3 h to 1 μM of ^{111}In-DTPA-F3 (22.17 MBq/nmol) or an equimolar amount of ^{111}In-DTPA, due to the incorporation of F3 into ^{111}In-DTPA. ^{111}In-DTPA-F3/^{111}In-DTPA ratios were calculated by dividing the mean absorbed radiation dose deposited in the membrane, cytoplasm, nucleoplasm or nucleolus after exposure to ^{111}In-DTPA-F3 by the mean absorbed radiation dose deposited in the same fraction after exposure to ^{111}In-DTPA. ^{111}In-DTPA-F3/^{111}In-DTPA ratios for the cell were calculated in a similar manner after combining the mean absorbed radiation dose deposited in the membrane, cytoplasm, nucleoplasm and nucleolus; while ^{111}In-DTPA-F3/^{111}In-DTPA ratios for the nucleus were calculated after combining the mean absorbed radiation dose deposited in the nucleoplasm and nucleolus. Values show mean fold-change ± SEM, n = 2–3.

nucleoplasm and nucleolus. The mean ^{111}In-DTPA-F3/^{111}In-DTPA ratio for the mean absorbed radiation dose deposited in the nucleus (Wilcoxon, P = 0.0313; T-test, P = 0.0182) and, in particular, the nucleolus (Wilcoxon, P = 0.0313; T-test, P = 0.0132) was significantly greater than unity (1). The mean ^{111}In-DTPA-F3/^{111}In-DTPA ratio for the mean absorbed radiation dose deposited in the nucleolus was greater than that of all other intracellular compartments, and was significantly different from that of the membrane (P = 0.0068) and cytoplasm (P = 0.0061). The mean ^{111}In-DTPA-F3/^{111}In-DTPA ratio for the mean absorbed radiation dose deposited in the nucleus was significantly different from that of the cytoplasm (P = 0.0463). Together with the clonogenic survival data (Chapter 4, Figure 4.4), this supported the hypothesis that the deposition of radiation dose in the nucleolus was likely to be responsible for the radiotoxicity of ^{111}In-DTPA-F3.

Since the ^{111}In-DTPA-F3/^{111}In-DTPA ratio of the level of mean absorbed radiation dose deposited in the nucleolus was higher than the ^{111}In-DTPA-F3/^{111}In-DTPA ratio of the level of mean absorbed radiation dose deposited in the nucleoplasm, it was hypothesised that the nucleolus-to-nucleoplasm ratio (No/Np ratio) of mean absorbed radiation dose (a measure of the distribution of mean absorbed radiation dose between the nucleolus and the nucleoplasm) would be greater after exposure of malignant cells to ^{111}In-DTPA-F3 compared to ^{111}In-DTPA (i.e. the incorporation of F3 into ^{111}In-DTPA would shift the distribution of radiation dose from the nucleoplasm to the nucleolus).

Figure 5.32 shows that the No/Np ratio of mean absorbed radiation dose deposited in malignant cells exposed to ^{111}In-DTPA-F3 or ^{111}In-DTPA. There was a trend of higher No/Np ratio of mean absorbed radiation dose after exposure of malignant cells to ^{111}In-DTPA-F3 compared to ^{111}In-DTPA. The No/Np ratio of mean absorbed radiation dose

Wilcoxon signed-rank test (significantly different from unity)

Cell	Membrane	Cytoplasm	Nucleus	Nucleoplasm	Nucleolus
0.3125	0.3125	0.2188	0.0313	0.1563	0.0313

One-sample T-test (significantly different from unity)

Cell	Membrane	Cytoplasm	Nucleus	Nucleoplasm	Nucleolus
0.3290	0.2351	0.1721	0.0182	0.0521	0.0132

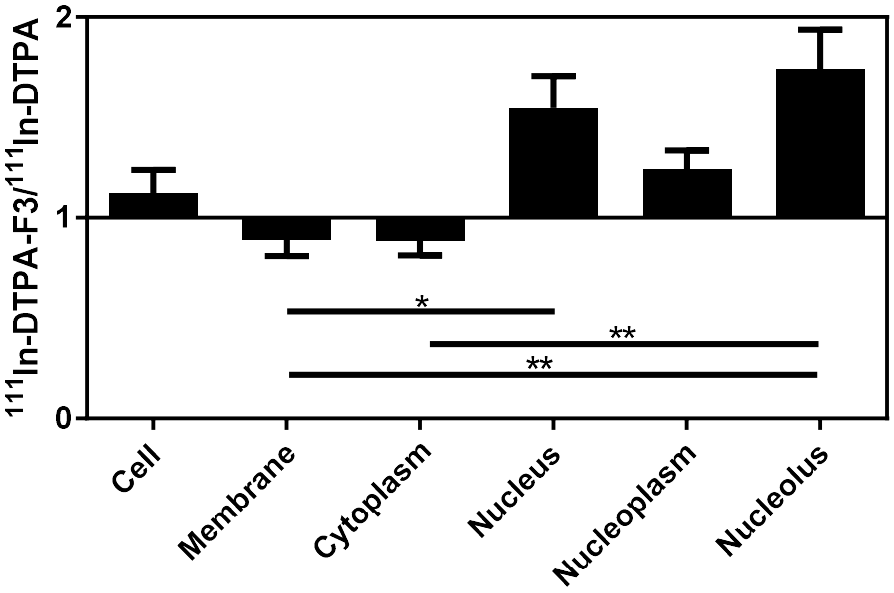

Figure 5.31. Mean fold-change in mean absorbed radiation dose deposited in the cell, membrane, cytoplasm, nucleus, nucleoplasm and nucleolus of malignant cells due to the incorporation of F3 into ^{111}In-DTPA

Mean fold-change in mean absorbed radiation dose (mean ^{111}In-DTPA-F3/^{111}In-DTPA ratio) deposited in the cell, membrane, cytoplasm, nucleus, nucleoplasm and nucleolus of MCF7, HCT116, MDA-MB-231/H2N, H322, MDA-MB-435, and U2OS cells exposed for 3 h to 1 μM of ^{111}In-DTPA-F3 (22.17 MBq/nmol) or an equimolar amount of ^{111}In-DTPA, due to the incorporation of F3 into ^{111}In-DTPA. Mean ^{111}In-DTPA-F3/^{111}In-DTPA ratios were calculated by taking the average of ^{111}In-DTPA-F3/^{111}In-DTPA ratios of MCF7, HCT116, MDA-MB-231/H2N, H322, MDA-MB-435, and U2OS cells (see Table 5.8). Values show mean fold-change ± SEM, n = 6. GraphPad Prism 6 software was used to test if the data followed a Gaussian distribution using a D'Agostino-Pearson omnibus test. Since the data did not follow a Gaussian distribution, medians were compared to a hypothetical value of 1 using non-parametric Wilcoxon signed-rank test. Nevertheless, parametric one-sample T-tests were also performed to test if means were significantly different from 1. A non-parametric Kruskal-Wallis one-way ANOVA with multiplicity adjusted P values (Dunn's post-hoc test) was also performed. *, $P < 0.05$; **, $P < 0.01$.

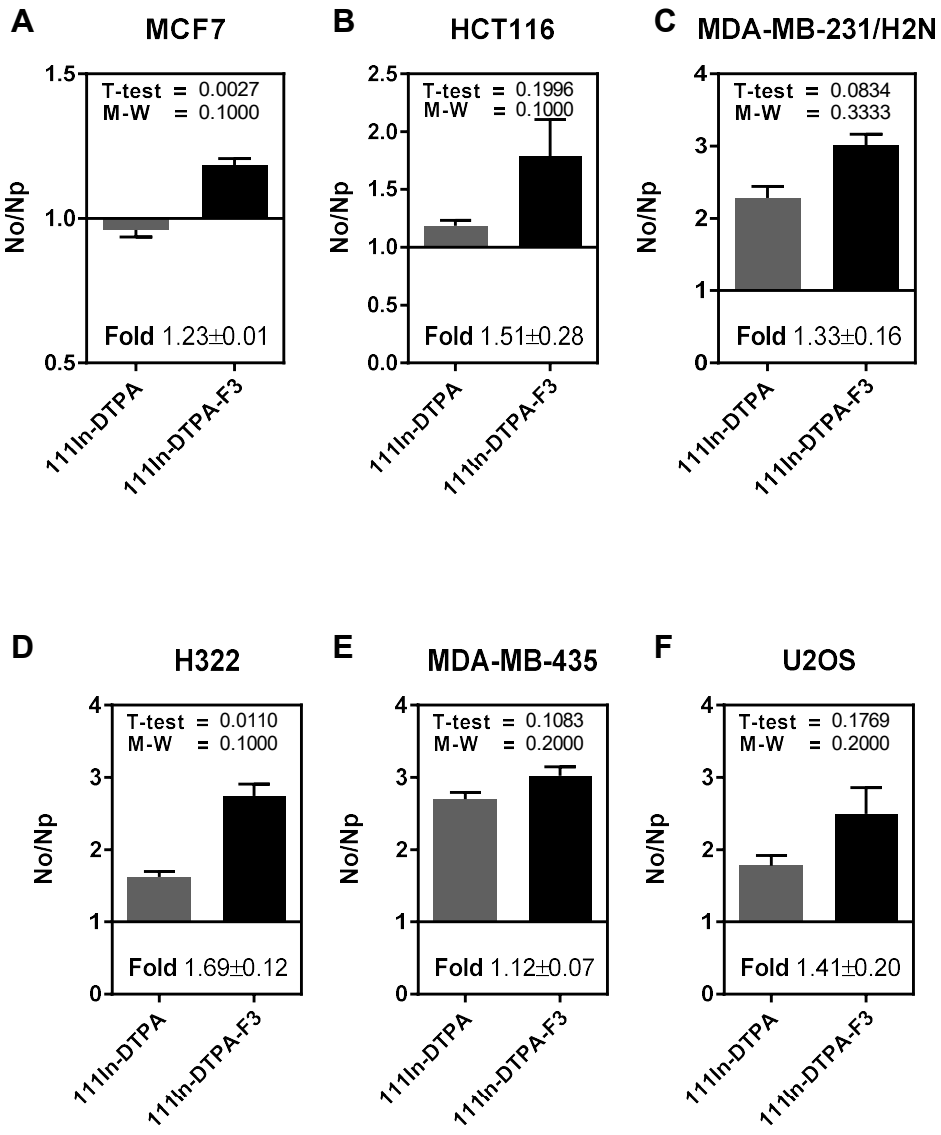

Figure 5.32. Distribution of radiation dose between the nucleolus and nucleoplasm of malignant cells exposed to ^{111}In-DTPA-F3 or ^{111}In-DTPA

Nucleolus-to-nucleoplasm ratio (No/Np ratio) of mean absorbed radiation dose deposited in (A) MCF7, (B) HCT116, (C) MDA-MB-231/H2N, (D) H322, (E) MDA-MB-435, and (F) U2OS cells exposed for 3 h to 1 μM of ^{111}In-DTPA-F3 (22.17 MBq/nmol) or an equimolar amount of ^{111}In-DTPA. Values show mean No/Np ratio ± SEM, n = 2–3. GraphPad Prism 6 software was used to test if the data followed a Gaussian distribution using a D'Agostino-Pearson omnibus test. Since the data did not follow a Gaussian distribution, means were compared using unpaired Mann-Whitney (M-W) tests with two-tailed P values. However, the unpaired, two-tailed M-W test has little statistical power and will never produce a P value of less than 0.1 for a sample size of 3 or less. Therefore, parametric T-tests with Welch's correction for unequal standard deviations (two-tailed P values) were also performed. Fold, fold increase in the No/Np ratio (mean ± SEM, n = 2–3) due to the incorporation of F3 into ^{111}In-DTPA (calculated by dividing the No/Np ratio on exposure to ^{111}In-DTPA-F3 by the No/Np ratio on exposure to ^{111}In-DTPA).

deposited in the MCF7 (M-W test, P = 0.1000; T-test, P = 0.0027), HCT116 (M-W test, P = 0.1000; T-test, P = 0.1996) and H322 (M-W test, P = 0.1000; T-test, P = 0.0110) cells after exposure to ^{111}In-DTPA-F3 was higher compared to ^{111}In-DTPA; although the differences between the No/Np ratio of mean absorbed radiation dose deposited in MDA-MB-231/H2N, MDA-MB-435 and U2OS cells after exposure to ^{111}In-DTPA-F3 was not statistically significantly different from ^{111}In-DTPA. Nevertheless, this supported the hypothesis that the incorporation of F3 into ^{111}In-DTPA could have shifted the distribution of nuclear mean absorbed radiation dose from the nucleoplasm to the nucleolus.

5.2.3. The level of cell kill produced by ^{111}In-DTPA-F3 is correlated with the localisation of cell-bound ^{111}In-DTPA-F3 in the nucleus

To assess the relationship between the level of cell kill produced by ^{111}In-DTPA-F3 and the proportion of cell-bound radioactivity associated with the membrane, cytoplasm, nucleus, nucleoplasm and nucleolus, Spearman correlations were generated using histograms that plotted the natural log of the surviving fraction after exposure of the malignant cells lines to ^{111}In-DTPA-F3 on the *x axis* and the percentage of cell-bound radioactivity associated with the membrane, cytoplasm, nucleus, nucleoplasm or nucleolus on the *y axis*.

Figure 5.33 shows that the level of cell death after a 3 h exposure to 0.1 μM of ^{111}In-DTPA-F3 (22.17 MBq/nmol) was not correlated with the percentage of cell-bound radioactivity associated with the membrane (Spearman R, 0.6000; P, 0.2417), cytoplasm (Spearman R, -0.6000; P, 0.2417), nucleoplasm (Spearman R, -0.8286; P, 0.0583) or nucleolus (Spearman R, 0.2571; P, 0.6583) after a 3 h exposure to 1 μM of

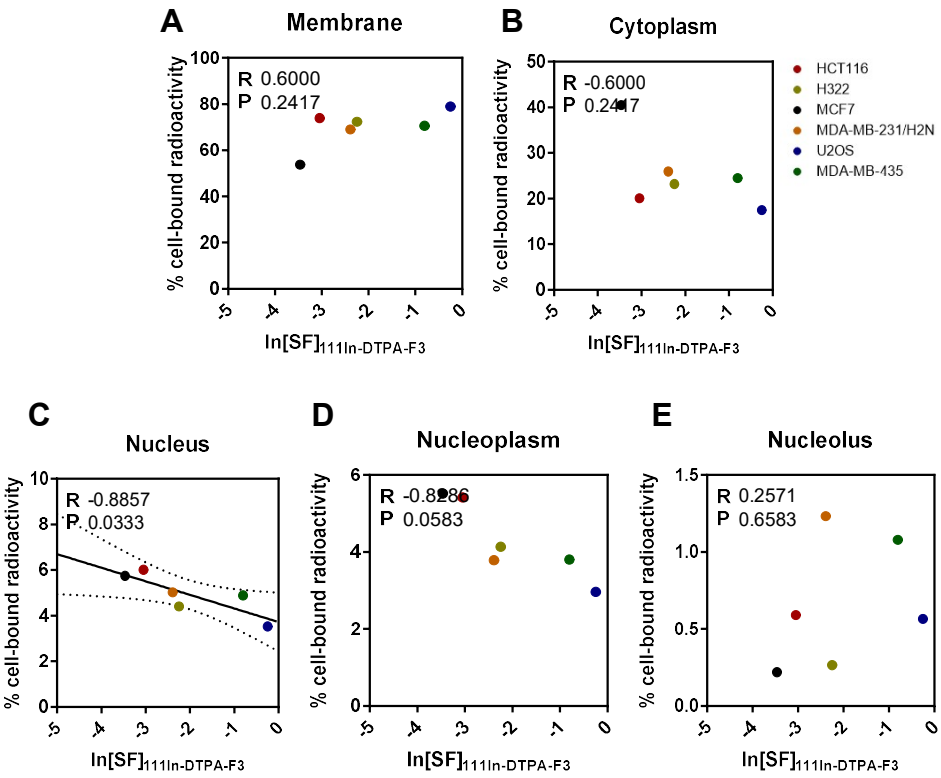

Figure 5.33. Correlation between the level of cell kill produced by ^{111}In-DTPA-F3 and the localisation of cell-bound ^{111}In-DTPA-F3 in the nucleus

Scatterplots showing the $\ln[SF]_{^{111}\text{In-DTPA-F3}}$ (natural log of the surviving fraction due to a 3 h exposure to 0.1 μM of ^{111}In-DTPA-F3 (22.17 MBq/nmol)) on the *x axis* (values show mean, n = 2–3) and the percentage cell-bound radioactivity in (A) membrane, (B) cytoplasm, (C) nucleus, (D) nucleoplasm or (E) nucleolus after 3 h exposure to 1 μM of ^{111}In-DTPA-F3 (22.17 MBq/nmol) on the *y axis* (values show mean, n = 2–3). GraphPad Prism 6 software was used to test if the data followed a Gaussian distribution using a D'Agostino-Pearson omnibus test. Since the data did not follow a Gaussian distribution, a nonparametric Spearman correlation (95% confidence interval) with two-tailed P values (shown) was used. R, Spearman R. A linear regression line with a 95% confidence band was also fitted to correlations with a P value < 0.05.

^{111}In-DTPA-F3 (22.17 MBq/nmol). However, the level of cell kill produced by ^{111}In-DTPA-F3 was correlated with the percentage of cell-bound radioactivity associated with the nucleus (Spearman R, -0.8857; P, 0.0333). Together, this suggested that the level of cell kill produced by ^{111}In-DTPA-F3 was determined by the localisation of cell-bound radioactivity in the nucleus.

To assess the relationship between the level of cell kill produced by ^{111}In-DTPA-F3 and the level of radioactivity associated with the cell, membrane, cytoplasm, nucleus, nucleoplasm and nucleolus, Spearman correlations were generated using histograms that plotted the natural log of the surviving fraction after exposure of the malignant cells lines to ^{111}In-DTPA-F3 on the *x axis* and the radioactivity in the cell, membrane, cytoplasm, nucleus, nucleoplasm or nucleolus on the *y axis*. Figure 5.34 shows that the level of cell kill produced after a 3 h exposure to 0.1 μM of ^{111}In-DTPA-F3 (22.17 MBq/nmol) was not correlated with the level of radioactivity associated with the cell (Spearman R, 0.8286; P = 0.0583), membrane (Spearman R, 0.8286; P = 0.0583), cytoplasm (Spearman R, 0.6000; P = 0.2417), nucleus (Spearman R, 0.6000; P = 0.2417), nucleoplasm (Spearman R, 0.6000; P = 0.2417) or nucleolus (Spearman R, 0.6000; P = 0.2417) after a 3 h exposure to 1 μM of ^{111}In-DTPA-F3 (22.17 MBq/nmol).

To assess the relationship between the level of cell kill produced by ^{111}In-DTPA-F3 and the level of radiation dose deposited in the cell, membrane, cytoplasm, nucleus, nucleoplasm and nucleolus, Spearman correlations were generated using histograms that plotted the natural log of the surviving fraction after exposure of the malignant cells lines to ^{111}In-DTPA-F3 on the *x axis* and the mean absorbed radiation dose deposited in the cell, membrane, cytoplasm, nucleus, nucleoplasm or nucleolus on the *y axis*. Figure 5.35 shows that the level of cell kill produced by ^{111}In-DTPA-F3 was not correlated with the level of mean absorbed radiation dose deposited in the cell

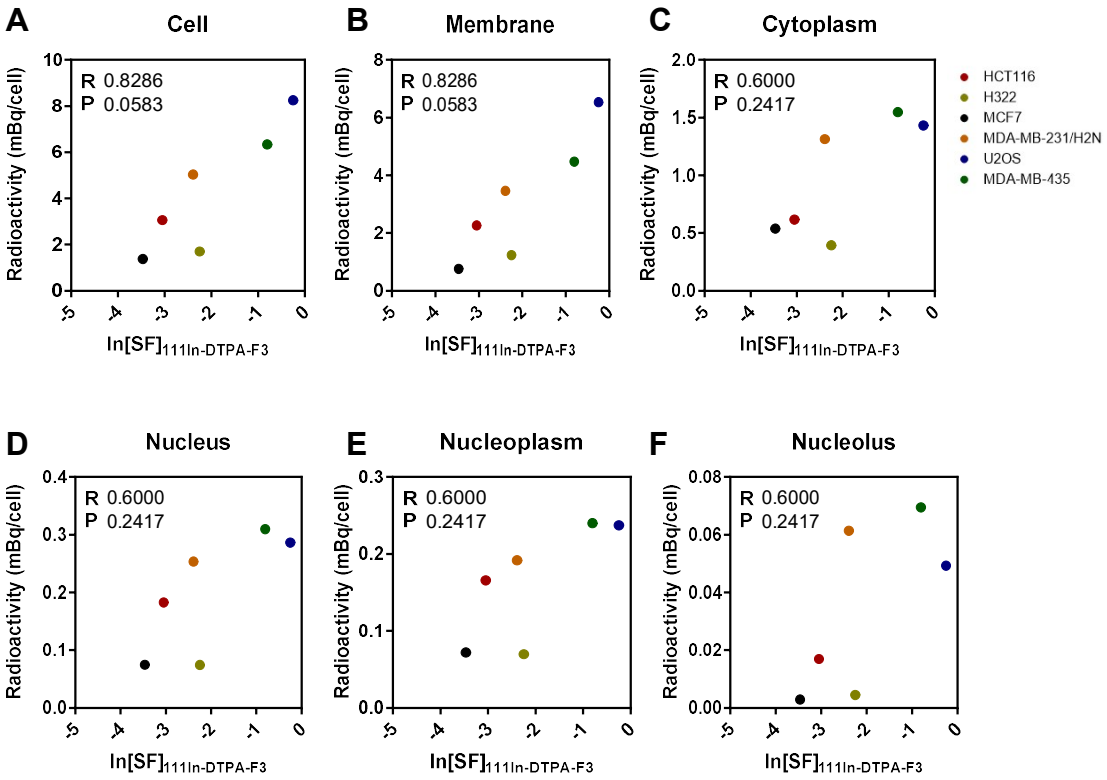

Figure 5.34. No correlation between the level of cell kill produced by ^{111}In-DTPA-F3 and the level of radioactivity delivered by ^{111}In-DTPA-F3 to the cell, membrane, cytoplasm, nucleus, nucleoplasm and nucleolus

Scatterplots showing the $\ln[SF]_{^{111}\text{In-DTPA-F3}}$ (natural log of the surviving fraction due to a 3 h exposure to 0.1 μM of ^{111}In-DTPA-F3 (22.17 MBq/nmol)) on the *x axis* (values show mean, n = 2–3) and the radioactivity in the (A) cell, (B) membrane, (C) cytoplasm, (D) nucleus, (E) nucleoplasm or (F) nucleolus after 3 h exposure to 1 μM of ^{111}In-DTPA-F3 (22.17 MBq/nmol) on the *y axis* (values show mean, n = 2–3). GraphPad Prism 6 software was used to test if the data followed a Gaussian distribution using a D'Agostino-Pearson omnibus test. Since the data did not follow a Gaussian distribution, a nonparametric Spearman correlation (95% confidence interval) with two-tailed P values (shown) was used. R, Spearman R.

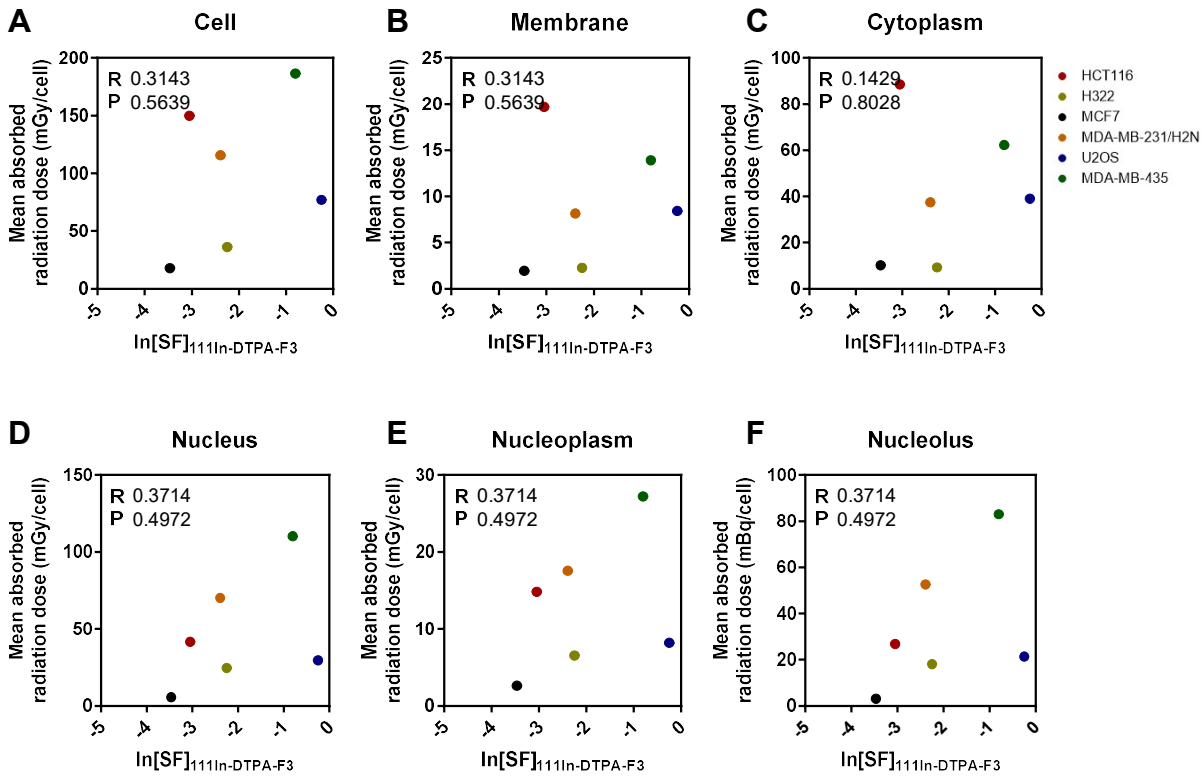

Figure 5.35. No correlation between the level of cell kill produced by ^{111}In-DTPA-F3 and the level of mean absorbed radiation dose deposited by ^{111}In-DTPA-F3 in the cell, membrane, cytoplasm, nucleus, nucleoplasm and nucleolus

Scatterplots showing ln[SF]$_{111\text{In-DTPA-F3}}$ (the natural log of the surviving fraction due to a 3 h exposure to 0.1 μM of ^{111}In-DTPA-F3 (22.17 MBq/nmol)) on the *x axis* (values show mean, n = 2–3) and the mean absorbed radiation dose in the (A) cell, (B) membrane, (C) cytoplasm, (D) nucleus, (E) nucleoplasm or (F) nucleolus after exposure 3 h to 1 μM of ^{111}In-DTPA-F3 (22.17 MBq/nmol) on the *y axis* (values show mean, n = 2–3). GraphPad Prism 6 software was used to test if the data followed a Gaussian distribution using a D'Agostino-Pearson omnibus test. Since the data did not follow a Gaussian distribution, a nonparametric Spearman correlation (95% confidence interval) with two-tailed P values (shown) was used. R, Spearman R.

(Spearman R, 0.3413; P = 0.5639), membrane (Spearman R, 0.3143; P = 0.5639), cytoplasm (Spearman R, 0.1429; P = 0.8028), nucleus (Spearman R, 0.3714; P = 0.4972), nucleoplasm (Spearman R, 0.3714; P = 0.4972) or nucleolus (Spearman R, 0.3714; P = 0.4972).

Together, this suggested that the localisation of cell-bound ^{111}In-DTPA-F3 in the nucleus determined the level of cell kill produced by ^{111}In-DTPA-F3, while the level of radioactivity or mean absorbed radiation dose deposited in the cell, membrane, cytoplasm, nucleus, nucleoplasm or nucleolus by ^{111}In-DTPA-F3 did not determine the level of cell kill produced by ^{111}In-DTPA-F3. Since the ^{111}In-DTPA-F3 was found to target the nucleolus, the radiosensitivity of the nucleolus to radiation dose deposited by ^{111}In-DTPA-F3 could vary depending on the malignant cell line.

5.2.4. The level of γH2AX foci, but not the level of cell kill, induced by ^{111}In-DTPA-F3 is correlated with the volume of the nucleolus

To assess the relationship between the level of γH2AX foci induced by ^{111}In-DTPA-F3 and the volume of the cell, nucleus and nucleolus or the number of nucleoli per cell, Spearman correlations were generated using histograms that plotted the absolute number of γH2AX foci after a 3 h exposure to 1 μM of ^{111}In-DTPA-F3 (22.17 MBq/nmol) on the *x axis* and the volume of the cell, nucleus or nucleolus or the number of nucleoli per cell on the *y axis*. Figure 5.36 shows that the absolute number of γH2AX foci after 3 h exposure to ^{111}In-DTPA-F3 was not significantly correlated with the volume of the cell (Spearman R, 0.9000; P = 0.0833) or nucleus (Spearman R, 0.9000; P = 0.0833) or the number of nucleoli per cell (Spearman R, 0.7000; P = 0.2333). However, the absolute number of γH2AX foci after 3 h exposure to ^{111}In-DTPA-F3 was correlated

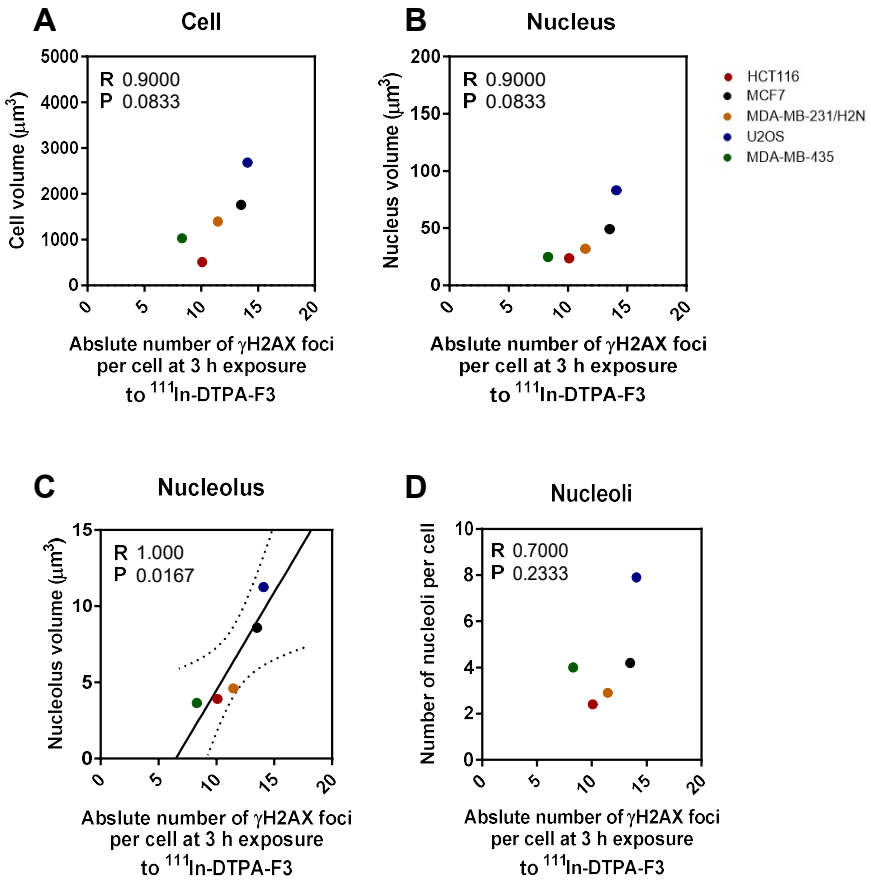

Figure 5.36. Correlation between the level of γH2AX foci induced by ^{111}In-DTPA-F3 and the volume of the nucleolus

Scatterplots showing the absolute number of γH2AX foci per cell at 3 h after exposure to 1 µM of ^{111}In-DTPA-F3 on the *x axis* (values show mean, n = 50) and the volume of the (A) cell, (B) nucleus or (C) nucleolus or (D) the number of nucleoli per cell on the *y axis* (values show mean, n = 10). GraphPad Prism 6 software was used to test if the data followed a Gaussian distribution using a D'Agostino-Pearson omnibus test. Since the data did not follow a Gaussian distribution, a nonparametric Spearman correlation (95% confidence interval) with two-tailed P values (shown) was used. R, Spearman R. A linear regression line with a 95% confidence band was also fitted to correlations with a P value < 0.05.

with the volume of the nucleolus (Spearman R, 1.0000; P = 0.0167). This suggested that the induction of γH2AX foci by ^{111}In-DTPA-F3 was dependent on the volume of the nucleolus, although the induction of γH2AX foci by ^{111}In-DTPA-F3 was not correlated with the level of cell kill produced by ^{111}In-DTPA-F3 (Chapter 4, Figure 4.12).

To assess the relationship between the level of cell kill produced by ^{111}In-DTPA-F3 and the number of nucleoli per cell or the volume of the cell, nucleus and nucleolus or the number of nucleoli per cell, Spearman correlations were generated using histograms that plotted the natural log of the surviving fraction of the malignant cell lines after exposure to ^{111}In-DTPA-F3 on the *x axis* and the volume of the cell, nucleus and nucleolus or the number of nucleoli per cell on the *y axis*. Figure 5.37 shows that the level of cell kill produced after a 3 h exposure to 0.1 μM of ^{111}In-DTPA-F3 (22.17 MBq/nmol) was not significantly correlated with the volume of the cell (Spearman R, 0.2571; P, 0.6583), nucleus (Spearman R, 0.1429; P, 0.8028) or nucleolus (Spearman R, -0.0286; P, > 0.9999), or with the number of nucleoli per cell (Spearman R, 0.2571; P, 0.6583). Thus, the volume of the cell, nucleus or nucleolus, and the number with the volume of the nucleolus (Spearman R, 1.0000; P = 0.0167). This suggested that the induction of γH2AX foci by ^{111}In-DTPA-F3 was dependent on the volume of the nucleolus, although the induction of γH2AX foci by ^{111}In-DTPA-F3 was not correlated with the level of cell kill produced by ^{111}In-DTPA-F3 (Chapter 4, Figure 4.12).

To assess the relationship between the level of cell kill produced by ^{111}In-DTPA-F3 and the number of nucleoli per cell or the volume of the cell, nucleus and nucleolus or the number of nucleoli per cell, Spearman correlations were generated using histograms that plotted the natural log of the surviving fraction of the malignant cell lines after exposure to ^{111}In-DTPA-F3 on the *x axis* and the volume of the cell, nucleus

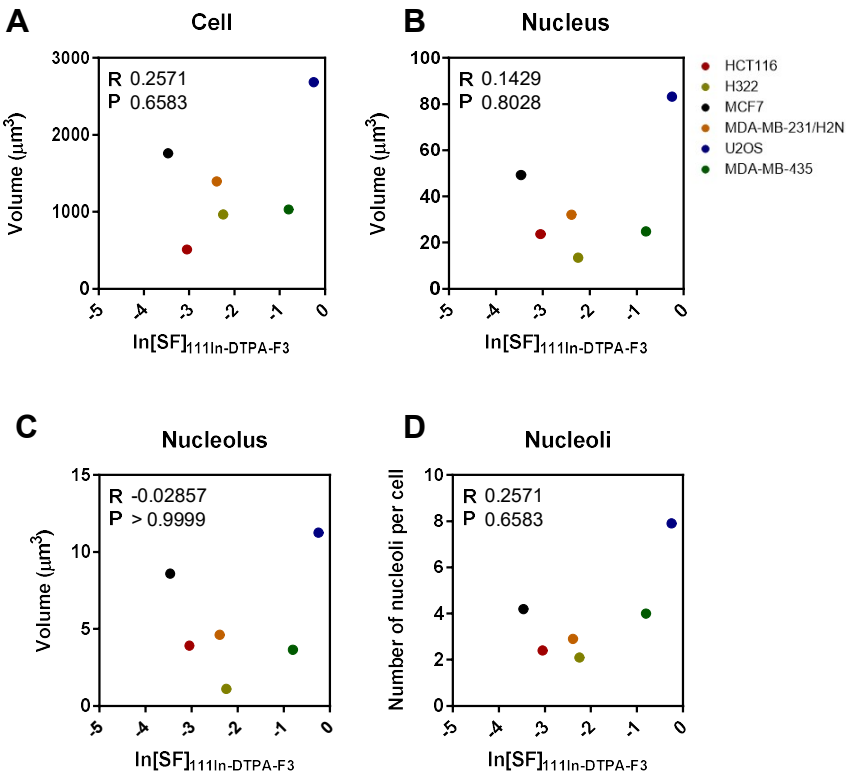

Figure 5.37. No correlation between the radiotoxicity of ^{111}In-DTPA-F3 and the number of nucleoli per cell or the volume of the cell, nucleus or nucleolus

Scatterplots showing the $\ln[SF]_{^{111}\text{In-DTPA-F3}}$ (the natural log of the surviving fraction after 3 h exposure to 0.1 µM of ^{111}In-DTPA-F3 (22.17 MBq/nmol)) on the *x axis* (values show mean, n = 2–3) and the volume of the (A) cell, (B) nucleus and (C) nucleolus or (D) the number of nucleoli per cell on the *y axis* (values show mean, n = 10). GraphPad Prism 6 software was used to test if the data followed a Gaussian distribution using a D'Agostino-Pearson omnibus test. Since the data did not follow a Gaussian distribution, a nonparametric Spearman correlation (95% confidence interval) with two-tailed P values (shown) was used. R, Spearman R.

and nucleolus or the number of nucleoli per cell on the *y axis*. Figure 5.37 shows that the level of cell kill produced after a 3 h exposure to 0.1 μM of ^{111}In-DTPA-F3 (22.17 MBq/nmol) was not significantly correlated with the volume of the cell (Spearman R, 0.2571; P, 0.6583), nucleus (Spearman R, 0.1429; P, 0.8028) or nucleolus (Spearman R, -0.0286; P, > 0.9999), or with the number of nucleoli per cell (Spearman R, 0.2571; P, 0.6583). Thus, the volume of the cell, nucleus or nucleolus, and the number of nucleoli per cell, did not determine the level of cell kill produced by ^{111}In-DTPA-F3.

5.3. Discussion

In this Chapter, internalisation assays showed that the uptake of radioactivity into malignant cells exposed for 3 h to 1 μM of ^{111}In-DTPA-F3 (22.17 MBq/nmol) was relatively modest (0.39±0.08–1.36±0.13%; 1.378±0.274–8.253±0.981 mBq/cell). The level of cell-bound ^{111}In-DTPA-F3 was in agreement with the internalisation experiments in Cornelissen *et al*. (2012b) that showed that 0.51±0.03% of 1 μM of ^{111}In-BnDTPA-F3 was taken up by MDA-MB-231/H2N cells by 2 h (Cornelissen*, et al.*, 2012b). The level of cell-bound ^{111}In-DTPA-F3 was also comparable to the level of cell-bound ^{111}In-DTPA (0.54±0.14–1.83±0.10%; 1.784±0.448–7.681±0.583 mBq/cell), an equimolar control lacking F3. Similarly, less than 1% of ^{213}Bi-DTPA (which also lacked F3) was reported in Vallon *et al*. (2012) to become associated with OVCAR-3 cells by 1 h. The level of cell-bound ^{111}In-DTPA-F3 was 35–123 fold lower than the level of cell-bound ^{111}In-DTPA-EGF (5 ng/mL; 3.7 MBq/μg) reported in Reilly *et al*. (2000) to be taken up by MDA-MB-435 cells by 3 h (48.1±10.0%) (Reilly*, et al.*, 2000). The uptake of ^{111}In-DTPA-F3 was also 7–26 fold lower compared to the uptake of ^{213}Bi-DTPA-F3, 10% of which was reported to be associated with OVCAR-3 cells after

1 h, while 6% was reported to be internalised into OVCAR-3 cells (4% remained on the membrane) (Vallon*, et al.*, 2012). This discrepancy may be due to different numbers of membrane NCL receptors depending on the cell line or the influence of different radionuclides on cell uptake.

The relatively modest uptake of ^{111}In-DTPA-F3 by malignant cells *in vitro* was also in agreement with the relatively modest tumour uptake of ^{111}In-BnDTPA-F3 when it was i.v. injected into MDA-MB-231/H2N xenograft-bearing athymic mice (Cornelissen*, et al.*, 2012b). Cornelissen *et al*. (2012b) performed SPECT imaging and biodistribution studies and showed that 3 h after i.v. injection the tumour uptake of ^{111}In-BnDTPA-F3 was relatively low (0.80±0.28% ID/g) and the tumour-to-muscle ratio was also relatively low (1.1) (Cornelissen*, et al.*, 2012b). Similarly, Bhojani *et al*. (2011) reported that the tumour uptake of ^{125}I-IBMF3 was relatively low at 30 min post i.v. injection of MDA-MB-435 xenograft-bearing athymic mice (1.05% ID/g) (Bhojani*, et al.*, 2011).

In contrast, ^{213}Bi-DTPA-$[F3]_2$ was found to be taken up at high levels in MDA-MB-435 xenografts in SCID mice (32% ID/g) and the tumour-to-blood and tumour-to-intestine ratios were also relatively high at 17.6:1 and 10.4:1, respectively (Drecoll*, et al.*, 2009). This discrepancy may have been due to the dimeric form of ^{213}Bi-DTPA-$[F3]_2$, since the additional mass of an extra F3 moiety could have reduced the rate of tumour washout and also doubled the number of receptors that could be targeted by a dimeric construct of ^{213}Bi-DTPA-$[F3]_2$, thereby increasing the ability of the dimeric construct to bind to membrane NCL-expressing malignant cells in comparison to a monomeric F3 construct.

The radiation dose that was deposited after 3 h exposure of malignant cell lines to ^{111}In-DTPA-F3 (cumulated radioactivity of 15,111±3.008–90,527±10.756 mBq·sec/cell) was also relatively modest (17.93±2.66–186.54±21.79 mGy/cell). This

level of radiation dose was 131–1366 fold lower than the level of radiation dose that was calculated by Reiley *et al.* (2000) to be deposited in MDA-MB-468 cells by 43 mBq/cell of ^{111}In-DTPA-EGF (24.5 Gy/cell) (Reilly*, et al.*, 2000).

The proportion of cell-bound ^{111}In-DTPA-F3 that was localised in the nucleus of malignant cells after 3 h was relatively low (3.53±0.56–6.01±0.52% of cell-bound ^{111}In-DTPA-F3). In contrast, Cornelissen *et al*. (2012b) reported that 37% of the cell-bound of ^{111}In-BnDTPA-F3 was localised in the nucleus after 30 min (Cornelissen*, et al.*, 2012b). This discrepancy may have been due to the fact that nuclear localisation of ^{111}In-BnDTPA-F3 was reported in Cornelissen *et al*. (2012) to increase rapidly and reach a plateau by 15 min, while uptake of ^{111}In-BnDTPA-F3 in the membrane and cytoplasm increased steadily and reached a plateau by 3–4 h. Therefore, the percentage of cell-bound ^{111}In-BnDTPA-F3 that was localised in the nucleus at 3 h would have been significantly less than the 37% at 30 min (Cornelissen*, et al.*, 2012b).

The radiation dose that was deposited in the nucleus after 3 h exposure of malignant cells to ^{111}In-DTPA-F3 was also relatively modest (5.75±0.60–110.33±17.00 mGy/cell). This was 175–1,134 fold lower than the level of radiation dose that was calculated by Reiley *et al.* (2000) to be deposited in the nucleus of MDA-MB-468 cells by 43 mBq/cell of ^{111}In-DTPA-EGF (19.28 Gy/cell) (Reilly*, et al.*, 2000).

A proportion of cell-bound ^{111}In-DTPA-F3 was also found to be associated with the nucleolus after 3 h exposure of malignant cells to ^{111}In-DTPA-F3 (0.22±0.02–1.23±0.13%). The level of radioactivity associated with the nucleolus after 3 h exposure of malignant cells to ^{111}In-DTPA-F3 was found to be 1.68±0.19–4.53±2.12 fold greater than ^{111}In-DTPA. The targeting of the nucleolus by ^{111}In-DTPA-F3 was in agreement with the report in Cornelissen *et al*. (2012b) of the colocalisation of

fluorescein-labelled F3 (FITC-F3) with NCL in the nucleolus of MD-MB-231/H2N cells *in vitro* (Cornelissen*, et al.*, 2012b)(Cornelissen*, et al.*, 2012b).

The radiation dose deposited in the nucleolus after 3 h exposure of malignant cells to ^{111}In-DTPA-F3 (3.11±0.31–83.08±13.54 mGy/cell), was 1.21±0.21–2.56±0.08 fold greater than the radiation dose deposited in the nucleolus by ^{111}In-DTPA. Further, the nucleolus-to-nucleoplasm ratio (No/Np ratio) of mean absorbed radiation dose after exposure of malignant cells to ^{111}In-DTPA-F3 was 1.23±0.01–1.69±0.02 fold higher compared to ^{111}In-DTPA, suggesting that the incorporation of F3 into ^{111}In-DTPA could have shifted the nuclear radiation dose from the nucleoplasm to the nucleolus.

Together with the clonogenic survival data (Chapter 4, Figure 4.4) that showed that ^{111}In-DTPA-F3, but not ^{111}In-DTPA, was significantly radiotoxic to malignant cells (except for U2OS cells which were not radiosensitive to ^{111}In-DTPA-F3), higher levels of uptake of radioactivity and deposition of radiation dose in the nucleolus of malignant cells exposed to ^{111}In-DTPA-F3 relative to ^{111}In-DTPA, supported the hypothesis that the localisation of ^{111}In-DTPA-F3 in the nucleolus was likely to be responsible for the radiotoxicity of ^{111}In-DTPA-F3.

Interestingly, the level of cell kill that was produced by ^{111}In-DTPA-F3 was found to correlate with the percentage of cell-bound ^{111}In-DTPA-F3 that was localised in the nucleus of the malignant cells. This correlation suggested that cell kill could only be produced by ^{111}In-DTPA-F3 after the translocation of greater than 3.72±0.47% of cell-bound radioactivity to the nucleus. This could explain why non-significant levels of cell kill (43%) were produced by the localisation of 3.53±0.56% of cell-bound ^{111}In-DTPA-F3 to the nucleus of U2OS cells, while the translocation of 4.40±0.55–6.01±0.52% of cell-bound ^{111}In-DTPA-F3 to the nucleus of MCF7, HCT116, MDA-MB-231/H2N, H322 and MDA-MB-435 cells produced statistically significant levels of cell kill (55–97%).

For every 0.60±0.20% (over the 3.72±0.47% threshold) of cell-bound ^{111}In-DTPA-F3 that was localised in the nucleus, 1 natural log of cell kill was produced by ^{111}In-DTPA-F3.

In contrast, the localisation of cell-bound ^{111}In-DTPA-F3 to the nucleoplasm or nucleolus was not correlated with the level of cell kill produced by ^{111}In-DTPA-F3, suggesting that the distribution of nuclear ^{111}In-DTPA-F3 between the nucleoplasm and nucleolus could be variable depending on the cell line. Indeed, the level of cell kill that was produced by exposing malignant cells to ^{111}In-DTPA-F3 was not found to correlate with the level of radioactivity in the nucleolus, or the level of radiation dose deposited in the nucleolus, after exposure of malignant cells to ^{111}In-DTPA-F3, although the incorporation of F3 into ^{111}In-DTPA was found to increase the deposition of mean absorbed radiation dose in the nucleolus and shift the distribution of nuclear mean absorbed radiation dose from the nucleoplasm to the nucleolus. Thus, the radiosensitivity of the nucleolus to the mean absorbed radiation dose deposited by ^{111}In-DTPA-F3 could vary depending on the malignant cell line.

The method for calculating the mean absorbed radiation dose assumed immediate uptake of radioactivity followed by elimination by radioactive decay up to 3 h. The weakness of this approach was that it did not account for ‘biological decay’, i.e. the rate of uptake/efflux of ^{111}In-DTPA-F3 in/from the membrane, cytoplasm, nucleoplasm and nucleolus over time. As mentioned, the level of uptake of ^{111}In-BnDTPA-F3 in the membrane and cytoplasm of MDA-MB-231/H2N cells reported in Cornelissen *et al*. (2012b) increased steadily and reached a plateau by 3–4 h, while the level of uptake of ^{111}In-BnDTPA-F3 in the nucleus increased rapidly and reached a plateau by 15 min. By not accounting for the biological decay of ^{111}In-DTPA-F3 (or ^{111}In-DTPA) the mean absorbed radiation dose may have been overestimated, but underestimated in

comparison to ^{111}In-DTPA-F3. Therefore, it cannot be excluded that a correlation between the level of cell kill produced by of ^{111}In-DTPA-F3 and the mean absorbed radiation dose deposited in the nucleolus could still be found if differences in the biological decay ^{111}In-DTPA-F3 between the malignant cell lines were taken into account.

It should also be noted that mean absorbed radiation dose is a homogeneous approximation of the energy absorbed over a given volume. In reality, the radiation dose deposited by ^{111}In-DTPA-F3 would have been highly inhomogeneous due to localised deposition of energy over very small volumes of several cubic nanometres (Kassis, 2011). Since inhomogeneous deposition of highly localised energy may be more likely to inactivate critical targets that are essential for cell survival, this may explain why targeting the nucleolus with relatively modest levels of ^{111}In-DTPA-F3 (0.22±0.02–5.42±0.39% of cell-bound; 0.003±0.000–0.070±0.013 mBq/cell) and relatively modest tumour accumulation of ^{111}In-BnDTPA-F3 (0.80±0.28% ID/g) (Cornelissen*, et al.*, 2012b), nonetheless produce significant levels of cell kill *in vitro* and significant inhibition of tumour growth *in vivo*, respectively.

Despite the lack of correlation between the level of cell kill produced by ^{111}In-DTPA-F3 and the level of γH2AX foci induced by ^{111}In-DTPA-F3, the volume of the nucleolus was found to correlate with the induction of γH2AX foci by ^{111}In-DTPA-F3. A potential reason for this may have been that polyploid malignant cells carrying additional copies of chromosomes 13, 14, 15, 21 and 22, in which the rDNA genes reside, could possess enlarged nucleoli as well as the extra genetic material to act as a substrate for the induction of a higher level of γH2AX foci. It is unlikely that the induction of γH2AX foci by ^{111}In-DTPA-F3 was merely a by-product of the deposition of radiation dose in the nucleus, and therefore the rate of repair of γH2AX foci may still be found to contribute,

at least in part, to the radiotoxicity of ^{111}In-DTPA-F3. In contrast, the volume of the nucleolus was not found to correlate with the level of cell kill produced by ^{111}In-DTPA-F3.

Since the nucleolus is not a discrete membrane-bound organelle, but rather is comprised of dynamic components in constant flux with the surrounding nucleoplasm, it is interesting to speculate that the inactivation of the nucleolus could be dependent on the level of ^{111}In-DTPA-F3 in the nucleoplasm and nucleolus. This could explain why a correlation was found between the level of cell kill produced by ^{111}In-DTPA-F3 and the localisation of ^{111}In-DTPA-F3 in the nucleus, but not to the nucleoplasm nor nucleolus, and yet the clonogenic survival and internalisation data supported the hypothesis that the radiotoxicity of ^{111}In-DTPA-F3 was caused by targeting the nucleolus.

The nucleolus contains >4,500 components, some of which contribute to distinct pathways that monitor ribosome biogenesis and others that regulate the MDM2-p53 pathway (Ahmad*, et al.*, 2009; Andersen*, et al.*, 2005; Leung*, et al.*, 2006). The nuclear translocation of ^{111}In-DTPA-F3 and inhomogeneous deposition of radiation dose in the nucleolus could result in the ionisation of nucleolar components which occupy a relatively compact 1.11±0.12–11.25±1.09 μm^3 volume. The emission of low energy (4 to 26 keV), short range (2 nm to 500 nm) Auger electrons from ^{111}In-DTPA-F3 could result in a high level of direct ionisations or indirect ionisations (mediated by ROS such as $\cdot O2^-$, H_2O_2, $\cdot OH$, and OH^-), causing damage to rDNA, rRNA, r-proteins, snoRNAs, snoRNPs and other nucleolar components concentrated in the follicular component (FC), dense follicular component (DFC) or granular component (GC) of the nucleolus. Inactivation of the nucleolus could interfere with the rate of transcription and processing of rRNA and assembly of the 40S and 60S r-subunits, and trigger the

nucleolar stress response which regulates the MDM2-p53 pathway (Boulon*, et al.*, 2010).

Damage to rDNA and rRNA by ^{111}In-DTPA-F3 may lead to the release of r-proteins from the nucleolus due to reduced biogenesis of the 40S and 60S r-subunits. Reduced pre-rRNA synthesis could alter interactions with snoRNAs and snoRNPs that mediate 2′-O-ribose methylation and pseudouridine formation during the processing of the 47S pre-rRNA and thereby decrease the abundance of the 28S, 5.8S and 18S rRNAs in the nucleolus (Dieci*, et al.*, 2009; Matera*, et al.*, 2007). Decreased abundance of the 28S, 5.8S and 18S rRNAs could reduce transient interactions with, and the nucleolar abundance of snoRNPs and non-ribosomal proteins required for the assembly of the 40S and 60S r-subunits (Andersen*, et al.*, 2005; Fatica and Tollervey, 2002; Tschochner and Hurt, 2003). Thus, uptake of ^{111}In-DTPA-F3 in the nucleolus might cause a reduction in ribosome biogenesis by interfering with the localisation of nucleolar proteins following increased rDNA damage and interference with rRNA transcription.

Reduced abundance of the 28S and 18S rRNAs due to damage to rDNA and pre-rRNA could also alter protein-rRNA and protein-protein interactions, leading to the release of r-proteins (RPL5, RPS6, RPS7, RPL11 and RPL23) from the nucleolus into the nucleoplasm. In the nucleoplasm, RPL5, RPS7, RPS6, RPL11 and RPL23 may bind to MDM2 (at its central acidic domain), preventing MDM2 from ubiquitylating p53 and therefore allowing p53 to induce cell cycle arrest and apoptosis (Boisvert*, et al.*, 2007; Fumagalli*, et al.*, 2009; Fumagalli*, et al.*, 2012; Holzel*, et al.*, 2010). Reduced rRNA transcription and r-protein depletion in the nucleolus may decrease the nuclear export of the 40S and 60S r-subunits, which might block the co-ribosomal export of

p53 from the nucleus to the cytoplasm. Together, this could result in the stabilisation of p53 in the nucleus (Boisvert*, et al.*, 2007).

The effects of damage caused by ^{111}In-DTPA-F3 to nucleolar proteins are more difficult to predict, but could result in the reorganisation of the nucleolar proteome, altering the localisation of many nucleolar and non-nucleolar components in a manner analogous to the induction of nucleolar stress (Boisvert*, et al.*, 2010; Boisvert and Lamond, 2010; Emmott*, et al.*, 2010; Lam*, et al.*, 2010; Moore*, et al.*, 2011). Induction of nucleolar stress by ^{111}In-DTPA-F3 may also trigger the induction of p53, since a non-stressed nucleolus is required for nuclear export and degradation of p53 (Boyd*, et al.*, 2011; Rubbi and Milner, 2003). Induction of nucleolar stress by ^{111}In-DTPA-F3 could also trigger the release of r-proteins from the nucleolus into the nucleoplasm (Boisvert*, et al.*, 2010; Boisvert and Lamond, 2010; Boisvert*, et al.*, 2007; Daniely*, et al.*, 2002; Emmott*, et al.*, 2010; Gjerset and Bandyopadhyay, 2006; Lam*, et al.*, 2010; Moore*, et al.*, 2011; Zhang and Lu, 2009).

Stabilisation and activation of p53 by ^{111}In-DTPA-F3 may repress Pol I (and III) transcription, reducing the bioavailability of the 47S and 5S rRNAs, respectively. The activation of p53 upregulates Pol II-transcribed genes, such as p21, Bax, Puma and Noxa, initiating the mitochondrial apoptotic pathway in the cytoplasm (Lee and Gu, 2010). Thus, the interference of ribosome biogenesis and induction of nucleolar stress by ^{111}In-DTPA-F3 could lead to p53-dependent cycle arrest and apoptosis.

The small molecules CX-3453 and CX-5461 have been developed specifically to target the nucleolus by inhibiting Pol I-mediated ribosome biogenesis. Drygin *et al.* (2011) reported that CX-5461 produced an anti-proliferative effect that ranged 1,667 fold depending on the malignant or normal cell line. Both CX-3453 and CX-5461 have also been shown to induce senescence and a range of different cell death pathways,

including p53-dependent apoptosis and p53-independent autophagy, depending on the malignant cell line (Bywater*, et al.*, 2012; Drygin*, et al.*, 2011; Drygin*, et al.*, 2009). This suggests that the cellular response to interference with the function of the nucleolus (at least through the inhibition of ribosome biogenesis) varies depending on the malignant cell line, and that malignant cell lines therefore may possess a range of dependencies on the function of the nucleolus (Drygin*, et al.*, 2011).

CX-3453 has been shown to bind GC-rich rDNA and redistribute NCL from the nucleolus to the nucleoplasm (Drygin*, et al.*, 2009), while CX-5461 has been shown to cause the release of RPL5 and RPL11 from the nucleolus, thereby inducing p53 (Bywater*, et al.*, 2012). Interestingly, cell lines carrying wild-type p53 have been found to be more sensitive to CX-5461 than p53 mutant or $p53^{-/-}$ cells (Bywater*, et al.*, 2012). However, ^{111}In-DTPA-F3 produced levels of cell kill for the p53 wild-type cells (U2OS, HCT116 and MCF7) that ranged from 43% to 97%, while the level of cell kill for the p53 mutant cells (MCF7, MDA-MB-231/H2N, H322 and MDA-MB-435) ranged from 55% to 91%. Thus, not all the p53 wild-type cell lines were found to be less radiosensitive to ^{111}In-DTPA-F3 than the p53 mutant cell lines, suggesting that the mechanism of cell kill by ^{111}In-DTPA-F3 may not be p53-dependent. It should however be noted that a relatively small number of p53 wild-type and p53 mutant cell lines were tested and therefore it cannot be excluded that a correlation with p53 status could still be found after testing a larger number of p53 wild-type and p53 mutant or $p53^{-/-}$ cell lines.

Targeting the nucleolus is a promising approach for Auger electron radionuclide therapy that may be effective regardless of p53 status, since ^{111}In-DTPA-F3 is significantly radiotoxic to a wide range of different cell lines *in vitro* independent of p53 status. However, it is hypothesised that perturbation of ribosome biogenesis or

induction of nucleolar stress with ^{111}In-DTPA-F3 may be more difficult to achieve in malignant cells with dysregulated growth factor signalling and upregulation of oncogenes that drive Pol I-transcription of pre-rRNA (Bakshi*, et al.*, 2008; Delloye-Bourgeois*, et al.*, 2012; Drygin*, et al.*, 2010; Grummt, 2003; Hannan*, et al.*, 2013; Mayer and Grummt, 2006; Romanova*, et al.*, 2009; Xiao and Grove, 2009). Figure 5.38 shows a how dysregulated growth factor signalling and activation of oncogenes may mitigate the radiotoxicity of ^{111}In-DTPA-F3.

In summary, ^{111}In-DTPA-F3 was found to target the nucleolus, in which it is taken up and deposits radiation dose. The level of cell kill caused by ^{111}In-DTPA-F3 to a variety of malignant cell lines was not ascribed to the level of radiation dose deposited in the nucleolus, but rather the localisation of cell-bound ^{111}In-DTPA-F3 in the nucleus, suggesting the level and distribution of radiation dose between the nucleolus and the nucleoplasm and the radiosensitivity of the nucleolus could vary depending on the cell line. Also, the induction of γH2AX foci by ^{111}In-DTPA-F3 was correlated with the volume of the nucleolus. More research is required to characterise the radiosensitivity of different malignant cell lines to ^{111}In-DTPA-F3 and the damage it is hypothesised to cause to nucleolar components.

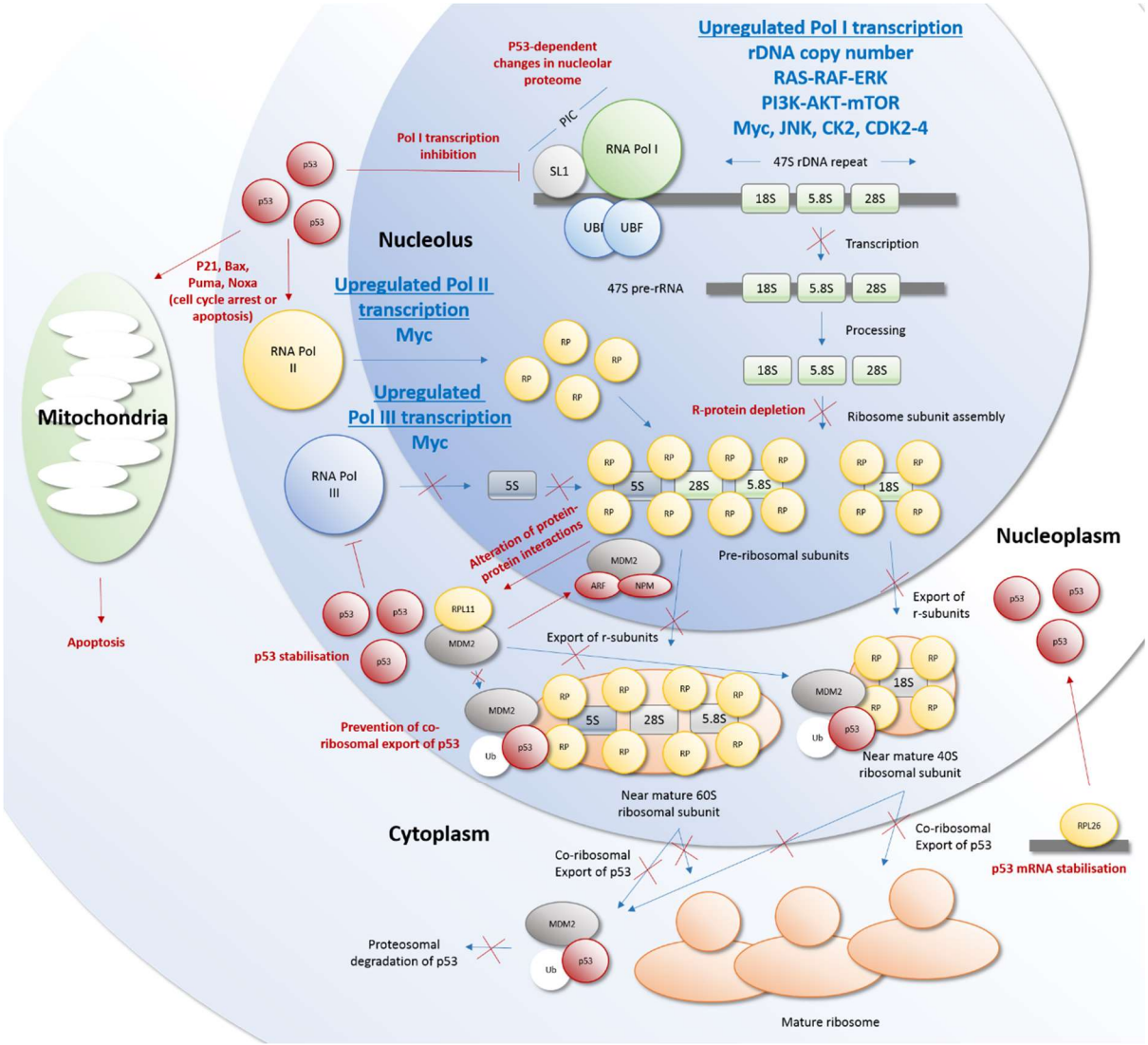

Figure 5.38. Potential mitigation of the predicted effects of ^{111}In-DTPA-F3

Accumulation of ^{111}In-DTPA-F3 in the nucleolus of malignant cells is hypothesised to interfere with ribosome biogenesis and induce the nucleolar stress response pathway, triggering the stabilisation and activation of p53 through alterations in protein-protein interactions and prevention of co-ribosomal export of p53 and MDM2. The predicted effects of uptake of ^{111}In-DTPA-F3 in the nucleolus are shown in red and include inhibition of Pol I-mediated rRNA transcription, the release of r-proteins from the nucleolus into the nucleoplasm, increased p53 levels, upregulation of p53 target genes (p21, Bax, Puma and Noxa), cell cycle arrest and apoptosis. Mechanisms by which malignant cells may mitigate the predicted effects of ^{111}In-DTPA-F3 are shown in blue and include upregulation of oncogenes that regulate Pol I, II, and III transcription. Adapted with permission from (Hein, *et al.*, 2013) and under creative common licence from (Boulon, *et al.*, 2010).

Chapter 6. Discussion

To summarise the results in Chapters 3, 4 and 5, F3 has been shown to increase the size of the nucleolus. F3, IR and F3 + IR altered the level of nucleolin (NCL) and nucleophosmin (NPM) in the nucleolus, redistributing both proteins to the nucleoplasm of U2OS cells. In contrast, F3 increased the level of Ki-67 in the nucleoplasm. ^{111}In-labelled F3 (^{111}In-DTPA-F3) was successfully radiosynthesised and was significantly radiotoxic to MCF7, HCT116, MDA-MB-231/H2N, H322 and MDA-MB-435 cells. ^{111}In-DTPA-F3 was not significantly radiotoxic to U2OS cells. The level of cell kill produced by ^{111}In-DTPA-F3 was highly variable (19 fold range in surviving fraction) depending on the malignant cell line. ^{111}In-DTPA-F3 was shown to induce higher levels of γH2AX foci compared to a control lacking F3 (^{111}In-DTPA). ^{111}In-DTPA-F3 was also shown to target the nucleolus: the level of radioactivity and radiation dose deposited in the nucleolus was greater after exposure of malignant cells to ^{111}In-DTPA-F3 compared to ^{111}In-DTPA. Further, the incorporation of F3 into ^{111}In-DTPA shifted the distribution of nuclear radiation dose from the nucleoplasm to the nucleolus. The level of cell kill produced by ^{111}In-DTPA-F3 was not correlated with cellular radiosensitivity to external γ-radiation; the level of γH2AX foci induced by ^{111}In-DTPA-F3; the volume of the cell, nucleus or nucleolus and the number of nucleoli per cell; nor the uptake of radioactivity or deposition of radiation dose in the cell, membrane, cytoplasm, nucleus, nucleoplasm or nucleolus. However, the level of cell kill produced by ^{111}In-DTPA-F3 was correlated with the localisation of cell-bound ^{111}In-DTPA-F3 in the nucleus, suggesting that the nucleolus might possess a range of radiosensitivities to Auger electrons depending on the cell line. Thus, ^{111}In-DTPA-F3 was radiotoxic where greater than 3.72±0.47% of cell-bound ^{111}In-DTPA-F3 is localised in the nucleus, and

1 natural log of cell kill was produced for every 0.60±0.20% (over the 3.72±0.47% threshold) of cell-bound ^{111}In-DTPA-F3 that was localised in the nucleus. Finally, the volume of the nucleolus was also correlated with the level of γH2AX foci induced by ^{111}In-DTPA-F3.

6.1. Future investigation of the radiotoxicity of ^{111}In-DTPA-F3

To the Author's knowledge, this is the first report of the combination of clonogenic assays, internalisation assays and single cell radiation dose modelling to assess the uptake and deposition of radiation dose in the nucleolus by an Auger electron-emitting radiotherapeutic agent. The measurement of the volumes of the cell, nucleus and nucleolus using z-stacks was an improvement on techniques which previously only measured the diameter of the cell or nucleus to generate concentric single cell models with membrane, cytoplasm and nucleus regions. The clonogenic survival assay was used as the gold standard assay to assess the radiotoxicity of ^{111}In-DTPA-F3. However, the limitations of the clonogenic survival assays included the limited number of malignant cell lines that were exposed to ^{111}In-DTPA-F3 and the single concentration (and specific activity) of ^{111}In-DTPA-F3 to which malignant cell lines were exposed. Since the level of cell kill produced by ^{111}In-DTPA-F3 varied widely (19 fold range in surviving fraction) depending on the cell line, clonogenic survival assays could be carried out on a wider range of malignant cell lines. Interestingly, cell lines with wild-type p53 status have been shown to be more sensitive to Pol I inhibition with CX-5461 than p53 mutant or p53$^{-/-}$ cells (Bywater*, et al.*, 2012). Although a correlation with p53 status and the level of cell kill produced by ^{111}In-DTPA-F3 was not observed here, future research could also focus on investigating the correlation between the

level of cell kill produced by ^{111}In-DTPA-F3 and p53 status. This could be achieved by utilising clonogenic assays in combination with internalisation assays and single cell radiation dose modelling as outlined below.

To examine the relationship between the level of cell kill produced by ^{111}In-DTPA-F3 and the range of cellular radiosensitivities to external γ-radiation, clonogenic survival assays could, in theory, be performed using a range of concentrations of ^{111}In-DTPA-F3, with a constant specific activity, in parallel with internalisation assays and single cell radiation dose modelling. The data obtained from these experiments would allow the radiation dose deposited by a range of concentrations ^{111}In-DTPA-F3 to the cell, membrane, cytoplasm, nucleus, nucleoplasm or nucleolus to be plotted on the *x axis* against the surviving fraction on the *y axis*. From this graph the D_0 (mGy/cell) could be calculated for a range of concentrations of ^{111}In-DTPA-F3.

Clonogenic survival assays could also be performed using a constant concentration of ^{111}In-DTPA-F3, but with a range of specific activities, in parallel with internalisation assays and single cell radiation dose modelling. The data obtained from these experiments would allow the radiation dose deposited by a range of specific activities of ^{111}In-DTPA-F3 in the cell, membrane, cytoplasm, nucleus, nucleoplasm or nucleolus to be plotted on the *x axis* against the surviving fraction on the *y axis*. From this graph the D_0 (mGy/cell) could be calculated for a range of specific activities of ^{111}In-DTPA-F3. Together, this could show how the D_0 values for a range of concentrations of ^{111}In-DTPA-F3 (of constant specific activity) differ to the D_0 values for a range of specific activities of ^{111}In-DTPA-F3 (of constant concentration).

A limitation to the approach of combining clonogenic assays with internalisation assays is that the level of radioactivity associated with the nucleolus can be extremely low, while the levels of radioactivity used to expose cells to ^{111}In-DTPA-F3 can be

relatively high. For samples at the low end of a dilution series of concentrations or specific activities of ^{111}In-DTPA-F3, the level of radioactivity taken up in the nucleolus may be below the detection limit of the γ-counter. In contrast, radiation safety and protection issues may arise when exposing cells to concentrations or specific activities of ^{111}In-DTPA-F3 at the high end of a dilution series.

Nevertheless, the D_0 for a range of concentrations and specific activities of ^{111}In-DTPA-F3 could be compared with the D_0 for a range of doses of external γ-radiation. The D_0 (or, alternatively, the LD_{37}) for ^{111}In-DTPA-F3 and external γ-radiation could be used to calculate the relative biological effectiveness (RBE) of ^{111}In-DTPA-F3. Using these data, correlations between the D_0 for ^{111}In-DTPA-F3 and the localisation of cell-bound ^{111}In-DTPA-F3, the uptake of radioactivity and deposition of radiation dose in the membrane, cytoplasm, nucleus, nucleoplasm and nucleolus could also be assessed.

NCL drives the proliferative activity of the cell (Derenzini*, et al.*, 1995). Since small interfering RNA (siRNA) against NCL mRNA has been shown to radiosensitise MCF7 cells (Goldstein*, et al.*, 2013), overexpressing NCL may attenuate the radiotoxicity of ^{111}In-DTPA-F3. NCL overexpression in cancer has been linked to upregulated rRNA synthesis and the proliferative activity of the cell (Abdelmohsen and Gorospe, 2012; Cong*, et al.*, 2014a; Derenzini*, et al.*, 1995). However, NCL depletion using NCL siRNA may also attenuate the level of cell kill produced by ^{111}In-DTPA-F3, because the internalisation of ^{111}In-BnDTPA-F3 has been reported in Cornelissen *et al*. (2012) to be blocked by anti-NCL antibodies that bind to membrane NCL and prevent the internalisation of NCL and ^{111}In-BnDTPA-F3 (Cornelissen*, et al.*, 2012b). Therefore, clonogenic survival assays could also be performed with NCL siRNA prior to exposure

of malignant cells to ^{111}In-DTPA-F3, to demonstrate that the radiotoxicity of ^{111}In-DTPA-F3 depends on the expression of NCL.

Similarly, NPM expression has been reported to confer increased cellular survival after exposure to UV (Wu*, et al.*, 2002a; Wu*, et al.*, 2002b), IR (Dalenc*, et al.*, 2002), hypoxia (Li*, et al.*, 2004), and actinomycin D (Yao*, et al.*, 2010). Therefore, clonogenic survival assays using cells transfected to overexpress NPM might also reveal that the effect of ^{111}In-DTPA-F3 can be attenuated due to overexpression of NPM.

The γH2AX assay was used to assess the induction of DNA double-strand breaks by a single concentration (and specific activity) of ^{111}In-DTPA-F3. However, the limitations of the γH2AX assay included the fact that γH2AX may have also been induced by replication stress induced by ^{111}In-DTPA-F3, and that counting the number of γH2AX foci in a single section through the nucleus using confocal microscopy does not strictly quantify the number of γH2AX foci per cell. Since the rate of repair of γH2AX foci has been shown to correlate with the level of cell kill produced by external X-radiation (Banath*, et al.*, 2004; MacPhail*, et al.*, 2003; Olive and Banath, 2004), the rate of repair of DNA double-strand breaks could also be assessed and correlated with the D_0 for ^{111}In-DTPA-F3 for a range of malignant cell lines. To do this, z-stacks showing γH2AX foci throughout the nucleus of malignant cells exposed to ^{111}In-DTPA-F3 could be obtained to quantify the number of γH2AX foci at a range of time points, including at 0 and 3 h exposure to ^{111}In-DTPA-F3 and then at 6 and 24 h, after replacing ^{111}In-DTPA-F3-containing medium with fresh medium at 3 h. The data obtained from these experiments would allow the rate of induction of γH2AX foci between 0 and 3 h and the rate of loss (or repair) of γH2AX foci between 3 and 24 h to be quantified. Neutral or alkaline single-cell gel electrophoresis (comet assays), which measure double-strand breaks or single-strand breaks, respectively, could also be performed in parallel

to obtain data complementary to the γH2AX assays. Together, these data could be correlated with the D_0 for ^{111}In-DTPA-F3 to assess whether the level of cell kill produced by ^{111}In-DTPA-F3 depends on the repair of DNA double-strand breaks or single-strand breaks.

Since ^{111}In-BnDTPA-F3 binds to NCL (Cornelissen*, et al.*, 2012b), and F3 alters the localisation of both NCL and NPM, which have been shown to have H2A/H2B (Angelov*, et al.*, 2006; Erard*, et al.*, 1988; Gaume*, et al.*, 2011; Goldstein*, et al.*, 2013; Kharrat*, et al.*, 1991) and H3/H4 (Hingorani*, et al.*, 2000; Okuwaki*, et al.*, 2001a; Okuwaki*, et al.*, 2001b) histone chaperone activity, future experiments could investigate the effect of ^{111}In-DTPA-F3 on chromatin condensation and decondensation. The micrococcal nuclease (MNase) assay could be used to analyse how readily chromatin, which is more sensitive to MNase digestion in relaxed state, is digested when cells are exposed to ^{111}In-DTPA-F3 or F3 alone (Terry and Vallis, 2012). These experiments may show whether ^{111}In-DTPA-F3 alters chromatin compaction.

Future experiments could also investigate the effect of chromatin compaction on the level of cell kill and γH2AX foci induced by ^{111}In-DTPA-F3. Hydroxamic acid vorinostat (SAHA), which inhibits DNA methyltransferase and causes chromatin relaxation through hypomethylation of CpG islands, has been shown to increase the number of γH2AX foci and enhance the level of cell kill produced by ^{111}In-DTPA-EGF, without altering its nuclear localisation (Terry and Vallis, 2012). Exposing malignant cells to ^{111}In-DTPA-F3 + SAHA may increase the level of γH2AX foci induced by ^{111}In-DTPA-F3. SAHA may increase the level of cell kill produced by ^{111}In-DTPA-F3 and ascribe chromatin decondensation and the induction of γH2AX foci to the mechanism underpinning the enhancement of the radiotoxicity of ^{111}In-DTPA-F3.

6.2. Future investigation of the effects of ^{111}In-DTPA-F3 on the nucleolus

F3 was found to cause the size (cross-sectional area) of the nucleolus of U2OS cells to increase, without altering the number of nucleoli inside the nucleus. This contrasts with the highly selective Pol I inhibitor CX-5461, which has been shown to cause multiple nucleoli to fuse to form a single nucleolus (Bywater*, et al.*, 2012). Immunofluorescence experiments staining for NCL could be performed to assess the effect of ^{111}In-DTPA-F3 on the volume, number and morphology of the nucleolus using z-stacks. F3 was found to reduce levels of NCL and NPM in the nucleolus, shifting the distribution of these proteins to the nucleoplasm. Future research could also focus on characterising the effects of ^{111}In-DTPA-F3 on proteins whose nucleolar localisation is influenced by NPM, such as the tumour suppressor ARF (Colombo*, et al.*, 2005; Kuo*, et al.*, 2004) and the cell cycle inhibitor p21 (Xiao*, et al.*, 2009). NPM is also required for the nuclear export of the r-protein RPL5 (Yu*, et al.*, 2006) and the near-mature ribosome subunits (Maggi*, et al.*, 2008), and therefore the cytoplasmic localisation of these ribosomal components could also be assessed and quantified by immunocytochemical staining of malignant cells exposed to ^{111}In-DTPA-F3.

Fluorescence imaging experiments are a low throughput approach to obtain quantitative information about the spatial and temporal dynamics of nucleolar proteins. MS-SILAC experiments would offer a high throughput alternative that could identify hundreds of proteins purified from cytoplasmic, nucleoplasmic and nucleolar fractions from malignant cell lines exposed over a range of time points to ^{111}In-DTPA-F3. This would permit spatial and temporal characterisation of dynamic changes in the cytoplasmic, nucleoplasmic and nucleolar proteomes after exposure of malignant cells

to ^{111}In-DTPA-F3. This approach could highlight novel interactions between nucleolar proteins and ^{111}In-DTPA-F3, since the nucleolar proteome has been shown by MS-SILAC to undergo complex reorganisation in response to different types of nucleolar stress (Boisvert*, et al.*, 2010; Boisvert and Lamond, 2010; Moore*, et al.*, 2011).

Future research could also focus on determining whether ^{111}In-DTPA-F3 reduces Pol I transcription of pre-rRNA and whether this effect can be altered by overexpression of NCL or NPM (Ginisty*, et al.*, 1999; Mongelard and Bouvet, 2007; Murano*, et al.*, 2008; Rickards*, et al.*, 2007; Roger*, et al.*, 2003; Srivastava and Pollard, 1999; Tuteja and Tuteja, 1998). In yeast, the high mobility group B (HMGB) protein HMO1 forms part of the Pol I transcription machinery (Gadal*, et al.*, 2002). HMGB proteins bind to DNA without sequence specificity, but with a preference for DNA that is distorted structurally. In mammalian cells, it is hypothesised that ^{111}In-DTPA-F3 (F3 is a fragment of HMGB2) may also interact directly with Pol I or the rDNA enhancer. The damage caused by Auger electrons to rDNA and rRNA in the nucleolus is hypothesised to interfere with ribosome biogenesis by interfering with Pol I-mediated transcription, rRNA processing and r-subunit assembly (Fatica and Tollervey, 2002; Olson*, et al.*, 2002). Immunochemical staining could be combined with fluorescence *in situ* hybridisation (FISH) to determine whether the colocalisation of Pol I components or transcription factors with rDNA genes is disrupted following exposure of malignant cells to ^{111}In-DTPA-F3. Also, the run-on assay could be used to examine whether ^{111}In-DTPA-F3 alters the rate of rRNA transcription. The run-on assay measures the amount of radiolabelled UTP- or non-radiolabelled BrU-incorporated into total RNA, which is then used to hybridise with full-length rDNA or a control (e.g. β-actin cDNA) blotted onto a filter (Cui and Tseng, 2004; Rohr*, et al.*, 2000; Wansink*, et al.*, 1993). The run-on assay could therefore quantify changes in the level of rRNA,

and therefore the rate of Pol I transcription in malignant cells exposed to ^{111}In-DTPA-F3 over a time course. Also, alteration of posttranslational processing of pre-rRNA by ^{111}In-DTPA-F3 could be assessed using FISH analysis of the levels of the 47S pre-rRNA in the nucleus and the mature 28S rRNA in the cytoplasm of malignant cells exposed to ^{111}In-DTPA-F3 (Cui and Tseng, 2004).

The rate of Pol I transcription of rRNA fluctuates with the cell cycle, with maximal Pol I transcription occurring in G_2 phase followed by a drop-off in rRNA transcription during mitosis that is not fully recovered until late G_1 phase because UBF is not active in early G_1 phase (Klein and Grummt, 1999). It would be interesting to correlate the rate of rRNA transcription in malignant cells synchronised in G_2, M, early G_1 or late G_1 phase of the cell cycle using the run-on assay with the D_0 of ^{111}In-DTPA-F3 obtained from malignant cells also synchronised in G_2, M, early G_1 or late G_1. This may reveal that the level of cell kill produced by ^{111}In-DTPA-F3 is dependent on the transcriptional activity of the nucleolus.

The effect of ^{111}In-DTPA-F3 on the integrity of the 47S pre-rRNA and the 32S, 28S and 18S rRNAs could also be analysed using 1% agarose gels after extraction of total cellular RNA (Roger*, et al.*, 2003). Further, the ability of malignant cells to process exogenous RNA could also be examined using extract from malignant cells exposed to ^{111}In-DTPA-F3. After cell extract has been appropriately stored to permit decay of ^{111}In-DTPA-F3, radiolabelled RNA species (47S pre-rRNA, 32S rRNA, etc.) could be mixed with or without cell extract and the products of RNA processing visualised using a 6% polyacrylamide gel (Ginisty*, et al.*, 1998).

Data from these experiments may suggest that ^{111}In-DTPA-F3 interferes with the production of the 28S rRNA by damaging machinery involved in rRNA processing. Repeat experiments could also be performed using cell extract purified from

cytoplasmic, nucleoplasmic, and nucleolar fractions from malignant cells exposed to ^{111}In-DTPA-F3. This may confirm that ^{111}In-DTPA-F3 interferes with rRNA processing in the nucleolus, but not the cytoplasm or nucleoplasm. The protein content of these fractions could also be separated using SDS-PAGE polyacrylamide gels. Alterations to the nucleolar proteome due to uptake of ^{111}In-DTPA-F3 in the nucleolus, which may reduce the abundance of the 28S, 5.8S and 18S rRNAs and affect transient interactions with r-proteins, snoRNPs and non-ribosomal proteins (Andersen*, et al.*, 2005; Fatica and Tollervey, 2002; Tschochner and Hurt, 2003), could then be analysed by staining global proteins with Coomassie or by identifying target proteins using Western blotting.

Induction of nucleolar stress has been reported to lead to the release of r-proteins from the nucleolus (Boisvert*, et al.*, 2010; Boisvert and Lamond, 2010; Boisvert*, et al.*, 2007; Zhang and Lu, 2009). In the nucleoplasm, RPL5, RPL11, RPL23 and RPS7 may bind to MDM2, preventing MDM2 from ubiquitylating p53 (Boisvert*, et al.*, 2007; Fumagalli*, et al.*, 2012; Holzel*, et al.*, 2010; Zhang and Lu, 2009). It has been suggested that these MDM2-binding proteins may have redundant MDM2 inhibiting activity or that they may function separately in sensing different types of nucleolar stress (Zhang and Lu, 2009). Co-immunoprecipitation could also be used to demonstrate the binding of RPL5, RPL11, RPL23 or RPS7 to MDM2 in the nucleoplasm fraction obtained from malignant cells exposed to ^{111}In-DTPA-F3. Immunofluorescence experiments could also be performed to confirm the redistribution of r-proteins from the nucleolus to the nucleoplasm.

6.3. Future investigation of cell cycle arrest and cell death induced by ^{111}In-DTPA-F3

Increased nucleoplasmic levels of Ki-67 mediated by F3 may reflect the accumulation of cells in early G_1 phase, since the level of Ki-67 in the nucleoplasm decreases as cells progress through interphase (Bridger, 1998). Therefore, cell cycle distribution could also be assessed by flow cytometry after exposure of malignant cells over a range of time points to ^{111}In-DTPA-F3. The cell death pathway induced by ^{111}In-DTPA-F3, like that induced by Pol I-specific inhibitors (Bywater*, et al.*, 2012; Drygin*, et al.*, 2011; Drygin*, et al.*, 2010), may be p53-dependent or p53-independent, depending on the cell line, since p53 wild-type and p53 mutant cell lines were both found to be radiosensitive to ^{111}In-DTPA-F3. Therefore, the level of p53, p53 target genes (such as p21, Bax, Puma and Noxa) and markers of apoptosis (cleaved caspase-3/7/9), could also be assessed by Western blotting, analysing cell lysate from malignant cells exposed over a range of time points to, and/or doses of ^{111}In-DTPA-F3 (Lee and Gu, 2010).

6.4. Conclusion

^{111}In-DTPA-F3 is a promising anti-cancer agent for Auger electron radionuclide therapy that targets the nucleolus of a wide range of malignant cells. The uptake of radioactivity and deposition of radiation dose in the nucleolus by ^{111}In-DTPA-F3 has been shown to be responsible for the radiotoxic effect of ^{111}In-DTPA-F3. The level of cell kill produced by ^{111}In-DTPA-F3 was found to be correlated with the localisation of cell-bound ^{111}In-DTPA-F3 in the nucleus, while the level of γH2AX foci induced by

^{111}In-DTPA-F3 was determined by the volume of the nucleolus. The nucleolus is a novel target for Auger electron radionuclide therapy that may possess a range of radiosensitivities to ^{111}In-DTPA-F3 depending on the malignant cell line.

7. Appendix

	$S(r_{No} \leftarrow r_{No})$	$S(r_{No} \leftarrow r_{Np})$	$S(r_{No} \leftarrow r_{Cy})$	$S(r_{No} \leftarrow r_{Me})$	$S(r_{Np} \leftarrow r_{No})$	$S(r_{Np} \leftarrow r_{Np})$	$S(r_{Np} \leftarrow r_{Cy})$	$S(r_{Np} \leftarrow r_{Me})$	$S(r_{Cy} \leftarrow r_{No})$	$S(r_{Cy} \leftarrow r_{Np})$	$S(r_{Cy} \leftarrow r_{Cy})$	$S(r_{Cy} \leftarrow r_{Me})$	$S(r_{Me} \leftarrow r_{No})$	$S(r_{Me} \leftarrow r_{Np})$	$S(r_{Me} \leftarrow r_{Cy})$	$S(r_{Me} \leftarrow r_{Me})$
MCF7	4.32E-02	1.20E-03	1.06E-04	1.81E-05	8.57E-03	1.53E-03	1.54E-04	2.88E-05	4.39E-04	4.76E-04	9.89E-04	4.77E-04	2.13E-05	2.79E-05	1.46E-04	1.27E-04
HCT116	8.28E-02	2.56E-03	3.57E-04	1.78E-04	1.69E-02	2.56E-03	3.89E-04	1.78E-04	1.65E-03	1.80E-03	4.54E-03	2.19E-03	1.81E-04	1.80E-04	4.59E-04	6.54E-04
MDA-MB-231/H2N	6.58E-02	2.06E-03	1.76E-04	3.64E-05	1.32E-02	2.06E-03	1.91E-04	4.18E-05	5.04E-04	5.45E-04	1.10E-03	5.29E-04	3.55E-05	4.27E-05	1.81E-04	1.43E-04
H322	2.64E-01	4.88E-03	1.87E-04	3.91E-05	2.78E-02	4.89E-03	2.05E-04	4.09E-05	4.05E-04	4.40E-04	8.30E-04	3.98E-04	3.63E-05	4.07E-05	1.84E-04	1.08E-04
MDA-MB-435	8.28E-02	2.56E-03	2.28E-04	1.91E-04	1.69E-02	2.56E-03	2.47E-04	6.98E-05	6.64E-04	7.16E-04	1.47E-03	7.10E-04	6.42E-05	6.94E-05	2.36E-04	1.97E-04
U20S	3.06E-02	1.03E-03	9.33E-05	1.02E-05	5.32E-03	1.04E-03	1.02E-04	1.44E-05	3.17E-04	3.50E-04	7.54E-04	3.64E-04	1.04E-05	1.43E-05	1.03E-04	9.42E-05

Table 7.1. S-values for single cell models

S-values (Gy/Bq·sec) were calculated by Dr Nadia Falzone. To calculate the mean absorbed dose $\overline{D}_k$ to a target region r_k from a source region r_h, the Author used the appropriate S-values as per the MIRD formalism, $\overline{D}_k = \tilde{A}_h S(r_k \leftarrow r_h)$, where $\tilde{A}_h$ is the cumulated radioactivity in source region r_h, and $S(r_k \leftarrow r_h)$ is the S-value for the radiation dose to the target region r_k per cumulated radioactivity in the source region r_h. r_{Me}, membrane region; r_{Cy}, cytoplasm region; r_{Np}, nucleoplasm region; r_{No}, nucleolus region.

BENTHAM SCIENCE PUBLISHERS LICENSE

TERMS AND CONDITIONS

Jan 31, 2016

This Agreement between Christopher Hillyar ("You") and Bentham Science Publishers ("Bentham Science Publishers") consists of your license details and the terms and conditions provided by Bentham Science Publishers and Copyright Clearance Center.

License Number	3767511313097
License date	Dec 10, 2015
Licensed Content Publisher	Bentham Science Publishers
Licensed Content Publication	Current Drug Discovery Technologies
Licensed Content Title	Targeting the Nucleus: An Overview of Auger-Electron Radionuclide Therapy
Licensed Content Author	Bart Cornelissen and Katherine A Vallis
Licensed Content Date	December 2010
I would like to...	Thesis/Dissertation
Requestor type	Academic institution
Format	Print, Electronic
Portion	chart/graph/table/figure
Number of charts/graphs/tables/figures	1
Rights for	Main product
Duration of use	Life of current edition
Creation of copies for the disabled	no
With minor editing privileges	yes
In the following language(s)	Original language of publication
With incidental promotional use	no
The lifetime unit quantity of new product	0 to 499
The requesting person/organization is:	Christopher Hillyar, Oxford University
Title of your thesis / dissertation	Auger electron radionuclide therapy utilising F3 peptide to target the nucleolus
Expected completion date	Jul 2015

Expected size (number of pages)	220
Billing Type	Invoice
Billing Address	Christopher Hillyar 22 Meyseys Close None None Oxford, United Kingdom OX3 7SF Attn: Christopher Hillyar
Requestor Location	Christopher Hillyar 22 Meyseys Close None None Oxford, United Kingdom OX3 7SF Attn: Christopher Hillyar
Billing Type	Invoice
Billing Address	Christopher Hillyar 22 Meyseys Close None None Oxford, United Kingdom OX3 7SF Attn: Christopher Hillyar
Total	0.00 GBP
Total	0.00 GBP

Terms and Conditions

STANDARD TERMS AND CONDITIONS FOR REPRODUCTION OF MATERIAL

Introduction
The publisher for this copyrighted material is Bentham Science Publishers Ltd. By clicking "accept" in connection with completing this licensing transaction, you agree that the following terms and conditions apply (along with the Billing and Payment terms and conditions established by Copyright Clearance Center, Inc. ("CCC"), at the time that you opened your CCC account and that are available at any time at http://myaccount.copyright.com).

Limited License
Publisher hereby grants to you a non-exclusive license to use this material. Licenses are for one-time use only with a maximum distribution equal to the number that you identified in the licensing process; any form of republication must be completed within 180 days from the date hereof (although copies prepared before then may be distributed thereafter); and any electronic posting is limited to a period of 180 days.

Geographic Rights: Scope
Licenses may be exercised anywhere in the world.

Altering/Modifying Material: Not Permitted
You may not alter or modify the material in any manner, nor may you translate the material into another language without permission from the Publisher.

Reservation of Rights
Publisher reserves all rights not specifically granted in the combination of (i) the license details provided by you and accepted in the course of this licensing transaction, (ii) these terms and conditions and (iii) CCC's Billing and Payment terms and conditions.

License Contingent on Payment
While you may exercise the rights licensed immediately upon issuance of the license at the end of the licensing process for the transaction, provided that you have disclosed complete and accurate details of your proposed use, no license is finally effective unless and until full payment is received from you (either by publisher or by CCC) as provided in CCC's Billing and Payment terms and conditions. If full payment is not received on a timely basis, then any license preliminarily granted shall be deemed automatically revoked and shall be void as if never granted. Further, in the event that you breach any of these terms and conditions or any of CCC's Billing and Payment terms and conditions, the license is automatically revoked and shall be void as if never granted. Use of materials as described in a revoked license, as well as any use of the materials beyond the scope of an unrevoked license, may constitute copyright infringement and publisher reserves the right to take any and all action to protect its copyright in the materials.

Copyright Notice: Disclaimer
It is a condition of this license that on all copies you republish, display or distribute you (i) provide full bibliographical information for the licensed material, including but not limited to author name, title and publication date of the work, volume and number if applicable, publisher name (Eureka Science Ltd.), page reference, (ii) include the statement, "Reprinted by permission of Eureka Science Ltd."; and (iii) include the copyright notice that appears in the work as published by Eureka Science Ltd..

Warranties: None
Publisher makes no representations or warranties with respect to the licensed material.

Indemnity
You hereby indemnify and agree to hold harmless publisher and CCC, and their respective officers, directors, employees and agents, from and against any and all claims arising out of your use of the licensed material other than as specifically authorized pursuant to this license.

No Transfer of License
This license is personal to you and may not be sublicensed, assigned, or transferred by you to any other person without publisher's written permission.

No Amendment Except in Writing
This license may not be amended except in a writing signed by both parties (or, in the case of publisher, by CCC on publisher's behalf).

Objection to Contrary Terms
Publisher hereby objects to any terms contained in any purchase order, acknowledgment, check endorsement or other writing prepared by you, which terms are inconsistent with these terms and conditions or CCC's Billing and Payment terms and conditions. These terms and conditions, together with CCC's Billing and Payment terms and conditions (which are incorporated herein), comprise the entire agreement between you and publisher (and CCC) concerning this licensing transaction. In the event of any conflict between your obligations established by these terms and conditions and those established by CCC's Billing and Payment terms and conditions, these terms and conditions shall control.

Jurisdiction: Not Required*
This license transaction shall be governed by and construed in accordance with the laws of the United Arab Emirates. You hereby agree to submit to the jurisdiction of the federal and state courts located in Dubai for purposes of resolving any disputes that may arise in connection with this licensing transaction.

Other Terms and Conditions:

v1.0

Questions? customercare@copyright.com or +1-855-239-3415 (toll free in the US) or +1-978-646-2777.

Our Ref: LA/IRAB/H121

17 July 2015

Dear Christopher Hillyar,

Material requested: 2 Figures – Fig2&4 from "Targets for Radiation-induced Cell Death: Target Replication During the Cell Cycle Evaluated in Cells Exposed to X-rays or 125I Decays", by K.G. Hofer, N. van Loon, M.H. Schneiderman & G.V. Dalrymple, published in International Journal of Radiation Biology, Vol64:2, pp205-216(1993)

Thank you for your correspondence requesting permission to reproduce the above mentioned material from our Journal in your printed thesis entitled 'Auger electron radionuclide therapy utilising F3 peptide to target the nucleolus' and posted in your university's repository - University of Oxford**.**

We will be pleased to grant entirely free permission on the condition that you acknowledge the original source of publication and insert a reference to the Journal's web site: www.tandfonline.com

Please note that this licence does not allow you to post our content on any third party websites or repositories.

Thank you for your interest in our Journal.

Yours sincerely

Lee-Ann

Lee-Ann Anderson – Permissions & Licensing Administrator, Journals

Routledge, Taylor & Francis Group

3 Park Square, Milton Park, Abingdon, Oxon, OX14 4RN, UK.

Tel: +44 (0)20 7017 7932

Fax:+44 (0)20 7017 6336

Web: www.tandfonline.com

e-mail: lee-ann.anderson@tandf.co.uk

ELSEVIER LICENSE
TERMS AND CONDITIONS

Jul 09, 2015

This is a License Agreement between Christopher Hillyar ("You") and Elsevier ("Elsevier") provided by Copyright Clearance Center ("CCC"). The license consists of your order details, the terms and conditions provided by Elsevier, and the payment terms and conditions.

All payments must be made in full to CCC. For payment instructions, please see information listed at the bottom of this form.

Supplier

Elsevier Limited
The Boulevard,Langford Lane
Kidlington,Oxford,OX5 1GB,UK

Registered Company Number

1982084

Customer name

Christopher Hillyar

Customer address

22 Meyseys Close

Oxford, OX3 7SF

License number

3664701256634

License date

Jul 09, 2015

Licensed content publisher

Elsevier

Licensed content publication

Trends in Molecular Medicine

Licensed content title

The nucleolus: an emerging target for cancer therapy

Licensed content author

Nadine Hein,Katherine M. Hannan,Amee J. George,Elaine Sanij,Ross D. Hannan

Licensed content date

November 2013

Licensed content volume number

19

Licensed content issue number

11

Number of pages

12

Start Page

643

End Page

654

Type of Use

reuse in a thesis/dissertation

Intended publisher of new work

other

Portion

figures/tables/illustrations

Number of figures/tables/illustrations

2

Format

both print and electronic

Are you the author of this Elsevier article?

No

Will you be translating?

No

Original figure numbers

Figure 1, Table 1

Title of your thesis/dissertation

Auger electron radionuclide therapy utilising F3 peptide to target the nucleolus

Expected completion date

Jul 2015

Estimated size (number of pages)

220

Elsevier VAT number

GB 494 6272 12

Permissions price

0.00 USD

VAT/Local Sales Tax

0.00 USD / 0.00 GBP

Total

0.00 USD

Terms and Conditions

INTRODUCTION

1. The publisher for this copyrighted material is Elsevier. By clicking "accept" in connection with completing this licensing transaction, you agree that the following terms and conditions apply to this transaction (along with the Billing and Payment terms and conditions established by Copyright Clearance Center, Inc. ("CCC"), at the time that you opened your Rightslink account and that are available at any time athttp://myaccount.copyright.com).

GENERAL TERMS

2. Elsevier hereby grants you permission to reproduce the aforementioned material subject to the terms and conditions indicated.

3. Acknowledgement: If any part of the material to be used (for example, figures) has appeared in our publication with credit or acknowledgement to another source, permission must also be sought from that source. If such permission is not obtained then that material may not be included in your publication/copies. Suitable acknowledgement to the source must be made, either as a footnote or in a reference list at the end of your publication, as follows:

"Reprinted from Publication title, Vol /edition number, Author(s), Title of article / title of chapter, Pages No., Copyright (Year), with permission from Elsevier [OR APPLICABLE SOCIETY COPYRIGHT OWNER]." Also Lancet special credit - "Reprinted from The Lancet, Vol. number, Author(s), Title of article, Pages No., Copyright (Year), with permission from Elsevier."

4. Reproduction of this material is confined to the purpose and/or media for which permission is hereby given.

5. Altering/Modifying Material: Not Permitted. However figures and illustrations may be altered/adapted minimally to serve your work. Any other abbreviations, additions, deletions and/or any other alterations shall be made only with prior written authorization of Elsevier Ltd. (Please contact Elsevier at permissions@elsevier.com)

6. If the permission fee for the requested use of our material is waived in this instance, please be advised that your future requests for Elsevier materials may attract a fee.

7. Reservation of Rights: Publisher reserves all rights not specifically granted in the combination of (i) the license details provided by you and accepted in the course of this licensing transaction, (ii) these terms and conditions and (iii) CCC's Billing and Payment terms and conditions.

8. License Contingent Upon Payment: While you may exercise the rights licensed immediately upon issuance of the license at the end of the licensing process for the transaction, provided that you have disclosed complete and accurate details of your proposed use, no license is finally effective unless and until full payment is received from you (either by publisher or by CCC) as provided in CCC's Billing and Payment terms and conditions. If full payment is not received on a timely basis, then any license preliminarily granted shall be deemed automatically revoked and shall be void as if never granted. Further, in the event that you breach any of these terms and conditions or any of CCC's Billing and Payment terms and conditions, the license is automatically revoked and shall be void as if never granted. Use of materials as described in a revoked license, as well as any use of the materials beyond the scope of an unrevoked license, may constitute copyright infringement and publisher reserves the right to take any and all action to protect its copyright in the materials.

9. Warranties: Publisher makes no representations or warranties with respect to the licensed material.

10. Indemnity: You hereby indemnify and agree to hold harmless publisher and CCC, and their respective officers, directors, employees and agents, from and against any and all claims arising out of your use of the licensed material other than as specifically authorized pursuant to this license.

11. No Transfer of License: This license is personal to you and may not be sublicensed, assigned, or transferred by you to any other person without publisher's written permission.

12. No Amendment Except in Writing: This license may not be amended except in a writing signed by both parties (or, in the case of publisher, by CCC on publisher's behalf).

13. Objection to Contrary Terms: Publisher hereby objects to any terms contained in any purchase order, acknowledgment, check endorsement or other writing prepared by you, which terms are inconsistent with these terms and conditions or CCC's Billing and Payment terms and conditions. These terms and conditions, together with CCC's Billing and Payment terms and conditions (which are incorporated herein), comprise the entire agreement between you and publisher (and CCC) concerning this licensing transaction. In the event of any

conflict between your obligations established by these terms and conditions and those established by CCC's Billing and Payment terms and conditions, these terms and conditions shall control.

14. Revocation: Elsevier or Copyright Clearance Center may deny the permissions described in this License at their sole discretion, for any reason or no reason, with a full refund payable to you. Notice of such denial will be made using the contact information provided by you. Failure to receive such notice will not alter or invalidate the denial. In no event will Elsevier or Copyright Clearance Center be responsible or liable for any costs, expenses or damage incurred by you as a result of a denial of your permission request, other than a refund of the amount(s) paid by you to Elsevier and/or Copyright Clearance Center for denied permissions.

LIMITED LICENSE

The following terms and conditions apply only to specific license types:

15. **Translation**: This permission is granted for non-exclusive world **English** rights only unless your license was granted for translation rights. If you licensed translation rights you may only translate this content into the languages you requested. A professional translator must perform all translations and reproduce the content word for word preserving the integrity of the article. If this license is to re-use 1 or 2 figures then permission is granted for non-exclusive world rights in all languages.

16. **Posting licensed content on any Website**: The following terms and conditions apply as follows: Licensing material from an Elsevier journal: All content posted to the web site must maintain the copyright information line on the bottom of each image; A hyper-text must be included to the Homepage of the journal from which you are licensing athttp://www.sciencedirect.com/science/journal/xxxxx or the Elsevier homepage for books athttp://www.elsevier.com; Central Storage: This license does not include permission for a scanned version of the material to be stored in a central repository such as that provided by Heron/XanEdu.

Licensing material from an Elsevier book: A hyper-text link must be included to the Elsevier homepage at http://www.elsevier.com . All content posted to the web site must maintain the copyright information line on the bottom of each image.

Posting licensed content on Electronic reserve: In addition to the above the following clauses are applicable: The web site must be password-protected and made available only to bona fide students registered on a relevant course. This permission is granted for 1 year only. You may obtain a new license for future website posting.

17. **For journal authors:** the following clauses are applicable in addition to the above:

Preprints:

A preprint is an author's own write-up of research results and analysis, it has not been peer-reviewed, nor has it had any other value added to it by a publisher (such as formatting, copyright, technical enhancement etc.).

Authors can share their preprints anywhere at any time. Preprints should not be added to or enhanced in any way in order to appear more like, or to substitute for, the final versions of articles however authors can update their preprints on arXiv or RePEc with their Accepted Author Manuscript (see below).

If accepted for publication, we encourage authors to link from the preprint to their formal publication via its DOI. Millions of researchers have access to the formal publications on ScienceDirect, and so links will help users to find, access, cite and use the best available version. Please note that Cell Press, The Lancet and some society-owned have different preprint policies. Information on these policies is available on the journal homepage.

Accepted Author Manuscripts: An accepted author manuscript is the manuscript of an article that has been accepted for publication and which typically includes author-incorporated changes suggested during submission, peer review and editor-author communications.

Authors can share their accepted author manuscript:

- – immediately
  - via their non-commercial person homepage or blog
  - by updating a preprint in arXiv or RePEc with the accepted manuscript
  - via their research institute or institutional repository for internal institutional uses or as part of an invitation-only research collaboration work-group
  - directly by providing copies to their students or to research collaborators for their personal use
  - for private scholarly sharing as part of an invitation-only work group on commercial sites with which Elsevier has an agreement
- – after the embargo period
  - via non-commercial hosting platforms such as their institutional repository
  - via commercial sites with which Elsevier has an agreement

In all cases accepted manuscripts should:

- – link to the formal publication via its DOI
- – bear a CC-BY-NC-ND license - this is easy to do
- – if aggregated with other manuscripts, for example in a repository or other site, be shared in alignment with our hosting policy not be added to or enhanced in any way to appear more like, or to substitute for, the published journal article.

Published journal article (JPA): A published journal article (PJA) is the definitive final record of published research that appears or will appear in the journal and embodies all value-adding publishing activities including peer review co-ordination, copy-editing, formatting, (if relevant) pagination and online enrichment.

Policies for sharing publishing journal articles differ for subscription and gold open access articles:

Subscription Articles: If you are an author, please share a link to your article rather than the full-text. Millions of researchers have access to the formal publications on ScienceDirect, and so links will help your users to find, access, cite, and use the best available version.

Theses and dissertations which contain embedded PJAs as part of the formal submission can be posted publicly by the awarding institution with DOI links back to the formal publications on ScienceDirect.

If you are affiliated with a library that subscribes to ScienceDirect you have additional private sharing rights for others' research accessed under that agreement. This includes use for classroom teaching and internal training at the institution (including use in course packs and courseware programs), and inclusion of the article for grant funding purposes.

Gold Open Access Articles: May be shared according to the author-selected end-user license and should contain a CrossMark logo, the end user license, and a DOI link to the formal publication on ScienceDirect.

Please refer to Elsevier's posting policy for further information.

18. **For book authors** the following clauses are applicable in addition to the above: Authors are permitted to place a brief summary of their work online only. You are not allowed to download and post the published electronic version of your chapter, nor may you scan the printed edition to create an electronic version. **Posting to a repository:** Authors are permitted to post a summary of their chapter only in their institution's repository.

19. **Thesis/Dissertation**: If your license is for use in a thesis/dissertation your thesis may be submitted to your institution in either print or electronic form. Should your thesis be published commercially, please reapply for permission. These requirements include permission for the Library and Archives of Canada to supply single copies, on demand, of the complete thesis and include permission for Proquest/UMI to supply single copies, on demand, of the complete thesis. Should your thesis be published commercially, please reapply for permission.

Theses and dissertations which contain embedded PJAs as part of the formal submission can be posted publicly by the awarding institution with DOI links back to the formal publications on ScienceDirect.

Elsevier Open Access Terms and Conditions

You can publish open access with Elsevier in hundreds of open access journals or in nearly 2000 established subscription journals that support open access publishing. Permitted third party re-use of these open access articles is defined by the author's choice of Creative Commons user license. See our open access license policy for more information.

Terms & Conditions applicable to all Open Access articles published with Elsevier:

Any reuse of the article must not represent the author as endorsing the adaptation of the article nor should the article be modified in such a way as to damage the author's honour or reputation. If any changes have been made, such changes must be clearly indicated.

The author(s) must be appropriately credited and we ask that you include the end user license and a DOI link to the formal publication on ScienceDirect.

If any part of the material to be used (for example, figures) has appeared in our publication with credit or acknowledgement to another source it is the responsibility of the user to ensure their reuse complies with the terms and conditions determined by the rights holder.

Additional Terms & Conditions applicable to each Creative Commons user license:

CC BY: The CC-BY license allows users to copy, to create extracts, abstracts and new works from the Article, to alter and revise the Article and to make commercial use of the Article (including reuse and/or resale of the Article by commercial entities), provided the user gives appropriate credit (with a link to the formal publication through the relevant DOI), provides a link to the license, indicates if changes were made and the licensor is not represented as endorsing the use made of the work. The full details of the license are available at http://creativecommons.org/licenses/by/4.0.

CC BY NC SA: The CC BY-NC-SA license allows users to copy, to create extracts, abstracts and new works from the Article, to alter and revise the Article, provided this is not done for commercial purposes, and that the user gives appropriate credit (with a link to the formal publication through the relevant DOI), provides a link to the license, indicates if changes were made and the licensor is not represented as endorsing the use made of the work. Further, any new works must be made available on the same conditions. The full details of the license are available at http://creativecommons.org/licenses/by-nc-sa/4.0.

CC BY NC ND: The CC BY-NC-ND license allows users to copy and distribute the Article, provided this is not done for commercial purposes and further does not permit distribution of the Article if it is changed or edited in any way, and provided the user gives appropriate credit (with a link to the formal publication through the relevant DOI), provides a link to the license, and that the licensor is not represented as endorsing the use made of the work. The full details of the license are available at http://creativecommons.org/licenses/by-nc-nd/4.0. Any commercial reuse of Open Access articles published with a CC BY NC SA or CC BY NC ND license requires permission from Elsevier and will be subject to a fee.

Commercial reuse includes:

- – Associating advertising with the full text of the Article
- – Charging fees for document delivery or access
- – Article aggregation
- – Systematic distribution via e-mail lists or share buttons

Posting or linking by commercial companies for use by customers of those companies.

20. **Other Conditions**:

v1.7

Questions? customercare@copyright.com or +1-855-239-3415 (toll free in the US) or +1-978-646-2777.

---

8. Bibliography

Abdelmohsen, K., and M. Gorospe. 2012. RNA-binding protein nucleolin in disease. *RNA biology*. 9:799-808.

Abdelmohsen, K., K. Tominaga, E.K. Lee, S. Srikantan, M.J. Kang, M.M. Kim, R. Selimyan, J.L. Martindale, X. Yang, F. Carrier, M. Zhan, K.G. Becker, and M. Gorospe. 2011. Enhanced translation by Nucleolin via G-rich elements in coding and non-coding regions of target mRNAs. *Nucleic acids research*. 39:8513-8530.

Adelstein, S.J. 1993. Merrill C. Sosman Lecture. The Auger process: a therapeutic promise? *AJR. American journal of roentgenology*. 160:707-713.

Ahmad, Y., F.M. Boisvert, P. Gregor, A. Cobley, and A.I. Lamond. 2009. NOPdb: Nucleolar Proteome Database--2008 update. *Nucleic acids research*. 37:D181-184.

Al-Baker, E.A., J. Boyle, R. Harry, and I.R. Kill. 2004. A p53-independent pathway regulates nucleolar segregation and antigen translocation in response to DNA damage induced by UV irradiation. *Experimental cell research*. 292:179-186.

Al-Baker, E.A., M. Oshin, C.J. Hutchison, and I.R. Kill. 2005. Analysis of UV-induced damage and repair in young and senescent human dermal fibroblasts using the comet assay. *Mechanisms of ageing and development*. 126:664-672.

Alberts, D.S., K.S. Griffith, G.E. Goodman, T.S. Herman, and E. Murray. 1980. Phase I clinical trial f mitoxantrone: a new anthracenedione anticancer drug. *Cancer chemotherapy and pharmacology*. 5:11-15.

Aldi, S., C. Della Giovampaola, R. Focarelli, A. Armini, M. Ziche, F. Finetti, and F. Rosati. 2009. A fucose-containing O-glycoepitope on bovine and human nucleolin. *Glycobiology*. 19:337-343.

Allain, F.H., P. Bouvet, T. Dieckmann, and J. Feigon. 2000. Molecular basis of sequence-specific recognition of pre-ribosomal RNA by nucleolin. *The EMBO journal*. 19:6870-6881.

Amsterdam, A., K.C. Sadler, K. Lai, S. Farrington, R.T. Bronson, J.A. Lees, and N. Hopkins. 2004. Many ribosomal protein genes are cancer genes in zebrafish. *PLoS biology*. 2:E139.

Andersen, J.S., Y.W. Lam, A.K. Leung, S.E. Ong, C.E. Lyon, A.I. Lamond, and M. Mann. 2005. Nucleolar proteome dynamics. *Nature*. 433:77-83.

Andrade, L.E., E.M. Tan, and E.K. Chan. 1993. Immunocytochemical analysis of the coiled body in the cell cycle and during cell proliferation. *Proceedings of the National Academy of Sciences of the United States of America*. 90:1947-1951.

Andrews, W.J., T. Panova, C. Normand, O. Gadal, I.G. Tikhonova, and K.I. Panov. 2013. Old drug, new target: ellipticines selectively inhibit RNA polymerase I transcription. *The Journal of biological chemistry*. 288:4567-4582.

Angelov, D., V.A. Bondarenko, S. Almagro, H. Menoni, F. Mongelard, F. Hans, F. Mietton, V.M. Studitsky, A. Hamiche, S. Dimitrov, and P. Bouvet. 2006. Nucleolin is a histone chaperone with FACT-like activity and assists remodeling of nucleosomes. *The EMBO journal*. 25:1669-1679.

Anthony, L.B., E.A. Woltering, G.D. Espenan, M.D. Cronin, T.J. Maloney, and K.E. McCarthy. 2002. Indium-111-pentetreotide prolongs survival in

gastroenteropancreatic malignancies. *Seminars in nuclear medicine*. 32:123-132.

Arabi, A., S. Wu, K. Ridderstrale, H. Bierhoff, C. Shiue, K. Fatyol, S. Fahlen, P. Hydbring, O. Soderberg, I. Grummt, L.G. Larsson, and A.P. Wright. 2005. c-Myc associates with ribosomal DNA and activates RNA polymerase I transcription. *Nature cell biology*. 7:303-310.

Areberg, J., A. Johnsson, and J. Wennerberg. 2000. In vitro toxicity of (191)Pt-labeled cisplatin to a human cervical carcinoma cell line (ME-180). *International journal of radiation oncology, biology, physics*. 46:1275-1280.

Areberg, J., J. Wennerberg, A. Johnsson, K. Norrgren, and S. Mattsson. 2001. Antitumor effect of radioactive cisplatin (191Pt) on nude mice. *International journal of radiation oncology, biology, physics*. 49:827-832.

Auger, P. 1923. Sur les rayons beta secondariees produits dans un gaz par des rayons X. *CRAS*. 44:1479-1481.

Bagshawe, K.D., K. Sharma, P.J. Southall, J.A. Boden, G.M. Boxer, T.A. Patridge, P. Antoniw, and R.B. Pedley. 1991. Selective uptake of toxic nucleoside (125IUdR) by resistant cancer. *The British journal of radiology*. 64:37-44.

Bailey, K.E., D.L. Costantini, Z. Cai, D.A. Scollard, Z. Chen, R.M. Reilly, and K.A. Vallis. 2007. Epidermal growth factor receptor inhibition modulates the nuclear localization and cytotoxicity of the Auger electron emitting radiopharmaceutical 111In-DTPA human epidermal growth factor. *Journal of nuclear medicine : official publication, Society of Nuclear Medicine*. 48:1562-1570.

Bakshi, R., S.K. Zaidi, S. Pande, M.Q. Hassan, D.W. Young, M. Montecino, J.B. Lian, A.J. van Wijnen, J.L. Stein, and G.S. Stein. 2008. The leukemogenic t(8;21) fusion protein AML1-ETO controls rRNA genes and associates with nucleolar-organizing regions at mitotic chromosomes. *Journal of cell science*. 121:3981-3990.

Banath, J.P., S.H. Macphail, and P.L. Olive. 2004. Radiation sensitivity, H2AX phosphorylation, and kinetics of repair of DNA strand breaks in irradiated cervical cancer cell lines. *Cancer Res*. 64:7144-7149.

Bartek, J., J. Lukas, and M. Strauss. 1996. A common path to tumor growth. *Oncology reports*. 3:237-240.

Bender, H., H. Takahashi, K. Adachi, P. Belser, S.H. Liang, M. Prewett, M. Schrappe, A. Sutter, U. Rodeck, and D. Herlyn. 1992. Immunotherapy of human glioma xenografts with unlabeled, 131I-, or 125I-labeled monoclonal antibody 425 to epidermal growth factor receptor. *Cancer research*. 52:121-126.

Bertwistle, D., M. Sugimoto, and C.J. Sherr. 2004. Physical and functional interactions of the Arf tumor suppressor protein with nucleophosmin/B23. *Molecular and cellular biology*. 24:985-996.

Bhatt, P., C. d'Avout, N.S. Kane, J.A. Borowiec, and A. Saxena. 2012. Specific domains of nucleolin interact with Hdm2 and antagonize Hdm2-mediated p53 ubiquitination. *The FEBS journal*. 279:370-383.

Bhojani, M.S., R. Ranga, G.D. Luker, A. Rehemtulla, B.D. Ross, and M.E. Van Dort. 2011. Synthesis and investigation of a radioiodinated F3 peptide analog as a SPECT tumor imaging radioligand. *PloS one*. 6:e22418.

Bishayee, A., D.V. Rao, L.G. Bouchet, W.E. Bolch, and R.W. Howell. 2000a. Protection by DMSO against cell death caused by intracellularly localized iodine-125, iodine-131 and polonium-210. *Radiation research*. 153:416-427.

Bishayee, A., D.V. Rao, and R.W. Howell. 2000b. Radiation protection by cysteamine against the lethal effects of intracellularly localized Auger electron, alpha- and beta-particle emitting radionuclides. *Acta oncologica*. 39:713-720.

Bloomer, W.D., and S.J. Adelstein. 1977. 5-125I-iododeoxyuridine as prototype for radionuclide therapy with Auger emitters. *Nature*. 265:620-621.

Bloomer, W.D., W.H. McLaughlin, R.A. Milius, R.R. Weichselbaum, and S.J. Adelstein. 1983. Estrogen receptor-mediated cytotoxicity using iodine-125. *Journal of cellular biochemistry*. 21:39-45.

Bodei, L., A.I. Kassis, S.J. Adelstein, and G. Mariani. 2003. Radionuclide therapy with iodine-125 and other auger-electron-emitting radionuclides: experimental models and clinical applications. *Cancer biotherapy & radiopharmaceuticals*. 18:861-877.

Boisvert, F.M., Y.W. Lam, D. Lamont, and A.I. Lamond. 2010. A quantitative proteomics analysis of subcellular proteome localization and changes induced by DNA damage. *Molecular & cellular proteomics : MCP*. 9:457-470.

Boisvert, F.M., and A.I. Lamond. 2010. p53-Dependent subcellular proteome localization following DNA damage. *Proteomics*. 10:4087-4097.

Boisvert, F.M., S. van Koningsbruggen, J. Navascues, and A.I. Lamond. 2007. The multifunctional nucleolus. *Nature reviews. Molecular cell biology*. 8:574-585.

Borer, R.A., C.F. Lehner, H.M. Eppenberger, and E.A. Nigg. 1989. Major nucleolar proteins shuttle between nucleus and cytoplasm. *Cell*. 56:379-390.

Boulon, S., B.J. Westman, S. Hutten, F.M. Boisvert, and A.I. Lamond. 2010. The nucleolus under stress. *Molecular cell*. 40:216-227.

Bouvet, P., J.J. Diaz, K. Kindbeiter, J.J. Madjar, and F. Amalric. 1998. Nucleolin interacts with several ribosomal proteins through its RGG domain. *The Journal of biological chemistry*. 273:19025-19029.

Boyd, M., S.H. Cunningham, M.M. Brown, R.J. Mairs, and T.E. Wheldon. 1999. Noradrenaline transporter gene transfer for radiation cell kill by 131I meta-iodobenzylguanidine. *Gene therapy*. 6:1147-1152.

Boyd, M., S.C. Ross, J. Dorrens, N.E. Fullerton, K.W. Tan, M.R. Zalutsky, and R.J. Mairs. 2006. Radiation-induced biologic bystander effect elicited in vitro by targeted radiopharmaceuticals labeled with alpha-, beta-, and auger electron-emitting radionuclides. *Journal of nuclear medicine : official publication, Society of Nuclear Medicine*. 47:1007-1015.

Boyd, M.T., N. Vlatkovic, and C.P. Rubbi. 2011. The nucleolus directly regulates p53 export and degradation. *The Journal of cell biology*. 194:689-703.

Bradley, E.W., P.C. Chan, and S.J. Adelstein. 1975. The radiotoxicity of iodine-125 in mammalian cells. I. Effects on the survival curve of radioiodine incorporated into DNA. *Radiation research*. 64:555-563.

Braun, N., T. Papadopoulos, and H.K. Muller-Hermelink. 1988. Cell cycle dependent distribution of the proliferation-associated Ki-67 antigen in human embryonic lung cells. *Virchows Archiv. B, Cell pathology including molecular pathology*. 56:25-33.

Bridger, J.M.K., I.; Lichter, P. 1998. Association of pKi-67 with satellite DNA of the human gennome in early G1 cells. *Chromosome Res*. 6:4951-4966.

Brons, S., B. Jakob, G. Taucher-Scholz, and G. Kraft. 2001. Heavy ion production of single- and double-strand breaks in plasmid DNA in aqueous solution. *Physica medica : PM : an international journal devoted to the applications of physics to*

medicine and biology : official journal of the Italian Association of Biomedical Physics. 17 Suppl 1:217-218.

Brown, D.D., and J.B. Gurdon. 1964. Absence of Ribosomal Rna Synthesis in the Anucleolate Mutant of Xenopus Laevis. *Proceedings of the National Academy of Sciences of the United States of America*. 51:139-146.

Bruno, S., and Z. Darzynkiewicz. 1992. Cell cycle dependent expression and stability of the nuclear protein detected by Ki-67 antibody in HL-60 cells. *Cell proliferation*. 25:31-40.

Budde, A., and I. Grummt. 1999. p53 represses ribosomal gene transcription. *Oncogene*. 18:1119-1124.

Burger, K., B. Muhl, T. Harasim, M. Rohrmoser, A. Malamoussi, M. Orban, M. Kellner, A. Gruber-Eber, E. Kremmer, M. Holzel, and D. Eick. 2010. Chemotherapeutic drugs inhibit ribosome biogenesis at various levels. *The Journal of biological chemistry*. 285:12416-12425.

Bywater, M.J., G. Poortinga, E. Sanij, N. Hein, A. Peck, C. Cullinane, M. Wall, L. Cluse, D. Drygin, K. Anderes, N. Huser, C. Proffitt, J. Bliesath, M. Haddach, M.K. Schwaebe, D.M. Ryckman, W.G. Rice, C. Schmitt, S.W. Lowe, R.W. Johnstone, R.B. Pearson, G.A. McArthur, and R.D. Hannan. 2012. Inhibition of RNA polymerase I as a therapeutic strategy to promote cancer-specific activation of p53. *Cancer cell*. 22:51-65.

Calabresi, P., S.S. Cardoso, S.C. Finch, M.M. Kligerman, C.F. Von Essen, M.Y. Chu, and A.D. Welch. 1961. Initial clinical studies with 5-iodo-2'-deoxyuridine. *Cancer research*. 21:550-559.

Capello, A., E.P. Krenning, B.F. Bernard, W.A. Breeman, M.P. van Hagen, and M. de Jong. 2004. Increased cell death after therapy with an Arg-Gly-Asp-linked somatostatin analog. *Journal of nuclear medicine : official publication, Society of Nuclear Medicine*. 45:1716-1720.

Carmo-Fonseca, M., J. Ferreira, and A.I. Lamond. 1993. Assembly of snRNP-containing coiled bodies is regulated in interphase and mitosis--evidence that the coiled body is a kinetic nuclear structure. *The Journal of cell biology*. 120:841-852.

Celis, J.E., P. Madsen, and J.B. Lauridsen. 1987. Mid to late S-phase replication of the nucleolus in lymphoid human Molt-4 cells. *Leukemia*. 1:568-571.

Chan, C., Z. Cai, R. Su, and R.M. Reilly. 2010. 111In- or 99mTc-labeled recombinant VEGF bioconjugates: in vitro evaluation of their cytotoxicity on porcine aortic endothelial cells overexpressing Flt-1 receptors. *Nuclear medicine and biology*. 37:105-115.

Chan, J.C., K.M. Hannan, K. Riddell, P.Y. Ng, A. Peck, R.S. Lee, S. Hung, M.V. Astle, M. Bywater, M. Wall, G. Poortinga, K. Jastrzebski, K.E. Sheppard, B.A. Hemmings, M.N. Hall, R.W. Johnstone, G.A. McArthur, R.D. Hannan, and R.B. Pearson. 2011. AKT promotes rRNA synthesis and cooperates with c-MYC to stimulate ribosome biogenesis in cancer. *Science signaling*. 4:ra56.

Chan, P.C., E. Lisco, H. Lisco, and S.J. Adelstein. 1978. Cell survival and cytogenetic responses to 125I-UdR in cultured mammalian cells. *Current topics in radiation research quarterly*. 12:426-435.

Chan, P.K., Y. Qi, J. Amley, and C.A. Koller. 1996. Quantitation of the nucleophosmin/B23-translocation using imaging analysis. *Cancer letters*. 100:191-197.

Chen, D., J. Shan, W.G. Zhu, J. Qin, and W. Gu. 2010. Transcription-independent ARF regulation in oncogenic stress-mediated p53 responses. *Nature*. 464:624-627.

Chen, J., K. Guo, and M.B. Kastan. 2012. Interactions of nucleolin and ribosomal protein L26 (RPL26) in translational control of human p53 mRNA. *The Journal of biological chemistry*. 287:16467-16476.

Chen, P., J. Wang, K. Hope, L. Jin, J. Dick, R. Cameron, J. Brandwein, M. Minden, and R.M. Reilly. 2006. Nuclear localizing sequences promote nuclear translocation and enhance the radiotoxicity of the anti-CD33 monoclonal antibody HuM195 labeled with 111In in human myeloid leukemia cells. *Journal of nuclear medicine : official publication, Society of Nuclear Medicine*. 47:827-836.

Chen, X., D.M. Kube, M.J. Cooper, and P.B. Davis. 2008. Cell surface nucleolin serves as receptor for DNA nanoparticles composed of pegylated polylysine and DNA. *Molecular therapy : the journal of the American Society of Gene Therapy*. 16:333-342.

Chinnam, M., and D.W. Goodrich. 2011. RB1, development, and cancer. *Current topics in developmental biology*. 94:129-169.

Christian, S., J. Pilch, M.E. Akerman, K. Porkka, P. Laakkonen, and E. Ruoslahti. 2003. Nucleolin expressed at the cell surface is a marker of endothelial cells in angiogenic blood vessels. *The Journal of cell biology*. 163:871-878.

Chu, W.M., Z. Wang, R.G. Roeder, and C.W. Schmid. 1997. RNA polymerase III transcription repressed by Rb through its interactions with TFIIIB and TFIIIC2. *The Journal of biological chemistry*. 272:14755-14761.

Chung, W.J., Y. Cui, F.Y. Huang, T.H. Tu, T.S. Yang, J.M. Lo, C.S. Chiang, and I.C. Hsu. 2014. (9)(9)mTc pyrene derivative complex causes double-strand breaks in dsDNA mainly through cluster-mediated indirect effect in aqueous solution. *PloS one*. 9:e108162.

Cioce, M., S. Boulon, A.G. Matera, and A.I. Lamond. 2006. UV-induced fragmentation of Cajal bodies. *The Journal of cell biology*. 175:401-413.

Cioce, M., and A.I. Lamond. 2005. Cajal bodies: a long history of discovery. *Annual review of cell and developmental biology*. 21:105-131.

Cole, A. 1969. Absorption of 20-eV to 50,000-eV electron beams in air and plastic. *Radiation research*. 38:7-33.

Colombo, E., P. Bonetti, E. Lazzerini Denchi, P. Martinelli, R. Zamponi, J.C. Marine, K. Helin, B. Falini, and P.G. Pelicci. 2005. Nucleophosmin is required for DNA integrity and p19Arf protein stability. *Molecular and cellular biology*. 25:8874-8886.

Colombo, E., J.C. Marine, D. Danovi, B. Falini, and P.G. Pelicci. 2002. Nucleophosmin regulates the stability and transcriptional activity of p53. *Nature cell biology*. 4:529-533.

Commerford, S.L., and D.D. Joel. 1979. Iododeoxyuridine administered to mice is de-iodinated and incorporated into DNA primarily as thymidylate. *Biochemical and biophysical research communications*. 86:112-118.

Cong, R., S. Das, J. Douet, J. Wong, M. Buschbeck, F. Mongelard, and P. Bouvet. 2014a. Interaction of nucleolin with ribosomal RNA genes and its role in RNA polymerase I transcription. *Nucleic acids research*. 42:181-192.

Cong, R., S. Das, J. Douet, J. Wong, M. Buschbeck, F. Mongelard, and P. Bouvet. 2014b. macroH2A1 histone variant represses rDNA transcription. *Nucleic acids research*. 42:181-192.

Cornelissen, B., S. Able, C. Kartsonaki, V. Kersemans, P.D. Allen, F. Cavallo, J.B. Cazier, M. Iezzi, J. Knight, R. Muschel, S. Smart, and K.A. Vallis. 2014. Imaging DNA damage allows detection of preneoplasia in the BALB-neuT model of breast cancer. *Journal of nuclear medicine : official publication, Society of Nuclear Medicine*. 55:2026-2031.

Cornelissen, B., S. Darbar, R. Hernandez, V. Kersemans, I. Tullis, P.R. Barber, S. Smart, B. Vojnovic, R. Reilly, and K.A. Vallis. 2011a. ErbB-2 blockade and prenyltransferase inhibition alter epidermal growth factor and epidermal growth factor receptor trafficking and enhance (111)In-DTPA-hEGF Auger electron radiation therapy. *Journal of nuclear medicine : official publication, Society of Nuclear Medicine*. 52:776-783.

Cornelissen, B., S. Darbar, V. Kersemans, D. Allen, N. Falzone, J. Barbeau, S. Smart, and K.A. Vallis. 2012a. Amplification of DNA damage by a gammaH2AX-targeted radiopharmaceutical. *Nuclear medicine and biology*. 39:1142-1151.

Cornelissen, B., V. Kersemans, S. Darbar, J. Thompson, K. Shah, K. Sleeth, M.A. Hill, and K.A. Vallis. 2011b. Imaging DNA damage in vivo using gammaH2AX-targeted immunoconjugates. *Cancer research*. 71:4539-4549.

Cornelissen, B., and K.A. Vallis. 2010. Targeting the nucleus: an overview of Auger-electron radionuclide therapy. *Current drug discovery technologies*. 7:263-279.

Cornelissen, B., A. Waller, S. Able, and K.A. Vallis. 2013. Molecular radiotherapy using cleavable radioimmunoconjugates that target EGFR and gammaH2AX. *Molecular cancer therapeutics*. 12:2472-2482.

Cornelissen, B., A. Waller, C. Target, V. Kersemans, S. Smart, and K.A. Vallis. 2012b. 111In-BnDTPA-F3: an Auger electron-emitting radiotherapeutic agent that targets nucleolin. *EJNMMI research*. 2:9.

Costantini, D.L., C. Chan, Z. Cai, K.A. Vallis, and R.M. Reilly. 2007. (111)In-labeled trastuzumab (Herceptin) modified with nuclear localization sequences (NLS): an Auger electron-emitting radiotherapeutic agent for HER2/neu-amplified breast cancer. *Journal of nuclear medicine : official publication, Society of Nuclear Medicine*. 48:1357-1368.

Costantini, D.L., K. McLarty, H. Lee, S.J. Done, K.A. Vallis, and R.M. Reilly. 2010. Antitumor effects and normal-tissue toxicity of 111In-nuclear localization sequence-trastuzumab in athymic mice bearing HER-positive human breast cancer xenografts. *Journal of nuclear medicine : official publication, Society of Nuclear Medicine*. 51:1084-1091.

Creancier, L., H. Prats, C. Zanibellato, F. Amalric, and B. Bugler. 1993. Determination of the functional domains involved in nucleolar targeting of nucleolin. *Molecular biology of the cell*. 4:1239-1250.

Crighton, D., A. Woiwode, C. Zhang, N. Mandavia, J.P. Morton, L.J. Warnock, J. Milner, R.J. White, and D.L. Johnson. 2003. p53 represses RNA polymerase III transcription by targeting TBP and inhibiting promoter occupancy by TFIIIB. *The EMBO journal*. 22:2810-2820.

Cui, C., and H. Tseng. 2004. Estimation of ribosomal RNA transcription rate in situ. *BioTechniques*. 36:134-138.

D'Angelo, G., R. Sciuto, M. Salvatori, I. Sperduti, G. Mantini, C.L. Maini, and G. Mariani. 2012. Targeted "bone-seeking" radiopharmaceuticals for palliative

treatment of bone metastases: a systematic review and meta-analysis. *The quarterly journal of nuclear medicine and molecular imaging : official publication of the Italian Association of Nuclear Medicine*. 56:538-543.

Dalenc, F., J. Drouet, I. Ader, C. Delmas, P. Rochaix, G. Favre, E. Cohen-Jonathan, and C. Toulas. 2002. Increased expression of a COOH-truncated nucleophosmin resulting from alternative splicing is associated with cellular resistance to ionizing radiation in HeLa cells. *International journal of cancer. Journal international du cancer*. 100:662-668.

Daniely, Y., D.D. Dimitrova, and J.A. Borowiec. 2002. Stress-dependent nucleolin mobilization mediated by p53-nucleolin complex formation. *Molecular and cellular biology*. 22:6014-6022.

David-Pfeuty, T. 1999. Potent inhibitors of cyclin-dependent kinase 2 induce nuclear accumulation of wild-type p53 and nucleolar fragmentation in human untransformed and tumor-derived cells. *Oncogene*. 18:7409-7422.

de Jong, M., W.A. Breeman, B.F. Bernard, A. van Gameren, E. de Bruin, W.H. Bakker, M.E. van der Pluijm, T.J. Visser, H.R. Macke, and E.P. Krenning. 1999a. Tumour uptake of the radiolabelled somatostatin analogue [DOTA0, TYR3]octreotide is dependent on the peptide amount. *European journal of nuclear medicine*. 26:693-698.

De Jong, M., W.A. Breeman, H.F. Bernard, P.P. Kooij, G.D. Slooter, C.H. Van Eijck, D.J. Kwekkeboom, R. Valkema, H.R. Macke, and E.P. Krenning. 1999b. Therapy of neuroendocrine tumors with radiolabeled somatostatin-analogues. *The quarterly journal of nuclear medicine : official publication of the Italian Association of Nuclear Medicine*. 43:356-366.

Dean, P., and B. Kenny. 2011. Cell-surface nucleolin is sequestered into EPEC microcolonies and may play a role during infection. *Microbiology*. 157:1761-1767.

Deisenroth, C., and Y. Zhang. 2010. Ribosome biogenesis surveillance: probing the ribosomal protein-Mdm2-p53 pathway. *Oncogene*. 29:4253-4260.

Delloye-Bourgeois, C., D. Goldschneider, A. Paradisi, G. Therizols, S. Belin, S. Hacot, M. Rosa-Calatrava, J.Y. Scoazec, J.J. Diaz, A. Bernet, and P. Mehlen. 2012. Nucleolar localization of a netrin-1 isoform enhances tumor cell proliferation. *Science signaling*. 5:ra57.

Derenzini, M., L. Montanaro, and D. Trere. 2009. What the nucleolus says to a tumour pathologist. *Histopathology*. 54:753-762.

Derenzini, M., and D. Ploton. 1991. Interphase nucleolar organizer regions in cancer cells. *International review of experimental pathology*. 32:149-192.

Derenzini, M., V. Sirri, A. Pession, D. Trere, P. Roussel, R.L. Ochs, and D. Hernandez-Verdun. 1995. Quantitative changes of the two major AgNOR proteins, nucleolin and protein B23, related to stimulation of rDNA transcription. *Experimental cell research*. 219:276-282.

Derenzini, M., D. Trere, A. Pession, M. Govoni, V. Sirri, and P. Chieco. 2000. Nucleolar size indicates the rapidity of cell proliferation in cancer tissues. *The Journal of pathology*. 191:181-186.

Derenzini, M., D. Trere, A. Pession, L. Montanaro, V. Sirri, and R.L. Ochs. 1998. Nucleolar function and size in cancer cells. *The American journal of pathology*. 152:1291-1297.

Derfus, A.M., A.A. Chen, D.H. Min, E. Ruoslahti, and S.N. Bhatia. 2007. Targeted quantum dot conjugates for siRNA delivery. *Bioconjugate chemistry*. 18:1391-1396.

Derui, L., D.V. Woo, J. Emrich, Z. Steplewski, U. Rodeck, D. Herlyn, H. Koprowski, C. Miyamoto, and L.W. Brady. 1992. Radiotoxicity of 125I-labeled monoclonal antibody 425 against cancer cells containing epidermal growth factor receptor. *American journal of clinical oncology*. 15:288-294.

DeSombre, E.R., A. Hughes, R.N. Hanson, and T. Kearney. 2000. Therapy of estrogen receptor-positive micrometastases in the peritoneal cavity with Auger electron-emitting estrogens--theoretical and practical considerations. *Acta oncologica*. 39:659-666.

DeSombre, E.R., A. Hughes, C.C. Landel, G. Greene, R. Hanson, and J.L. Schwartz. 1996. Cellular and subcellular studies of the radiation effects of Auger electron-emitting estrogens. *Acta oncologica*. 35:833-840.

DeSombre, E.R., R.C. Mease, A. Hughes, P.V. Harper, O.T. DeJesus, and A.M. Friedman. 1988. Bromine-80m-labeled estrogens: Auger electron-emitting, estrogen receptor-directed ligands with potential for therapy of estrogen receptor-positive cancers. *Cancer Res*. 48:899-906.

DeSombre, E.R., B. Shafii, R.N. Hanson, P.C. Kuivanen, and A. Hughes. 1992. Estrogen receptor-directed radiotoxicity with Auger electrons: specificity and mean lethal dose. *Cancer Res*. 52:5752-5758.

Dhar, S.K., and D.K. St Clair. 2009. Nucleophosmin blocks mitochondrial localization of p53 and apoptosis. *The Journal of biological chemistry*. 284:16409-16418.

Dieci, G., M. Preti, and B. Montanini. 2009. Eukaryotic snoRNAs: a paradigm for gene expression flexibility. *Genomics*. 94:83-88.

Dimario, P.J. 2004. Cell and molecular biology of nucleolar assembly and disassembly. *International review of cytology*. 239:99-178.

Ding, Y., N. Song, C. Liu, T. He, W. Zhuo, X. He, Y. Chen, X. Song, Y. Fu, and Y. Luo. 2012. Heat shock cognate 70 regulates the translocation and angiogenic function of nucleolin. *Arteriosclerosis, thrombosis, and vascular biology*. 32:e126-134.

Dohan, O., A. De la Vieja, V. Paroder, C. Riedel, M. Artani, M. Reed, C.S. Ginter, and N. Carrasco. 2003. The sodium/iodide Symporter (NIS): characterization, regulation, and medical significance. *Endocrine reviews*. 24:48-77.

Draptchinskaia, N., P. Gustavsson, B. Andersson, M. Pettersson, T.N. Willig, I. Dianzani, S. Ball, G. Tchernia, J. Klar, H. Matsson, D. Tentler, N. Mohandas, B. Carlsson, and N. Dahl. 1999. The gene encoding ribosomal protein S19 is mutated in Diamond-Blackfan anaemia. *Nature genetics*. 21:169-175.

Drecoll, E., F.C. Gaertner, M. Miederer, B. Blechert, M. Vallon, J.M. Muller, A. Alke, C. Seidl, F. Bruchertseifer, A. Morgenstern, R. Senekowitsch-Schmidtke, and M. Essler. 2009. Treatment of peritoneal carcinomatosis by targeted delivery of the radio-labeled tumor homing peptide bi-DTPA-[F3]2 into the nucleus of tumor cells. *PloS one*. 4:e5715.

Drygin, D., A. Lin, J. Bliesath, C.B. Ho, S.E. O'Brien, C. Proffitt, M. Omori, M. Haddach, M.K. Schwaebe, A. Siddiqui-Jain, N. Streiner, J.E. Quin, E. Sanij, M.J. Bywater, R.D. Hannan, D. Ryckman, K. Anderes, and W.G. Rice. 2011. Targeting RNA polymerase I with an oral small molecule CX-5461 inhibits ribosomal RNA synthesis and solid tumor growth. *Cancer research*. 71:1418-1430.

Drygin, D., W.G. Rice, and I. Grummt. 2010. The RNA polymerase I transcription machinery: an emerging target for the treatment of cancer. *Annual review of pharmacology and toxicology*. 50:131-156.

Drygin, D., A. Siddiqui-Jain, S. O'Brien, M. Schwaebe, A. Lin, J. Bliesath, C.B. Ho, C. Proffitt, K. Trent, J.P. Whitten, J.K. Lim, D. Von Hoff, K. Anderes, and W.G. Rice. 2009. Anticancer activity of CX-3543: a direct inhibitor of rRNA biogenesis. *Cancer research*. 69:7653-7661.

Dundr, M., T. Misteli, and M.O. Olson. 2000. The dynamics of postmitotic reassembly of the nucleolus. *The Journal of cell biology*. 150:433-446.

Ebert, B.L., J. Pretz, J. Bosco, C.Y. Chang, P. Tamayo, N. Galili, A. Raza, D.E. Root, E. Attar, S.R. Ellis, and T.R. Golub. 2008. Identification of RPS14 as a 5q- syndrome gene by RNA interference screen. *Nature*. 451:335-339.

Egyhazi, E., A. Pigon, J.H. Chang, S.H. Ghaffari, T.D. Dreesen, S.E. Wellman, S.T. Case, and M.O. Olson. 1988. Effects of anti-C23 (nucleolin) antibody on transcription of ribosomal DNA in Chironomus salivary gland cells. *Experimental cell research*. 178:264-272.

Emmott, E., C. Smith, S.R. Emmett, B.K. Dove, and J.A. Hiscox. 2010. Elucidation of the avian nucleolar proteome by quantitative proteomics using SILAC and changes in cells infected with the coronavirus infectious bronchitis virus. *Proteomics*. 10:3558-3562.

Endl, E., and J. Gerdes. 2000. Posttranslational modifications of the KI-67 protein coincide with two major checkpoints during mitosis. *Journal of cellular physiology*. 182:371-380.

Endl, E., P. Steinbach, R. Knuchel, and F. Hofstadter. 1997. Analysis of cell cycle-related Ki-67 and p120 expression by flow cytometric BrdUrd-Hoechst/7AAD and immunolabeling technique. *Cytometry*. 29:233-241.

Epperly, M.W., K.M. Damodaran, W.H. McLaughlin, K.M. Pillai, and W.D. Bloomer. 1991. Radiotoxicity of 17 alpha-[125I]iodovinyl-11 beta-methoxyestradiol in MCF-7 human breast cancer cells. *The Journal of steroid biochemistry and molecular biology*. 39:729-734.

Erard, M.S., P. Belenguer, M. Caizergues-Ferrer, A. Pantaloni, and F. Amalric. 1988. A major nucleolar protein, nucleolin, induces chromatin decondensation by binding to histone H1. *European journal of biochemistry / FEBS*. 175:525-530.

Escande-Geraud, M.L., M.C. Azum, J.L. Tichadou, and N. Gas. 1985. Correlation between rDNA transcription and distribution of a 100 kD nucleolar protein in CHO cells. *Experimental cell research*. 161:353-363.

Essler, M., F.C. Gartner, F. Neff, B. Blechert, R. Senekowitsch-Schmidtke, F. Bruchertseifer, A. Morgenstern, and C. Seidl. 2012. Therapeutic efficacy and toxicity of 225Ac-labelled vs. 213Bi-labelled tumour-homing peptides in a preclinical mouse model of peritoneal carcinomatosis. *European journal of nuclear medicine and molecular imaging*. 39:602-612.

Faraggi, M., I. Gardin, C. de Labriolle-Vaylet, J.L. Moretti, and B.D. Bok. 1994. The influence of tracer localization on the electron dose rate delivered to the cell nucleus. *Journal of nuclear medicine : official publication, Society of Nuclear Medicine*. 35:113-119.

Fasih, A., H. Fonge, Z. Cai, J.V. Leyton, I. Tikhomirov, S.J. Done, and R.M. Reilly. 2012. (1)(1)(1)In-Bn-DTPA-nimotuzumab with/without modification with nuclear translocation sequence (NLS) peptides: an Auger electron-emitting

radioimmunotherapeutic agent for EGFR-positive and trastuzumab (Herceptin)-resistant breast cancer. *Breast cancer research and treatment*. 135:189-200.

Fatica, A., and D. Tollervey. 2002. Making ribosomes. *Current opinion in cell biology*. 14:313-318.

Fetherston, J., E. Werner, and R. Patterson. 1984. Processing of the external transcribed spacer of murine rRNA and site of action of actinomycin D. *Nucleic acids research*. 12:7187-7198.

Fischer, T., K. Schomacker, and H. Schicha. 2008. Diethylstilbestrol (DES) labeled with Auger emitters: potential radiopharmaceutical for therapy of estrogen receptor-positive tumors and their metastases? *International journal of radiation biology*. 84:1112-1122.

Foltz, D.R., L.E. Jansen, A.O. Bailey, J.R. Yates, 3rd, E.A. Bassett, S. Wood, B.E. Black, and D.W. Cleveland. 2009. Centromere-specific assembly of CENP-a nucleosomes is mediated by HJURP. *Cell*. 137:472-484.

Foltz, D.R., L.E. Jansen, B.E. Black, A.O. Bailey, J.R. Yates, 3rd, and D.W. Cleveland. 2006. The human CENP-A centromeric nucleosome-associated complex. *Nature cell biology*. 8:458-469.

Fontoura, B.M., E.A. Sorokina, E. David, and R.B. Carroll. 1992. p53 is covalently linked to 5.8S rRNA. *Molecular and cellular biology*. 12:5145-5151.

Frehlick, L.J., J.M. Eirin-Lopez, and J. Ausio. 2007. New insights into the nucleophosmin/nucleoplasmin family of nuclear chaperones. *BioEssays : news and reviews in molecular, cellular and developmental biology*. 29:49-59.

Friedberg, E.C. 2001. How nucleotide excision repair protects against cancer. *Nature reviews. Cancer*. 1:22-33.

Fujiki, H., T. Watanabe, and M. Suganuma. 2014. Cell-surface nucleolin acts as a central mediator for carcinogenic, anti-carcinogenic, and disease-related ligands. *Journal of cancer research and clinical oncology*. 140:689-699.

Fumagalli, S., A. Di Cara, A. Neb-Gulati, F. Natt, S. Schwemberger, J. Hall, G.F. Babcock, R. Bernardi, P.P. Pandolfi, and G. Thomas. 2009. Absence of nucleolar disruption after impairment of 40S ribosome biogenesis reveals an rpL11-translation-dependent mechanism of p53 induction. *Nature cell biology*. 11:501-508.

Fumagalli, S., V.V. Ivanenkov, T. Teng, and G. Thomas. 2012. Suprainduction of p53 by disruption of 40S and 60S ribosome biogenesis leads to the activation of a novel G2/M checkpoint. *Genes & development*. 26:1028-1040.

Gadal, O., S. Labarre, C. Boschiero, and P. Thuriaux. 2002. Hmo1, an HMG-box protein, belongs to the yeast ribosomal DNA transcription system. *The EMBO journal*. 21:5498-5507.

Gaidamakova, E.K., R.D. Neumann, and I.G. Panyutin. 2004. Antisense radiotherapy: targeting full-size mdrl mRNA with 125I-labelled oligonucleotides. *International journal of radiation biology*. 80:889-893.

Gallo, R.C., J. Whang-Peng, and R.H. Adamson. 1971. Studies on the antitumor activity, mechanism of action, and cell cycle effects of camptothecin. *Journal of the National Cancer Institute*. 46:789-795.

Gardette, M., C. Viallard, S. Paillas, J.L. Guerquin-Kern, J. Papon, N. Moins, P. Labarre, N. Desbois, P. Wong-Wah-Chung, S. Palle, T.D. Wu, J.P. Pouget, E. Miot-Noirault, J.M. Chezal, and F. Degoul. 2014. Evaluation of two (125)I-radiolabeled acridine derivatives for Auger-electron radionuclide therapy of melanoma. *Investigational new drugs*. 32:587-597.

Garrett, C., Y. Wataya, and D.V. Santi. 1979. Thymidylate synthetase. Catalysis of dehalogenation of 5-bromo- and 5-iodo-2'-deoxyuridylate. *Biochemistry*. 18:2798-2804.

Gaume, X., K. Monier, F. Argoul, F. Mongelard, and P. Bouvet. 2011. In vivo Study of the Histone Chaperone Activity of Nucleolin by FRAP. *Biochemistry research international*. 2011:187624.

Gautier, T., M. Robert-Nicoud, M.N. Guilly, and D. Hernandez-Verdun. 1992. Relocation of nucleolar proteins around chromosomes at mitosis. A study by confocal laser scanning microscopy. *Journal of cell science*. 102 (Pt 4):729-737.

Gazda, H.T., M.R. Sheen, A. Vlachos, V. Choesmel, M.F. O'Donohue, H. Schneider, N. Darras, C. Hasman, C.A. Sieff, P.E. Newburger, S.E. Ball, E. Niewiadomska, M. Matysiak, J.M. Zaucha, B. Glader, C. Niemeyer, J.J. Meerpohl, E. Atsidaftos, J.M. Lipton, P.E. Gleizes, and A.H. Beggs. 2008. Ribosomal protein L5 and L11 mutations are associated with cleft palate and abnormal thumbs in Diamond-Blackfan anemia patients. *American journal of human genetics*. 83:769-780.

Gaze, M.N., R.J. Mairs, S.M. Boyack, T.E. Wheldon, and A. Barrett. 1992. 131I-meta-iodobenzylguanidine therapy in neuroblastoma spheroids of different sizes. *British journal of cancer*. 66:1048-1052.

Gerbi, S.A., A.V. Borovjagin, and T.S. Lange. 2003. The nucleolus: a site of ribonucleoprotein maturation. *Current opinion in cell biology*. 15:318-325.

Ghisolfi-Nieto, L., G. Joseph, F. Puvion-Dutilleul, F. Amalric, and P. Bouvet. 1996. Nucleolin is a sequence-specific RNA-binding protein: characterization of targets on pre-ribosomal RNA. *Journal of molecular biology*. 260:34-53.

Ghisolfi, L., A. Kharrat, G. Joseph, F. Amalric, and M. Erard. 1992. Concerted activities of the RNA recognition and the glycine-rich C-terminal domains of nucleolin are required for efficient complex formation with pre-ribosomal RNA. *European journal of biochemistry / FEBS*. 209:541-548.

Ghoshal, K., and S.T. Jacob. 1997. An alternative molecular mechanism of action of 5-fluorouracil, a potent anticancer drug. *Biochemical pharmacology*. 53:1569-1575.

Ginisty, H., F. Amalric, and P. Bouvet. 1998. Nucleolin functions in the first step of ribosomal RNA processing. *The EMBO journal*. 17:1476-1486.

Ginisty, H., G. Serin, L. Ghisolfi-Nieto, B. Roger, V. Libante, F. Amalric, and P. Bouvet. 2000. Interaction of nucleolin with an evolutionarily conserved pre-ribosomal RNA sequence is required for the assembly of the primary processing complex. *The Journal of biological chemistry*. 275:18845-18850.

Ginisty, H., H. Sicard, B. Roger, and P. Bouvet. 1999. Structure and functions of nucleolin. *Journal of cell science*. 112 (Pt 6):761-772.

Ginj, M., K. Hinni, S. Tschumi, S. Schulz, and H.R. Maecke. 2005. Trifunctional somatostatin-based derivatives designed for targeted radiotherapy using auger electron emitters. *Journal of nuclear medicine : official publication, Society of Nuclear Medicine*. 46:2097-2103.

Gjerset, R.A., and K. Bandyopadhyay. 2006. Regulation of p14ARF through subnuclear compartmentalization. *Cell cycle*. 5:686-690.

Goddu, S.M., Budinger, T.F. 1997. MIRD Cellular S Values: Self-absorbed dose per unit cumulated activity for selected radionuclides and monoenergetic electron and alpha particle emitters incorporated into different cell compartments. *SNM Inc*.

Goddu, S.M., R.W. Howell, and D.V. Rao. 1994. Cellular dosimetry: absorbed fractions for monoenergetic electron and alpha particle sources and S-values for radionuclides uniformly distributed in different cell compartments. *Journal of nuclear medicine : official publication, Society of Nuclear Medicine*. 35:303-316.

Goldsmith, S.J. 2010. Radioimmunotherapy of lymphoma: Bexxar and Zevalin. *Seminars in nuclear medicine*. 40:122-135.

Goldstein, M., F.A. Derheimer, J. Tait-Mulder, and M.B. Kastan. 2013. Nucleolin mediates nucleosome disruption critical for DNA double-strand break repair. *Proceedings of the National Academy of Sciences of the United States of America*. 110:16874-16879.

Gomez-Roman, N., C. Grandori, R.N. Eisenman, and R.J. White. 2003. Direct activation of RNA polymerase III transcription by c-Myc. *Nature*. 421:290-294.

Govoni, M., F. Farabegoli, A. Pession, and F. Novello. 1994. Inhibition of topoisomerase II activity and its effect on nucleolar structure and function. *Experimental cell research*. 211:36-41.

Grandori, C., N. Gomez-Roman, Z.A. Felton-Edkins, C. Ngouenet, D.A. Galloway, R.N. Eisenman, and R.J. White. 2005. c-Myc binds to human ribosomal DNA and stimulates transcription of rRNA genes by RNA polymerase I. *Nature cell biology*. 7:311-318.

Greco, A. 2009. Involvement of the nucleolus in replication of human viruses. *Reviews in medical virology*. 19:201-214.

Grosshans, H., K. Deinert, E. Hurt, and G. Simos. 2001. Biogenesis of the signal recognition particle (SRP) involves import of SRP proteins into the nucleolus, assembly with the SRP-RNA, and Xpo1p-mediated export. *The Journal of cell biology*. 153:745-762.

Grummt, I. 2003. Life on a planet of its own: regulation of RNA polymerase I transcription in the nucleolus. *Genes & development*. 17:1691-1702.

Grummt, I., and C.S. Pikaard. 2003. Epigenetic silencing of RNA polymerase I transcription. *Nature reviews. Molecular cell biology*. 4:641-649.

Gurumurthy, M., C.H. Tan, R. Ng, L. Zeiger, J. Lau, J. Lee, A. Dey, R. Philp, Q. Li, T.M. Lim, D.H. Price, D.P. Lane, and S.H. Chao. 2008. Nucleophosmin interacts with HEXIM1 and regulates RNA polymerase II transcription. *Journal of molecular biology*. 378:302-317.

Haaf, T., and D.C. Ward. 1996. Inhibition of RNA polymerase II transcription causes chromatin decondensation, loss of nucleolar structure, and dispersion of chromosomal domains. *Experimental cell research*. 224:163-173.

Hamilton, G., A.G. Abraham, J. Morton, O. Sampson, D.E. Pefani, S. Khoronenkova, A. Grawenda, A. Papaspyropoulos, N. Jamieson, C. McKay, O. Sansom, G.L. Dianov, and E. O'Neill. 2014. AKT regulates NPM dependent ARF localization and p53mut stability in tumors. *Oncotarget*. 5:6142-6167.

Hampton, E.G., and M.L. Eidinoff. 1961. Administration of 5-iododeoxyuridine-I-131 in the mouse and rat. *Cancer research*. 21:345-352.

Han, G., Z.P. Kortylewicz, T. Enke, and J. Baranowska-Kortylewicz. 2014. Co-targeting androgen receptor and DNA for imaging and molecular radiotherapy of prostate cancer: in vitro studies. *The Prostate*. 74:1634-1646.

Hanakahi, L.A., H. Sun, and N. Maizels. 1999. High affinity interactions of nucleolin with G-G-paired rDNA. *The Journal of biological chemistry*. 274:15908-15912.

Handwerger, K.E., and J.G. Gall. 2006. Subnuclear organelles: new insights into form and function. *Trends in cell biology*. 16:19-26.

Handwerger, K.E., Z. Wu, C. Murphy, and J.G. Gall. 2002. Heat shock induces mini-Cajal bodies in the Xenopus germinal vesicle. *Journal of cell science*. 115:2011-2020.

Hannan, K.M., R.D. Hannan, S.D. Smith, L.S. Jefferson, M. Lun, and L.I. Rothblum. 2000a. Rb and p130 regulate RNA polymerase I transcription: Rb disrupts the interaction between UBF and SL-1. *Oncogene*. 19:4988-4999.

Hannan, K.M., B.K. Kennedy, A.H. Cavanaugh, R.D. Hannan, I. Hirschler-Laszkiewicz, L.S. Jefferson, and L.I. Rothblum. 2000b. RNA polymerase I transcription in confluent cells: Rb downregulates rDNA transcription during confluence-induced cell cycle arrest. *Oncogene*. 19:3487-3497.

Hannan, K.M., E. Sanij, L.I. Rothblum, R.D. Hannan, and R.B. Pearson. 2013. Dysregulation of RNA polymerase I transcription during disease. *Biochimica et biophysica acta*. 1829:342-360.

Hardie, D.G. 2005. New roles for the LKB1-->AMPK pathway. *Current opinion in cell biology*. 17:167-173.

Haupt, Y., R. Maya, A. Kazaz, and M. Oren. 1997. Mdm2 promotes the rapid degradation of p53. *Nature*. 387:296-299.

Hein, N., K.M. Hannan, A.J. George, E. Sanij, and R.D. Hannan. 2013. The nucleolus: an emerging target for cancer therapy. *Trends in molecular medicine*. 19:643-654.

Heine, M.A., M.L. Rankin, and P.J. DiMario. 1993. The Gly/Arg-rich (GAR) domain of Xenopus nucleolin facilitates in vitro nucleic acid binding and in vivo nucleolar localization. *Molecular biology of the cell*. 4:1189-1204.

Heitz, E. 1931. Nukleolar und chromosomen in der gattung. *Vicia Planta*. 15:495–505.

Heix, J., A. Vente, R. Voit, A. Budde, T.M. Michaelidis, and I. Grummt. 1998. Mitotic silencing of human rRNA synthesis: inactivation of the promoter selectivity factor SL1 by cdc2/cyclin B-mediated phosphorylation. *The EMBO journal*. 17:7373-7381.

Henke, E., J. Perk, J. Vider, P. de Candia, Y. Chin, D.B. Solit, V. Ponomarev, L. Cartegni, K. Manova, N. Rosen, and R. Benezra. 2008. Peptide-conjugated antisense oligonucleotides for targeted inhibition of a transcriptional regulator in vivo. *Nature biotechnology*. 26:91-100.

Hernandez-Verdun, D. 2006. Nucleolus: from structure to dynamics. *Histochemistry and cell biology*. 125:127-137.

Herrera, A.H., and M.O. Olson. 1986. Association of protein C23 with rapidly labeled nucleolar RNA. *Biochemistry*. 25:6258-6264.

Hillyar, C.R., B. Cornelissen, and K.A. Vallis. 2014. Uptake, internalization and nuclear translocation of radioimmunotherapeutic agents. *Therapeutic delivery*. 5:319-335.

Hillyar, C.R.K., J.C.; Vallis, K.A.; Cornelissen, B. 2015. PET and SPECT imaging for the acceleration of anti-cancer drug development. *Curr. Drug. Tar.*

Hingorani, K., A. Szebeni, and M.O. Olson. 2000. Mapping the functional domains of nucleolar protein B23. *The Journal of biological chemistry*. 275:24451-24457.

Hirano, K., Y. Miki, Y. Hirai, R. Sato, T. Itoh, A. Hayashi, M. Yamanaka, S. Eda, and M. Beppu. 2005. A multifunctional shuttling protein nucleolin is a macrophage receptor for apoptotic cells. *The Journal of biological chemistry*. 280:39284-39293.

Hofer, K.G., C.R. Harris, and J.M. Smith. 1975. Rdiotoxicity of intracellular 67Ga, 125I and 3H. Nuclear versus cytoplasmic radiation effects in murine L1210

leukaemia. *International journal of radiation biology and related studies in physics, chemistry, and medicine*. 28:225-241.

Hofer, K.G., N. van Loon, M.H. Schneiderman, and G.V. Dalrymple. 1993. Targets for radiation-induced cell death: target replication during the cell cycle evaluated in cells exposed to X-rays or 125I decays. *International journal of radiation biology*. 64:205-216.

Hofland, L.J., W.A. Breeman, E.P. Krenning, M. de Jong, M. Waaijers, P.M. van Koetsveld, H.R. Macke, and S.W. Lamberts. 1999. Internalization of [DOTA degrees,125I-Tyr3]Octreotide by somatostatin receptor-positive cells in vitro and in vivo: implications for somatostatin receptor-targeted radio-guided surgery. *Proceedings of the Association of American Physicians*. 111:63-69.

Holzel, M., M. Orban, J. Hochstatter, M. Rohrmoser, T. Harasim, A. Malamoussi, E. Kremmer, G. Langst, and D. Eick. 2010. Defects in 18 S or 28 S rRNA processing activate the p53 pathway. *The Journal of biological chemistry*. 285:6364-6370.

Horn, H.F., and K.H. Vousden. 2008. Cooperation between the ribosomal proteins L5 and L11 in the p53 pathway. *Oncogene*. 27:5774-5784.

Hou, D.Y., A.W. Hamburger, J.L. Beach, and Y. Maruyama. 1989a. Killing of human lung cancer cells using a new [111In]bleomycin complex [111In]BLMC. *Cancer investigation*. 7:543-550.

Hou, D.Y., H. Hoch, G.S. Johnston, K.C. Tsou, R.J. Farkas, and E.E. Miller. 1985a. Use of 111In-bleomycin for combining radiotherapy and chemotherapy on glioma-bearing mice. *Journal of surgical oncology*. 29:71-77.

Hou, D.Y., H. Hoch, G.S. Johnston, K.C. Tsou, A.E. Jones, R.J. Farkas, E.E. Miller, and S.M. Larson. 1985b. A new 111In-bleomycin complex for combined radiotherapy and chemotherapy. *Journal of surgical oncology*. 29:91-98.

Hou, D.Y., and Y. Maruyama. 1990. Enhanced killing of human small cell lung cancer by hyperthermia and indium-111-bleomycin complex. *Journal of surgical oncology*. 44:5-9.

Hou, D.Y., and Y. Maruyama. 1992. Distribution of 111In-bleomycin complex in small cell lung cancer cells by autoradiography. *Journal of surgical oncology*. 49:93-97.

Hou, D.Y., Y. Maruyama, and J.R. Drago. 1992. Chromosome aberrations of human small cell lung cancer induced by a new 111In-bleomycin complex. *Journal of surgical oncology*. 51:236-242.

Hou, D.Y., J.V. Ordonez, R.J. Cross, D.D. Ross, and Y. Maruyama. 1989b. Killing lung cancer cells at cell-cycle phase by a new indium-111-bleomycin complex. *Journal of surgical oncology*. 40:73-78.

Hovanessian, A.G., C. Soundaramourty, D. El Khoury, I. Nondier, J. Svab, and B. Krust. 2010. Surface expressed nucleolin is constantly induced in tumor cells to mediate calcium-dependent ligand internalization. *PloS one*. 5:e15787.

Howell, R.W., A.I. Kassis, S.J. Adelstein, D.V. Rao, H.A. Wright, R.N. Hamm, J.E. Turner, and K.S. Sastry. 1994. Radiotoxicity of platinum-195m-labeled trans-platinum (II) in mammalian cells. *Radiation research*. 140:55-62.

Hsu, B. 1980. The use of herbs as anticancer agents. *The American journal of Chinese medicine*. 8:301-306.

Hu, Q., G. Gu, Z. Liu, M. Jiang, T. Kang, D. Miao, Y. Tu, Z. Pang, Q. Song, L. Yao, H. Xia, H. Chen, X. Jiang, X. Gao, and J. Chen. 2013. F3 peptide-functionalized

PEG-PLA nanoparticles co-administrated with tLyp-1 peptide for anti-glioma drug delivery. *Biomaterials*. 34:1135-1145.

Huang, Y., H. Shi, H. Zhou, X. Song, S. Yuan, and Y. Luo. 2006. The angiogenic function of nucleolin is mediated by vascular endothelial growth factor and nonmuscle myosin. *Blood*. 107:3564-3571.

Inder, K.L., C. Lau, D. Loo, N. Chaudhary, A. Goodall, S. Martin, A. Jones, D. van der Hoeven, R.G. Parton, M.M. Hill, and J.F. Hancock. 2009. Nucleophosmin and nucleolin regulate K-Ras plasma membrane interactions and MAPK signal transduction. *The Journal of biological chemistry*. 284:28410-28419.

Itahana, K., K.P. Bhat, A. Jin, Y. Itahana, D. Hawke, R. Kobayashi, and Y. Zhang. 2003. Tumor suppressor ARF degrades B23, a nucleolar protein involved in ribosome biogenesis and cell proliferation. *Molecular cell*. 12:1151-1164.

Jaaskela-Saari, H.A., R. Grenman, H.A. Ramsay, J. Tarkkanen, T. Paavonen, and K.J. Kairemo. 2005. Indium-111-bleomycin complex in squamous cell cancer xenograft tumors of nude mice. *Cancer biotherapy & radiopharmaceuticals*. 20:426-435.

Jackson, S.P., and J. Bartek. 2009. The DNA-damage response in human biology and disease. *Nature*. 461:1071-1078.

Jacobson, M.R., and T. Pederson. 1998. Localization of signal recognition particle RNA in the nucleolus of mammalian cells. *Proceedings of the National Academy of Sciences of the United States of America*. 95:7981-7986.

James, N.J., G.J. Howell, J.H. Walker, and G.E. Blair. 2010. The role of Cajal bodies in the expression of late phase adenovirus proteins. *Virology*. 399:299-311.

Jordan, P., and M. Carmo-Fonseca. 1998. Cisplatin inhibits synthesis of ribosomal RNA in vivo. *Nucleic acids research*. 26:2831-2836.

Kairemo, K.J., H.A. Ramsay, T.K. Paavonen, H.A. Jaaskela-Saari, M. Tagesson, K. Ljunggren, and S.E. Strand. 1997. Biokinetics of indium-111-bleomycin complex in head and neck cancer--implementations for radiochemotherapy. *Cancer detection and prevention*. 21:83-90.

Kairemo, K.J., H.A. Ramsay, M. Tagesson, A.P. Jekunen, T.K. Paavonen, H.A. Jaaskela-Saari, K. Liewendahl, K. Ljunggren, S. Savolainen, and S.E. Strand. 1996. Indium-111 bleomycin complex for radiochemotherapy of head and neck cancer--dosimetric and biokinetic aspects. *European journal of nuclear medicine*. 23:631-638.

Kam, B.L., J.J. Teunissen, E.P. Krenning, W.W. de Herder, S. Khan, E.I. van Vliet, and D.J. Kwekkeboom. 2012. Lutetium-labelled peptides for therapy of neuroendocrine tumours. *European journal of nuclear medicine and molecular imaging*. 39 Suppl 1:S103-112.

Kaminski, M.S., A.D. Zelenetz, O.W. Press, M. Saleh, J. Leonard, L. Fehrenbacher, T.A. Lister, R.J. Stagg, G.F. Tidmarsh, S. Kroll, R.L. Wahl, S.J. Knox, and J.M. Vose. 2001. Pivotal study of iodine I 131 tositumomab for chemotherapy-refractory low-grade or transformed low-grade B-cell non-Hodgkin's lymphomas. *Journal of clinical oncology : official journal of the American Society of Clinical Oncology*. 19:3918-3928.

Karagiannis, T.C., P.N. Lobachevsky, and R.F. Martin. 2000. Cytotoxicity of an 125I-labelled DNA ligand. *Acta oncologica*. 39:681-685.

Kassis, A.I. 2004. The amazing world of auger electrons. *International journal of radiation biology*. 80:789-803.

Kassis, A.I. 2011. Molecular and cellular radiobiological effects of Auger emitting radionuclides. *Radiation protection dosimetry*. 143:241-247.

Kassis, A.I., S.J. Adelstein, C. Haydock, and K.S. Sastry. 1980. Radiotoxicity of 75Se and 35S: theory and application to a cellular model. *Radiation research*. 84:407-425.

Kassis, A.I., S.J. Adelstein, C. Haydock, and K.S. Sastry. 1983. Thallium-201: an experimental and a theoretical radiobiological approach to dosimetry. *Journal of nuclear medicine : official publication, Society of Nuclear Medicine*. 24:1164-1175.

Kassis, A.I., S.J. Adelstein, C. Haydock, K.S. Sastry, K.D. McElvany, and M.J. Welch. 1982. Lethality of Auger electrons from the decay of bromine-77 in the DNA of mammalian cells. *Radiation research*. 90:362-373.

Kassis, A.I., F. Fayad, B.M. Kinsey, K.S. Sastry, and S.J. Adelstein. 1989. Radiotoxicity of an 125I-labeled DNA intercalator in mammalian cells. *Radiation research*. 118:283-294.

Kassis, A.I., F. Fayad, B.M. Kinsey, K.S. Sastry, R.A. Taube, and S.J. Adelstein. 1987a. Radiotoxicity of 125I in mammalian cells. *Radiation research*. 111:305-318.

Kassis, A.I., K.S. Sastry, and S.J. Adelstein. 1985. Intracellular distribution and radiotoxicity of chromium-51 in mammalian cells: Auger-electron dosimetry. *Journal of nuclear medicine : official publication, Society of Nuclear Medicine*. 26:59-67.

Kassis, A.I., K.S. Sastry, and S.J. Adelstein. 1987b. Kinetics of uptake, retention, and radiotoxicity of 125IUdR in mammalian cells: implications of localized energy deposition by Auger processes. *Radiation research*. 109:78-89.

Kassis, A.I., M.A. Walicka, and S.J. Adelstein. 2000. Double-strand break yield following 125I decay--effects of DNA conformation. *Acta oncologica*. 39:721-726.

Kearney, T., A. Hughes, R.N. Hanson, and E.R. DeSombre. 1999. Radiotoxicity of Auger electron-emitting estrogens in MCF-7 spheroids: a potential treatment for estrogen receptor-positive tumors. *Radiation research*. 151:570-579.

Kenneth, N.S., B.A. Ramsbottom, N. Gomez-Roman, L. Marshall, P.A. Cole, and R.J. White. 2007. TRRAP and GCN5 are used by c-Myc to activate RNA polymerase III transcription. *Proceedings of the National Academy of Sciences of the United States of America*. 104:14917-14922.

Kerr, L.E., J.L. Birse-Archbold, D.M. Short, A.L. McGregor, I. Heron, D.C. Macdonald, J. Thompson, G.J. Carlson, J.S. Kelly, J. McCulloch, and J. Sharkey. 2007. Nucleophosmin is a novel Bax chaperone that regulates apoptotic cell death. *Oncogene*. 26:2554-2562.

Kersemans, V., B. Cornelissen, M.D. Minden, J. Brandwein, and R.M. Reilly. 2008a. Drug-resistant AML cells and primary AML specimens are killed by 111In-anti-CD33 monoclonal antibodies modified with nuclear localizing peptide sequences. *Journal of nuclear medicine : official publication, Society of Nuclear Medicine*. 49:1546-1554.

Kersemans, V., K. Kersemans, and B. Cornelissen. 2008b. Cell penetrating peptides for in vivo molecular imaging applications. *Current pharmaceutical design*. 14:2415-2447.

Kharrat, A., J. Derancourt, M. Doree, F. Amalric, and M. Erard. 1991. Synergistic effect of histone H1 and nucleolin on chromatin condensation in mitosis: role of a phosphorylated heteromer. *Biochemistry*. 30:10329-10336.

Kidani, Y., M. Noji, and T. Tashiro. 1980. Antitumor activity of platinum(II) complexes of 1,2-diamino-cyclohexane isomers. *Gan*. 71:637-643.

Kill, I.R. 1996. Localisation of the Ki-67 antigen within the nucleolus. Evidence for a fibrillarin-deficient region of the dense fibrillar component. *Journal of cell science*. 109 (Pt 6):1253-1263.

Kinsella, T.J., P.P. Dobson, and J.B. Mitchell. 1986. Interaction of iododeoxyuridine and its primary metabolite, iodouracil on radiation response. *International journal of radiation oncology, biology, physics*. 12:1519-1522.

Klein, J., and I. Grummt. 1999. Cell cycle-dependent regulation of RNA polymerase I transcription: the nucleolar transcription factor UBF is inactive in mitosis and early G1. *Proceedings of the National Academy of Sciences of the United States of America*. 96:6096-6101.

Koch, C.J., and H.J. Burki. 1975. The oxygen-enhancement ratio for reproductive death induced by 3H or 125I damage in mammalian cells. *International journal of radiation biology and related studies in physics, chemistry, and medicine*. 28:417-425.

Korgaonkar, C., L. Zhao, M. Modestou, and D.E. Quelle. 2002. ARF function does not require p53 stabilization or Mdm2 relocalization. *Molecular and cellular biology*. 22:196-206.

Korppi-Tommola, T., H. Huhmar, H.J. Aronen, P. Penttila, J. Hiltunen, S. Savolainen, M.E. Kallio, and K. Liewendahl. 1999. 111In-labelled bleomycin complex for the differentiation of high- and low-grade gliomas. *Nuclear medicine communications*. 20:145-152.

Kortylewicz, Z.P., E. Mack, C.A. Enke, K.A. Estes, R.L. Mosley, and J. Baranowska-Kortylewicz. 2015. Preclinical evaluation of investigational radiopharmaceutical RISAD-P intended for use as a diagnostic and molecular radiotherapy agent for prostate cancer. *The Prostate*. 75:8-22.

Kressler, D., E. Hurt, and J. Bassler. 2010. Driving ribosome assembly. *Biochimica et biophysica acta*. 1803:673-683.

Krisch, R.E., F. Krasin, and C.J. Sauri. 1976. DNA breakage, repair and lethality after 125I decay in rec+ and recA strains of Escherichia coli. *International journal of radiation biology and related studies in physics, chemistry, and medicine*. 29:37-50.

Krisch, R.E., F. Krasin, and C.J. Sauri. 1978. DNA breakage, repair, and lethality accompanying 125I decay in microorganisms. *Current topics in radiation research quarterly*. 12:355-368.

Krisch, R.E., and R.D. Ley. 1974. Induction of lethality and DNA breakage by the decay of iodine-125 in bacteriophage T4. *International journal of radiation biology and related studies in physics, chemistry, and medicine*. 25:21-30.

Krisch, R.E., and C.J. Sauri. 1975. Further studies of DNA damage and lethality from the decay of iodine-125 in bacteriophages. *International journal of radiation biology and related studies in physics, chemistry, and medicine*. 27:553-560.

Kriss, J.P., L. Tung, and S. Bond. 1962. The distribution and fate of iododeoxycytidine in the mouse and rat. *Cancer research*. 22:1257-1264.

Kruhlak, M., E.E. Crouch, M. Orlov, C. Montano, S.A. Gorski, A. Nussenzweig, T. Misteli, R.D. Phair, and R. Casellas. 2007. The ATM repair pathway inhibits

RNA polymerase I transcription in response to chromosome breaks. *Nature*. 447:730-734.

Kruse, J.P., and W. Gu. 2008. SnapShot: p53 posttranslational modifications. *Cell*. 133:930-930 e931.

Kubbutat, M.H., S.N. Jones, and K.H. Vousden. 1997. Regulation of p53 stability by Mdm2. *Nature*. 387:299-303.

Kuo, M.L., W. den Besten, D. Bertwistle, M.F. Roussel, and C.J. Sherr. 2004. N-terminal polyubiquitination and degradation of the Arf tumor suppressor. *Genes & development*. 18:1862-1874.

Kurki, S., K. Peltonen, L. Latonen, T.M. Kiviharju, P.M. Ojala, D. Meek, and M. Laiho. 2004. Nucleolar protein NPM interacts with HDM2 and protects tumor suppressor protein p53 from HDM2-mediated degradation. *Cancer cell*. 5:465-475.

Kwekkeboom, D.J., W.H. Bakker, B.L. Kam, J.J. Teunissen, P.P. Kooij, W.W. de Herder, R.A. Feelders, C.H. van Eijck, M. de Jong, A. Srinivasan, J.L. Erion, and E.P. Krenning. 2003. Treatment of patients with gastro-entero-pancreatic (GEP) tumours with the novel radiolabelled somatostatin analogue [177Lu-DOTA(0),Tyr3]octreotate. *European journal of nuclear medicine and molecular imaging*. 30:417-422.

Lam, Y.W., V.C. Evans, K.J. Heesom, A.I. Lamond, and D.A. Matthews. 2010. Proteomics analysis of the nucleolus in adenovirus-infected cells. *Molecular & cellular proteomics : MCP*. 9:117-130.

Lam, Y.W., Lamond, A.I. 2006. Isolation of nucleoli.In: Celis, J.E., Editor. Thir Edition. *Elsevier Academic Press*. 2:103-108.

Lane, D.P. 1992. Cancer. p53, guardian of the genome. *Nature*. 358:15-16.

Lapeyre, B., F. Amalric, S.H. Ghaffari, S.V. Rao, T.S. Dumbar, and M.O. Olson. 1986. Protein and cDNA sequence of a glycine-rich, dimethylarginine-containing region located near the carboxyl-terminal end of nucleolin (C23 and 100 kDa). *The Journal of biological chemistry*. 261:9167-9173.

Le Mevel, B.P., R.K. Oldham, S.A. Wells, and R.B. Herberman. 1973. An evaluation of 125I-iododeoxyuridine as a cellular label for in vitro assays: kinetics of incorporation and toxicity. *Journal of the National Cancer Institute*. 51:1551-1558.

Lee, J.T., and W. Gu. 2010. The multiple levels of regulation by p53 ubiquitination. *Cell death and differentiation*. 17:86-92.

Lemm, I., C. Girard, A.N. Kuhn, N.J. Watkins, M. Schneider, R. Bordonne, and R. Luhrmann. 2006. Ongoing U snRNP biogenesis is required for the integrity of Cajal bodies. *Molecular biology of the cell*. 17:3221-3231.

Leung, A.K., J.S. Andersen, M. Mann, and A.I. Lamond. 2003. Bioinformatic analysis of the nucleolus. *The Biochemical journal*. 376:553-569.

Leung, A.K., D. Gerlich, G. Miller, C. Lyon, Y.W. Lam, D. Lleres, N. Daigle, J. Zomerdijk, J. Ellenberg, and A.I. Lamond. 2004. Quantitative kinetic analysis of nucleolar breakdown and reassembly during mitosis in live human cells. *The Journal of cell biology*. 166:787-800.

Leung, A.K., L. Trinkle-Mulcahy, Y.W. Lam, J.S. Andersen, M. Mann, and A.I. Lamond. 2006. NOPdb: Nucleolar Proteome Database. *Nucleic acids research*. 34:D218-220.

Li, J., X. Zhang, D.P. Sejas, G.C. Bagby, and Q. Pang. 2004. Hypoxia-induced nucleophosmin protects cell death through inhibition of p53. *The Journal of biological chemistry*. 279:41275-41279.

Li, L., T.S. Quang, E.J. Gracely, J.H. Kim, J.G. Emrich, T.E. Yaeger, J.M. Jenrette, S.C. Cohen, P. Black, and L.W. Brady. 2010. A Phase II study of anti-epidermal growth factor receptor radioimmunotherapy in the treatment of glioblastoma multiforme. *Journal of neurosurgery*. 113:192-198.

Lin, S.Y., K. Makino, W. Xia, A. Matin, Y. Wen, K.Y. Kwong, L. Bourguignon, and M.C. Hung. 2001. Nuclear localization of EGF receptor and its potential new role as a transcription factor. *Nature cell biology*. 3:802-808.

Linden, O., C. Hindorf, E. Cavallin-Stahl, W.A. Wegener, D.M. Goldenberg, H. Horne, T. Ohlsson, L. Stenberg, S.E. Strand, and J. Tennvall. 2005. Dose-fractionated radioimmunotherapy in non-Hodgkin's lymphoma using DOTA-conjugated, 90Y-radiolabeled, humanized anti-CD22 monoclonal antibody, epratuzumab. *Clinical cancer research : an official journal of the American Association for Cancer Research*. 11:5215-5222.

Lindstrom, M.S. 2009. Emerging functions of ribosomal proteins in gene-specific transcription and translation. *Biochemical and biophysical research communications*. 379:167-170.

Lindstrom, M.S., A. Jin, C. Deisenroth, G. White Wolf, and Y. Zhang. 2007. Cancer-associated mutations in the MDM2 zinc finger domain disrupt ribosomal protein interaction and attenuate MDM2-induced p53 degradation. *Molecular and cellular biology*. 27:1056-1068.

Liu, H.T., and B.Y. Yung. 1999. In vivo interaction of nucleophosmin/B23 and protein C23 during cell cycle progression in HeLa cells. *Cancer letters*. 144:45-54.

Llanos, S., P.A. Clark, J. Rowe, and G. Peters. 2001. Stabilization of p53 by p14ARF without relocation of MDM2 to the nucleolus. *Nature cell biology*. 3:445-452.

Lo, H.W., S.C. Hsu, and M.C. Hung. 2006. EGFR signaling pathway in breast cancers: from traditional signal transduction to direct nuclear translocalization. *Breast cancer research and treatment*. 95:211-218.

Lobachevsky, P.N., and R.F. Martin. 2004. Plasmid DNA breakage by decay of DNA-associated auger emitters: experiments with 123I/125I-iodoHoechst 33258. *International journal of radiation biology*. 80:915-920.

Lorenzato, M., P. Abboud, C. Lechki, F. Browarnyj, M.F. O'Donohue, D. Ploton, and J.J. Adnet. 2000. Proliferation assessment in breast cancer: a double-staining technique for AgNOR quantification in MIB-1 positive cells especially adapted for image cytometry. *Micron*. 31:151-159.

Losfeld, M.E., D.E. Khoury, P. Mariot, M. Carpentier, B. Krust, J.P. Briand, J. Mazurier, A.G. Hovanessian, and D. Legrand. 2009. The cell surface expressed nucleolin is a glycoprotein that triggers calcium entry into mammalian cells. *Experimental cell research*. 315:357-369.

Lyon, C.E., K. Bohmann, J. Sleeman, and A.I. Lamond. 1997. Inhibition of protein dephosphorylation results in the accumulation of splicing snRNPs and coiled bodies within the nucleolus. *Experimental cell research*. 230:84-93.

Ma, N., S. Matsunaga, H. Takata, R. Ono-Maniwa, S. Uchiyama, and K. Fukui. 2007. Nucleolin functions in nucleolus formation and chromosome congression. *Journal of cell science*. 120:2091-2105.

MacCallum, D.E., and P.A. Hall. 1999. Biochemical characterization of pKi67 with the identification of a mitotic-specific form associated with hyperphosphorylation and altered DNA binding. *Experimental cell research*. 252:186-198.

MacPhail, S.H., J.P. Banath, T.Y. Yu, E.H. Chu, H. Lambur, and P.L. Olive. 2003. Expression of phosphorylated histone H2AX in cultured cell lines following exposure to X-rays. *International journal of radiation biology*. 79:351-358.

Maggi, L.B., Jr., M. Kuchenruether, D.Y. Dadey, R.M. Schwope, S. Grisendi, R.R. Townsend, P.P. Pandolfi, and J.D. Weber. 2008. Nucleophosmin serves as a rate-limiting nuclear export chaperone for the Mammalian ribosome. *Molecular and cellular biology*. 28:7050-7065.

Mahajan, P.B. 1994. Modulation of transcription of rRNA genes by rapamycin. *International journal of immunopharmacology*. 16:711-721.

Mairs, R.J., W. Angerson, M.N. Gaze, T. Murray, J.W. Babich, R. Reid, and C. McSharry. 1991a. The distribution of alternative agents for targeted radiotherapy within human neuroblastoma spheroids. *British journal of cancer*. 63:404-409.

Mairs, R.J., W.J. Angerson, J.W. Babich, and T. Murray. 1991b. Differential penetration of targeting agents into multicellular spheroids derived from human neuroblastoma. *Progress in clinical and biological research*. 366:495-501.

Mariani, G., A. Cei, P. Collecchi, J. Baranowska-Kortylewicz, A.D. Van den Abbeele, L. Di Luca, R. Di Stefano, P. Viacava, E.M. Ferdeghini, S. Di Sacco, and et al. 1993. Tumor targeting in vivo and metabolic fate of 5-[iodine-125]iodo-2'-deoxyuridine following intratumoral injection in patients with colorectal cancer. *Journal of nuclear medicine : official publication, Society of Nuclear Medicine*. 34:1175-1183.

Marshall, L., N.S. Kenneth, and R.J. White. 2008. Elevated tRNA(iMet) synthesis can drive cell proliferation and oncogenic transformation. *Cell*. 133:78-89.

Martin, R.F., T.R. Bradley, and G.S. Hodgson. 1979. Cytotoxicity of an 125I-labeled DNA-binding compound that induces double-stranded DNA breaks. *Cancer research*. 39:3244-3247.

Matera, A.G., R.M. Terns, and M.P. Terns. 2007. Non-coding RNAs: lessons from the small nuclear and small nucleolar RNAs. *Nature reviews. Molecular cell biology*. 8:209-220.

Mathe, G., M. Hayat, F. De Vassal, L. Schwarzenberg, M. Schneider, J.R. Schlumberger, C. Jasmin, and C. Rosenfeld. 1970. Methoxy-9-ellipticine lactate. 3. Clinical screening: its action in acute myeloblastic leukaemia. *Revue europeenne d'etudes cliniques et biologiques. European journal of clinical and biological research*. 15:541-545.

Mayer, C., and I. Grummt. 2006. Ribosome biogenesis and cell growth: mTOR coordinates transcription by all three classes of nuclear RNA polymerases. *Oncogene*. 25:6384-6391.

McClintock, B. 1934. The relationship of a particular chromosomal element to the development of the nucleoli in Zea mays. *Z. Zellforsch Mikrosk* 21:294–398.

McCluskey, A.G., R.J. Mairs, A. Sorensen, T. Robson, H.O. McCarthy, S.L. Pimlott, J.W. Babich, S. Champion, and M. Boyd. 2013. Gamma irradiation and targeted radionuclides enhance the expression of the noradrenaline transporter transgene controlled by the radio-inducible p21(WAF1/CIP1) promoter. *Radiation research*. 179:282-292.

McEwan, A.J., B. Shapiro, J.C. Sisson, W.H. Beierwaltes, and D.M. Ackery. 1985. Radio-iodobenzylguanidine for the scintigraphic location and therapy of adrenergic tumors. *Seminars in nuclear medicine*. 15:132-153.

McGann, S., and E.R. Horton. 2015. Radium-223 Dichloride: A Novel Treatment Option for Castration-Resistant Prostate Cancer Patients With Symptomatic Bone Metastases. *The Annals of pharmacotherapy*.

McLaughlin, W.H., K.M. Pillai, J.P. Edasery, R.D. Blumenthal, and W.D. Bloomer. 1989. [125I]iodotamoxifen cytotoxicity in cultured human (MCF-7) breast cancer cells. *Journal of steroid biochemistry*. 33:515-519.

McStay, B., and I. Grummt. 2008. The epigenetics of rRNA genes: from molecular to chromosome biology. *Annual review of cell and developmental biology*. 24:131-157.

Meitner, L. 1922. Uber die Enstehung der beta-Strahl-Spektren radioaktiver Substanzen. *Zeitschrift fur Physik A Hadrons and Nuclei*. 9.

Mekhail, K., M. Khacho, A. Carrigan, R.R. Hache, L. Gunaratnam, and S. Lee. 2005. Regulation of ubiquitin ligase dynamics by the nucleolus. *The Journal of cell biology*. 170:733-744.

Mekhail, K., L. Rivero-Lopez, M. Khacho, and S. Lee. 2006. Restriction of rRNA synthesis by VHL maintains energy equilibrium under hypoxia. *Cell cycle*. 5:2401-2413.

Michel, R.B., A.V. Rosario, P.M. Andrews, D.M. Goldenberg, and M.J. Mattes. 2005. Therapy of small subcutaneous B-lymphoma xenografts with antibodies conjugated to radionuclides emitting low-energy electrons. *Clinical cancer research : an official journal of the American Association for Cancer Research*. 11:777-786.

Miyazaki, N., and K. Shinohara. 1993. Cell killing induced by decay of 125I during the cell cycle: comparison of 125I-antipyrine with 125I-bovine serum albumin. *Radiation research*. 133:182-186.

Momand, J., G.P. Zambetti, D.C. Olson, D. George, and A.J. Levine. 1992. The mdm-2 oncogene product forms a complex with the p53 protein and inhibits p53-mediated transactivation. *Cell*. 69:1237-1245.

Mongelard, F., and P. Bouvet. 2007. Nucleolin: a multiFACeTed protein. *Trends in cell biology*. 17:80-86.

Moore, H.M., B. Bai, F.M. Boisvert, L. Latonen, V. Rantanen, J.C. Simpson, R. Pepperkok, A.I. Lamond, and M. Laiho. 2011. Quantitative proteomics and dynamic imaging of the nucleolus reveal distinct responses to UV and ionizing radiation. *Molecular & cellular proteomics : MCP*. 10:M111 009241.

Morency, E., M. Sabra, F. Catez, P. Texier, and P. Lomonte. 2007. A novel cell response triggered by interphase centromere structural instability. *The Journal of cell biology*. 177:757-768.

Moss, T., F. Langlois, T. Gagnon-Kugler, and V. Stefanovsky. 2007. A housekeeper with power of attorney: the rRNA genes in ribosome biogenesis. *Cellular and molecular life sciences : CMLS*. 64:29-49.

Moy, T.I., and P.A. Silver. 1999. Nuclear export of the small ribosomal subunit requires the ran-GTPase cycle and certain nucleoporins. *Genes & development*. 13:2118-2133.

Mukudai, Y., S. Kubota, H. Kawaki, S. Kondo, T. Eguchi, K. Sumiyoshi, T. Ohgawara, T. Shimo, and M. Takigawa. 2008. Posttranscriptional regulation of chicken

ccn2 gene expression by nucleophosmin/B23 during chondrocyte differentiation. *Molecular and cellular biology*. 28:6134-6147.

Murano, K., M. Okuwaki, M. Hisaoka, and K. Nagata. 2008. Transcription regulation of the rRNA gene by a multifunctional nucleolar protein, B23/nucleophosmin, through its histone chaperone activity. *Molecular and cellular biology*. 28:3114-3126.

Murayama, A., K. Ohmori, A. Fujimura, H. Minami, K. Yasuzawa-Tanaka, T. Kuroda, S. Oie, H. Daitoku, M. Okuwaki, K. Nagata, A. Fukamizu, K. Kimura, T. Shimizu, and J. Yanagisawa. 2008. Epigenetic control of rDNA loci in response to intracellular energy status. *Cell*. 133:627-639.

Naora, H., I. Takai, M. Adachi, and H. Naora. 1998. Altered cellular responses by varying expression of a ribosomal protein gene: sequential coordination of enhancement and suppression of ribosomal protein S3a gene expression induces apoptosis. *The Journal of cell biology*. 141:741-753.

Ocampo-Garcia, B.E., C.L. Santos-Cuevas, L.M. De Leon-Rodriguez, R. Garcia-Becerra, D. Ordaz-Rosado, M.A. Luna-Guitierrez, N.P. Jimenez-Mancilla, M.E. Romero-Pina, and G. Ferro-Flores. 2013. Design and biological evaluation of (9)(9)mTc-N(2)S(2)-Tat(49-57)-c(RGDyK): a hybrid radiopharmaceutical for tumors expressing alpha(v)beta(3) integrins. *Nuclear medicine and biology*. 40:481-487.

Ofir-Rosenfeld, Y., K. Boggs, D. Michael, M.B. Kastan, and M. Oren. 2008. Mdm2 regulates p53 mRNA translation through inhibitory interactions with ribosomal protein L26. *Mol Cell*. 32:180-189.

Okuwaki, M., A. Iwamatsu, M. Tsujimoto, and K. Nagata. 2001a. Identification of nucleophosmin/B23, an acidic nucleolar protein, as a stimulatory factor for in vitro replication of adenovirus DNA complexed with viral basic core proteins. *Journal of molecular biology*. 311:41-55.

Okuwaki, M., K. Matsumoto, M. Tsujimoto, and K. Nagata. 2001b. Function of nucleophosmin/B23, a nucleolar acidic protein, as a histone chaperone. *FEBS letters*. 506:272-276.

Oliner, J.D., J.A. Pietenpol, S. Thiagalingam, J. Gyuris, K.W. Kinzler, and B. Vogelstein. 1993. Oncoprotein MDM2 conceals the activation domain of tumour suppressor p53. *Nature*. 362:857-860.

Olive, P.L., and J.P. Banath. 2004. Phosphorylation of histone H2AX as a measure of radiosensitivity. *International journal of radiation oncology, biology, physics*. 58:331-335.

Olivier, M., M. Hollstein, and P. Hainaut. 2010. TP53 mutations in human cancers: origins, consequences, and clinical use. *Cold Spring Harbor perspectives in biology*. 2:a001008.

Olson, M.O., and M. Dundr. 2005. The moving parts of the nucleolus. *Histochemistry and cell biology*. 123:203-216.

Olson, M.O., K. Hingorani, and A. Szebeni. 2002. Conventional and nonconventional roles of the nucleolus. *International review of cytology*. 219:199-266.

Otake, Y., S. Soundararajan, T.K. Sengupta, E.A. Kio, J.C. Smith, M. Pineda-Roman, R.K. Stuart, E.K. Spicer, and D.J. Fernandes. 2007. Overexpression of nucleolin in chronic lymphocytic leukemia cells induces stabilization of bcl2 mRNA. *Blood*. 109:3069-3075.

Otte, A., R. Herrmann, A. Heppeler, M. Behe, E. Jermann, P. Powell, H.R. Maecke, and J. Muller. 1999. Yttrium-90 DOTATOC: first clinical results. *European journal of nuclear medicine*. 26:1439-1447.

Pandit-Taskar, N., S.M. Larson, and J.A. Carrasquillo. 2014. Bone-seeking radiopharmaceuticals for treatment of osseous metastases, Part 1: alpha therapy with 223Ra-dichloride. *Journal of nuclear medicine : official publication, Society of Nuclear Medicine*. 55:268-274.

Pang, Q., T.A. Christianson, T. Koretsky, H. Carlson, L. David, W. Keeble, G.R. Faulkner, A. Speckhart, and G.C. Bagby. 2003. Nucleophosmin interacts with and inhibits the catalytic function of eukaryotic initiation factor 2 kinase PKR. *The Journal of biological chemistry*. 278:41709-41717.

Pasieka, J.L., A.J. McEwan, and O. Rorstad. 2004. The palliative role of 131I-MIBG and 111In-octreotide therapy in patients with metastatic progressive neuroendocrine neoplasms. *Surgery*. 136:1218-1226.

Pederson, T. 1998. The plurifunctional nucleolus. *Nucleic acids research*. 26:3871-3876.

Pich, A., L. Chiusa, and E. Margaria. 2000. Prognostic relevance of AgNORs in tumor pathology. *Micron*. 31:133-141.

Pickering, B.F., D. Yu, and M.W. Van Dyke. 2011. Nucleolin protein interacts with microprocessor complex to affect biogenesis of microRNAs 15a and 16. *The Journal of biological chemistry*. 286:44095-44103.

Piron, B., S. Paillas, V. Boudousq, A. Pelegrin, C. Bascoul-Mollevi, N. Chouin, I. Navarro-Teulon, and J.P. Pouget. 2014. DNA damage-centered signaling pathways are effectively activated during low dose-rate Auger radioimmunotherapy. *Nuclear medicine and biology*. 41 Suppl:e75-83.

Pomplun, E., J. Booz, and D.E. Charlton. 1987. A Monte Carlo simulation of Auger cascades. *Radiation research*. 111:533-552.

Poortinga, G., K.M. Hannan, H. Snelling, C.R. Walkley, A. Jenkins, K. Sharkey, M. Wall, Y. Brandenburger, M. Palatsides, R.B. Pearson, G.A. McArthur, and R.D. Hannan. 2004. MAD1 and c-MYC regulate UBF and rDNA transcription during granulocyte differentiation. *The EMBO journal*. 23:3325-3335.

Poortinga, G., M. Wall, E. Sanij, K. Siwicki, J. Ellul, D. Brown, T.P. Holloway, R.D. Hannan, and G.A. McArthur. 2011. c-MYC coordinately regulates ribosomal gene chromatin remodeling and Pol I availability during granulocyte differentiation. *Nucleic acids research*. 39:3267-3281.

Porkka, K., P. Laakkonen, J.A. Hoffman, M. Bernasconi, and E. Ruoslahti. 2002. A fragment of the HMGN2 protein homes to the nuclei of tumor cells and tumor endothelial cells in vivo. *Proceedings of the National Academy of Sciences of the United States of America*. 99:7444-7449.

Porteous, D.D. 1971. The toxicity of 125 IUdR in cultured mouse BP8 tumour cells. *British journal of cancer*. 25:594-597.

Pouget, J.P., L. Santoro, L. Raymond, N. Chouin, M. Bardies, C. Bascoul-Mollevi, H. Huguet, D. Azria, P.O. Kotzki, M. Pelegrin, E. Vives, and A. Pelegrin. 2008. Cell membrane is a more sensitive target than cytoplasm to dense ionization produced by auger electrons. *Radiation research*. 170:192-200.

Prusoff, W.H. 1963. A Review of Some Aspects of 5-Iododeoxyuridine and Azauridine. *Cancer research*. 23:1246-1259.

Quang, T.S., and L.W. Brady. 2004. Radioimmunotherapy as a novel treatment regimen: 125I-labeled monoclonal antibody 425 in the treatment of high-grade

brain gliomas. *International journal of radiation oncology, biology, physics*. 58:972-975.

Radford, I.R., G.S. Hodgson, and J.P. Matthews. 1988. Critical DNA target size model of ionizing radiation-induced mammalian cell death. *International journal of radiation biology*. 54:63-79.

Raska, I. 2003. Oldies but goldies: searching for Christmas trees within the nucleolar architecture. *Trends in cell biology*. 13:517-525.

Ravanat, J.L., T. Douki, and J. Cadet. 2001. Direct and indirect effects of UV radiation on DNA and its components. *Journal of photochemistry and photobiology. B, Biology*. 63:88-102.

Reddy, G.R., M.S. Bhojani, P. McConville, J. Moody, B.A. Moffat, D.E. Hall, G. Kim, Y.E. Koo, M.J. Woolliscroft, J.V. Sugai, T.D. Johnson, M.A. Philbert, R. Kopelman, A. Rehemtulla, and B.D. Ross. 2006. Vascular targeted nanoparticles for imaging and treatment of brain tumors. *Clinical cancer research : an official journal of the American Association for Cancer Research*. 12:6677-6686.

Reilly, R.M., P. Chen, J. Wang, D. Scollard, R. Cameron, and K.A. Vallis. 2006. Preclinical pharmacokinetic, biodistribution, toxicology, and dosimetry studies of 111In-DTPA-human epidermal growth factor: an auger electron-emitting radiotherapeutic agent for epidermal growth factor receptor-positive breast cancer. *Journal of nuclear medicine : official publication, Society of Nuclear Medicine*. 47:1023-1031.

Reilly, R.M., R. Kiarash, R.G. Cameron, N. Porlier, J. Sandhu, R.P. Hill, K. Vallis, A. Hendler, and J. Gariepy. 2000. 111In-labeled EGF is selectively radiotoxic to human breast cancer cells overexpressing EGFR. *Journal of nuclear medicine : official publication, Society of Nuclear Medicine*. 41:429-438.

Rey, J.P., R. Scott, and H. Muller. 1993. Induction and removal of interstrand crosslinks in the ribosomal RNA genes of lymphoblastoid cell lines from patients with Fanconi anemia. *Mutation research*. 289:171-180.

Rickards, B., S.J. Flint, M.D. Cole, and G. LeRoy. 2007. Nucleolin is required for RNA polymerase I transcription in vivo. *Molecular and cellular biology*. 27:937-948.

Ridanpaa, M., H. van Eenennaam, K. Pelin, R. Chadwick, C. Johnson, B. Yuan, W. vanVenrooij, G. Pruijn, R. Salmela, S. Rockas, O. Makitie, I. Kaitila, and A. de la Chapelle. 2001. Mutations in the RNA component of RNase MRP cause a pleiotropic human disease, cartilage-hair hypoplasia. *Cell*. 104:195-203.

Riley, K.J., and L.J. Maher, 3rd. 2007. p53 RNA interactions: new clues in an old mystery. *Rna*. 13:1825-1833.

Rodriguez, M.S., J.M. Desterro, S. Lain, D.P. Lane, and R.T. Hay. 2000. Multiple C-terminal lysine residues target p53 for ubiquitin-proteasome-mediated degradation. *Molecular and cellular biology*. 20:8458-8467.

Roger, B., A. Moisand, F. Amalric, and P. Bouvet. 2003. Nucleolin provides a link between RNA polymerase I transcription and pre-ribosome assembly. *Chromosoma*. 111:399-407.

Rohr, O., C. Schwartz, C. Hery, D. Aunis, M. Tardieu, and E. Schaeffer. 2000. The nuclear receptor chicken ovalbumin upstream promoter transcription factor interacts with HIV-1 Tat and stimulates viral replication in human microglial cells. *The Journal of biological chemistry*. 275:2654-2660.

Romanova, L., A. Grand, L. Zhang, S. Rayner, N. Katoku-Kikyo, S. Kellner, and N. Kikyo. 2009. Critical role of nucleostemin in pre-rRNA processing. *The Journal of biological chemistry*. 284:4968-4977.

Rubbi, C.P., and J. Milner. 2003. Disruption of the nucleolus mediates stabilization of p53 in response to DNA damage and other stresses. *The EMBO journal*. 22:6068-6077.

Rudra, D., and J.R. Warner. 2004. What better measure than ribosome synthesis? *Genes & development*. 18:2431-2436.

Ruggero, D., S. Grisendi, F. Piazza, E. Rego, F. Mari, P.H. Rao, C. Cordon-Cardo, and P.P. Pandolfi. 2003. Dyskeratosis congenita and cancer in mice deficient in ribosomal RNA modification. *Science*. 299:259-262.

Salvat, F., Fernandez-Varea, J.M., Sempau, J. 2011. PENELOPE-2011: A code system for Monte Carlo simulation of electron and photon transport. *NEA*.

Santoro, L., S. Boutaleb, V. Garambois, C. Bascoul-Mollevi, V. Boudousq, P.O. Kotzki, M. Pelegrin, I. Navarro-Teulon, A. Pelegrin, and J.P. Pouget. 2009. Noninternalizing monoclonal antibodies are suitable candidates for 125I radioimmunotherapy of small-volume peritoneal carcinomatosis. *Journal of nuclear medicine : official publication, Society of Nuclear Medicine*. 50:2033-2041.

Sasaki, M., K. Kawahara, M. Nishio, K. Mimori, R. Kogo, K. Hamada, B. Itoh, J. Wang, Y. Komatsu, Y.R. Yang, H. Hikasa, Y. Horie, T. Yamashita, T. Kamijo, Y. Zhang, Y. Zhu, C. Prives, T. Nakano, T.W. Mak, T. Sasaki, T. Maehama, M. Mori, and A. Suzuki. 2011. Regulation of the MDM2-P53 pathway and tumor growth by PICT1 via nucleolar RPL11. *Nature medicine*. 17:944-951.

Savino, T.M., J. Gebrane-Younes, J. De Mey, J.B. Sibarita, and D. Hernandez-Verdun. 2001. Nucleolar assembly of the rRNA processing machinery in living cells. *The Journal of cell biology*. 153:1097-1110.

Savkur, R.S., and M.O. Olson. 1998. Preferential cleavage in pre-ribosomal RNA byprotein B23 endoribonuclease. *Nucleic acids research*. 26:4508-4515.

Schillaci, O., and G. Simonetti. 2004. Fusion imaging in nuclear medicine--applications of dual-modality systems in oncology. *Cancer biotherapy & radiopharmaceuticals*. 19:1-10.

Schlosser, I., M. Holzel, M. Murnseer, H. Burtscher, U.H. Weidle, and D. Eick. 2003. A role for c-Myc in the regulation of ribosomal RNA processing. *Nucleic acids research*. 31:6148-6156.

Schlumberger, M.J. 1998. Papillary and follicular thyroid carcinoma. *The New England journal of medicine*. 338:297-306.

Schmidt-Zachmann, M.S., C. Dargemont, L.C. Kuhn, and E.A. Nigg. 1993. Nuclear export of proteins: the role of nuclear retention. *Cell*. 74:493-504.

Schmidt-Zachmann, M.S., and E.A. Nigg. 1993. Protein localization to the nucleolus: a search for targeting domains in nucleolin. *Journal of cell science*. 105 (Pt 3):799-806.

Schmidt, A., and G. Hotz. 1973. The occurrence of double-strand breaks in coliphage T1-DNA by iodine-125 decay. *International journal of radiation biology and related studies in physics, chemistry, and medicine*. 24:307-313.

Scholzen, T., and J. Gerdes. 2000. The Ki-67 protein: from the known and the unknown. *Journal of cellular physiology*. 182:311-322.

Schwab, M.S., and C. Dreyer. 1997. Protein phosphorylation sites regulate the function of the bipartite NLS of nucleolin. *European journal of cell biology*. 73:287-297.

Schwartz, J.L., R. Mustafi, A. Hughes, and E.R. DeSombre. 1996. DNA and chromosome breaks induced by iodine-123-labeled estrogen in Chinese hamster ovary cells. *Radiation research*. 146:151-158.

Sengupta, S., T.R. Peterson, and D.M. Sabatini. 2010. Regulation of the mTOR complex 1 pathway by nutrients, growth factors, and stress. *Molecular cell*. 40:310-322.

Sengupta, T.K., S. Bandyopadhyay, D.J. Fernandes, and E.K. Spicer. 2004. Identification of nucleolin as an AU-rich element binding protein involved in bcl-2 mRNA stabilization. *The Journal of biological chemistry*. 279:10855-10863.

Serin, G., G. Joseph, C. Faucher, L. Ghisolfi, G. Bouche, F. Amalric, and P. Bouvet. 1996. Localization of nucleolin binding sites on human and mouse pre-ribosomal RNA. *Biochimie*. 78:530-538.

Shav-Tal, Y., J. Blechman, X. Darzacq, C. Montagna, B.T. Dye, J.G. Patton, R.H. Singer, and D. Zipori. 2005. Dynamic sorting of nuclear components into distinct nucleolar caps during transcriptional inhibition. *Molecular biology of the cell*. 16:2395-2413.

Sherman, S.I. 2003. Thyroid carcinoma. *Lancet*. 361:501-511.

Sherr, C.J., and J.D. Weber. 2000. The ARF/p53 pathway. *Current opinion in genetics & development*. 10:94-99.

Sirri, V., P. Roussel, and D. Hernandez-Verdun. 2000. In vivo release of mitotic silencing of ribosomal gene transcription does not give rise to precursor ribosomal RNA processing. *The Journal of cell biology*. 148:259-270.

Sirri, V., S. Urcuqui-Inchima, P. Roussel, and D. Hernandez-Verdun. 2008. Nucleolus: the fascinating nuclear body. *Histochemistry and cell biology*. 129:13-31.

Sleeman, J.E., P. Ajuh, and A.I. Lamond. 2001. snRNP protein expression enhances the formation of Cajal bodies containing p80-coilin and SMN. *Journal of cell science*. 114:4407-4419.

Soundararajan, S., L. Wang, V. Sridharan, W. Chen, N. Courtenay-Luck, D. Jones, E.K. Spicer, and D.J. Fernandes. 2009. Plasma membrane nucleolin is a receptor for the anticancer aptamer AS1411 in MV4-11 leukemia cells. *Molecular pharmacology*. 76:984-991.

Srivastava, M., and H.B. Pollard. 1999. Molecular dissection of nucleolin's role in growth and cell proliferation: new insights. *FASEB journal : official publication of the Federation of American Societies for Experimental Biology*. 13:1911-1922.

Stefanovsky, V.Y., G. Pelletier, R. Hannan, T. Gagnon-Kugler, L.I. Rothblum, and T. Moss. 2001. An immediate response of ribosomal transcription to growth factor stimulation in mammals is mediated by ERK phosphorylation of UBF. *Molecular cell*. 8:1063-1073.

Stein, T., D. Crighton, L.J. Warnock, J. Milner, and R.J. White. 2002. Several regions of p53 are involved in repression of RNA polymerase III transcription. *Oncogene*. 21:5540-5547.

Sun, X.X., M.S. Dai, and H. Lu. 2007. 5-fluorouracil activation of p53 involves an MDM2-ribosomal protein interaction. *The Journal of biological chemistry*. 282:8052-8059.

Sundqvist, A., G. Liu, A. Mirsaliotis, and D.P. Xirodimas. 2009. Regulation of nucleolar signalling to p53 through NEDDylation of L11. *EMBO reports*. 10:1132-1139.

Swaminathan, V., A.H. Kishore, K.K. Febitha, and T.K. Kundu. 2005. Human histone chaperone nucleophosmin enhances acetylation-dependent chromatin transcription. *Molecular and cellular biology*. 25:7534-7545.

Szebeni, A., B. Mehrotra, A. Baumann, S.A. Adam, P.T. Wingfield, and M.O. Olson. 1997. Nucleolar protein B23 stimulates nuclear import of the HIV-1 Rev protein and NLS-conjugated albumin. *Biochemistry*. 36:3941-3949.

Szebeni, A., and M.O. Olson. 1999. Nucleolar protein B23 has molecular chaperone activities. *Protein science : a publication of the Protein Society*. 8:905-912.

Tajrishi, M.M., R. Tuteja, and N. Tuteja. 2011. Nucleolin: The most abundant multifunctional phosphoprotein of nucleolus. *Communicative & integrative biology*. 4:267-275.

Takagi, M., M.J. Absalon, K.G. McLure, and M.B. Kastan. 2005. Regulation of p53 translation and induction after DNA damage by ribosomal protein L26 and nucleolin. *Cell*. 123:49-63.

Taneja, N., M. Davis, J.S. Choy, M.A. Beckett, R. Singh, S.J. Kron, and R.R. Weichselbaum. 2004. Histone H2AX phosphorylation as a predictor of radiosensitivity and target for radiotherapy. *The Journal of biological chemistry*. 279:2273-2280.

Tao, W., and A.J. Levine. 1999. P19(ARF) stabilizes p53 by blocking nucleo-cytoplasmic shuttling of Mdm2. *Proceedings of the National Academy of Sciences of the United States of America*. 96:6937-6941.

Terry, S.Y., and K.A. Vallis. 2012. Relationship between chromatin structure and sensitivity to molecularly targeted auger electron radiation therapy. *International journal of radiation oncology, biology, physics*. 83:1298-1305.

Thisgaard, H., B.B. Olsen, J.H. Dam, P. Bollen, J. Mollenhauer, and P.F. Hoilund-Carlsen. 2014. Evaluation of Cobalt-Labeled Octreotide Analogs for Molecular Imaging and Auger Electron-Based Radionuclide Therapy. *Journal of nuclear medicine : official publication, Society of Nuclear Medicine*. 55:1311-1316.

Tschochner, H., and E. Hurt. 2003. Pre-ribosomes on the road from the nucleolus to the cytoplasm. *Trends in cell biology*. 13:255-263.

Tuteja, N., N.W. Huang, D. Skopac, R. Tuteja, S. Hrvatic, J. Zhang, S. Pongor, G. Joseph, C. Faucher, F. Amalric, and et al. 1995. Human DNA helicase IV is nucleolin, an RNA helicase modulated by phosphorylation. *Gene*. 160:143-148.

Tuteja, N., K. Rahman, R. Tuteja, and A. Falaschi. 1991. DNA helicase IV from HeLa cells. *Nucleic acids research*. 19:3613-3618.

Tuteja, R., and N. Tuteja. 1998. Nucleolin: a multifunctional major nucleolar phosphoprotein. *Critical reviews in biochemistry and molecular biology*. 33:407-436.

Ugrinova, I., K. Monier, C. Ivaldi, M. Thiry, S. Storck, F. Mongelard, and P. Bouvet. 2007. Inactivation of nucleolin leads to nucleolar disruption, cell cycle arrest and defects in centrosome duplication. *BMC molecular biology*. 8:66.

Valentin, G. 1836. Repertorium für Anatomie und Physiologie. *Verlag von Veit und Comp*. 1:1-293.

Valentin, G. 1839. Repertorium für Anatomie und Physiologie. *Verlag von Veit und Comp*. 4:1-275.

Valkema, R., M. De Jong, W.H. Bakker, W.A. Breeman, P.P. Kooij, P.J. Lugtenburg, F.H. De Jong, A. Christiansen, B.L. Kam, W.W. De Herder, M. Stridsberg, J.

Lindemans, G. Ensing, and E.P. Krenning. 2002. Phase I study of peptide receptor radionuclide therapy with [In-DTPA]octreotide: the Rotterdam experience. *Seminars in nuclear medicine*. 32:110-122.

Valkema, R., S. Pauwels, L.K. Kvols, R. Barone, F. Jamar, W.H. Bakker, D.J. Kwekkeboom, H. Bouterfa, and E.P. Krenning. 2006. Survival and response after peptide receptor radionuclide therapy with [90Y-DOTA0,Tyr3]octreotide in patients with advanced gastroenteropancreatic neuroendocrine tumors. *Seminars in nuclear medicine*. 36:147-156.

Vallis, K.A., R.M. Reilly, D. Scollard, P. Merante, A. Brade, S. Velauthapillai, C. Caldwell, I. Chan, M. Freeman, G. Lockwood, N.A. Miller, B. Cornelissen, J. Petronis, and K. Sabate. 2014. Phase I trial to evaluate the tumor and normal tissue uptake, radiation dosimetry and safety of (111)In-DTPA-human epidermal growth factor in patients with metastatic EGFR-positive breast cancer. *American journal of nuclear medicine and molecular imaging*. 4:181-192.

Vallon, M., C. Seidl, B. Blechert, Z. Li, K.P. Gilbertz, A. Baumgart, M. Aichler, A. Feuchtinger, F.C. Gaertner, F. Bruchertseifer, A. Morgenstern, A.K. Walch, R. Senekowitsch-Schmidtke, and M. Essler. 2012. Enhanced efficacy of combined 213Bi-DTPA-F3 and paclitaxel therapy of peritoneal carcinomatosis is mediated by enhanced induction of apoptosis and G2/M phase arrest. *European journal of nuclear medicine and molecular imaging*. 39:1886-1897.

van Riggelen, J., A. Yetil, and D.W. Felsher. 2010. MYC as a regulator of ribosome biogenesis and protein synthesis. *Nature reviews. Cancer*. 10:301-309.

Verheijen, R., H.J. Kuijpers, R.O. Schlingemann, A.L. Boehmer, R. van Driel, G.J. Brakenhoff, and F.C. Ramaekers. 1989. Ki-67 detects a nuclear matrix-associated proliferation-related antigen. I. Intracellular localization during interphase. *Journal of cell science*. 92 (Pt 1):123-130.

Vlatkovic, N., M.T. Boyd, and C.P. Rubbi. 2014. Nucleolar control of p53: a cellular Achilles' heel and a target for cancer therapy. *Cell Mol Life Sci*. 71:771-791.

Wade, M., Y.C. Li, and G.M. Wahl. 2013. MDM2, MDMX and p53 in oncogenesis and cancer therapy. *Nature reviews. Cancer*. 13:83-96.

Wagner, R. 1835. Einige Bemerkungen und Fragen über das Keimbläschen (vesicular germinativa). *Einige Bemerkungen und Fragen über das Keimbläschen* 373-377.

Waldherr, C., M. Pless, H.R. Maecke, T. Schumacher, A. Crazzolara, E.U. Nitzsche, A. Haldemann, and J. Mueller-Brand. 2002. Tumor response and clinical benefit in neuroendocrine tumors after 7.4 GBq (90)Y-DOTATOC. *Journal of nuclear medicine : official publication, Society of Nuclear Medicine*. 43:610-616.

Walicka, M.A., S.J. Adelstein, and A.I. Kassis. 1998a. Indirect mechanisms contribute to biological effects produced by decay of DNA-incorporated iodine-125 in mammalian cells in vitro: clonogenic survival. *Radiation research*. 149:142-146.

Walicka, M.A., S.J. Adelstein, and A.I. Kassis. 1998b. Indirect mechanisms contribute to biological effects produced by decay of DNA-incorporated iodine-125 in mammalian cells in vitro: double-strand breaks. *Radiation research*. 149:134-141.

Walicka, M.A., S.J. Adelstein, and A.I. Kassis. 2001. Chemical modification of 5-[125I]iodo-2'-deoxyuridine toxicity in mammalian cells in vitro. *International journal of radiation biology*. 77:625-630.

Walicka, M.A., Y. Ding, S.J. Adelstein, and A.I. Kassiss. 2000. Toxicity of DNA-incorporated iodine-125: quantifying the direct and indirect effects. *Radiation research*. 154:326-330.

Walicka, M.A., Y. Ding, A.M. Roy, R.S. Harapanhalli, S.J. Adelstein, and A.I. Kassis. 1999. Cytotoxicity of [125I]iodoHoechst 33342: contribution of scavengeable effects. *International journal of radiation biology*. 75:1579-1587.

Walker, K.A., R. Mairs, T. Murray, T.E. Hilditch, T.E. Wheldon, A. Gregor, and I.M. Hann. 1990. Tumor spheroid model for the biologically targeted radiotherapy of neuroblastoma micrometastases. *Cancer Res*. 50:1000s-1002s.

Wang, M., A.L. Caruano, M.R. Lewis, L.A. Meyer, R.P. VanderWaal, and C.J. Anderson. 2003. Subcellular localization of radiolabeled somatostatin analogues: implications for targeted radiotherapy of cancer. *Cancer Res*. 63:6864-6869.

Wang, W., A. Budhu, M. Forgues, and X.W. Wang. 2005. Temporal and spatial control of nucleophosmin by the Ran-Crm1 complex in centrosome duplication. *Nature cell biology*. 7:823-830.

Wansink, D.G., W. Schul, I. van der Kraan, B. van Steensel, R. van Driel, and L. de Jong. 1993. Fluorescent labeling of nascent RNA reveals transcription by RNA polymerase II in domains scattered throughout the nucleus. *The Journal of cell biology*. 122:283-293.

Warner, J.R. 1999. The economics of ribosome biosynthesis in yeast. *Trends in biochemical sciences*. 24:437-440.

Warner, J.R., and K.B. McIntosh. 2009. How common are extraribosomal functions of ribosomal proteins? *Molecular cell*. 34:3-11.

Warters, R.L., and K.G. Hofer. 1977. Radionuclide toxicity in cultured mammalian cells. Elucidation of the primary site for radiation-induced division delay. *Radiation research*. 69:348-358.

Watanabe, N., H. Sawai, I. Ogihara-Umeda, S. Tanada, E.E. Kim, Y. Yonekura, and Y. Sasaki. 2006. Molecular therapy of human neuroblastoma cells using Auger electrons of 111In-labeled N-myc antisense oligonucleotides. *Journal of nuclear medicine : official publication, Society of Nuclear Medicine*. 47:1670-1677.

Weber, J.D., L.J. Taylor, M.F. Roussel, C.J. Sherr, and D. Bar-Sagi. 1999. Nucleolar Arf sequesters Mdm2 and activates p53. *Nature cell biology*. 1:20-26.

Weber, W., J. Weber, and R. Senekowitsch-Schmidtke. 1996. Therapeutic effect of m-[131I]- and m-[125I]iodobenzylguanidine on neuroblastoma multicellular tumor spheroids of different sizes. *Cancer Res*. 56:5428-5434.

White, R.J., D. Trouche, K. Martin, S.P. Jackson, and T. Kouzarides. 1996. Repression of RNA polymerase III transcription by the retinoblastoma protein. *Nature*. 382:88-90.

Wicki, A., D. Wild, V. Pretre, R. Mansi, A. Orleth, J.C. Reubi, C. Rochlitz, C. Mamot, H.R. Macke, and G. Christofori. 2014. Synergism of peptide receptor-targeted Auger electron radiation therapy with anti-angiogenic compounds in a mouse model of neuroendocrine tumors. *EJNMMI research*. 4:9.

Willimott, S., and S.D. Wagner. 2010. Post-transcriptional and post-translational regulation of Bcl2. *Biochemical Society transactions*. 38:1571-1575.

Winer, I., S. Wang, Y.E. Lee, W. Fan, Y. Gong, D. Burgos-Ojeda, G. Spahlinger, R. Kopelman, and R.J. Buckanovich. 2010. F3-targeted cisplatin-hydrogel

nanoparticles as an effective therapeutic that targets both murine and human ovarian tumor endothelial cells in vivo. *Cancer Res*. 70:8674-8683.

Witzig, T.E., L.I. Gordon, F. Cabanillas, M.S. Czuczman, C. Emmanouilides, R. Joyce, B.L. Pohlman, N.L. Bartlett, G.A. Wiseman, N. Padre, A.J. Grillo-Lopez, P. Multani, and C.A. White. 2002. Randomized controlled trial of yttrium-90-labeled ibritumomab tiuxetan radioimmunotherapy versus rituximab immunotherapy for patients with relapsed or refractory low-grade, follicular, or transformed B-cell non-Hodgkin's lymphoma. *Journal of clinical oncology : official journal of the American Society of Clinical Oncology*. 20:2453-2463.

Woo, D.V., D. Li, J.A. Mattis, and Z. Steplewski. 1989. Selective chromosomal damage and cytotoxicity of 125I-labeled monoclonal antibody 17-1a in human cancer cells. *Cancer research*. 49:2952-2958.

Wu, M.H., J.H. Chang, C.C. Chou, and B.Y. Yung. 2002a. Involvement of nucleophosmin/B23 in the response of HeLa cells to UV irradiation. *International journal of cancer. Journal international du cancer*. 97:297-305.

Wu, M.H., J.H. Chang, and B.Y. Yung. 2002b. Resistance to UV-induced cell-killing in nucleophosmin/B23 over-expressed NIH 3T3 fibroblasts: enhancement of DNA repair and up-regulation of PCNA in association with nucleophosmin/B23 over-expression. *Carcinogenesis*. 23:93-100.

Wyman, C., and R. Kanaar. 2006. DNA double-strand break repair: all's well that ends well. *Annual review of genetics*. 40:363-383.

Xiao, J., Z. Zhang, G.G. Chen, M. Zhang, Y. Ding, J. Fu, M. Li, and J.P. Yun. 2009. Nucleophosmin/B23 interacts with p21WAF1/CIP1 and contributes to its stability. *Cell cycle*. 8:889-895.

Xiao, L., and A. Grove. 2009. Coordination of Ribosomal Protein and Ribosomal RNA Gene Expression in Response to TOR Signaling. *Current genomics*. 10:198-205.

Xue, L.Y., N.J. Butler, G.M. Makrigiorgos, S.J. Adelstein, and A.I. Kassis. 2002. Bystander effect produced by radiolabeled tumor cells in vivo. *Proceedings of the National Academy of Sciences of the United States of America*. 99:13765-13770.

Xue, Z., and T. Melese. 1994. Nucleolar proteins that bind NLSs: a role in nuclear import or ribosome biogenesis? *Trends in cell biology*. 4:414-417.

Yang, T.H., W.H. Tsai, Y.M. Lee, H.Y. Lei, M.Y. Lai, D.S. Chen, N.H. Yeh, and S.C. Lee. 1994. Purification and characterization of nucleolin and its identification as a transcription repressor. *Molecular and cellular biology*. 14:6068-6074.

Yao, Z., S. Duan, D. Hou, W. Wang, G. Wang, Y. Liu, L. Wen, and M. Wu. 2010. B23 acts as a nucleolar stress sensor and promotes cell survival through its dynamic interaction with hnRNPU and hnRNPA1. *Oncogene*. 29:1821-1834.

Yasui, L., A. Hughes, and E. DeSombre. 2001a. Relative biological effectiveness of accumulated 125IdU and 125I-estrogen decays in estrogen receptor-expressing MCF-7 human breast cancer cells. *Radiation research*. 155:328-334.

Yasui, L.S., A. Hughes, and E.R. DeSombre. 1996. DNA damage induction by 125I-estrogen. *Acta oncologica*. 35:841-847.

Yasui, L.S., A. Hughes, and E.R. Desombre. 2001b. Cytotoxicity of 125I-oestrogen decay in non-oestrogen receptor-expressing human breast cancer cells, MDA-231 and oestrogen receptor-expressing MCF-7 cells. *International journal of radiation biology*. 77:955-962.

Yu, Y., L.B. Maggi, Jr., S.N. Brady, A.J. Apicelli, M.S. Dai, H. Lu, and J.D. Weber. 2006. Nucleophosmin is essential for ribosomal protein L5 nuclear export. *Molecular and cellular biology*. 26:3798-3809.

Zeller, K.I., T.J. Haggerty, J.F. Barrett, Q. Guo, D.R. Wonsey, and C.V. Dang. 2001. Characterization of nucleophosmin (B23) as a Myc target by scanning chromatin immunoprecipitation. *The Journal of biological chemistry*. 276:48285-48291.

Zhai, W., and L. Comai. 2000. Repression of RNA polymerase I transcription by the tumor suppressor p53. *Molecular and cellular biology*. 20:5930-5938.

Zhang, B., H. Wang, B. Jiang, P. Liang, M. Liu, G. Deng, and X. Xiao. 2010. Nucleolin/C23 is a negative regulator of hydrogen peroxide-induced apoptosis in HUVECs. *Cell stress & chaperones*. 15:249-257.

Zhang, Y., and H. Lu. 2009. Signaling to p53: ribosomal proteins find their way. *Cancer cell*. 16:369-377.

Zhao, J., X. Yuan, M. Frodin, and I. Grummt. 2003. ERK-dependent phosphorylation of the transcription initiation factor TIF-IA is required for RNA polymerase I transcription and cell growth. *Molecular cell*. 11:405-413.

Zhou, Y., K.M. Schmitz, C. Mayer, X. Yuan, A. Akhtar, and I. Grummt. 2009. Reversible acetylation of the chromatin remodelling complex NoRC is required for non-coding RNA-dependent silencing. *Nature cell biology*. 11:1010-1016.

Zou, Y., J. Wu, R.J. Giannone, L. Boucher, H. Du, Y. Huang, D.K. Johnson, Y. Liu, and Y. Wang. 2008. Nucleophosmin/B23 negatively regulates GCN5-dependent histone acetylation and transactivation. *The Journal of biological chemistry*. 283:5728-5737.